Integration and Validation of Flow Image Quantification (Flow-IQ) System

Jason Bradley Carneal

A thesis submitted to the Faculty of the Virginia Polytechnic Institute and State University in partial fulfillment of the requirements for the degree of

Master of Science

in

Engineering Mechanics

September 2004

Approved by _____
Dr. Pavlos Vlachos, Chairperson of Supervisory Committee

_____
Dr. Demetri Telionis

_____
Dr. Marty Johnson

Keywords: DPIV, Wall Shear, Spray, Particle Sizing, Elliptical Gaussian Profile

ABSTRACT

Integration and Validation of Flow Image Quantification (Flow-IQ) System

Jason B. Carneal

The first aim of this work was to integrate, validate, and document, a digital particle image quantification (Flow-IQ) software package developed in conjunction with and supported by Aeroprobe Corporation. The system is tailored towards experimental fluid mechanics applications. The second aim of this work was to test the performance of DPIV algorithms in wall shear flows, and to test the performance of several particle sizing algorithms for use in spray sizing and average diameter calculation. Several particle sizing algorithms which assume a circular particle profile were tested with DPIV data on spray atomization, including three point Guassian, four point Gaussian, and least squares algorithms. A novel elliptical diameter estimation scheme was developed which does not limit the measurement to circular patterns. The elliptic estimator developed in this work is able to estimate the diameter of a particle with an elliptic shape, and assumes that the particle is axisymmetric about the x or y axis. Two elliptical schemes, the true and averaged elliptical estimators, were developed and compared to the traditional three point Gaussian diameter estimator using theoretical models. If elliptical particles are theoretically used, the elliptical sizing schemes perform drastically better than the traditional scheme, which is limited to diameter measurements in the x-direction. The error of the traditional method in determining the volume of an elliptical particle increases dramatically with the eccentricity. Monte Carlo Simulations were also used to characterize the error associated with wall shear measurements using DPIV. Couette flow artificial images were generated with various shear rates at the wall. DPIV analysis was performed on these images using PIV algorithms developed by other researchers, including the traditional multigrid method, a dynamically-adaptive DPIV scheme, and a control set with no discrete window offset. The error at the wall was calculated for each data set. The dynamically adaptive scheme was found to estimate the velocity near the wall with less error than the no discrete window offset and traditional multigrid algorithms. The shear rate was found to be the main factor in the error in the velocity measurement. In wall shear velocity measurement, the mean (bias) error was an order of magnitude greater than the RMS (random) error. A least squares scheme was used to correct for this bias error with favorable results. The major contribution of this effort stems from providing a novel elliptical particle sizing scheme for use in DPIV, and quantifies the error associated with wall shear measurements using several DPIV algorithms. A test bed and comprehensive user's manual for Flow-IQ v2.2 was also developed in this work.

ACKNOWLEDGMENTS

The author is truly at a loss when it comes to thanks in relation to this work. The reason for this loss is the difficulty of imagining anyone who would want to be associated with a pile of paper that will never make any real or imaginary difference in the world as we know it. However, the one saving grace of the acknowledgements section is that of all the theses I have picked up, the acknowledgements are the only section I have bothered to read. So, therefore, for people like me reading this now, I must submit:

My deepest thanks to my parents for raising me with a healthy disrespect for all those in authority. I also owe them the need for people to earn their respect from me, rather than simply respecting them for their shiny titles, medals, and pieces of paper. Thank you again, mom and dad, for teaching me to be my own person, and to hell with anyone who would have me any other way.

Thank you to my precious wife, Catherine, whose example of unending kindness inspires me every day to be more understanding and accepting of the world around me. You truly are my anchor.

Thank you to my brother, for his inspiring zest for life, and the affirmation that family and friends must always take a front burner on the stove of life.

Thank you my friends, both at home and at school, for making this appalling waste of time, if anything, more enjoyable and memorable. To Yaz, Ali, Jose, and Jagibbs for many hours of support, venting time, and comradery. To Schwartz, for keeping the dream alive.

And finally, to anyone who is reading this thesis now, for putting it down before continuing on and wasting any more of your precious time on this earth.

Dream out loud.

Everything you know is wrong.

-interference from zoo tv

TABLE OF CONTENTS

LIST OF FIGURES

CHAPTER 1

1 BACKGROUND AND INTRODUCTION

1.1 Motivation

The purpose of this work is to expand the usability and accuracy of Digital Particle Image Velocimetry (DPIV) in several significant applications. These applications include whole-field particle diameter and mass flux calculations in sprays, the measurement of wall shear, and the performance of novel sizing techniques on DPIV velocity measurement accuracy. The first focus of this work is the analysis of errors associated with particle diameter and velocity measurements using DPIV in conjunction with novel particle sizing techniques. PIV allows a full two-dimensional analysis of particle diameter as compared to the traditional Phase Doppler Anemometry (PDA) measurements. This paper explores the application and performance of novel particle sizing techniques to the measurement of particle diameter and mass flux in sprays. The second focus of this paper is the performance of traditional and novel PIV algorithms in the measurement of wall shear. Wall shear, especially in boundary layer analyses, contributes significant error to velocity measurements using DPIV. This work explores the errors involved in the measurement of shear rate with DPIV and provides some novel methods for correcting these errors. The third portion of this work explores the application of novel sizing techniques to displacement estimation algorithms used in DPIV, and the errors associated with each method.

1.2 Particle Image Velocimetry

1.2.1 Method

Particle Image Velocimetry (PIV) is the process of analyzing consecutive digital images of data using cross correlation in regions of interest to estimate a displacement in the image. This displacement is then converted to a velocity using the frame rate of the camera, which is a known experimental parameter. A great deal of study has been performed on PIV and methods to improve the accuracy of the method. Digital Particle Image Velocimetry (DPIV) has emerged as a

standard in global flow measurements. In this technique, a fluid is seeded with neutrally buoyant, reflective microparticles and interrogated with a sheet of light expanded from a high-power laser (Willert and Gharib, 1991)). Reflected light from the particles is recorded using a digital CMOS camera with high frame rate (generally 30 Hz). Time-resolved systems (TRDPIV) such as the one developed and employed by our group use CMOS cameras with kHz sampling rates (Abiven and Vlachos, 2002). Images of the seeded flow are captured successively within a very short time interval, so that the particles in a single frame appear in the previous and subsequent frames as well. Velocity is obtained by measuring the displacement between particles in successive frames through cross-correlation (Westerweel, 1997). The two accepted ways of resolving displacement are DPIV and DPTV.

DPIV applications typically use digital imaging technology, since it is possible to acquire and store a large amount of data on a computer. Digital images are characterized by their intensity pixel values corresponding to the ones given by the camera sensors. One pixel thus defines the smallest element of a digital image. In DPIV, images are usually coded in an 8-bit grayscale, with each pixel taking a value between 0 and 255. An intensity value of 0 represents a black pixel, and an intensity value of 255 represents a white pixel (Abiven and Vlachos, 2002).

In DPIV, the target image pair is divided into subdivisions called interrogation windows. Each subdivision is processed independently to calculate a local velocity vector. The subdivisions are determined by the grid spacing and interrogation window size. Grid spacing is the space between measurements in the image. For example, a grid spacing of 4 pixels means that the final output will have a velocity every 4 pixels in the image, or a 64 X 64 grid of velocity measurements for an image size of 256 pixels. Typically, interrogation window sizes range from 8 to 128 pixels, depending on the size of the digital image and the seed particle size and seeding density. Figure 1.1 below illustrates an image broken down into four interrogation windows with no overlap on the left. This case represents no overlap between the velocity measurements. On the right, the 50% overlap case is shown, along with the resulting measurement grid (Abiven and Vlachos, 2002).

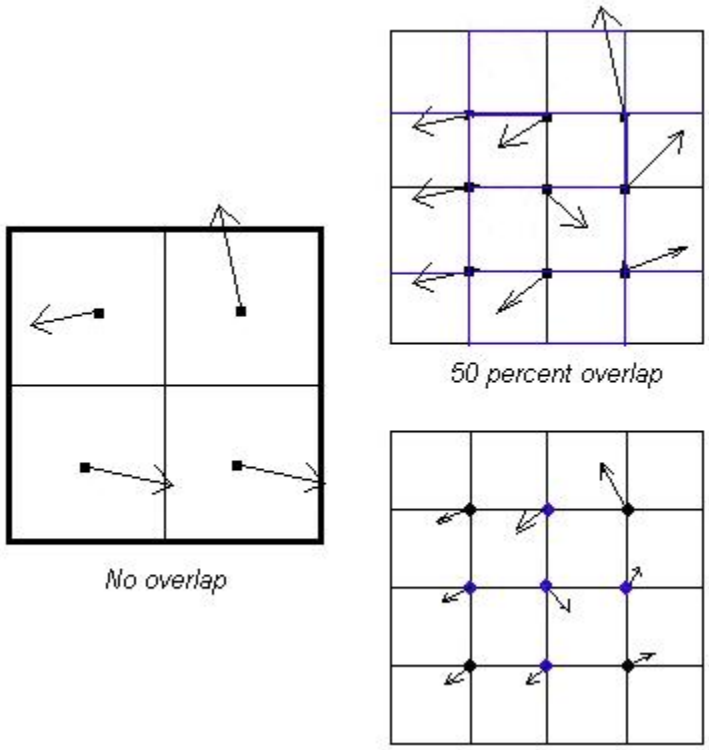

Figure 1.1: Illustration of interrogation windows and overlap

In order to get a displacement out of each interrogation window, a process called cross-correlation is performed. Typically, fast-Fourier transforms (FFT's) are used to calculate the cross-correlation between two corresponding interrogation windows from successive images. However, direct correlation and normalized methods have also been used in the past. Figure 1.2 illustrates the DPIV process. In essence, the cross-correlation shifts the second window across the first, and sums the matching values. At the point where the images match best, the correlation is at its peak value. This peak is located and provides the best estimate for the displacement of the particles in the window (Abiven and Vlachos, 2002).

There are several sources of error in DPIV that prevent the deterministic evaluation of the flow field. Particles are moving in and out of a frame, and the particles within the same window do not necessarily have diverse velocities. Also, particles might appear differently from one frame to the other in terms of light intensity or shape as they move within the light sheet. The combination of

all these phenomena coupled with noise from the recording media constitute a random process that introduces significant error levels to the measurement (Abiven and Vlachos, 2002).

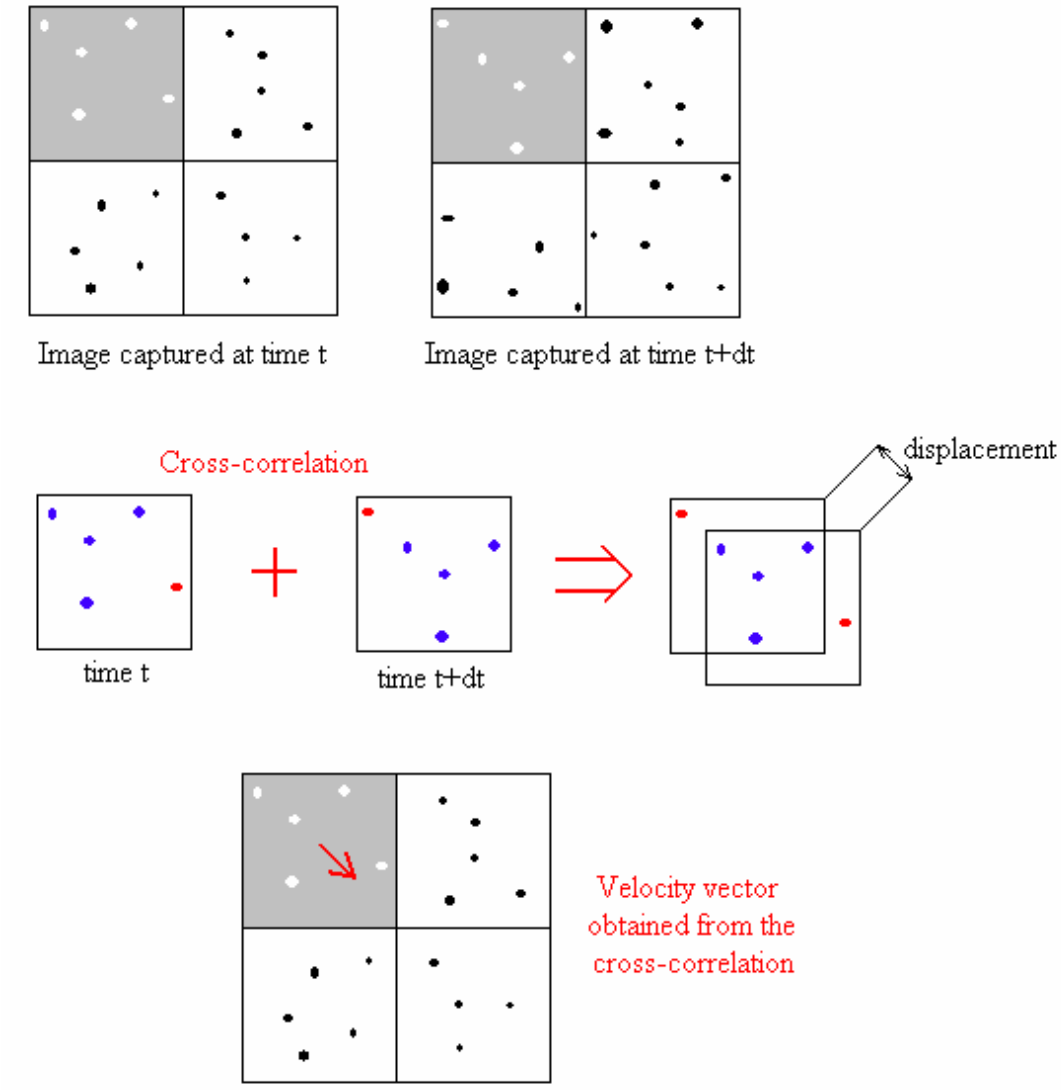

Figure 1.2: Cross-correlation procedure

Both DPIV and DPTV use digital images as an input. A typical experimental setup for DPIV is shown below in Figure 1.3.

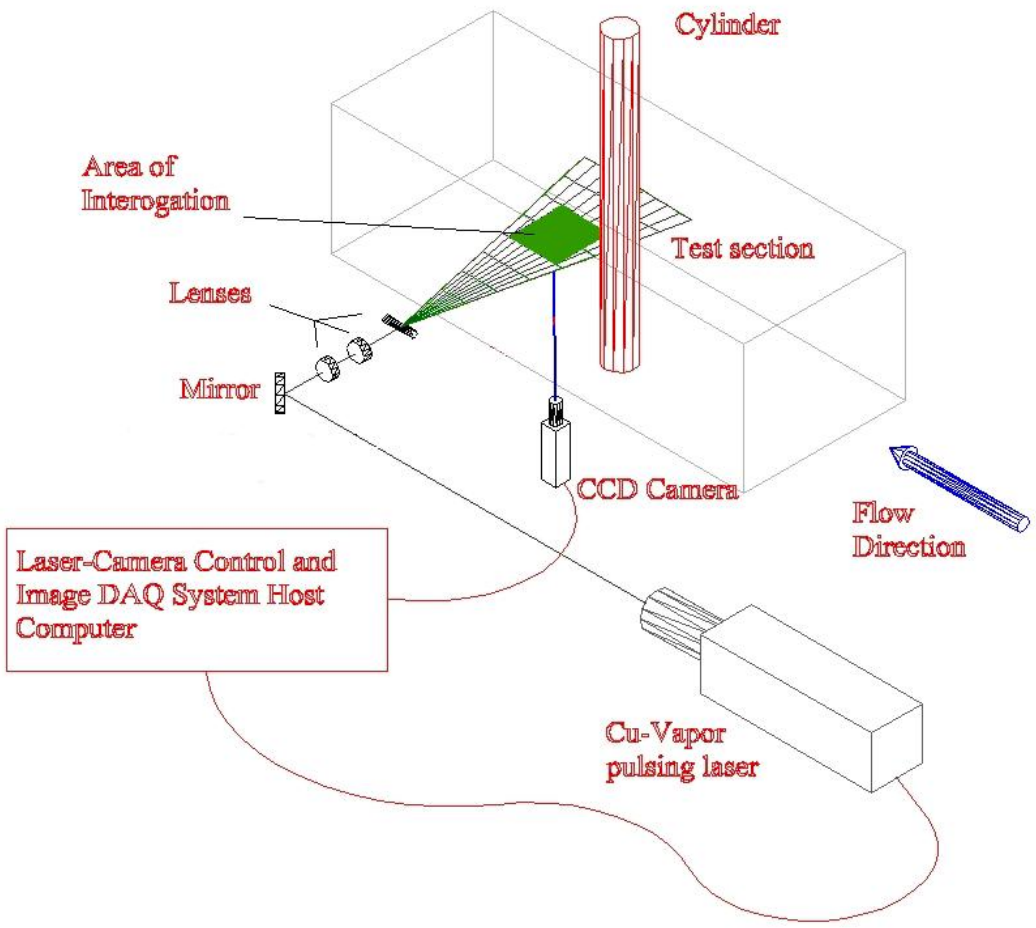

Figure 1.3: Generic experimental setup

In Figure 1.3 above, the experimental setup for flow around a cylinder is shown. The test section can be anything from an airfoil to a biological system. The area of interrogation is fixed to observe the desired region of fluid behavior in a given experiment.

The origin of DPIV hails back to traditional qualitative particle-flow visualizations. The early work of Meynard (1983) established the foundations of its present form. Over the past two decades, several publications have appeared on the application and improvement of the PIV method (Hasselinc, 1988; Adrian, 1991, 1996; Grant, 1994, 1997). Willert and Gharib (1991), Westerweel (1993a,b), and Huang and Gharib (1997) established the digital implementation of PIV, which replaced traditional photographic methods. The DPIV technique is illustrated below in Figure 1.4 (Abiven and Vlachos, 2002).

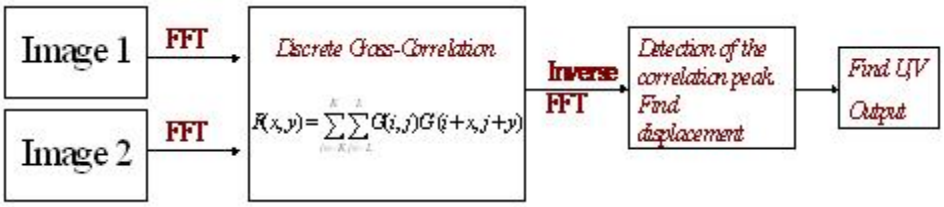

Figure 1.4: Block Diagram for the estimation of velocity vectors

The standard implementation of the method uses a single-exposure, double-frame, digital cross-correlation approach. CCD cameras are commercially available that can sample at frame rates of 1000 fps or higher. The velocity field calculated in DPIV can be treated as a linear transfer function that corresponds to the displacement between two consecutive images. This transfer function can be interpreted in a statistical manner by incorporating second-order statistical moments of the image patterns (Westerweel, 1993a, 1997). In this manner, a statistical cross-correlation between the particle patterns of two successive images is performed in order to calculate the velocity field. A typical cross-correlation implementation of the velocity evaluation algorithm will produce a velocity grid with a vector every 8 to 16 pixels with an uncertainty of the velocity on the order of 0.1 pixels.

1.2.2 Image Processing and Maximum Resolvable Displacement

DPIV algorithms can benefit greatly through the use of image pre-processing tasks to remove boundaries and reduce the effects of noise in the data. Since the images used in DPIV are purely digital, image pre-processing tools were developed to allow direct phase separation within the flow. Khalitov and Longmire (1999) presented an image-based approach for resolving two-phase flows between a flow tracer and a solid phase. In this work, previously implemented methods by Abiven and Vlachos (2002) were used, including dynamic thresholding, Gaussian smoothing, Laplacian edge detection, filtering, erosion, and many more. These techniques are included in Chapter 5, Flow-IQ documentation.

In order to satisfy the Nyquist frequency criterion, the measured displacement must be smaller than one-half the length of the interrogation window in order to prevent aliasing effects.. However, previous work (Keane and Adrian, 1990) illustrated that the statistical cross correlation

velocity evaluation has the maximum confidence levels when the displacement is less than one quarter of the interrogation window size. In this work, one quarter of the interrogation window size is referred to as the maximum resolvable displacement.

1.2.3 Traditional Multigrid Technique

The tradidtional iterative multigrid DPIV employs a first cross-correlation pass in order to generate an initial predictor of the velocity-field. On the subsequent passes, the size of the interrogation window is dynamically allocated, based on the results from the previous step (Scarano & Rieuthmuller, 1999) as shown by figure 1.5.

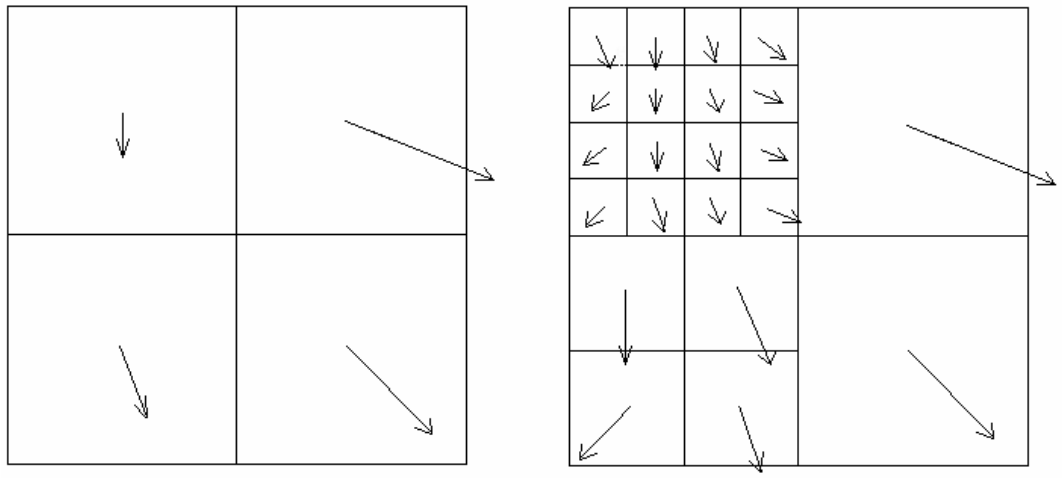

Figure 1.5: Traditional Multigrid Method

Each initial window is broken down into several windows. The size of the consecutive windows depends on the velocity obtained from the first pass.

1.2.4 Discrete Window Offset

The window offset feature introduced by Westerweel (1997) represented a real breakthrough in DPIV. This feature significantly improves the accuracy of the DPIV method. Using the first estimate obtained from the initial DPIV pass, a second pass is applied by shifting the interrogation window in the second image by the rounded displacement found during the first pass. The first

pass is subject to particles going in and out of the interrogation area, while the second pass dramatically reduces this effect, as illustrated by the Figure 1.6. This process is known as First Order Discrete Window Offset DPIV. The second cross-correlation pass after shifting the second image interrogation window by the previously estimated displacement provides a more accurate velocity evaluation (Abiven and Vlachos, 2002).

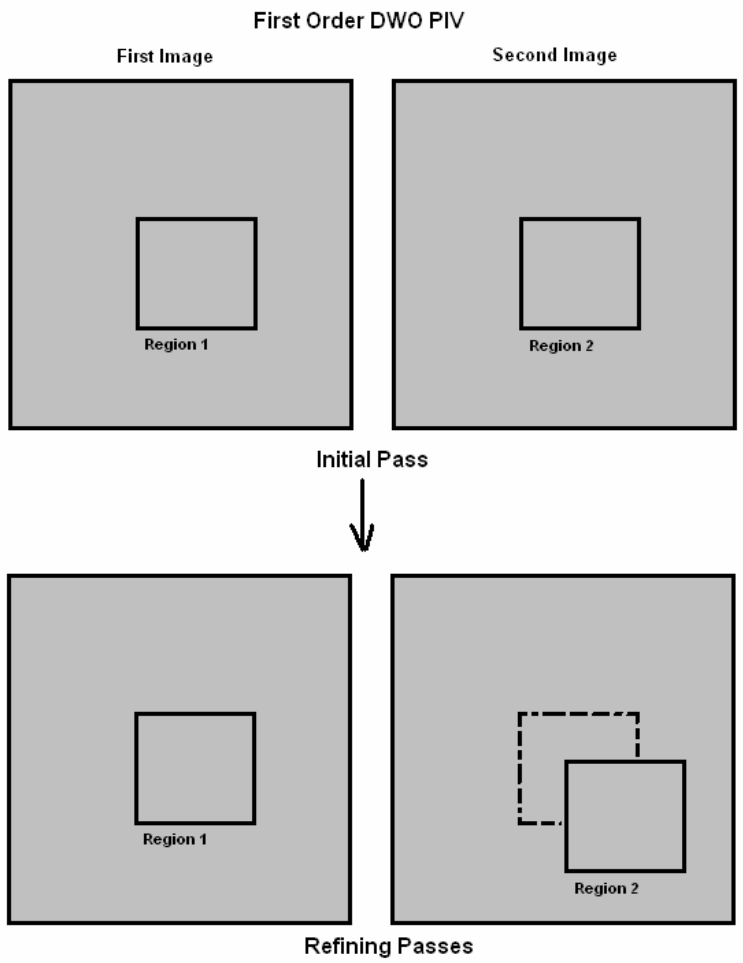

Figure 1.6: First Order Discrete Window Offset

The second cross-correlation is preformed between two windows that contain the same particles. The signal to noise is drastically increased during this operation. The iterative nature of this process significantly reduces the effects of spatial averaging, which improves the resolution and accuracy of system (Abiven and Vlachos, 2002).

Wereley and Meinhart (2001) developed a second-order accurate DPIV scheme that further reduced the errors associated with velocity measurement, particularly in vertical flowfields. This method, known as Second Order Discrete Window Offset PIV, is illustrated below in Figure 1.7.

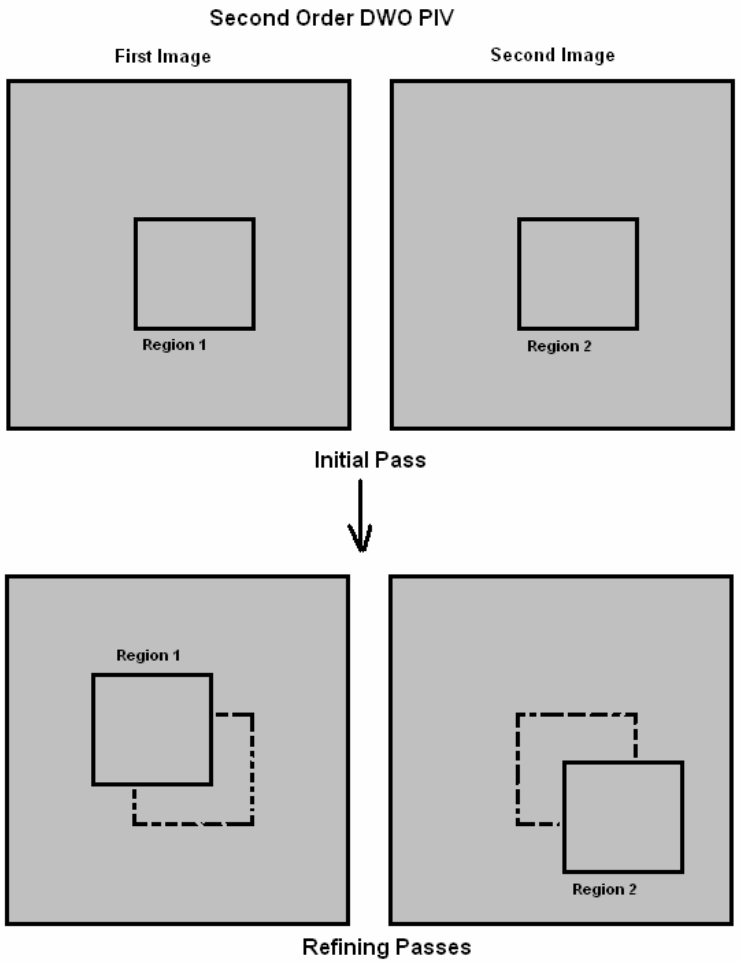

Figure 1.7: Second Order Discrete Window Offset PIV

In Second Order Discrete Window Offset PIV, the interrogation windows are shifted in both images by a value half of the initial estimate. If the initial estimate is an odd number, then one window is shifted by the floor of half of the estimate, and the other is shifted by the ceiling of the initial estimate. This process reduces the error of the method in relation to vortical flows.

1.3 Particle Tracking Velocimetry

Digital Particle Tracking Velocimetry is defined as the tracking of particles as they progress in DPIV data. The DPTV method used in this work utilizes the output from particle sizing and PIV algorithms to track particles. The particles in two consecutive frames are detected, and the local velocity from PIV is used to search for a particle within a given radius of the expected velocity. If a particle is found, this particle is used to estimate the displacement between this particle and the particle from the original frame . Other developed methods use size, shape, brightness, or closeness criteria for particle differentiation and identification. The difference in particle position serves as the displacement estimation in DPTV. The major difficulty in DPTV is the ability to distinguish unique particles. However, DPTV eliminates the averaging effect seen in DPIV results. The Hybrid DPTV method (Abiven and Vlachos, 2002) is used in this work.

DPTV is classified in the same general category as DPIV, since they are similar methods based on similar fundamentals (Dracos and Gruen, 1998; Adrian et. al., 1995; Prasad and Adrian, 1993; Adrian, 1996). In DPTV, the velocity is determined from the displacement of particles within a fixed time interval. The major experimental difference between the methods is that the DPTV algorithms need low seeding density, whereas PIV algorithms require relatively high seeding density. Seeding density is the number of tracer particles in a given frame or window. DPTV is limited to slower flows than PIV (Abiven and Vlachos, 2002).

Guezennec and Kiritsis (1990) developed the first DPTV algorithms based on DPIV, which uses the DPIV output as a priori knowledge for the search of particles. The estimation of the displacement is uncomplicated. A simple search radius is input by the user in order to define the search area around the predicted velocity from DPIV results. Most particles will be detected by a correctly-designed DPTV algorithm, given optimal experimental conditions (Abiven and Vlachos, 2002).

1.4 Error Analysis

The major error analysis technique used in this work is the Monte Carlo Simulation. In a Monte Carlo Simulation for PIV, artificial data with a known displacement field are generated. Then, the PIV method in question is performed on the artificial data. Errors are calculated by comparing the

PIV output with the known input. The major error sources are bias error and random error. Bias error, or mean error, represents a true bias in the measurement and indicates a consistent error in the measurement. Random error, or RMS error, quantifies the expected error in the measurement that does not fit a specific pattern. Total error is the complete error of the measurement, and consists of the random and bias errors summed in quadrature. The equations for total, bias, and random error are given below in equations 1.4.1 to 1.4.3. The reliability of this error analysis increases with the number of measurements performed in the simulation.

$$E_{total}(\mathrm{j}) = \left[\frac{1}{N} \sum_{n=1}^{N} \left| D_r(\mathrm{i},\ \mathrm{j}) - D_m(\mathrm{i},\ \mathrm{j}) \right|^2 \right]^{1/2} \qquad \text{(Eq. 1.4.1)}$$

$$E_{mb}(\mathrm{j}) = \left| D_r(\mathrm{i},\ \mathrm{j}) - \frac{1}{N} \sum_{n=1}^{N} D_m(\mathrm{i},\ \mathrm{j}) \right| \qquad \text{(Eq. 1.4.2)}$$

$$E_{rms}(\mathrm{j}) = \left[\frac{1}{N} \sum_{n=1}^{N} \left(D_m(\mathrm{i},\ \mathrm{j}) - \frac{1}{\mathrm{N}} \sum_{n=1}^{\mathrm{N}} D_m(\mathrm{i},\ \mathrm{j}) \right)^2 \right]^{1/2} \qquad \text{(Eq. 1.4.3)}$$

In equations 1.4.1 through 1.4.3, D_m is the measured displacement, D_r is the real (known) displacement, N is the number of measurements performed in the simulation, E_{total} is the total error of the measurement, E_{mb} is the bias error of the measurement, and E_{rms} is the random error of the measurement.

Chapter 2

2 PIV SIZING OF SPRAY DATA, ANALYSIS AND COMPARISON TO PDA

The purpose of this chapter was to explore the performance of the conventional sizing techniques developed by Brady et al. (2002) in a real-world spray atomization experiment. DPIV analysis was performed on a 60-degree conical, high-pressure spray that generated a poly-dispersed droplet distribution. Measurements were preformed for five planes parallel to the spray axis, and separated by 4mm. A CMOS camera recorded the DPIV images at sampling rate of 10 KHz. Advanced image processing techniques were employed to identify the droplets and calculate their diameter using the novel Flow-IQ software. Subsequently, the size distribution of each droplet was quantified using geometric optics theory to convert the droplet image information to the true droplet size. The droplet sizes from our direct imaging DPIV system were validated using a Phase Doppler Particle Analyzer (PDPA). The calculated sizes from the direct imaging methodology were found to agree with the measured PDPA results for droplets images larger than 3 to 4 pixels. Resolution limitations introduced inaccuracy for smaller droplets. This preliminary effort illustrates the potential of performing global time resolved size measurements using a simple DPIV configuration based on CMOS imaging technology.

2.1 Introduction

Simultaneous time resolved velocity and size measurements are limited to single point methodologies using Phase-Doppler Particle Analyzer (PDPA). Although these methods can measure with high accuracy the particle velocity and size they are limited by the requirement of spherical particles (Kim et al. 1999). In the case of spay atomization this requirement is not satisfied since the droplets deform, forming ellipsoids. In addition, single point methodologies do not reveal the global temporal variation of the flow. The above limitations generate the need for alternative, global measurement methodologies based on visualization techniques.

The dynamics of spray-droplet break-up, and the accurate measurement of droplet sizes and velocities in high-pressure sprays is an increasingly important problem in fluid mechanics. During

the past decade there has been a wide spread use of DPIV techniques employed on the analysis of single phase or multi-phase flow systems. DPIV measurements provide global instantaneous velocity distributions revealing the internal structure of the flow. However, despite the numerous advances of the method in polydispersed multi-phase flows, very few attempts have been made to deliver simultaneous velocity, size, and shape quantification of the dispersed phase (Abiven et al., 2002).

Simultaneous time resolved velocity and size measurements are limited to single point methodologies using Phase-Doppler Particle Analyzer (PDPA). Although these methods can measure with high accuracy the particle velocity and size they are limited by the requirement of spherical particles (Kim et al. 1999). In the case of spay atomization this requirement is not satisfied since the droplets deform, forming ellipsoids. In addition, single point methodologies do not reveal the global temporal variation of the flow. The above limitations generate the need for alternative, global measurement methodologies based on visualization techniques.

Khalitov and Longmire (2002) presented an image-based approach for resolving two-phase flows between a flow tracer and a solid phase. In their approach they were able to successfully discriminate the coexisting phases in the flow by employing image-processing principles. However, they did not carry out any size quantification. Recent efforts combine size measurements with DPIV using either fluorescence-Mie scattering ratio (Boedec and Simoens 2001) or interferometry principles (Damaschke et el. 2002) to carry out the sizing tasks. Boedec and Simoens (2001) by employing a fluorescence-Mie scattering ratio methodology were able to accurately measure the velocity and size distribution in a high-pressure spray. However, such implementations require complicated experimental setups, multiple cameras, optical filters and calibration for the fluorescence intensity quantification. Damaschke et el. (2002) use Global Phase Doppler (GPD) which is an interferometry based methodology where the particle/droplet diameter is proportional to the number of fringes formed by out of focus particle images. Despite the high accuracy and the global character of the method, the optical resolution of the system can be a limiting parameter soon generating overlapping particle images because of the out of focus effects while it is limited to small interrogation areas.

Pereira et al. (2000) introduced an out-of-focus method for size measurements based on a defocusing DPIV principle applied on liquid bubble flows. Using the out of focus images of the recorded bubbles enhances the capabilities of conventional DPIV systems by allowing bubble/droplet size information in two-phase flows. An off-axis aperture collecting light from a point source (bubble) generates an out-of-focus image. By collecting the information of the light intensity, the particle pattern, and the blurriness for each image pair, the method resolves both the velocity and the size of the bubble. In addition, by analyzing the intensity of the defocused particle, Airy disks can provide information for the out-of-plane velocity component. This method requires a minimum of three cameras in order to overcome measurements ambiguities.

This discussion although not comprehensive, represents some of the most recent and significant contributions in simultaneous global velocity and size quantification methods. However, all of the above methods do not resolve the time depended characteristics of the flow since they are limited to sampling rates in the order of 15-30Hz. Especially in the case of spray atomization where the natural unsteadiness of the flow is the dominant parameter that governs the break-up dynamics sampling rates in the order of KHz are necessary.

2.1.1 Conventional Particle Sizing Techniques

The conventional particle sizing techniques used in this work were developed by Brady et al. (2002). These techniques include the three point Gaussian, four point Gaussian, continuous four point, and continuous least squares particle sizing algorithms. Before the methods are introduced, a discussion of the assumptions made in the traditional algorithms is given below.

2.1.1.1 Axis-symmetric Gaussian Shape

The conventional particle sizing techniques follow the assumption that an axis-symmetric Gaussian shape can be used to approximate the intensity distribution of the light scattered from small particles. Adrian and Yao (1985) showed that the Airy distribution of the point spread function from a diffraction limited lens can be very closely characterized as a Gaussian function. If the point spread function and the geometric image are Gaussian shaped, then the intensity distribution can also be closely approximated by a Gaussian.

In a PIV data set, the recorded particle image, d_t can be expressed in terms of the particle diameter, d, the diffraction limited spot diameter, d_s, and the resolution of the recording medium, d_r. This relationship is shown below in Equations 2.1 to 2.3.

$$d_t^{\,2} = d_e^{\,2} + d_r^{\,2} \qquad \text{(Eq. 2.1)}$$

$$d_s = 2.44(M+1)f\#\lambda \qquad \text{(Eq. 2.2)}$$

$$d_e = (M^2 d^2 + d_s^{\,2})^{1/2} \qquad \text{(Eq. 2.3)}$$

In these equations, M is the magnification, f# is the numerical aperture of the lens, and λ is the wavelength of a coherent monochromatic light source. Equation 1.4.3 includes the combined effects of the optical system's magnification and diffraction on the particle image when optical aberrations are not present.

Gaussian fitting schemes such as the three-point estimator and local-least squares estimator reduce the error associated with particle center estimation of a geometric image when compared to more traditional methods such as center of mass (Udrea et al. 1996; Marxen et al. 2000, Willert and Gharib 1991). In addition, these techniques also decrease the peak locking effect in the bias-error when compared to centroid analysis (Willert and Gharib, 1991).

The use of the conventional Gaussian sizing schemes for finding particle positions has been documented further in Brady et al. (2002). Other studies, such as Marxen et al. (2000), have also investigated the use of the three point fit as a sizing algorithm. The conventional Gaussian sizing techniques developed by Brady et al. (2002) are given in the following sections.

2.1.1.2 Three Point Gaussian Fit

The traditional three-point Gaussian estimator is a simple one-dimensional approximation of the geometric particle image.

$$a_i = I_O e^{-\frac{(x_i - x_c)^2}{2\sigma^2}} \qquad \text{(Eq. 2.4)}$$

The three independent variables Io, σ, and x_c represent the maximum intensity, the Gaussian distribution standard deviation and the center position, respectively. If the three points chosen to solve these equations are the maximum intensity pixel, and the two neighboring pixels along the x-axis, then the standard three-point Gaussian estimator can be derived (Willert and Gharib 1991).

$$x_c = x_o + \frac{\ln a_{o-1} - \ln a_{o+1}}{2(\ln a_{o-1} + \ln a_{o+1} - 2\ln a_o)} \qquad \text{(Eq. 2.5)}$$

The equation for finding the y center position is identical to equation 2.5 above. The diameter measurement is directly related to the variance. The variance is given below in equation 2.6.

$$\sigma^2 = \frac{\ln a_{o+1} - \ln a_o}{(x_o - x_c)^2 - (x_{o+1} - x_c)^2} \qquad \text{(Eq 2.6)}$$

The three point estimator is computationally fast, and very easy to implement (Brady et al., 2002). The major limitation of the diameter measurements made in Brady et al. are the use of a single dimension as the diameter measurement and the assumption that the particles are, in fact, circular in profile.

2.1.1.3 Four Point Gaussian Estimator

The four point Gaussian estimator was developed in order to overcome the limitations of the three-point Gaussian fit and allow determining the center and diameter of a particle when it contains saturated pixels. In this scheme, saturated particles do not contribute to the measurement of diameter. The removal of saturated pixels from the calculation allows for a more accurate estimation of the Gaussian shape of the particle, and reduces the error of the method (Brady et al., 2002).

In order to derive the four point Gaussian estimator, Brady et al. (2002) considered the two-dimensional intensity distribution given below in equation 2.7.

$$a_i = I_o e^{-\frac{(x_i - x_c)^2 + (y_i - y_c)^2}{2\sigma^2}} \qquad \text{(Eq. 2.7)}$$

Four independent intensities were solved in order to arrive at the following set of equations. These intensities were used to derive equation 1.4.8 below, which is the equation used for variance in the four point Gaussian scheme.

$$\alpha_1 = x_4^2(y_2 - y_3) + (x_2^2 + (y_2 - y_3)(y_2 - y_4))(y_3 - y_4) + x_3^2(y_4 - y_2)$$
$$\alpha_2 = x_4^2(y_3 - y_1) + x_3^2(y_1 - y_4) - (x_1^2 + (y_1 - y_3)(y_1 - y_4))(y_3 - y_4)$$
$$\alpha_3 = x_4^2(y_2 - y_1) + x_2^2(y_1 - y_4) - (x_1^2 + (y_1 - y_2)(y_1 - y_4))(y_2 - y_4)$$
$$\alpha_4 = x_3^2(y_2 - y_1) + x_2^2(y_1 - y_3) - (x_1^2 + (y_1 - y_2)(y_1 - y_3))(y_2 - y_3)$$
$$\sigma^2 = \frac{(x_4 - x_c)^2 + (y_4 - y_c)^2 - (x_3 - x_c)^2 - (y_3 - y_c)^2}{2(\ln(a_3) - \ln(a_4))} \quad \text{(Eq. 2.8)}$$

If the points selected are the same as the three point estimator, then equation 2.8 reduces to equation 2.6. The points selected for the four-point Gaussian estimation are by no means arbitrary and will not always yield a unique solution. Two conditions must be met for the method to produce a solution. Firstly, a_3 cannot be equal to a_4, or the denominator in equation 2.8 will go to zero. The second criterion is that the four selected points cannot all lie in a circle of any arbitrary center or radius (Brady et al., 2002).

2.1.1.4 Continuous Four Point Fit

The three and four point fits will contain an error even without the presence of noise sources due to the digital medium pixel discretization. In order to address this error, Brady et al. (2002) developed a continuous four point scheme. The continuous four point fit eliminates the systematic error introduced by pixel descretization. The continuous four point scheme corrects for pixel discretization through equating an integrated Gaussian profile over each pixel with the discrete gray value (Brady et al., 2002).

$$a_i = \iint I_o e^{-\frac{(x_i - x_c)^2 + (y_i - y_c)^2}{2\sigma^2}} dydx \quad \text{(Eq. 2.9)}$$

Equation 2.9 cannot be solved in closed-form, and the expanded equations are shown below in Equation 2.10 where Erf is the error function. In this equation, x_i and y_i represent the position of the lower corner of each pixel (Brady et al., 2002).

$$\mathbf{a_i} = \frac{\pi \mathbf{I_o} \sigma^2}{2} (\mathbf{Erf}[\frac{(\mathbf{x_i} - \mathbf{x_c})}{\sqrt{2}\sigma}] - \mathbf{Erf}[\frac{(\mathbf{x_i} + 1 - \mathbf{x_c})}{\sqrt{2}\sigma}])(\mathbf{Erf}[\frac{(\mathbf{y_i} - \mathbf{y_c})}{\sqrt{2}\sigma}] - \mathbf{Erf}[\frac{(\mathbf{y_i} + 1 - \mathbf{y_c})}{\sqrt{2}\sigma}]) \quad \text{(Eq. 2.10)}$$

Brady et al. (2002) used a form of the Powell dogleg optimization routine to solve these nonlinear equations. The same point selection criteria in the four point Gaussian fit apply to the continuous four point fit.

2.1.1.5 Continuous Least Squares Gaussian Fit

The continuous least squares scheme, developed by Brady et al. (2002) is an integrated local least square fit. Similarly to the continuous four point fit, introduced above, this scheme improves the error by taking into account the discretization error of the individual pixels. The equation for the continuous least squares fit is given below in equation 2.11

$$\chi^2 = \sum (a_i - \iint I_o e^{-\frac{(x_i - x_c)^2 + (y_i - y_c)^2}{2\sigma^2}} dydx)^2 \qquad \text{(Eq. 2.11)}$$

In equation 2.11, χ^2 was minimized using a Gauss-Newton algorithm. Point selection was determined by the 3X3 area surrounding the peak intensity pixel (Brady et al, 2002).

2.2 Experimental Methods and Materials

This work relied heavily on the experimental and computational resources available in the ESM Fluid Mechanics Laboratory at Virginia Tech. A summary of the major resources used in this work is found below. The objective of this pilot experiment was to demonstrate the ability of the system to characterize the time depended characteristics of a poly-dispersed distribution of droplets by resolving the individual velocities and their apparent size.

2.2.1 Spray Generation

The spray employed in this study was generated using a 60deg cone angle nozzle and a pressure of approximately 10Psi was applied. A low-speed, annular co-flow was introduced but was not seeded. The water pressure going through the spray nozzle was delivered using a high-precision computer controlled gear pump and was varied as a sinusoid with a desired offset at 10Hz frequency.

2.2.2 DPIV System

The spray data used in this work was acquired using the DPIV system in the ESM Fluid Mechanics Laboratory at Virginia Tech. A diagram of the system is shown below in Figure 2.1. The system includes a 60-Watt copper-vapor laser for illumination and a Phantom V4 CMOS

digital camera for data acquisition. This system allows data acquisition up to a frame rate of 1kHz. The camera has a resolution of 512X512 pixels. The spray data used in this work was taken at a resolution of 256X256 pixels.

A 10KHz pulsing Copper Vapor Laser was used to deliver a sheet of light with illumination energy of 5 mJ. The laser sheet was passed through a cylindrical lens and focused into a vertical plane parallel to the axis of the spray. A Phantom-V CMOS camera placed normal of the laser sheet captured the water droplets with pixel resolution of 256x256 and a frame rate of 10 KHz and total sampling time of 1 sec. A second Phantom–IV CMOS camera with resolution of 128x128 and sampling rate of 10KHz was employed in order to record off-axis-images in a stereo DPIV configuration. A calibration target was used to assure that the interrogation areas of the two cameras overlap and subsequently used for the reconstruction of the images. Due to space limitations in this paper and the preliminary nature of this study, we will not elaborate on the three-dimensional measurements.

The laser and the camera were synchronized in order to operate in a single pulse per frame mode. The camera is equipped with an internal shutter, which was set at 10microsecs in order to reduce the ambient background light thus increasing the signal to noise ratio of the images. The laser pulse and the shutter trigger to the camera were synchronized and controlled with a PC/workstation. A multifunction National Instruments 6025E board was used to control the data acquisition. Two 20MHz digital counters with timing resolution of 50nsecs were used to generate the sequence of pulses necessary to accurately trigger the laser and the camera. Once the laser and the camera received the trigger pulses, a feedback signal was recorded in order to assure the accurate timing of the process. The overall timing uncertainly of the control system accounting also for the laser pulse jitter was estimated in the order of 1nsec which is negligible for the velocity ranges of approximately 10m/s measured during this experiment.

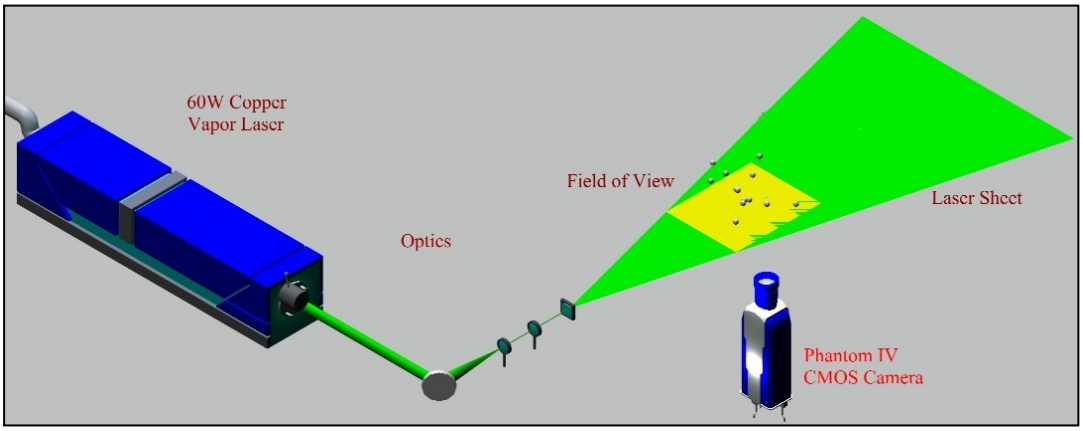

Figure 2.1: ESM Fluid Mechanics Laboratory DPIV system.

2.2.3 DPIV Software

The DPIV software used throughout this work consisted of in-house software. For the spray particle sizing results with tradtitional sizing algorithms, DPIV version 1.0 was used. DPIV version 1.0 is a DPIV software package developed by Aeroprobe, Inc. This software includes DPIV algorithms, sizing algorithms, particle tracking velocimetry, image pre-processing, and post-processing options for DPIV in a single Windows-based platform. The user's manual for DPIV version 1.0, written by the author of this work, can be found in Appendix A.

DOS-based DPIV software was also used in this work in the wall shear studies. This software gives the user the ability to select several processing algorithms not yet available in DPIV v1.0, and allows processing at high speed in a DOS environment. This software is known as "Ultimate," and was developed by Claude Abiven and Dr. Pavlos Vlachos in the ESM Fluid Mechanics Laboratory at Virginia Tech.

2.2.4 PDA System

To confirm the feasibility of this method and quantify the accuracy of our system, a validation experiment comparing our system and a PDA system was performed. A one-dimensional Phase Doppler Particle Analyzer (PDPA) was used to measure the spray droplet size and velocity in the axial direction. It was a commercial system consisting of an integrated optical unit, a signal

processor, and software for system setup, data acquisition and data analysis. The integrated optical unit encompassed a 10-mW He-Ne laser as the laser source (λ = 632.8 nm). Transmition was via a fiber optic probe, 60-mm in diameter, which encompassed necessary optics to transmit the red laser beams with an initial beam separation of 38mm. The focal length of the lens used for the transmitting probe was 400-mm. The PDA receiver was another fiber optical probe, 60-mm in diameter, with a focal length of 160-mm. It was positioned in the forward scatter mode, at a scattering angle of 35 degrees, to allow measurements of droplet size in the reflection mode. Given this arrangement, the fringe spacing was 6.67 μm with probe volume dimensions of approximately 250 μm in all directions. The PDA receiver probe was configured for a maximum particle diameter of 147 μm. A refractive index of n = 1.334 was assumed for the water spray droplets.

Sampling at a point was performed for 60 seconds or 100,000 particle counts. The average data rate in the core of the spray was approximately 1 kHz, this rate decreasing as the probe volume interrogated the edges of the spray. Autocorrelations at various points in the spray (near the core) gave an integral time scale of approximately 2.5 ms. Consequently, the statistical uncertainty of the mean PDA data (velocity and particle size) was estimated at less than 1%.

The signal processor used FFT technology to determine the velocity and phase difference. Three detectors were used to extend the diameter range without compromising resolution. The resolution of the system was 16 bits on the selected bandwidth (typically 3.75 MHz), thus yielding negligible velocity and phase resolution uncertainty.

The location of the PDA probe volume was fixed in space while the spray was traversed relative to it so that measurement data can be obtained over several points along a cross-plane located approximately 15-mm from the nozzle.

A total of 189 measurement points within a plane approximately 15mm above the spray with a total sampling time of 1min were acquired.

Figure 2 below shows (a) the experimental setup employed in this study including the two cameras and the Dantec PDA system, (b) a view of the high-pressure conical spray illuminated by the laser sheet, and (c) a schematic overview of the timing, synchronization and control arrangement.

The experiment involved the acquisition of several planes parallel to the center plane of the spray. A total of five planes placed at -8, -4, 0, 4, and 8 mm with respect to the center plane were acquired reconstructing a volume of the flow. The volumetric data were subsequently used to generate the statistical distributions of the droplet sizes for horizontal planes (normal to the spray axis). These statistics were compared with the corresponding PDA measurements

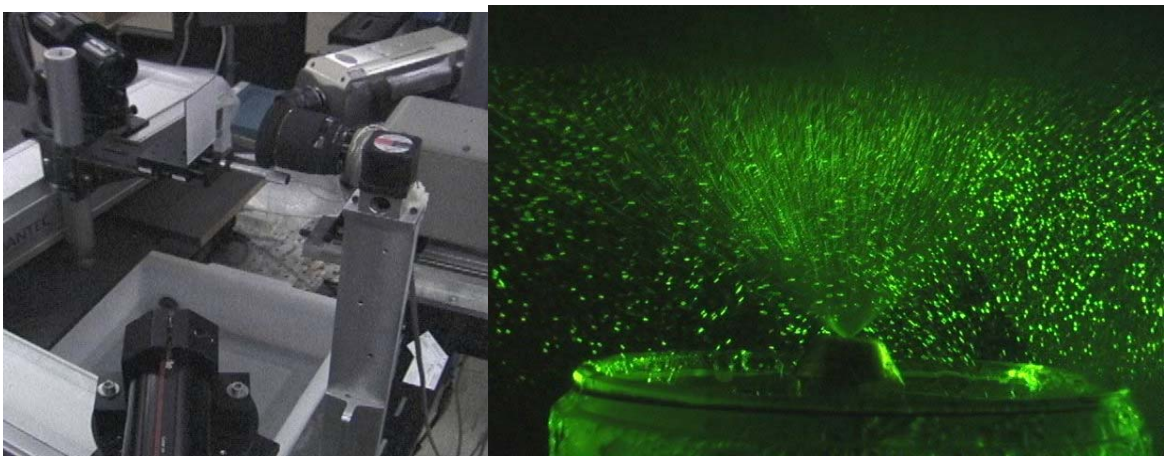

(a) (b)

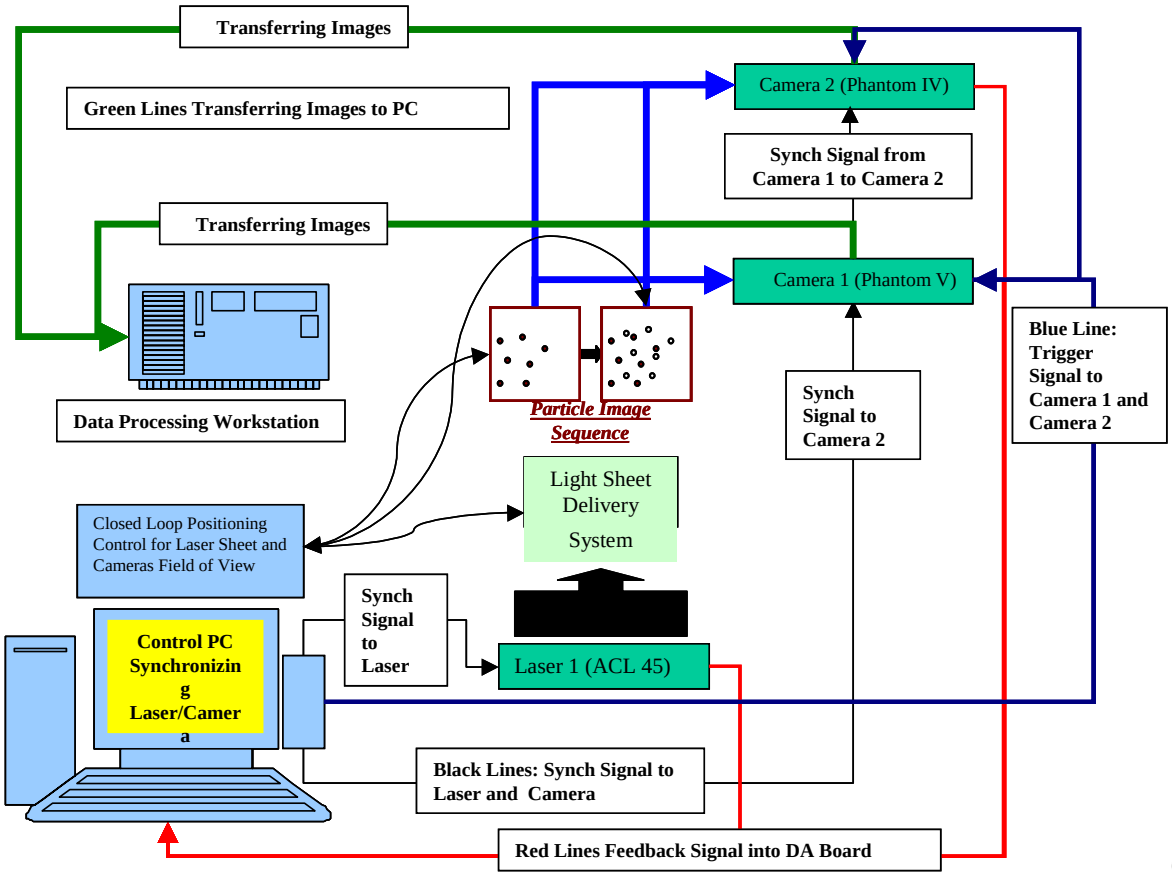

(c)

Figure 2.2: Experimental Setup for the Spray PIV and PDPA experiment

2.2.5 Computational and Computer Resources

Since the majority of this work was performed using simulations and massive amounts of data, the computational and computer resources available were key components of this work. The computational aspects of this work were performed on three personal computers. These resources included a desktop computer with a 2.8GHz Pentium IV processor and 512MB of RAM, a desktop with a 1.8GHz Pentium IV processor and 256MB of RAM, and a laptop with a 2.4GHz Pentium IV processor and 512MB of RAM.

Another resource used heavily in this work were both in-house and purchased programs available in the ESM Fluid Mechanics Laboratory. The in-house programs included DPIV version 1.0, a particle image velocimetry and sizing program developed by Aeroprobe Corporation, which was used to perform all of the spray sizing results presented in this paper. The artificial images used in this work were created using in-house artificial image generation software developed by Claude Abiven in the ESM Fluid Mechanics laboratory. The DPIV analyses used in the wall shear Monte Carlo simulations were performed using Ultimate, a DOS-based particle image velocimetry program developed by Dr. Pavlos Vlachos of the Mechanical Engineering Department at Virginia Tech. Several other programs were used in order to produce the results presented in this work. The researcher relied heavily upon MATLAB 6.5 for data analysis and presentation.

2.3 Spray DPIV/PDA Comparison

In order to provide a comparison between DPIV and PDA data, the particle size histogram and average diameter for each method was calculated and compared. Spray data from a previous experiment was analyzed using our DPIV version 1.0b software. Image preprocessing was used in this experiment. A basic thresholding of 20 (intensity 0-255) and subsequent dynamic thresholding were used on the images in order to generate the data presented in this work. The data contained a DPIV dataset at -8, -4, 0, 4, and 8 mm from the center of the spray. An example picture from the 0mm dataset at the center of the spray is shown below in Figure 2.3.

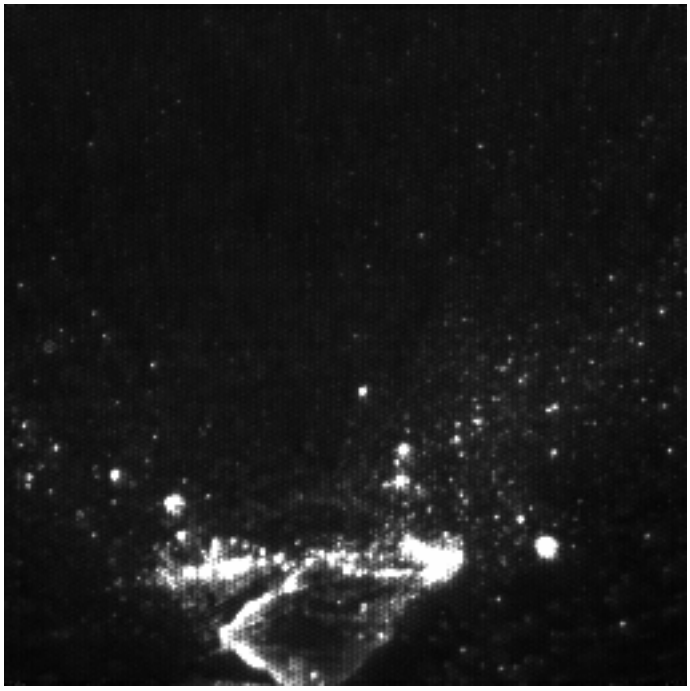

Figure 2.3: Example Digital Particle Image Velocimetry Spray Data, 0mm Plane

Each of these datasets included 16,304 images similar to the one shown in Figure 2.2. Each of these frames was analyzed using each method studied in this work. The methods used in this work were the three-point Gaussian, four-point Gaussian, continuous four-point Gaussian, and continuous least-squares sizing methods. A total of 81,520 images were processed using each method, combining to a total of 326,080 images processed. The experimental magnification in this experiment was approximately 24 microns per pixel. Diffraction terms were included in all of the diameter conversions and analysis. Bin ranges were matched for each method in order to provide completely comparable histograms between measurement techniques.

2.3.1 Histogram Analysis

The output from each method was analyzed in MATLAB to produce histograms for each method. Histograms were created for each plane of data. The total volume and total method histograms were also calculated. In order to account for multiply-counted particles in the histogram, particle tracking was run on the complete set of images, and tracked particles were removed to produce the compensated DPIV histograms. These histograms were compared to PDA data over various diameter ranges in order to quantify the performance of DPIV sizing techniques with respect to

traditional particle sizing techniques. All histograms were normalized with the total particle population in order to produce probability density functions (pdf's) for analysis.

2.3.2 Average diameter Analysis

In order to calculate the average diameter in the DPIV data, a volume was constructed with user-definable resolution. The volume was constructed such that the z component moved across planes of data with the x and y direction in the plane of the DPIV data. The output from each method was scanned and each particle was added to a region of the volume. If the x and y position of a particle was in a particular region, the average diameter was updated assuming the particle to be a perfect sphere.

2.4 Particle Sizing Results

This section presents the results for the traditional sizing algorithms used in this experiment and their histogram comparison to PDA measurements, and the average diameter analysis performed in this work.

2.4.1 Full-Range Results

The full theoretical range of the PIV sizing methods extends to less than one pixel diameter. However, at these low diameters, the error in the PIV measurement increases dramatically. It is, however, important to characterize the behavior of the PIV sizing methodologies on real data at these diameters. The magnification in this experiment was approximately 24 microns per pixel (diffraction terms were included in the calculation of the magnification factor). Therefore, the approximate lower limit of detectable diameter in this experiment is approximately 15 to 20 microns. The PDA system used in this experiment could resolve diameters as low as 0.5 microns. Therefore, in this particular experimental setup, the PIV method could not resolve diameters at the lower range of the PDA data. The full results from the 0mm plane are shown below in Figure 2.4.

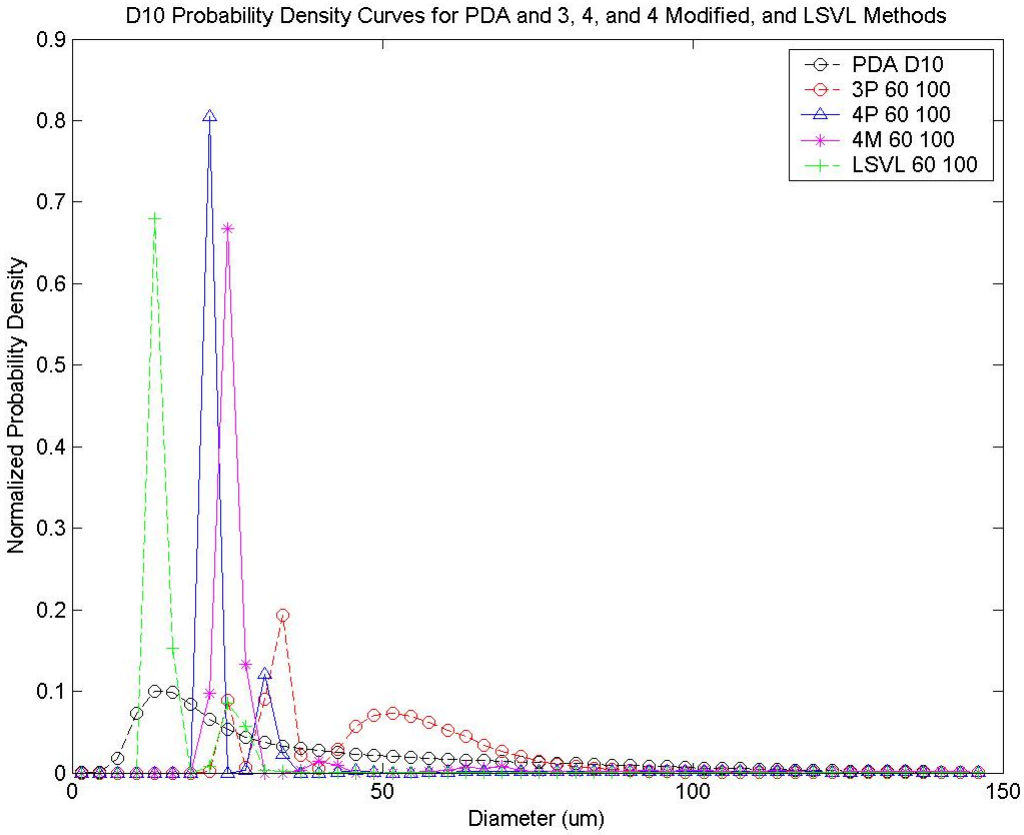

Figure 2.4: Full Results for All Sizing Methods and PDA, 0mm Plane

The results in Figure 2.4 show that there is a significant locking on particles in the 20 to 30 micron range for all of the PIV sizing algorithms. The correlation coefficients for the three point Gaussian, four point Gaussian, continuous four point Gaussian, and the continuous least squares are 0.1465 , 0.2762, 0.2465, and 0.5882, respectively for this plane

2.4.2 Limited-Range Results

The sizing algorithms used in this portion of the experiment were the three point Gaussian, four point Gaussian, four point continuous, and continuous least squares algorithms. Histogram results for each plane were generated, as well as an average histogram results for all of the combined planes. Figure 2.5 below shows the single plane results for each method in the 0mm plane, which is located in the direct center of the spray. The PDA results are also shown below in Figure 2.5.

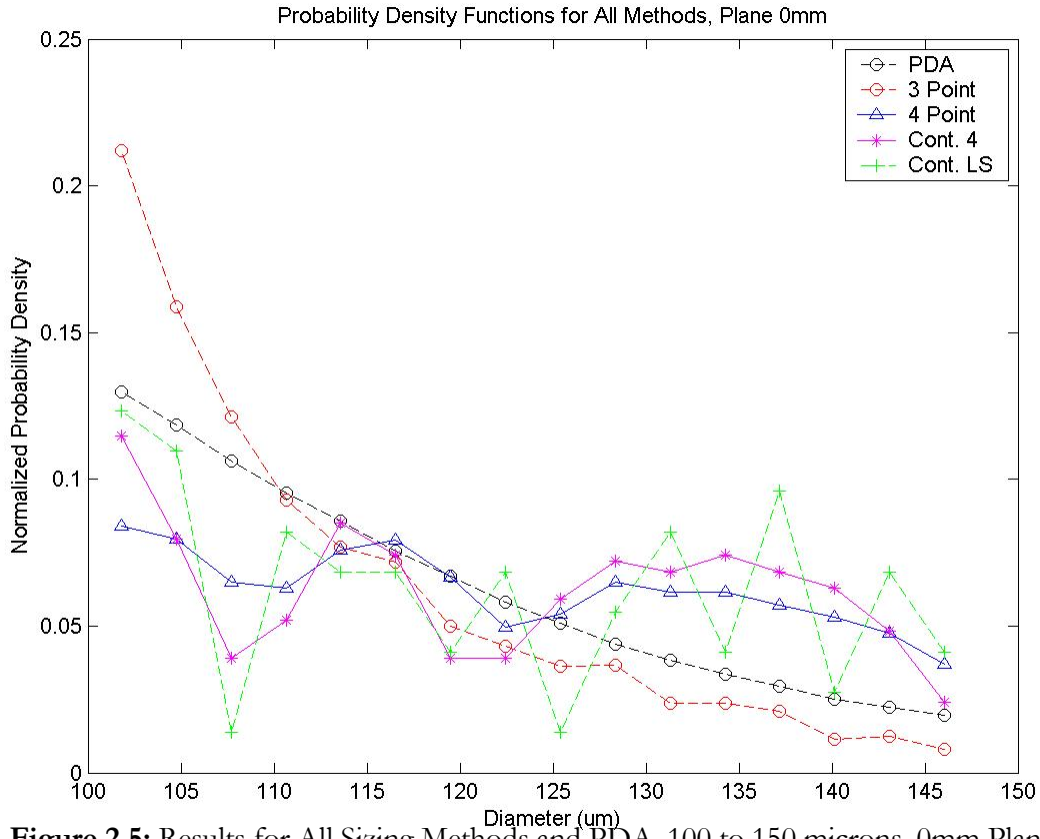

Figure 2.5: Results for All Sizing Methods and PDA, 100 to 150 microns, 0mm Plane

The results in Figure 2.5 show that the histogram for the three point Gaussian method matches best with the PDA measurements in the range from 100 microns to 150 microns. This range corresponds to approximately 4.2 to 6.25 pixels diameter in consideration of the overall magnification factor of 24 microns per pixel. The three point Gaussian method follows the PDA trend closely, exhibiting a correlation coefficient of 0.9571. The four point Gaussian and continuous four point Gaussian algorithms exhibit a bias toward higher diameters as compared to PDA measurement. The correlation coefficients for the four point Gaussian, continuous four point Gaussian, and the continuous least squares are 0.7916, 0.4130, and 0.4144, respectively for the 0mm plane. The continuous least squares pdf exhibits a high degree of noise over this range of diameter measurement, which stems from the low number of relative particles successfully detected.

The histograms for the positive and negative 4mm displacement (measured from the center of the spray) are shown below in Figures 2.6 and 2.7. The results in Figures 2.6 and 2.7 also show that the histogram for the three point Gaussian method matches best with the PDA measurements in

the range from 100 microns to 150 microns. The three point Gaussian method again follows the PDA trend with a correlation coefficient of 0.9728. In the +4mm plane, the four point Gaussian and continuous four point Gaussian algorithms exhibit the same trend as in the 0mm plane, a bias towards the higher diameters. The correlation coefficients for the four point Gaussian, continuous four point Gaussian, and the continuous least squares are 0.8904, 0.6692, and 0.5745, respectively for the +4mm plane. The same general trends appear in the -4mm plane. but the histograms are more erratic than in the +4mm plane results for the four point Gaussian and four point continuous sizing algorithms. In the -4mm plane, the correlation coefficients for the three point Gaussian, four point Gaussian, continuous four point Gaussian, and the continuous least squares are 0.9761, 0.5558, 0.1957, and 0.5496, respectively. These results show that the 3 point Gaussian performs much better in comparison to the PDA measurements than all of the other PIV sizing methods.

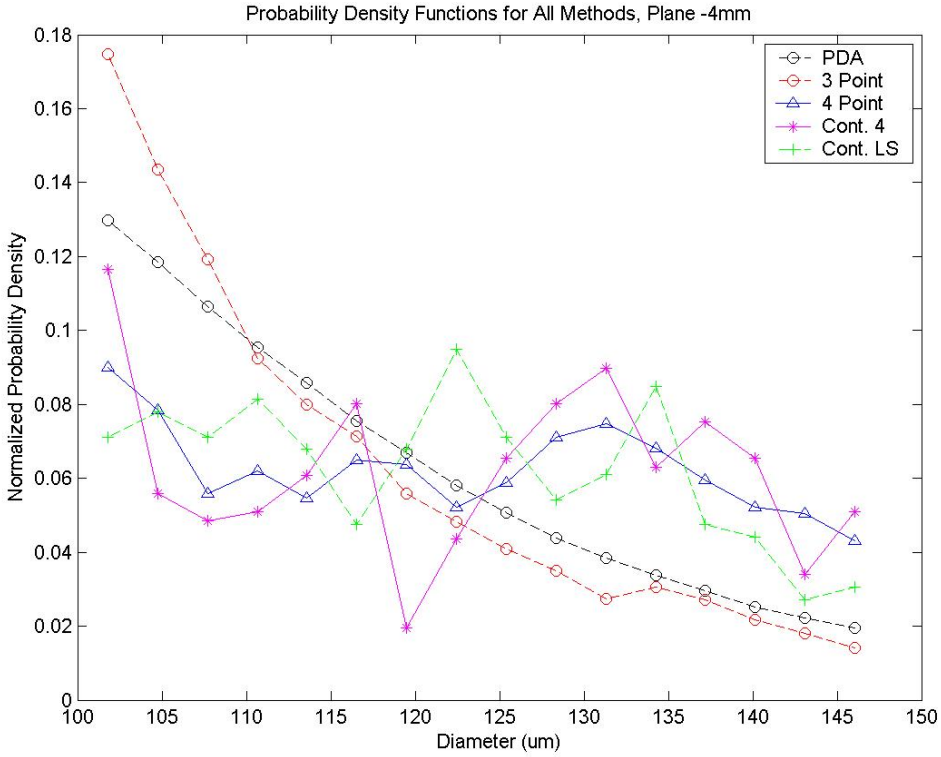

Figure 2.6: Histogram Results for - 4mm Spray Plane, All Sizing Methods

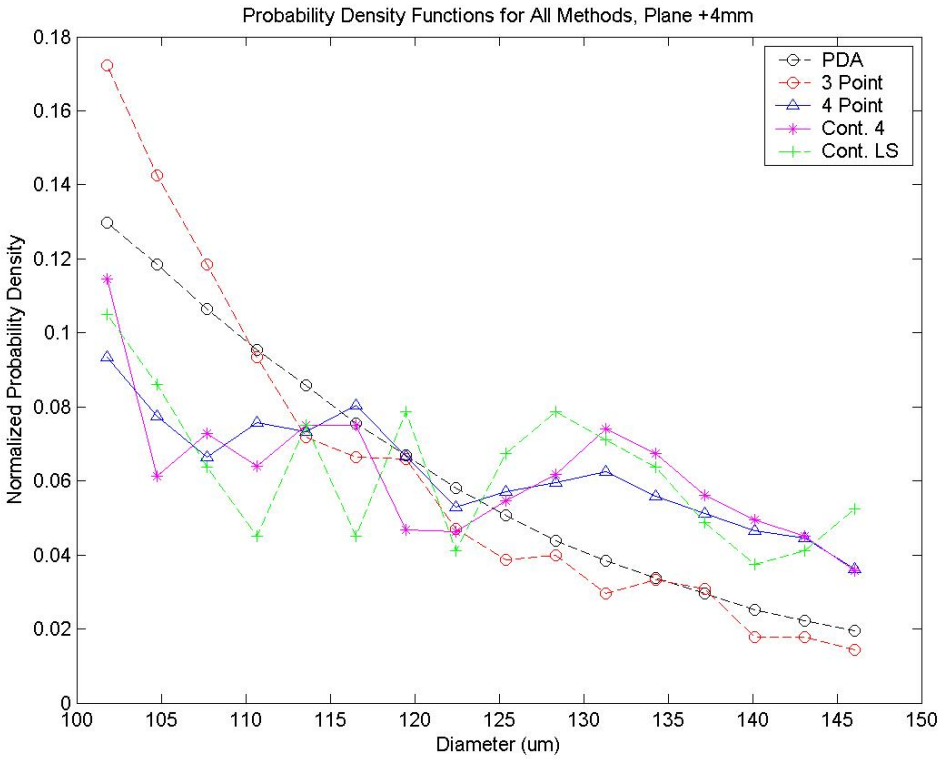

Figure 2.7: Histogram Results for + 4mm Spray Plane, All Sizing Methods

The histograms for the positive and negative 8mm displacement (measured from the center of the spray) are shown below in Figure 2.8. Figure 2.8 shows the same general trends in the +/- 8mm planes as seen in Figure 2.5 for the 0mm plane, except that the four point method performs better than in the previously analyzed frames in the +8mm case. In the +8mm plane, the correlation coefficients for the three point Gaussian, four point Gaussian, continuous four point Gaussian, and the continuous least squares are 0.9697, 0.9642, 0.6892, and 0.3265, respectively. In the -8mm plane, the correlation coefficients for the three point Gaussian, four point Gaussian, continuous four point Gaussian, and the continuous least squares are 0.9699, 0.7605, 0.1798, and 0.3060, respectively. The discrepancies between the 4 point, 4 point continuous, and least squares methods are most likely due to the absence of sufficient points in the data to arrive at a solution for diameter.

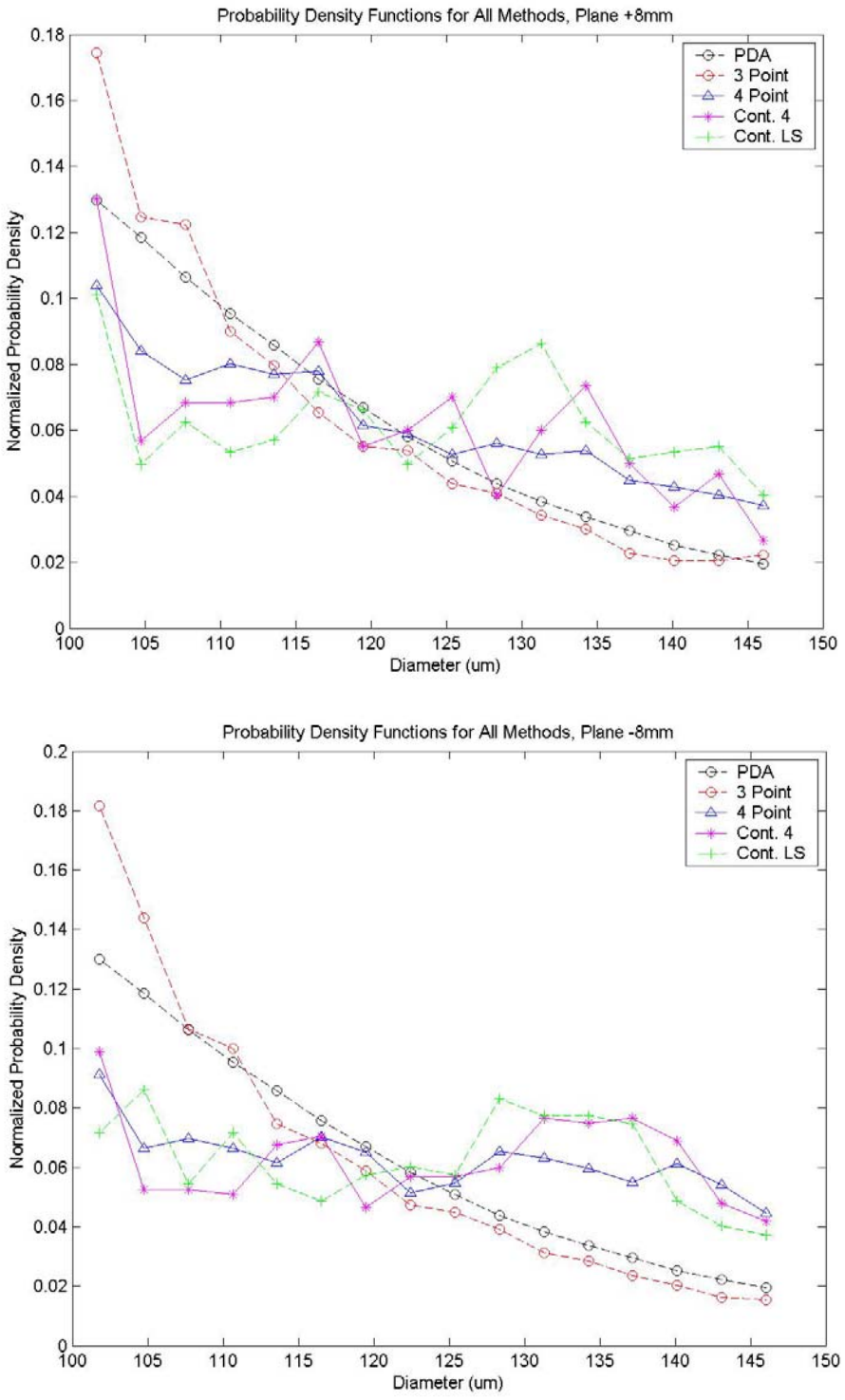

Figure 2.8: Histogram Results for +/- 8mm Spray Plane, All Sizing Methods.

The averaged results for the combined five planes (0mm, -4mm, -8mm, +4mm, and +8mm) are shown below in Figure 2.9. In order to generate these results, all of the particle populations were added together, separated into bins, and normalized with the total particle population. These results represent the average across all of the data planes considered in this work. In this case, the correlation coefficients for the three point Gaussian, four point Gaussian, continuous four point Gaussian, and the continuous least squares are 0.9728, 0.8915, 0.5658, and 0.5883, respectively. Figure 2.9 shows that the histogram for the three point Gaussian method matches best with the PDA measurements in the range from 100 microns to 150 microns. The four point Gaussian, continuous four point Gaussian, and continuous least squares all exhibit a bias toward higher diameters as compared to the PDA measurement. Therefore, all of the above results show that in this experiment, the 3 point Gaussian diameter estimation technique performs most accurately when compared with the corresponding PDA measurements over a range of 100 to 150 microns.

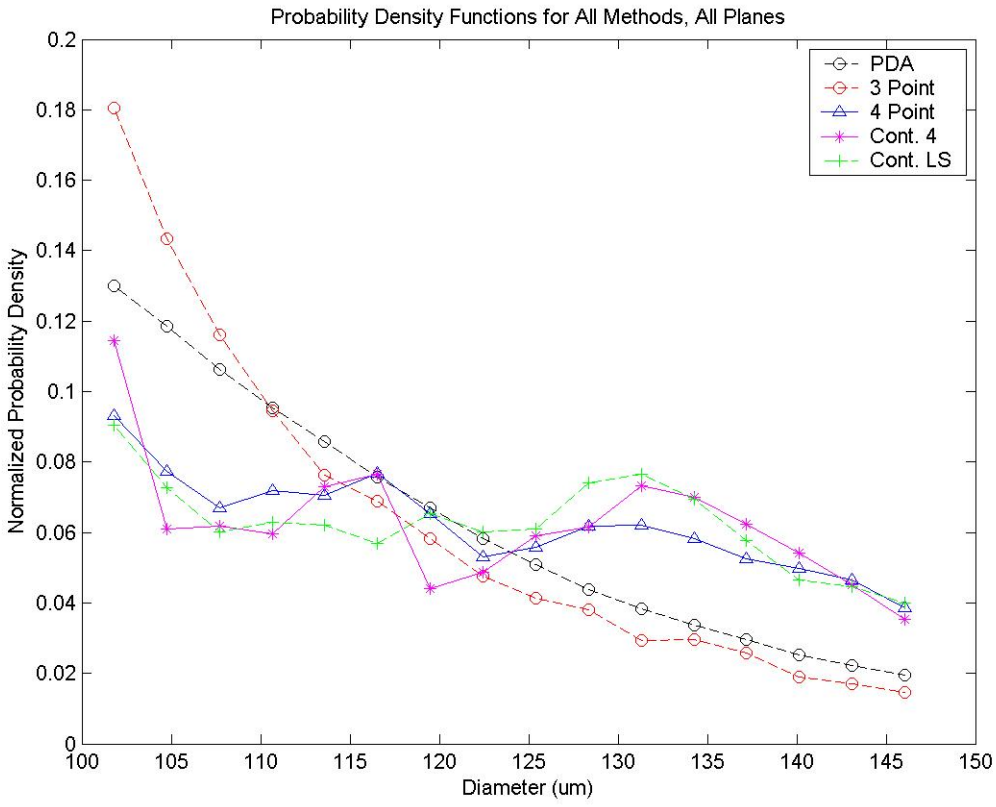

Figure 2.9: Plane-Averaged Histogram Results for All PIV Sizing Methods

The performance of the three point Gaussian estimator is shown in more detail below in Figure 2.10.

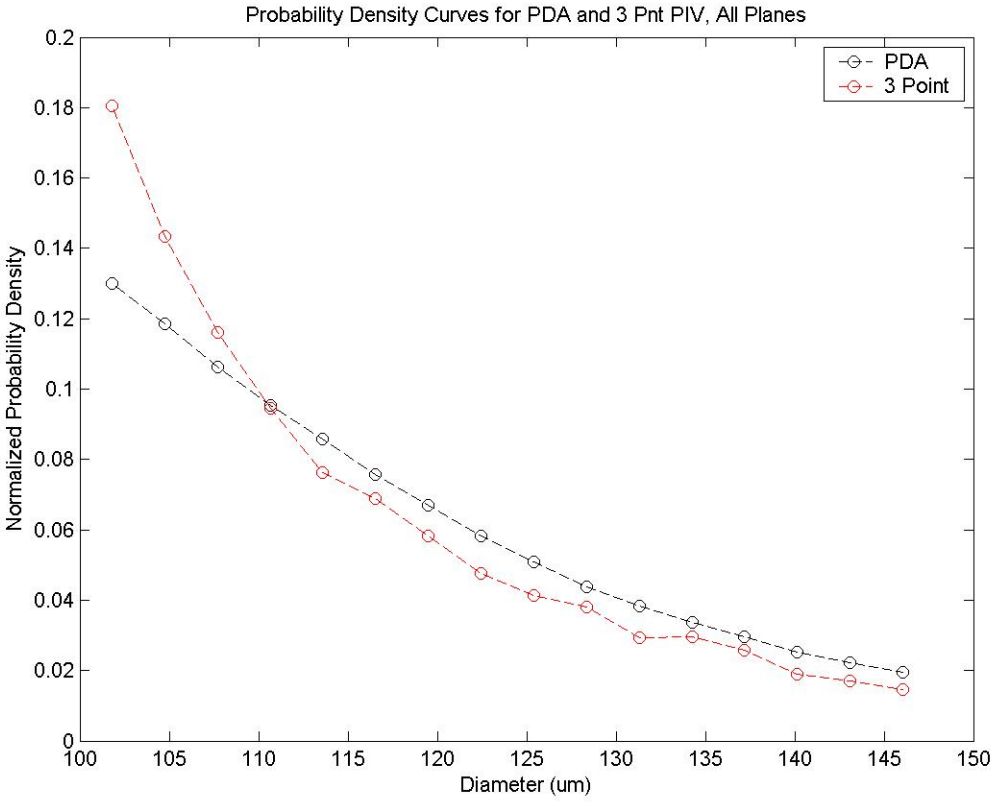

Figure 2.10: Plane-Averaged Results for 3 Point Gaussian Method and PDA.

The particle population is also an important factor in this experiment. Table 2.1 below lists the particle populations detected using the DPIV software for the 0mm plane. Table 2.1 shows that the 3 point Gaussian produces a result at a rate approximately 99.71 percent of the detected particle population, while the four point Guassian scheme produces results at approximately 19.40 percent. The 4 point continuous algorithm and the continuous least squares produce the lowest success rates, at approximately 3.187 and 3.280 percent, respectively. Each method was performed

on the same images with identical image preprocessing procedures, and therefore the number of particles fed to each algorithm for diameter estimation was identical.

Sizing Method	Particle Population (Number of Successes)	Average Successes Per Frame	Total Number of Particle Detected	Success Rate (%)
3 point Gaussian	554,497	34.7	556,111	99.71
4 point Gaussian	107,868	6.7	556,111	19.40
4 point Continuous	17,726	1.1	556,111	3.187
Continuous Least Squares	21,187	1.3	556,111	3.810

Table 2.1: Particle Population for Each Method, 0mm Plane

Table 2.2 below shows the correlation coefficient for each of the methods in tabulated form. Figure 2.11 shows the results in Table 2.2 in graphical form.

Correlation Coefficient for Each Plane, Each Sizing Method				
Plane (mm)	3 point	4 point	4 mod	lsvl
-8	0.9699	0.7605	0.1798	0.306
-4	0.9761	0.5558	0.1957	0.5496
0	0.9571	0.7916	0.413	0.4144
4	0.9728	0.8904	0.6692	0.5745
8	0.9697	0.9642	0.6892	0.3265
Plane Averaged	0.9728	0.8915	0.5658	0.5883

Table 2.2: Particle Population for Each Method, 0mm Plane

The results from Tables 2.1 and 2.2, along with Figure 2.11, show that only the 3 point method succeeds at a reliable rate above 99 percent and exhibits a high value of the correlation coefficient when compared to the PDA measurement over a diameter range from 100 to 150 microns. The other conventional sizing methods did not perform adequately in this experiment, exhibiting success rates ranging from 3 to 20 percent. The other methods also exhibited low values for the correlation coefficient throughout the planes. The plane averaged correlation coefficient was 0.8915 for the 4 point Gaussian, 0.5658 for the continuous 4 point Gaussian, and 0.5883 for the continuous least squares fit.

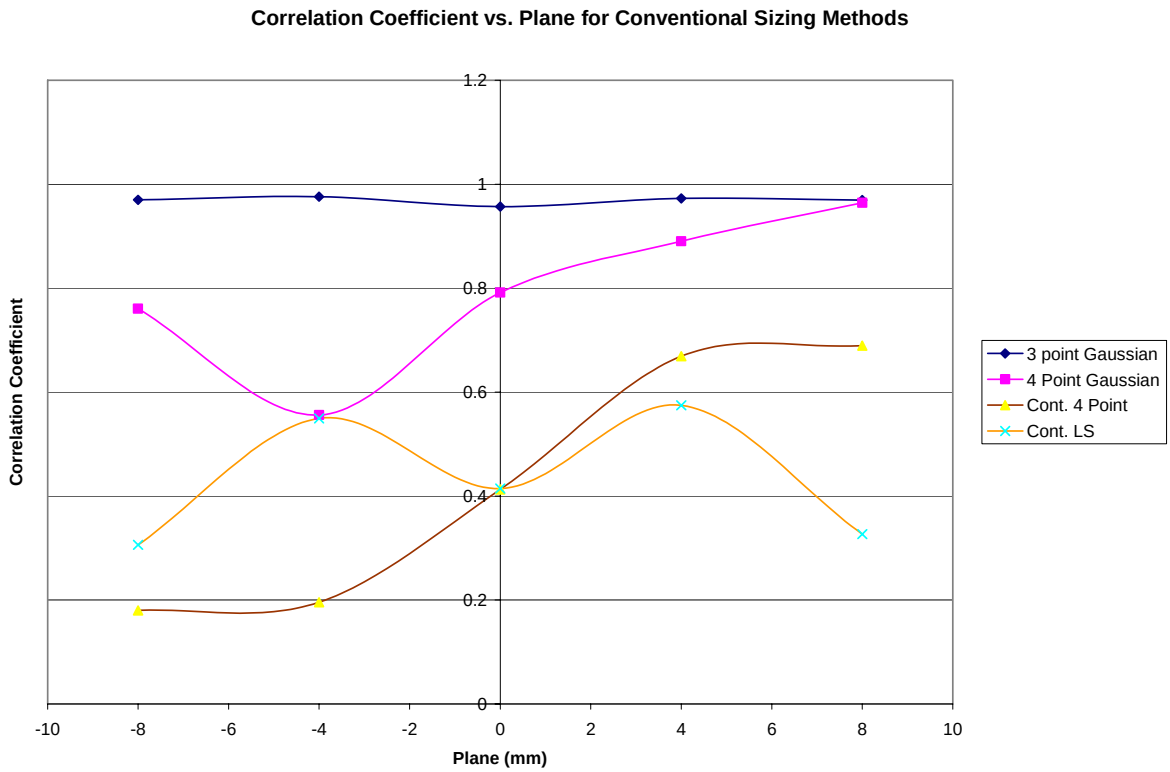

Figure 2.11: Correlation Coefficient vs. Plane for Conventional Sizing Methods.

2.4.3 Average Diameter

In addition to histogram analyses, average diameter calculations provide another comparison tool between the PIV and PDA diameter measurement techniques. The 3-D isosurface plot for the average diameter for all of the spray planes is shown below in Figure 2.12. Figure 2.12 was generated using the 0mm, +4mm, and +8mm results for the 3 point Gaussian sizing scheme and reconstructing a volume using Tecplot 10. The data from each plane was scanned and counted into 16 pixel bins with 50 percent overlap. The grid spacing in Figure 2.12 is 8 pixels, which allows a grid of 32X32X5 for the entire volume. The average diameter was calculated assuming spherical particles. Figure 2.12 was generated in Tecplot using isosurfaces between values of 54, 63, and 72. The results in Figure 2.12 were smoothed for 3 passes using the built-in smoothing functionality of Tecplot 10.

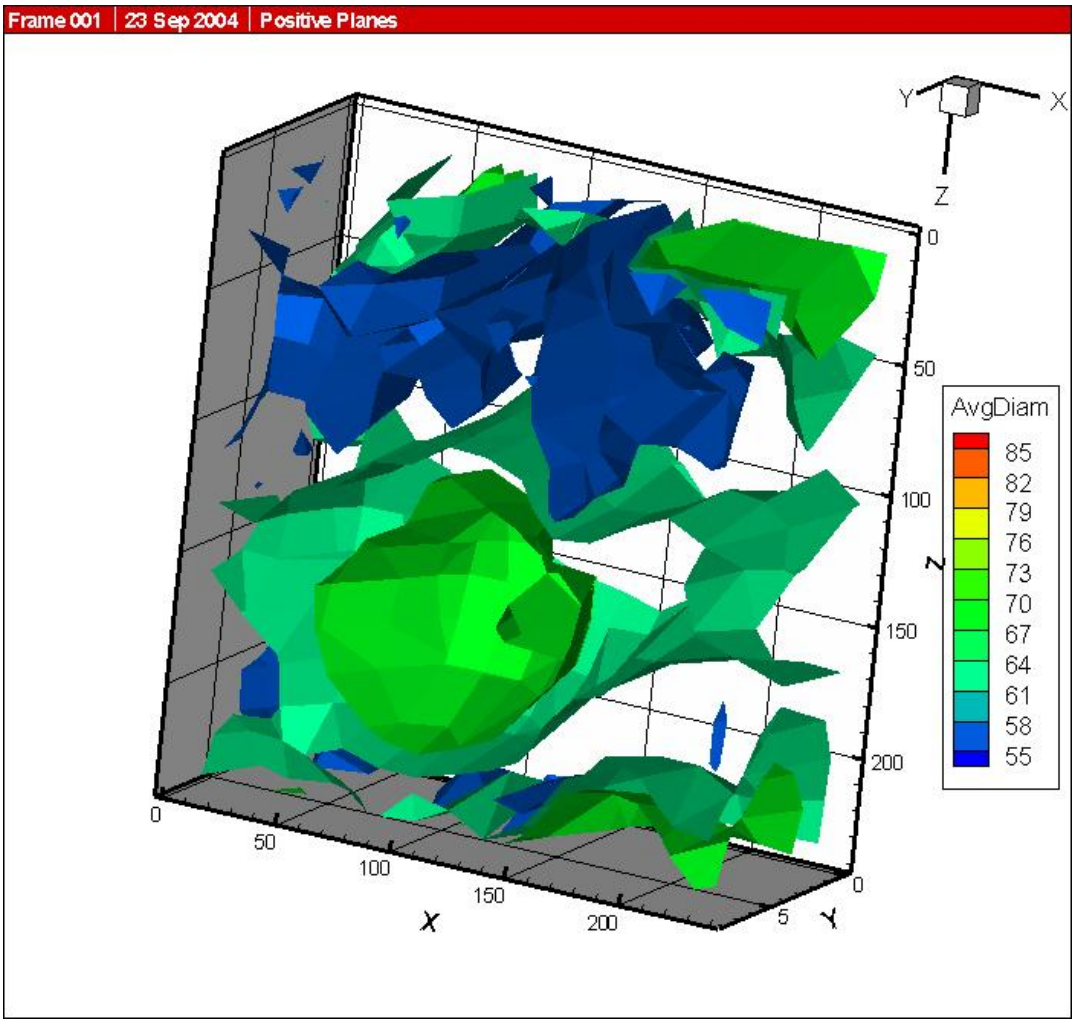

Figure 2.12: 3-D Isosurface Plot of Average Diameter

In Figure 2.12, the spray is located at (X,Y,Z) = (120,0,256). Figure 2.12 shows clearly shows the volume reconstruction of the spray. The ligament can be clearly seen at in the bright green area. Figure 2.12 shows that the larger particles are located near the ligament, and the average particle diameter decreases as the distance from the spray increases. Since this analysis allows the complete reconstruction of the entire volume, y plane slices may be extracted from the volume in order to compare the average diameter at a certain height above the spray with the PDA measurements.

The slice of the reconstructed volume at an exact height of 15.4 mm is shown below in Figure 2.13. This elevation was located at 61.3097 pixels below the top of the spray images, or at an elevation in the z plane of 194.69 pixels. The magnification used to find the corresponding region was 79.1 microns per pixel.

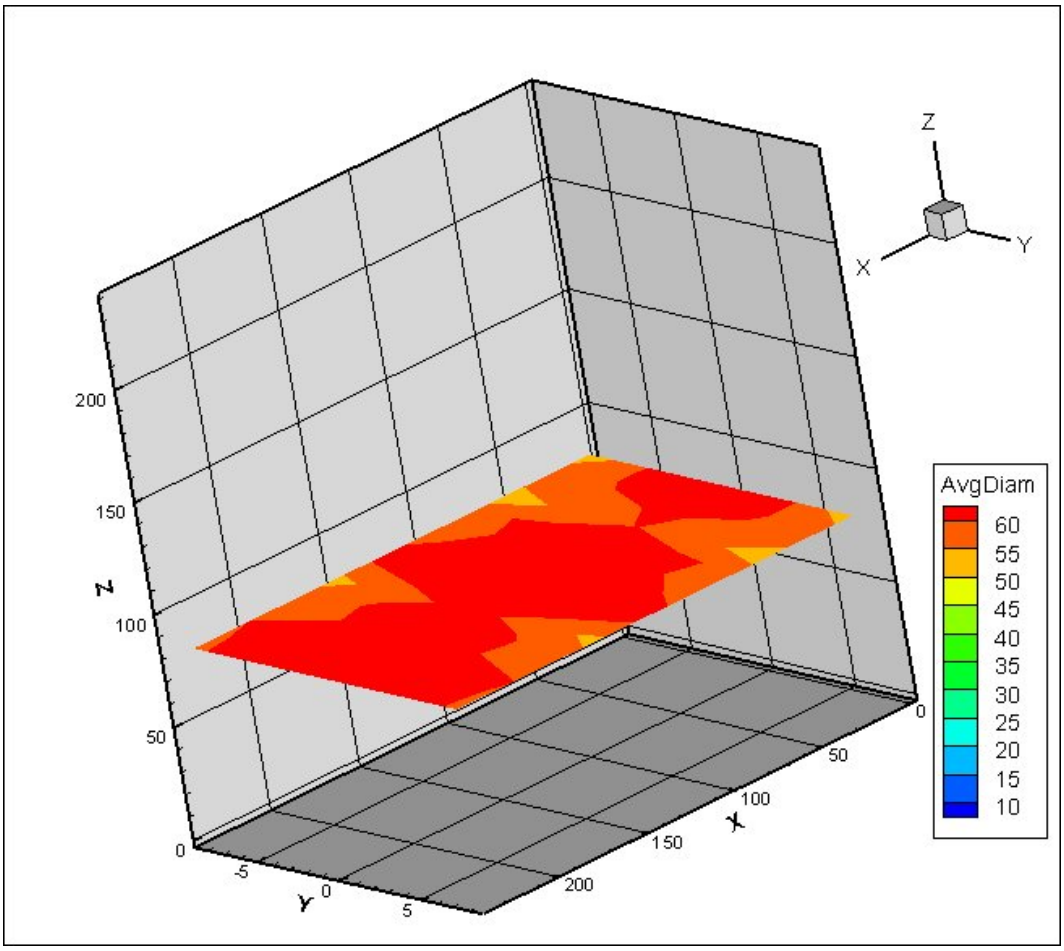

Figure 2.13: Corresponding Slice Height in 3-D.

The out-of-plane average diameter results for the 3 point Gaussian PIV sizing method are shown below in Figure 2.14. The PDA measurement is also shown in Figure 2.14, and was taken at an elevation above the spray of 15.4mm. The PIV planes shown in Figure 2.14 are located at z = 16, z = 32, z = 48, and z = 64 pixels. The grid spacing used in the out-of-plane results was 16 pixels. The results in Figure 2.14 show that the PIV sizing results agree with the PDA measurement, are about 40 microns higher than the PDA measurement in the center of the spray. On the outer edge of the analyzed domain, the values are approximately 10 to 20 percent higher than the PDA measurement. This discrepancy can be explained by the design of the experiment, which did not allow the PIV system to detect particles smaller than 2 pixels. The previous histogram analysis shows that the 3 point Gaussian method detects no particles below the 44 micron range. Therefore, the average diameter detected by the 3 point Gaussian cannot be less than 44 pixels. On the other hand, the PDA can resolve down to 1.4 microns in diameter. The PDA measurement accounts for all particles above 2 microns in diameter, while the PIV system used in

this experiment could only resolve 24 micron particles or greater. The mismatch between the resolvable diameters results in the discrepancy between the two systems. The units in Figure 2.14 are average diameter in microns.

Figure 2.14 shows that the 3 point Gaussian fit overestimates the average diameter in comparison to the PDA measurement. In the matching ranges, the PDA reaches a maximum level of 40 microns. The PIV values do not drop below 50 microns. Therefore, the PIV error ranges from 25% of the PDA to around 1000% in the center of the flow. The reason for this discrepancy, again, is the inability of the PIV 3 point method to resolve diameters below 25 microns in diameter. Even though a population of 25 micron particles exists in the data, the data shown in Figure 2.14 is the average particle diameter passing through bins of 16 pixels square, or 1.6 square millimeters. A bin size of 1.6 square millimeters is more than enough to capture particles of several sizes in this experiment. This means that for every 25 micron particle that passes through the center at 15.4mm above the spray, a larger particle traverses the same area within the entire data set. Therefore, the PIV method cannot produce results in this analysis for diameters less than 25 pixels at the minimum under ideal bin selection criteria, while the PDA measurement can resolve down to 1.4 microns. Therefore, due to the limitations of the PIV method, this analysis cannot produce a viable comparison between the PDA and PIV methods for this data set.

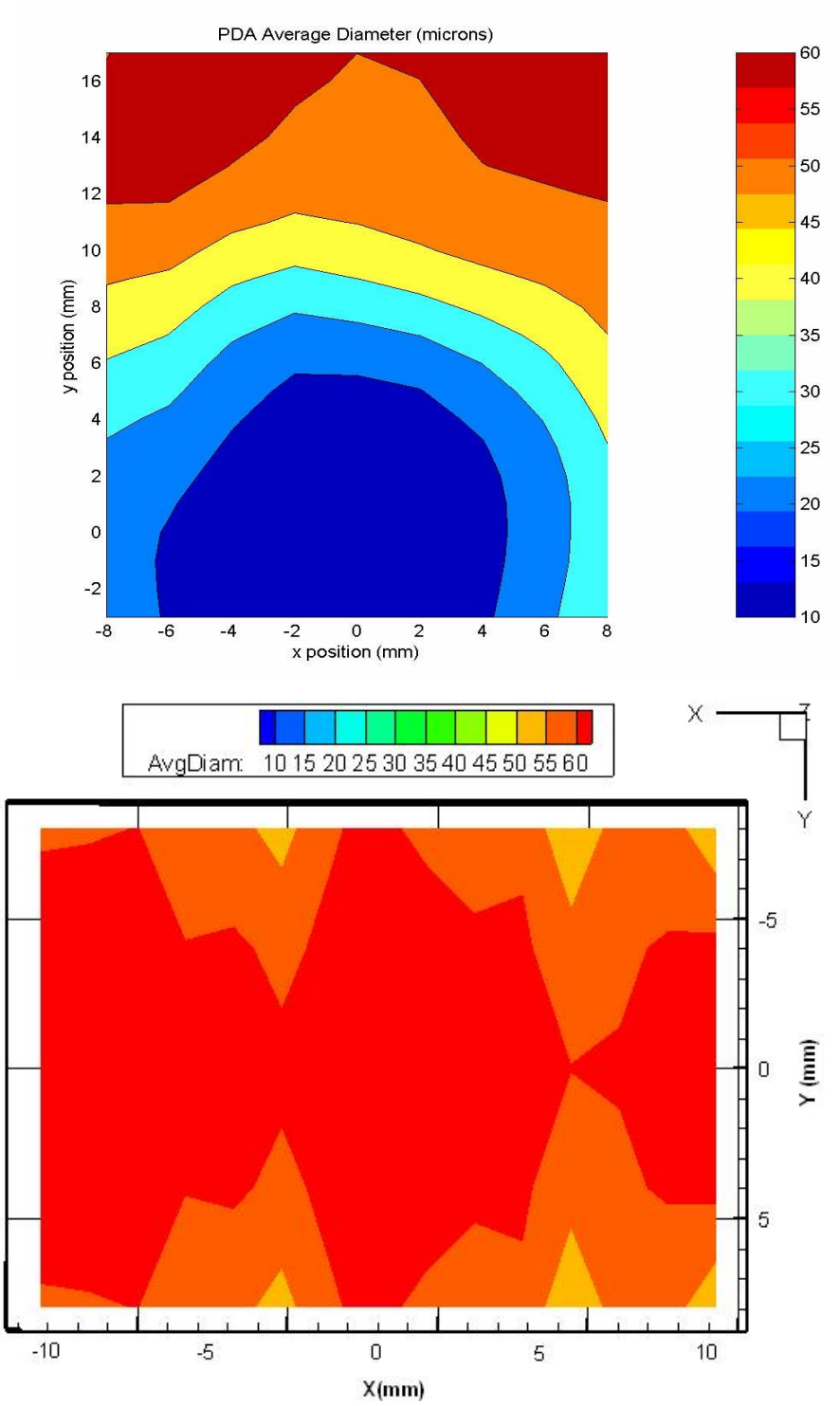

Figure 2.14: PDA and 3 Point Gaussian PIV Average Diameter, z = 15.4mm

2.4.4 PTV-Corrected Histograms

PTV was performed on the spray data for the 0mm plane case using the 3 point Gaussian sizing method. The PTV method used in this portion of the work was the Basic Trajectory option in Flow-IQ v2.2. Histograms were generated for the tracking, the 3 point fit, and the compensated tracking algorithm. The PTV compensated histogram was obtained by subtracting the tracking algorithm from the overall 3 point Gaussian results. The tracking histogram was generated by histogramming the average diameter of each tracked particle. The average diameter for a tracked particle was calculated by using all of the occurrences of the particle throughout the data files. Most of the particles in this study were tracked through only two frames. The results for the 3 point Gaussian fit, the particle tracking, and the PTV compensated histograms are shown below in Figure 2.15.

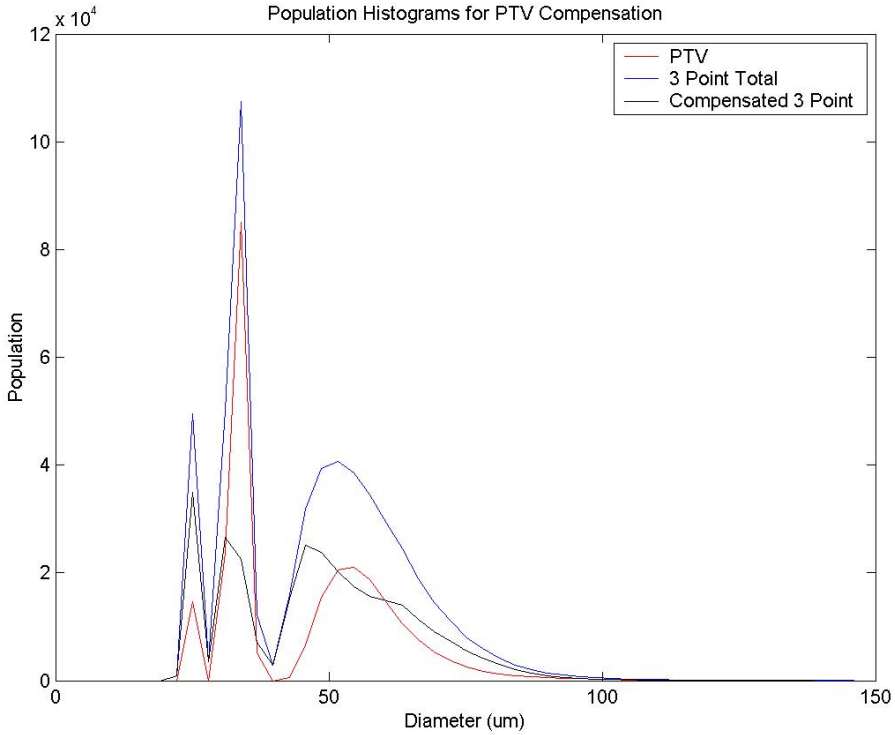

Figure 2.15: Total Population Histograms for 3 Point Guassian, Tracking, and PTV-compensated methods, Spray 0mm plane.

Figure 2.15 shows that approximately 80 percent of the particles detected at the 25 and 44 micron points were tracked using PTV. Approximately half of the particles from the 50 to 90 micron range were tracked between frames. Therefore, the compensation using PTV decreases the overall population bias towards the lower diameters for the 3 point Gaussian method. In order to compare the methods to the PDA measurement, probability density functions were generated by dividing the populations shown in Figure 2.15 with the total population for each corresponding method. These results are shown below in Figure 2.16.

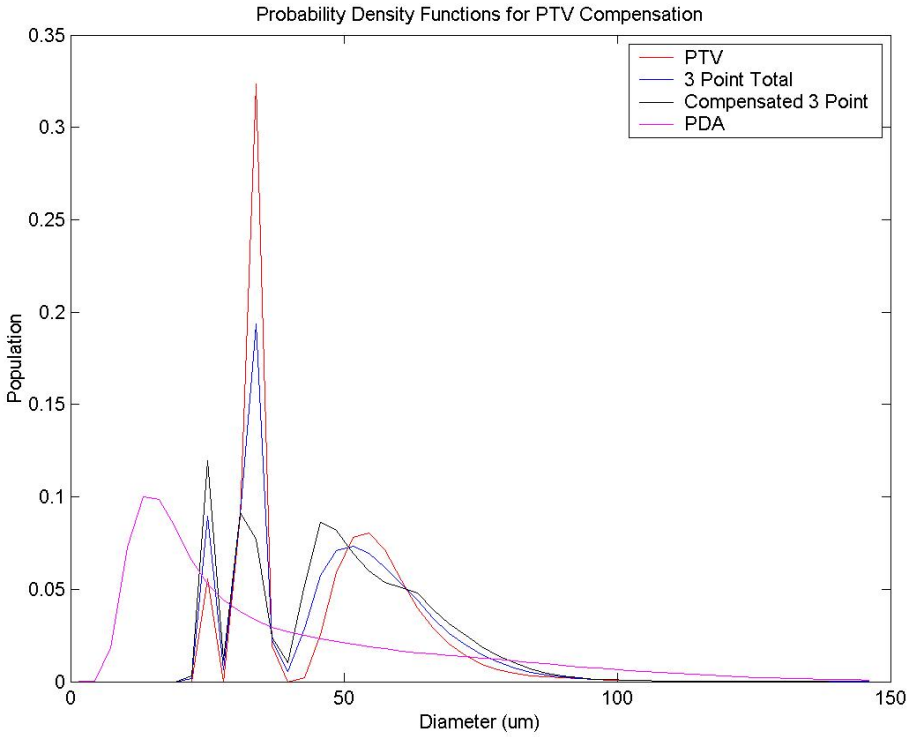

Figure 2.16: PDA, 3 point Gaussian, PTV, and PTV-compensated PDF's, 0mm plane

Figure 2.16 above shows that the PTV and PTV-compensated pdf's are much closer to the PDA measurement than the full 3 point Guassian results. The correlation coefficients with the PDA measurement for each of the methods shown in Figure 2.16 are listed below in Table 2.3.

Method	Correlation Coefficient
3 Point Guassian (Full Results)	0.1465
Tracked 3 Point Gaussian	0.1099
PTV-Compensated 3 Point Gaussian	0.1677

Table 2.3: PTV Correlation Coefficients for Full Range Results, 0 mm Plane

The correlation coefficient for the PTV-compensated algorithm is 14.5% higher than the correlation coefficient of the 3 point Gaussian sizing method alone. The PTV-compensated comparison with the PDA sizing method is shown in greater detail in Figure 2.17.

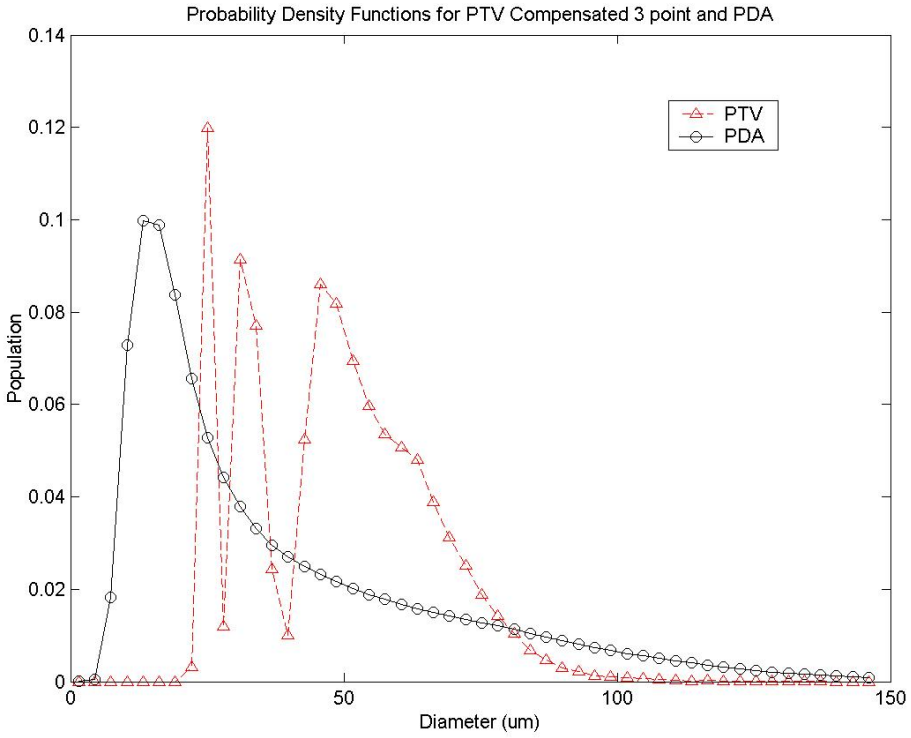

Figure 2.17: PTV-compensated and PDA histograms, 0mm plane

Figure 2.17 shows that the PTV compensated method significantly improves the estmation of diameter population at the lower diameters. However, the correlation coefficient is still very low, due to the inability of the 3 point method to resolve diameters smaller than 25 microns. Therefore, the methods were also analyzed over the 100 to 150 micron range, as in the previous sections. The histogram results for the 100 to 150 micron diameter range are shown below in Figure 2.18. Figure 2.18 shows the total population for the PIV/PTV methods and the probability density functions for the PIV, PDA, and PTV methods. Figure 2.18 suggests that the PTV 3 point

Gaussian method improves the correlation of the PIV method with the PDA measurement. A list of the correlation coefficients over the 100 to 150 micron range is given in Table 2.4.

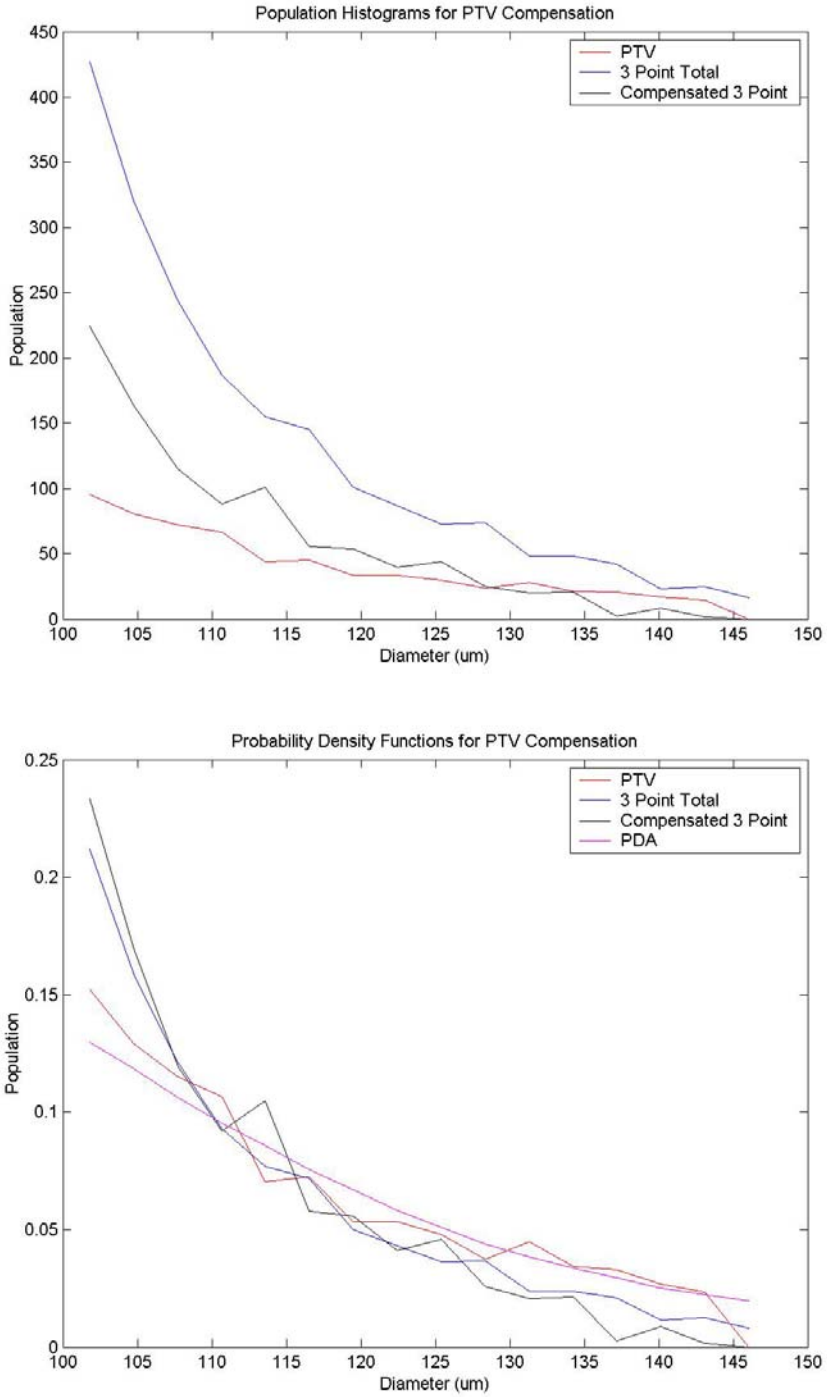

Figure 2.18: Population for PIV/PTV methods and PDF's for PIV, PDA, and PTV

Method	Correlation Coefficient
3 Point Guassian (Full Results)	0.9571
Tracked 3 Point Gaussian	0.9759
PTV-Compensated 3 Point Gaussian	0.9558

Table 2.4: PTV Correlation Coefficients for 100 to 150 um Range, 0 mm Plane

Table 2.4 shows that the tracking method improves the correlation coefficient of the method, since the tracked histogram matched the PDA better at diameters less than 110 microns. The compensated histogram is shown below in Figure 2.19.

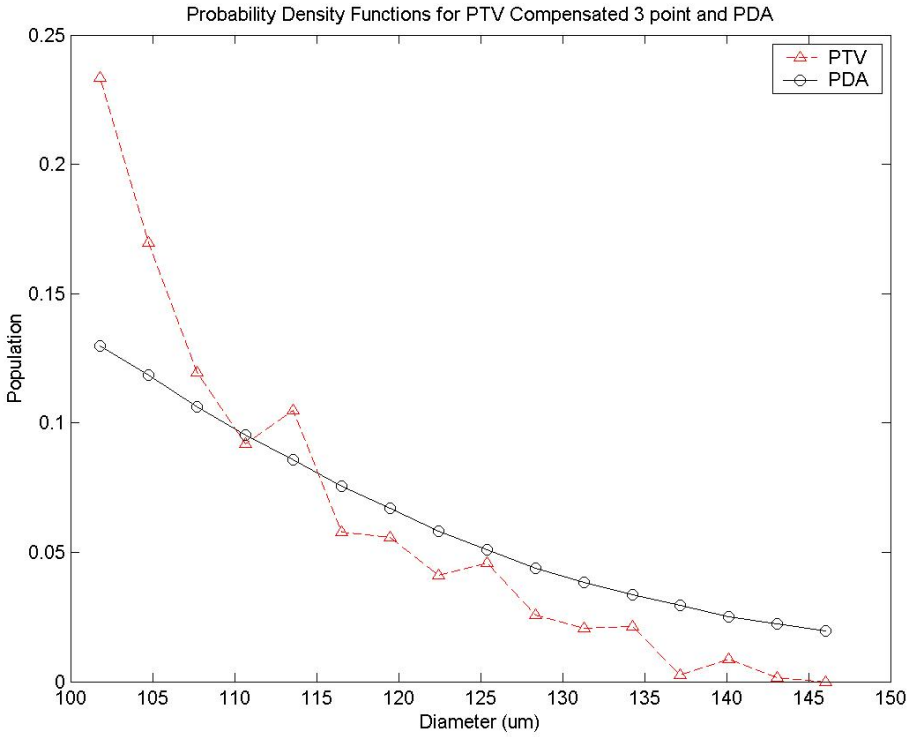

Figure 2.19: Tracking Compensation and PDA for 100 to 150 micron range.

The correlation coefficient between the PDA and the compensated PTV method may improve over different diameter ranges. The exploration of different diameters will be left to future researcher in the particle sizing arena.

2.5 Conclusions and Future Work

The particle sizing portion of this work showed that the design of DPIV experiments is vital for the accurate measurement of particle size using PIV sizing methodologies. An experiment must contain particles that are at least 3 pixels in diameter in the PIV data plane in order to produce

accurate results. Therefore, the minimum suggested particle diameter for sizing with PIV methods is approximately 3 pixels. This conclusion is in agreement with the errors reported in Brady et al. (2002), which showed that at diameters less than 3 pixels, the conventional PIV sizing methods exhibit increasing error as particle diameter decreases. The spray results analyzed in this work did not take this criterion into consideration at the time of data acquisition, and only portions of the analyzed data were accurate. Therefore, it is the conclusion of this work that PIV experiments that include sizing as a project goal should be designed with sufficient magnification to provide a minimum of 3 pixels diameter for all particles the experimenters wish to size. This means that the burden of producing accurate sizing results depends heavily on the appropriate setup and design of the PIV experiment. New spray experiments are underway to test this criterion, and preliminary results show that experiments with sufficient magnification produce results that match closely with PDA measurements across the entire range of particle diameters. The PTV method has shown initial promise in improving the correlation coefficient of PIV sizing methodologies with the traditional PDA methods. Future work should focus on the improvement of the PTV-corrected method for PIV particle sizing.

The spray sizing analysis completed in this work should be extended to further experiments with adequate optical design to perform PIV average diameter analysis. This work showed that the optimal design should magnify all desired particles to a minimum of three pixels diameter in order to provide accurate spray sizing results. The new elliptical sizing methods should also be tested on real data in order to determine their performance in real-world experiments.

2.6 Summary of Original Contribution

The original contribution of this work is the application of the sizing methods developed by previous researchers to an entire set of spray atomization data. No new sizing methods were developed or used in the spray sizing portion of this work. The histogram analysis found that the 3 point Gaussian sizing method exhibited a correlation coefficient of up to 0.9728 when compared to the PDA method over a range of 100 to 150 microns in diameter (4 to 7 pixels in diameter). Although the PIV average diameter results in this section do not agree with the PDA measurement, several important observations were made from this analysis. The PIV experiment must be designed to have sufficient magnification, such that the particles the experimentor(s) wish

to size are greater than 3 pixels in diameter in the PIV data. Over the detectable range of PIV sizing (greater than 3 pixels in diameter), the PIV sizing method performed with a correlation coefficient of up to 0.9728 when compared statistically to the PDA sizing method. Therefore, the major finding of this work is the conclusion that PIV sizing experiments must be carefully designed to provide the necessary particle size for comparable results to PDA measurements. This work was performed as a validation of the particle sizing methodologies as an application of the new sizing software in a real experiment. The only original algorithm in this work is the PTV-corrected method for particle sizing, which will be further developed by future researchers.

Chapter 3

3 ELLIPTICAL PARTICLE SIZING METHOD

The purpose of this chapter is to explore the development of a novel elliptical sizing algorithm developed by the author. Previous sizing methodologies have made the assumption that particles are spherical in shape, and present a circular profile in DPIV data. In some applications, this assumption can be justified. However, in several applications, such as spray atomization, droplets or seed particles deform and may present elliptical profiles in DPIV data. Therefore, this work explores the development of an elliptical sizing method that is not limited to circular profiles. Monte Carlo simulations were also performed in order to validate the performance of the method on simulated DPIV data.

3.1 Introduction

In this work, an elliptical particle sizing technique was developed in order to overcome the assumption that all particles in a flow field are spherical. The assumption of spherical particles introduces error into the measurement of diameter using the conventional PIV sizing schemes presented above in Chapter 2. In order to create an elliptical particle, the intensity in the x and y directions were assumed to be jointly Gaussian, identically independent random variables.

Two random variables x and y are considered Jointly Gaussian is their joint pdf is defined as (Stark and Woods, 1986):

$$f_{XY}(x,y) = \frac{1}{2\pi\sigma_x\sigma_y\sqrt{1-\rho^2}} e^{\left(\frac{-1}{2(1-\rho^2)} \left\{ \left(\frac{x-\mu_x}{\sigma_x} \right)^2 - 2\rho \frac{(x-\mu_x)(y-\mu_y)}{\sigma_x\sigma_y} + \left(\frac{y-\mu_y}{\sigma_y} \right)^2 \right\} \right)} \qquad \text{(Eq. 3.1)}$$

where σ_x is the standard deviation in the x direction, σ_y is the standard deviation in the y direction, μ_x is the mean of the x variable , μ_y is the mean of the y variable, and ρ is the correlation coefficient between the x and y random variables.

When the x and y are considered to by identically independent random variables ($\rho = 0$), equation 3.1 reduces to:

$$f_{XY}(x, y) = \frac{1}{2\pi\sigma_x\sigma_y} e^{\left(\frac{-1}{2}\left\{\left(\frac{x-\mu_x}{\sigma_x}\right)^2 + \left(\frac{y-\mu_y}{\sigma_y}\right)^2\right\}\right)} \quad \text{(Eq. 3.2)}$$

This equation describes an elliptical Gaussian curvature, whose semimajor axis is related to the greater of σ_x or σ_y, and whose simeminor axis is related to the lesser of σ_x or σ_y. The semimajor and semiminor axes are the particle width in the x and y direction. An ellipse is shown below in Figure 3.1 (Harris and Stocker, 1998).

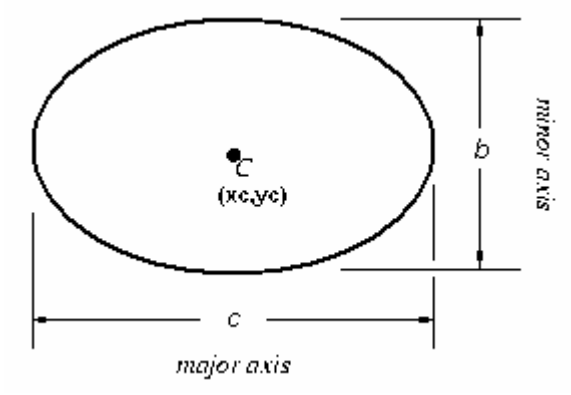

Figure 3.1: Diagram of an ellipse.

Brady et. al. (2004) examined particles using the assumption that particle distributions were normally distributed i.i.r.v.'s with σ_x equal to σ_y, which produces a circular distribution as shown below in Figure 3.2.

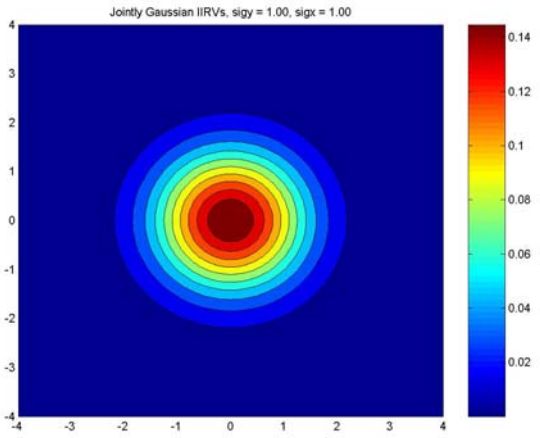

Figure 3.2: Jointly Gaussian IIRV's with $\sigma_x = \sigma_y$.

For a circular particle, Brady et. al. showed that for circular particles, σ_x and σ_y are given by the following equations.

$$x_c = x_o + \frac{\ln a_{o-1} - \ln a_{o+1}}{2(\ln a_{o-1} + \ln a_{o+1} - 2\ln a_o)} \quad \text{(Eq. 3.3)}$$

$$y_c = y_o + \frac{\ln a_{o-1} - \ln a_{o+1}}{2(\ln a_{o-1} + \ln a_{o+1} - 2\ln a_o)} \quad \text{(Eq. 3.4)}$$

$$\sigma^2 = \frac{\ln a_{o+1} - \ln a_o}{(x_o - x_c)^2 - (x_{o+1} - x_c)^2} \quad \text{(Eq. 3.5)}$$

$$d = \sqrt{2\sigma} \quad \text{(Eq. 3.6)}$$

$$a_i = I_o e^{-\frac{(x_i - x_c)^2}{2\sigma^2}} \quad \text{(Eq. 3.7)}$$

Where a_0 and a_{0+1} are the intensities at the center pixel and the pixel to the right of the center pixel, x_0 and x_{0+1} are the pixel positions of the center and right pixel, x_0 and x_{0+1} are the pixel positions of the center and right pixel, respectively, and *d* is the estimated diameter of the particle.

For an elliptical particle the above equations are reduced to the following equations for σ_x, σ_y, *b*, and *c*, where *b* and *c* are the semimajor and semiminor axes.

$$\sigma_x^{\,2} = \frac{\ln a_{xo+1} - \ln a_{xo}}{(x_{xo} - x_c)^2 - (x_{xo+1} - x_c)^2} \qquad \text{(Eq. 3.8)}$$

$$\sigma_y^{\,2} = \frac{\ln a_{yo+1} - \ln a_{yo}}{(y_{yo} - y_c)^2 - (y_{yo+1} - y_c)^2} \qquad \text{(Eq. 3.9)}$$

$$b = \sqrt{2\sigma_x} \qquad \text{(Eq. 3.10)}$$

$$c = \sqrt{2\sigma_y} \qquad \text{(Eq. 3.11)}$$

Figure 3.3 below shows some example plots of jointly Gaussian i.i.r.v.'s with various values of σ_x and σ_y. Using these equations, elliptical particles can be accurately sized. This distribution can be used to size particles that do not exhibit a circular shape, such as elliptical droplets, streaked particles, particles detected in regions of high background noise or non-symmetric cross-correlation distribution peaks.

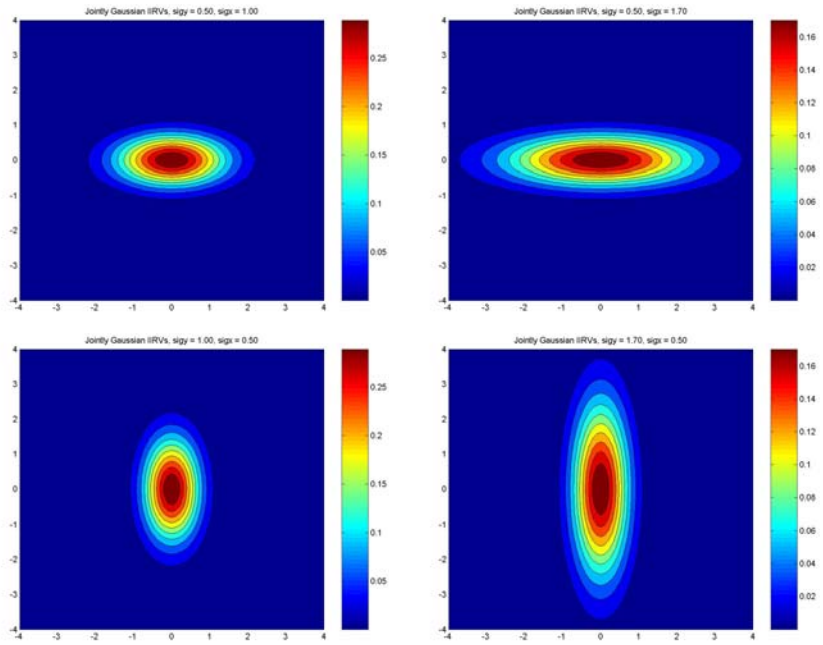

Figure 3.3: Jointly Gaussian IIIRV's with various values of σ_x and σ_y.

Errors were calculated in this work as the difference between the actual area of the particle and the measured area of the particle. The area of an ellipse is simply πbc, where b is the semimajor axis of the ellipse, and c is the semiminor axis of the ellipse. The eccentricity of an ellipse, which describes the shape of the ellipse, is defined below in equation 3.11.

$$e = \sqrt{1 - \frac{b^2}{c^2}} \qquad \text{(Eq. 3.12)}$$

The eccentricity varies from 0 to 1 for an ellipse, since the semiminor axis is by definition less than the semimajor axis.

3.2 Elliptical Particle Sizing Scheme Methods and Materials

A theoretical analysis of the elliptical sizing method was performed. Monte Carlo simulations of the performance of the method will be left to future research.

3.3 Elliptical Particle Sizing Results

The theoretical advantages of using an elliptical particle sizing algorithm are explored in the following section. These results provide the basis for future work in the development of elliptical

sizing techniques. Section 3.3.2 presents the experimental portion of this work, which consists of Monte Carlo simulations in order to determine the performance of the elliptical sizing method in simulated data.

3.3.1 Theoretical Foundations

The conventional 3 point sizing method takes only the x direction into account when sizing particle. This procedure can certainly be improved by the addition of a y component to the diameter measurement. The particle may either as a true ellipse, or as a sphere by averaging the x and y diameter measurements. This analysis assumes that the ellipse is axisymmetric around the x and y axes.

The error associated with the measurement, in this work, is considered as the percent difference in area of the measured particle as compared to the actual area of the particle. The percent difference is defined below in Equation 3.12.

$$\%_{err} = \frac{A_{meas} - A_{true}}{A_{true}} \qquad \text{(Eq. 3.13)}$$

The area of the conventional method is simply πd^2, where d is the measured diameter of the particle in the x direction. The theoretical error of the traditional method when x is the semimajor axis of the ellipse is given by Equation 3.13, which reduces to Equation 3.14.

$$e_{\%xmaj} = \frac{\pi b^2 - \pi bc}{\pi bc} \qquad \text{(Eq. 3.14)}$$

$$e_{\%xmaj} = \frac{b}{c} - 1 \qquad \text{(Eq. 3.15)}$$

The theoretical error of the traditional method when x is the semiminor axis of the ellipse is given by Equation 3.15, which reduces to Equation 3.16.

$$e_{\%x\min} = \frac{\pi c^2 - \pi bc}{\pi bc} \qquad \text{(Eq. 3.16)}$$

$$e_{\%x\min} = \frac{c}{b} - 1 \qquad \text{(Eq. 3.17)}$$

The theoretical error of the averaged elliptic sizing method, where the diameter is considered to be the average of the semiminor and semimajor axes, is given by Equation 3.17. This equation reduces to Equation 3.18.

$$e_{\%xavg} = \frac{\pi\left(\frac{b+c}{2}\right)^2 - \pi bc}{\pi bc} \qquad \text{(Eq. 3.18)}$$

$$e_{\%xavg} = \frac{b}{4c} + \frac{c}{4b} - \frac{1}{2} \qquad \text{(Eq. 3.19)}$$

The theoretical error of the true elliptic sizing method, where the area is defined as πbc, is identically zero.

Figure 3.4 below shows the theoretical error introduced by using only the x direction as a measurement of an ellipse with varying eccentricity. Eccentricity is defined as the square root of one minus the square of the ratio of the semiminor axis to the semimajor axis.

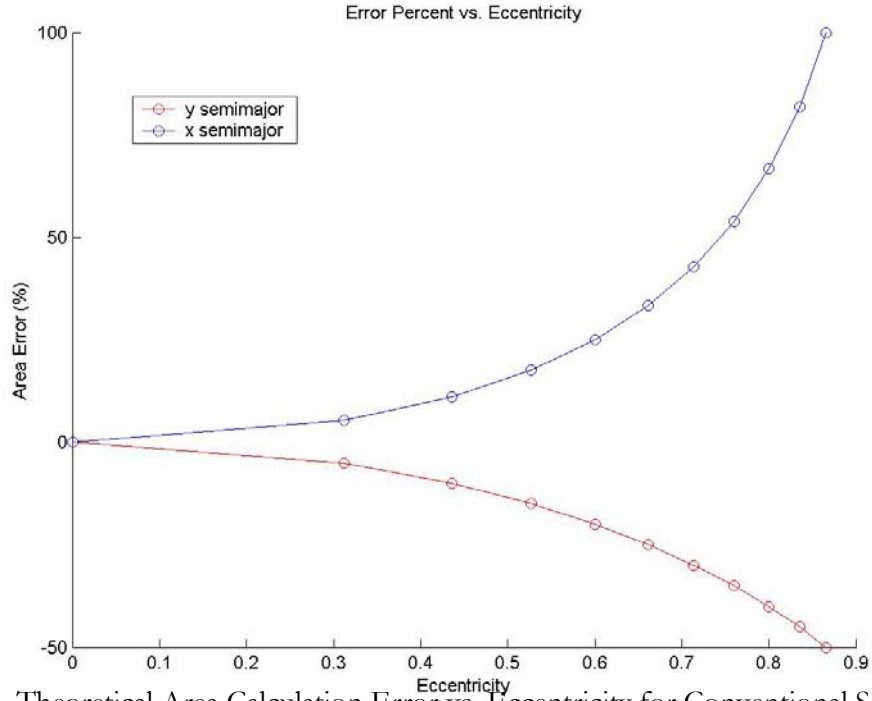

Figure 3.4: Theoretical Area Calculation Error vs. Eccentricity for Conventional Sizing Method

Figure 3.4 above shows that, theoretically, the error introduced by measuring the diameter with only the x information diverges as the eccentricity increases. At an eccentricity of 0.866, the error is 100 percent for the case of an x semimajor axis, and -50 percent for the case of a y semimajor axis. This analysis was performed in order to demonstrate the need for improvement in the three point Gaussian sizing method. Another presentation of the theoretical error introduced by the 3 point Gaussian sizing method is shown below in Figure 3.5. These errors are plotted as a function of axis ratio for the case of x and y semimajor axes.

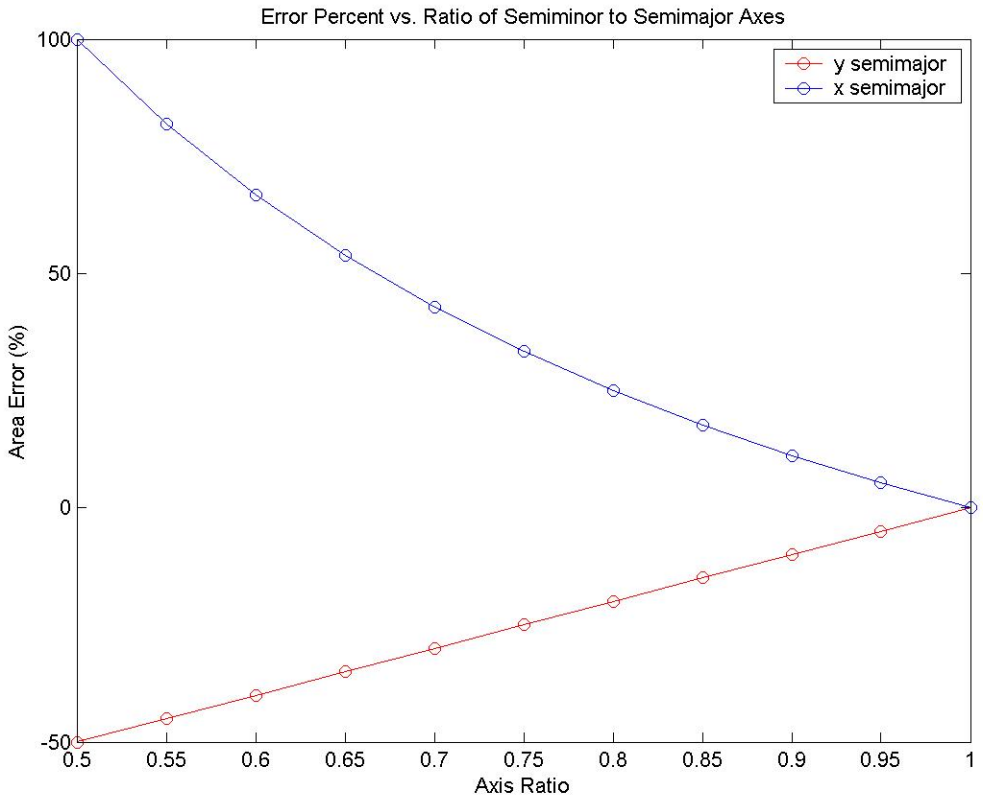

Figure 3.5: Theoretical Error vs. Axis Ratio for 3 point Gaussian Sizing Method

Figure 3.5 above is more intuitively obvious, as the error diverges when the discrepancy between the semimajor and semiminor axes increases.

The novel sizing methods presented in this work are the averaged elliptic and true elliptic sizing methods. The averaged elliptic method uses the average of the two axes to arrive at a measurement diameter. The true elliptic method sizes a particle using the two independent measurements, thus forming a true ellipse. The theoretical error for the averaged elliptic and true

elliptic methods are compared to the theoretical error for the 3 point Gaussian sizing method in Figures 3.6 and 3.7 below.

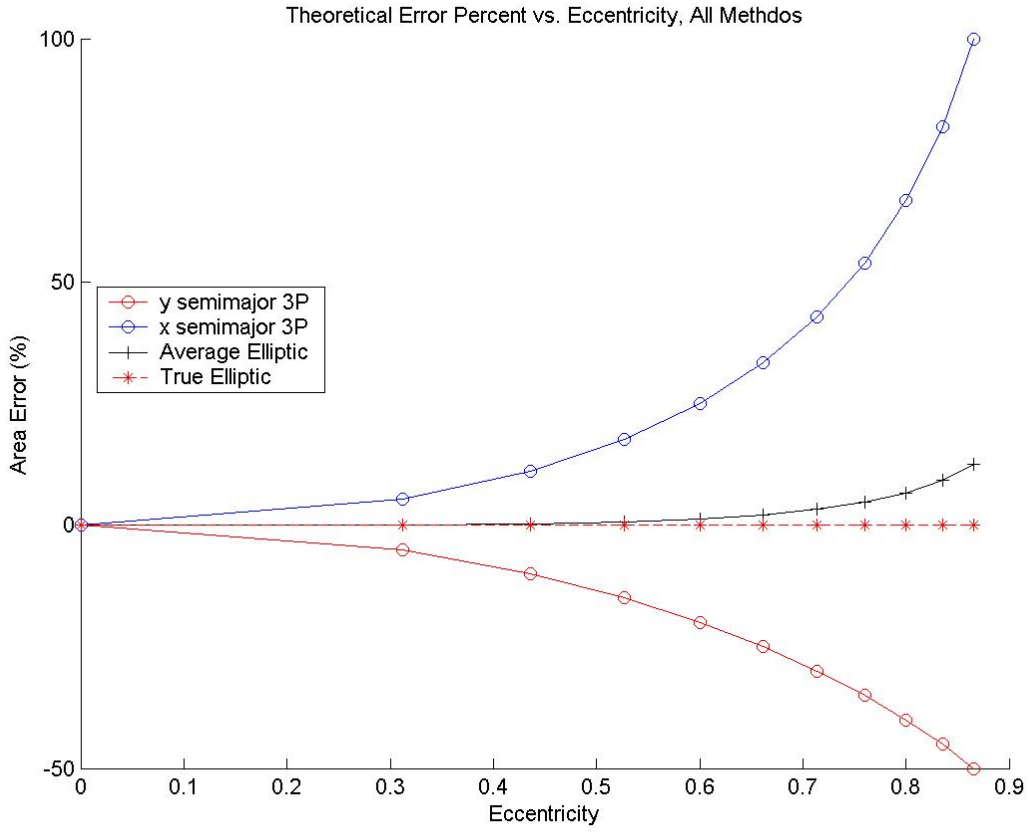

Figure 3.6: Theoretical Percent Error for 3 Point Gaussian, Averaged Elliptic, and True Elliptic Sizing Methods

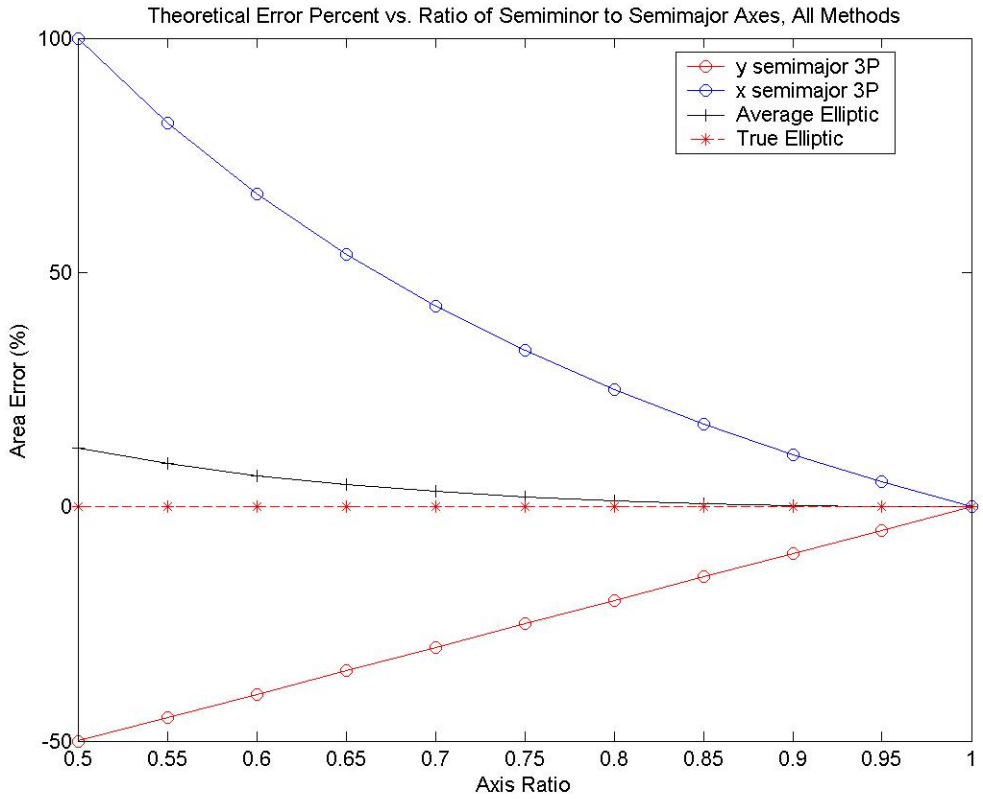

Figure 3.7: Theoretical Percent Error for 3 Point Gaussian, Averaged Elliptic, and True Elliptic Sizing Methods

The above results show that the averaged elliptic sizing method, in theory, reduces the error in the measurement by 5 to 10 times, maxing at 12.5 percent at an eccentricity of 0.866 and an axis ratio of 0.5. It is also interesting to note that the averaged elliptic sizing method exhibits the same error whether the x-axis is the semimajor axis or the semiminor axis. Therefore, the true elliptic and averaged elliptic sizing methods exhibit the ability to correct for non-spherical particles within a flowfield, while the conventional 3 point Gaussian exhibits an error that diverges greatly with eccentricity. However, the theoretical calculations presented above do not account for the error introduced by pixel discretization. Future work in this area will include Monte Carlo Simulations of the elliptical sizing algorithm and its performance comparison to traditional Gaussian particle sizing methodologies.

3.3.2 Experimental Analysis

Monte Carlo Simulations were used in order to characterize the performance of the elliptical sizing method on simulated PIV data. A total of 5000 images were generated with particles with

eccentricities varying from 0 (circular) to 0.8660 (50 percent difference between the semimajor and semiminor axes). Two example images are shown below in Figure 3.8. The generated images were 32 X 32 pixels square and the center of the particle was forced to be located at (x,y) = (7.25,7.25) in order to fix the particles within the image.

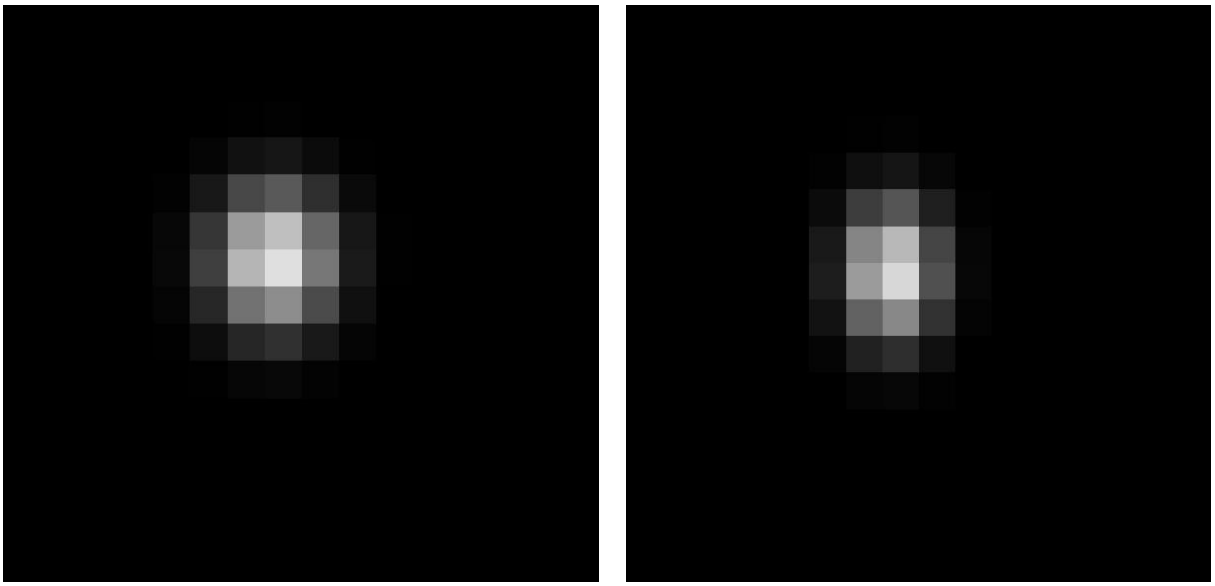

Figure 3.8: Sample Monte Carlo Simulation Images.

The images used in this experiment were generated using MatLAB 6.0. The profiles were assumed to be elliptical Gaussian profiles as developed in the introduction of this chapter. The pixel values were obtained by integration of the elliptical Gaussian profile over the pixel area in order to simulate the optics of a CCD device. The traditional and novel elliptical sizing methods were performed on each image, and the error was calculated according to Equation 3.13. The results obtained from this analysis follow.

In order to test the methods on a basic level, circular particles were generated in order to provide a baseline method to ensure that the different methods developed in this work agreed with the traditional 3 point Gaussian method. The total error in the diameter measurement is shown below in Figures 3.9 and 3.10. To generate Figure 3.10, the error values shown in Figure 3.9 were averaged over 250 measurements, which generated 20 data points over the data range from 2.8 pixels to 5.6 pixels in steps of 0.14 pixels.

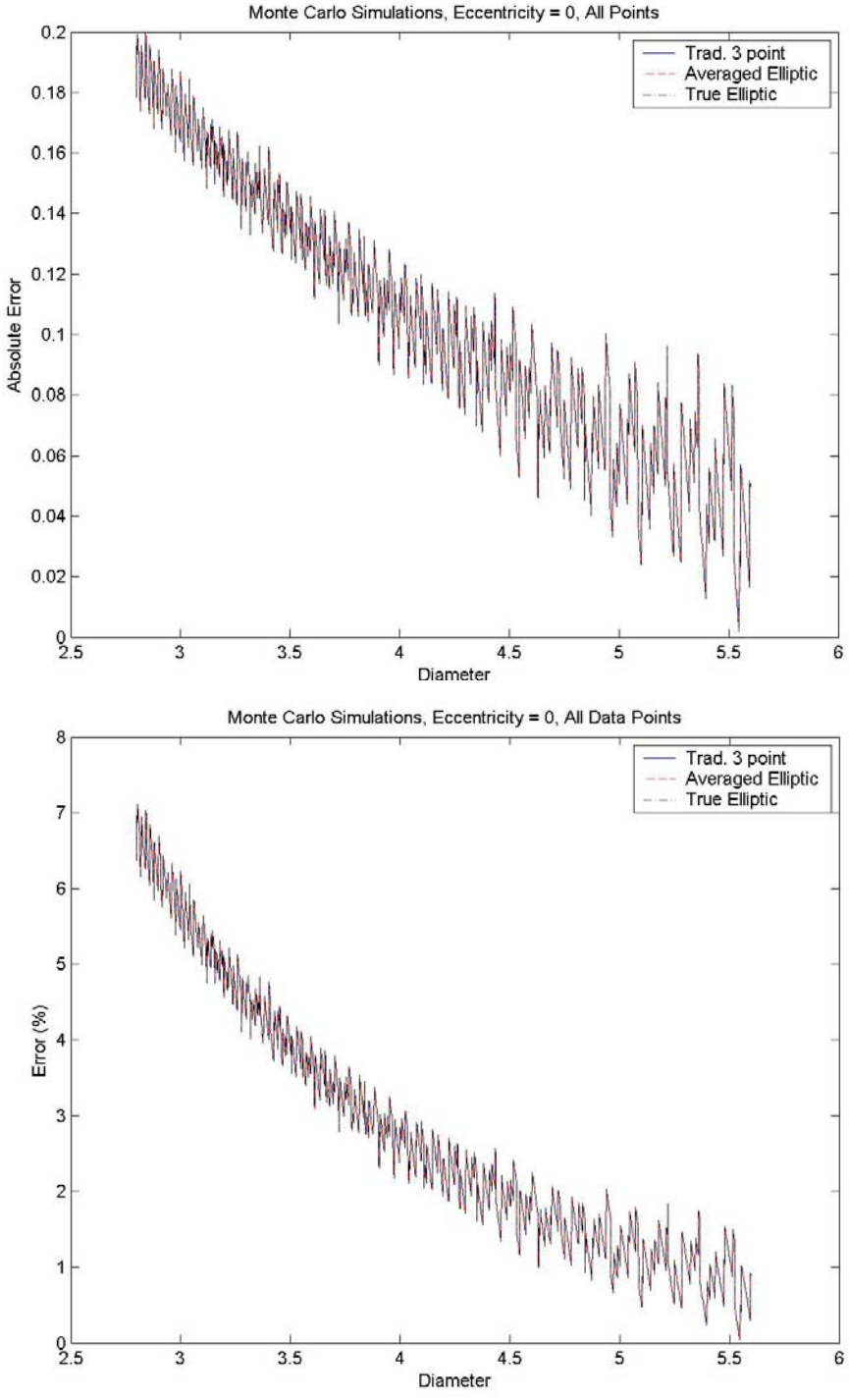

Figure 3.9: All Data Points for Eccentricity = 0, Diameter range 2.8 to 5.6 pixels

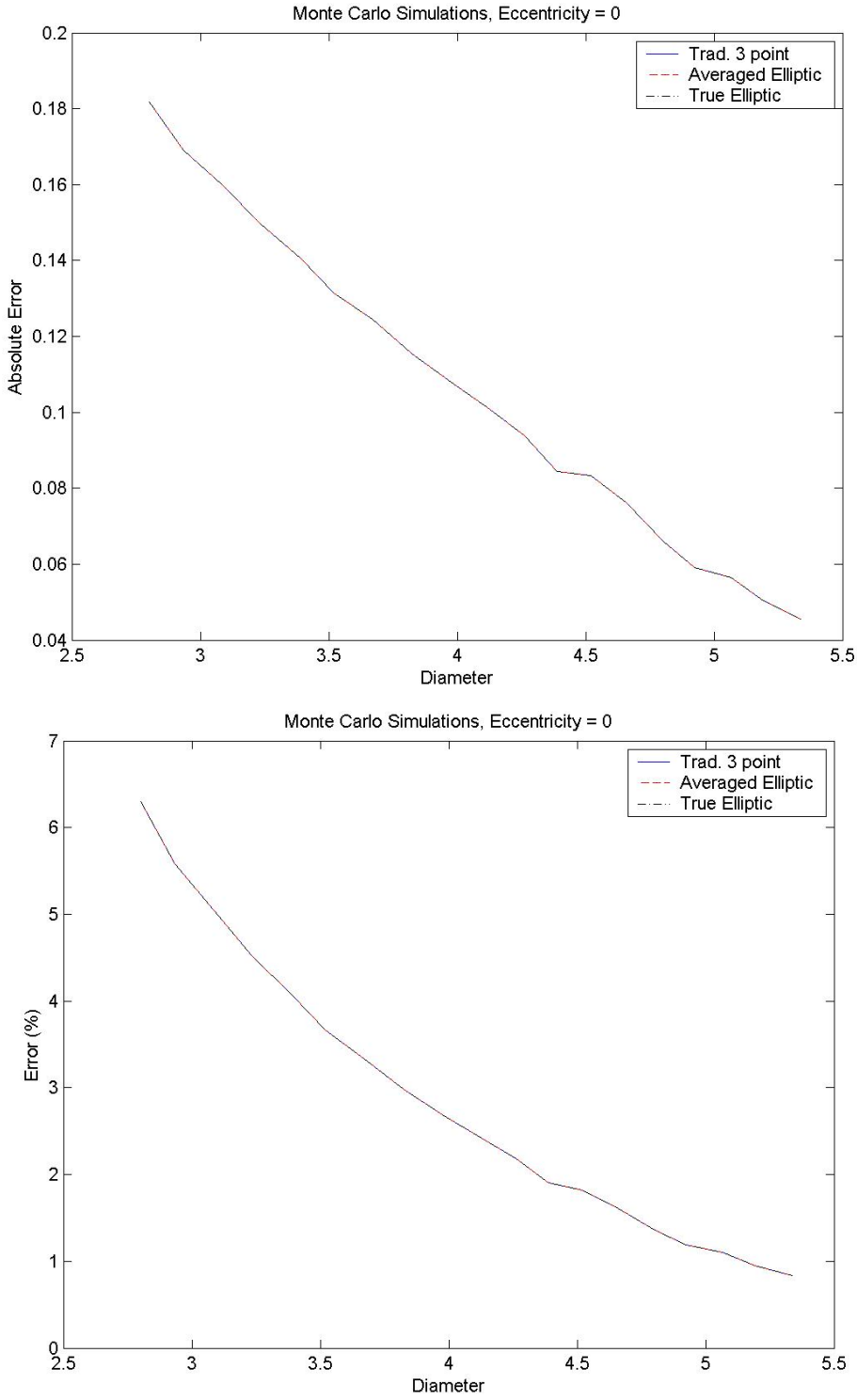

Figure 3.10: Averaged Total Error over 250 points, Eccentricity = 0.

Figures 3.9 and 3.10 above show that the 3 point Gaussian, averaged elliptic, and true elliptic sizing methods perform with a correlation coefficient of 1.00. The correlation coefficient is unity between all of the methods for the case of no eccentricity. The absolute and percent error shown in Figures 3.9 and 3.10 agree with previous results obtained by Brady et al. (2002) in their study of the 3 point Gaussian sizing scheme. Since the zero eccentricity case has been established, the performance of the various sizing methods are explored in the following paragraphs.

There are several ways to present the error analysis in this section. The first approach used to determine the errors associated with the diameter measurement was to calculate the error in the x and y diameters. For the 3 point Gaussian fit, the x diameter is the only calculated diameter, and therefore this diameter is used as a comparison to the actual y diameter in this simulation. The averaged elliptic method assumes a spherical shape with the average of the diameter in the two directions. Therefore, for the averaged elliptic method, the average diameter was compared to the actual diameter in the x and y directions. For the true elliptic fit, the corresponding diameters were compared. The results from this analysis are shown below in Figure 3.11 and 3.12. The same procedure for Figures 3.9 and 3.10 were used to generate these graphs. Figure 3.11 shows the comparative absolute and percentage error in the x and y diameter measurements versus x diameter, and Figure 3.12 shows the comparative errors in the x and y diameter measurements versus eccentricity. For the images used to obtain these results, the x diameter was chosen at random in a range from 2.8 to 5.6 pixels in diameter. The y diameter was held constant at 5.6 pixels in order to fix the eccentricity range from 0 to 0.8660.

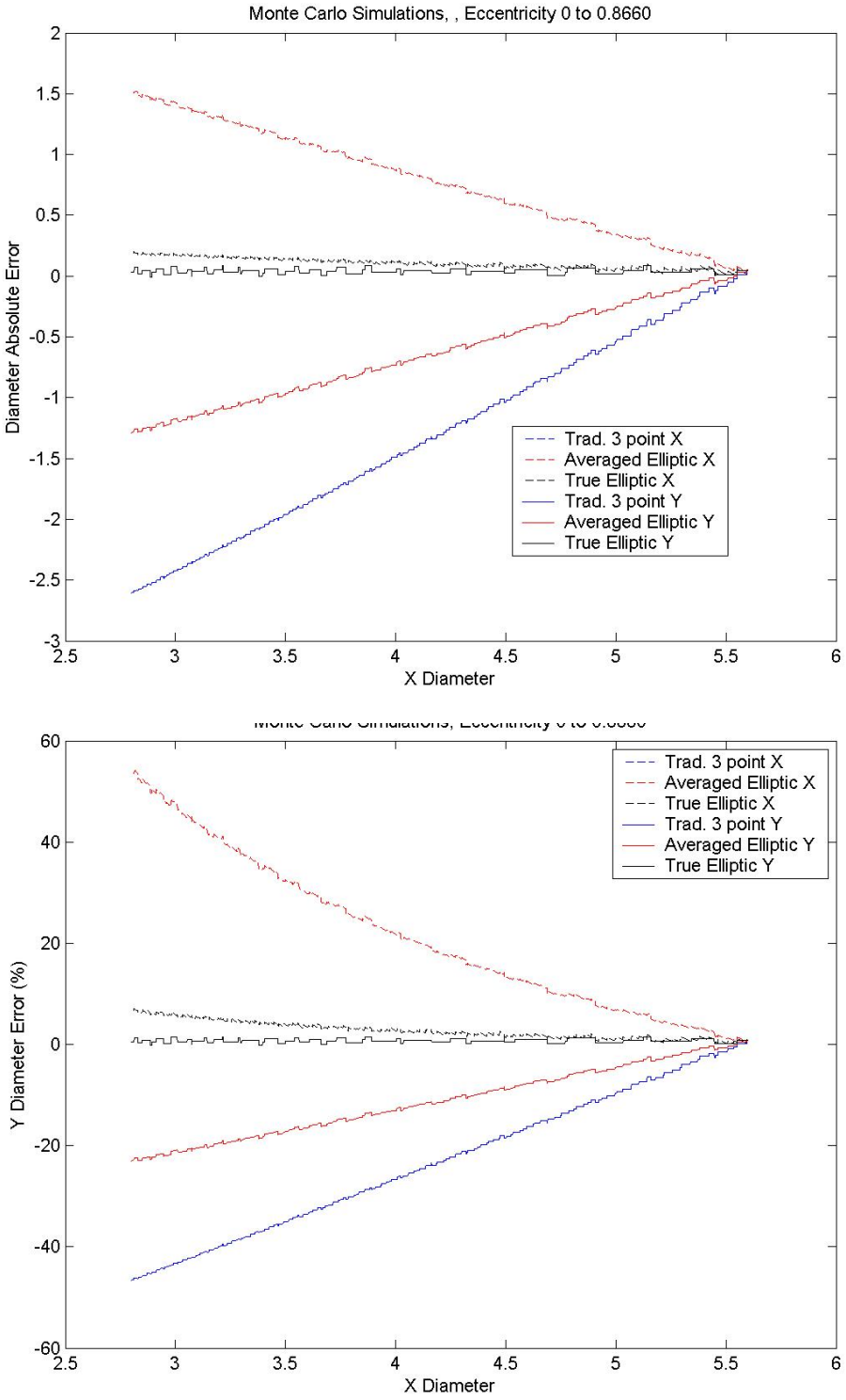

Figure 3.11: Error in the x and y diameter measurements vs. x diameter

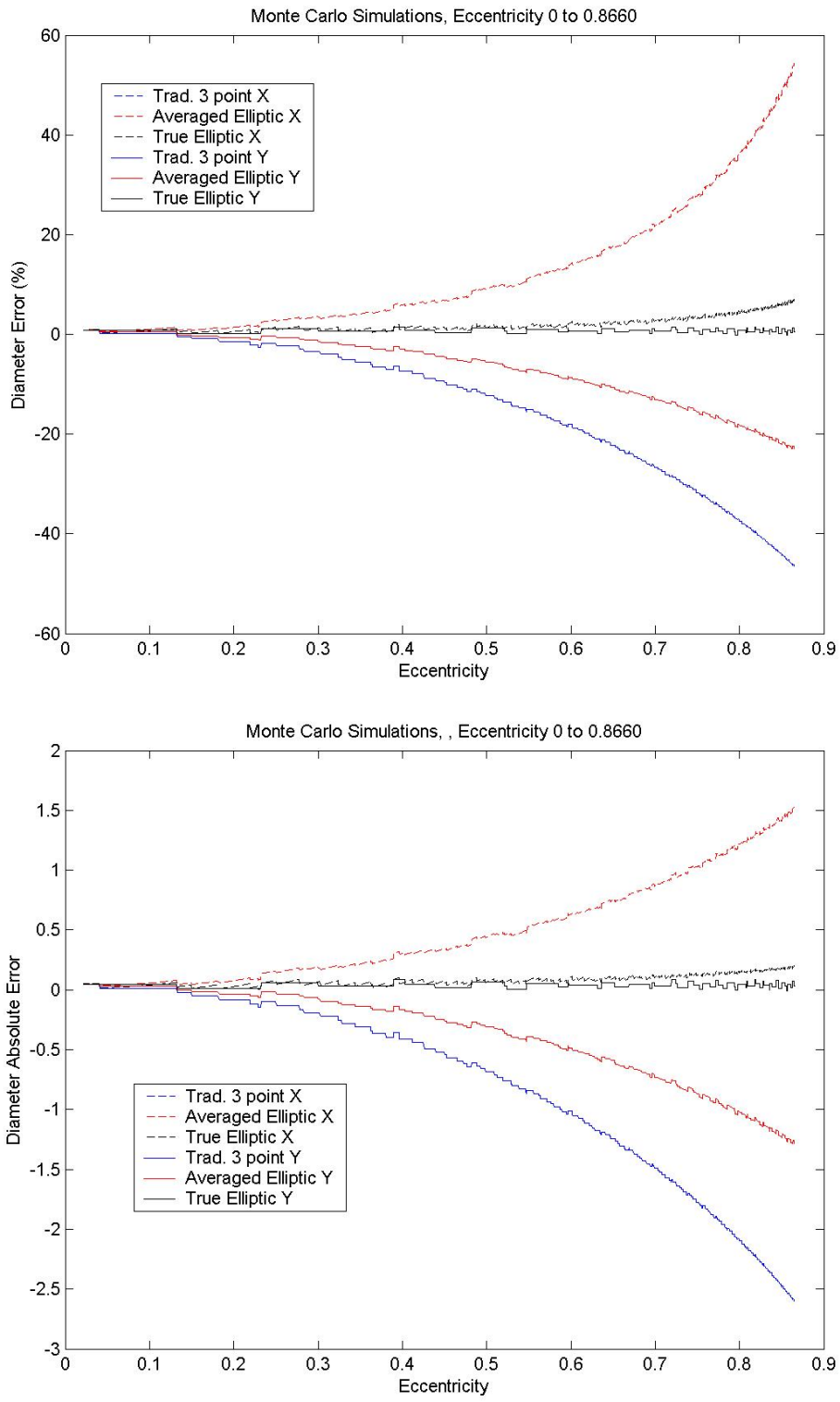

Figure 3.12: X and Y diameter vs. Eccentricity for each sizing method

Figures 3.11 and 3.12 above shows that the true elliptical sizing method exhibits a correlation coefficient of 1.00 with the 3 point Gaussian in relation to x diameter. The averaged elliptic method exhibits diverging error in the x and y diameter measurement as eccentricity increases. This phenomenon should be expected, since the averaged elliptic method uses the average of the two diameters and assumes a spherical particle profile. Therefore, when the x diameter is less than the y diameter, the averaged elliptic method will overestimate the x diameter and underestimate the y diameter. This behavior is clearly visible in Figures 3.11 and 3.12. The true elliptic sizing method exhibits the lowest error in the y direction, since the true elliptic method is the only method that performs a true sizing scheme in the y direction. Figures 3.11 and 3.12 show the behavior of each sizing method with respect to diameter and eccentricity. Figure 3.12 shows that the true elliptical sizing method performs identically with the traditional 3 point Gaussian sizing scheme in the x direction. However, the 3 point Gaussian method exhibits error that reaches a level of -50% at an eccentricity of 0.8660, which corresponds to an axis ratio x/y of 0.50.

Another method for calculating the error associated with the various sizing methods is the area estimation. In this section, the actual area was compared to the estimated area by the various sizing schemes. Therefore, this section deals with the area in the projected area of a particle image in DPIV data. The area error results from the Monte Carlo Simulations are shown below in Figure 3.13. The error was plotted as a function of eccentricity. For the data shown in Figure 3.13, the x axis was considered to be the semimajor axis.

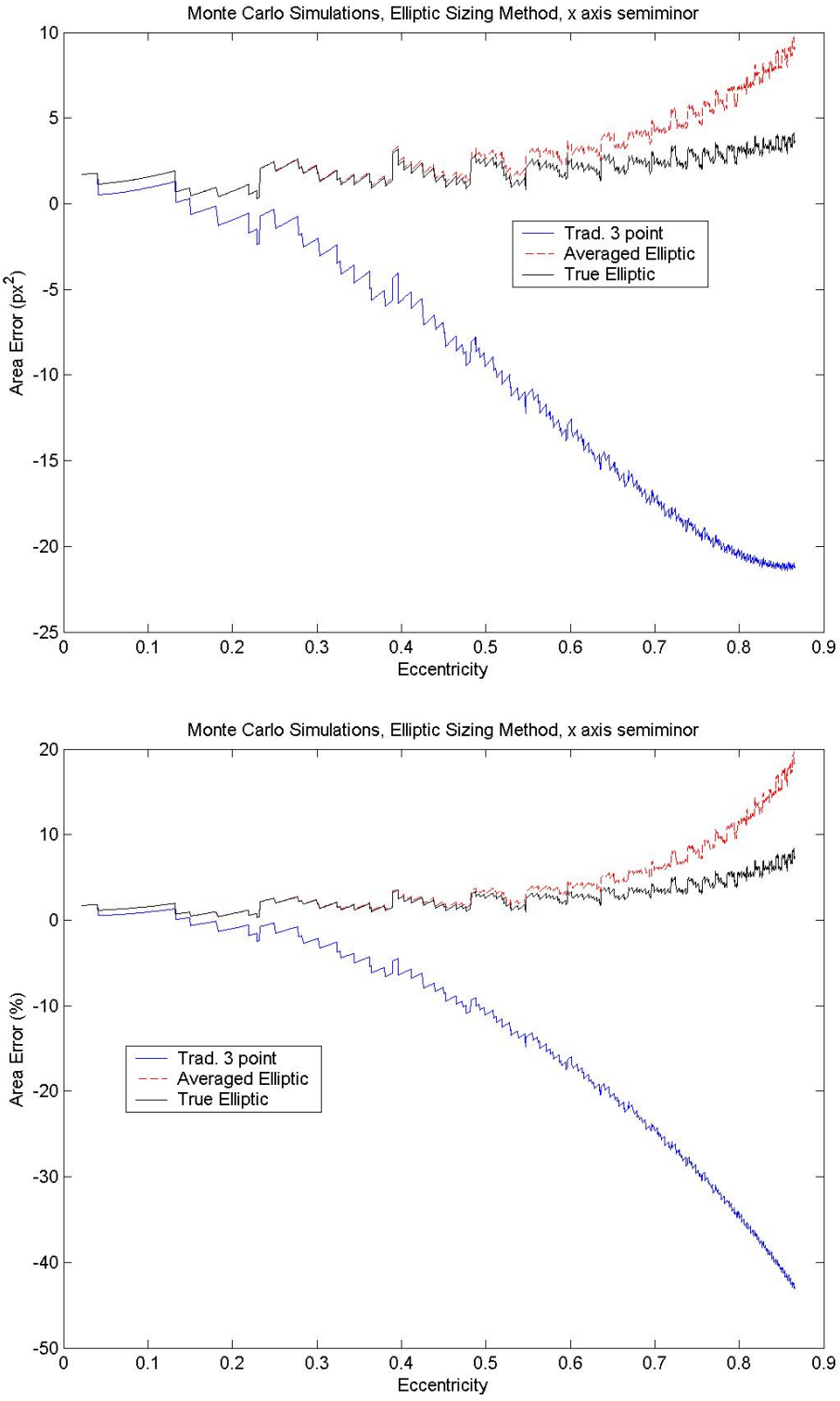

Figure 3.13: Area absolute and percent error for all sizing methods

Figure 3.13 shows that the pixel intensity discretization introduces significant error into the measurement of particle area. The errors are higher than the theoretical errors by approximately 10 to 20 percent. However, the trends in Figure 3.9 agree with the theoretical findings in Section 3.3.1 for the averaged elliptic method. The true elliptic method exhibits higher error than the traditional 3 point method for eccentricities less than 0.60. The error for the averaged elliptic method is lower than the traditional 3 point Gaussian method by approximately 5% at an eccentricity of 0.03. The error is decreased by using the averaged elliptic method by approximately 80 percent when compared to the traditional 3 point Gaussian method. These results show that the averaged elliptic method performs the best out of the three methods tested in this section.

3.4 Conclusions and Future Work.

In this chapter, an elliptical sizing methodology was introduced and tested using Monte Carlo simulations. These studies found that for particles of elliptical profile, the averaged elliptic method performs the best in the measurement of particle area. The trends seen in the Monte Carlo Simulations agree with the trends predicted by theory. Therefore, the elliptical sizing method has been theoretically introduced and validated experimentally using Monte Carlo Simulations.

Future work in the particle sizing area should concentrate on the development of more adaptive sizing algorithms that can dynamically adapt to size a given particle based on its intensity profile. Monte Carlo simulations should be performed in order to confirm the theoretically-improved performance of the elliptical sizing method. The next step in the evolution of the Gaussian sizing methods is the development of a rotation for the elliptic Gaussian profile and conversion from the pixel domain to a rotated pixel domain. This rotated elliptic Gaussian profile could accurately detect particles that are deformed and not restricted to the normal Cartesian coordinate system. This sizing scheme could either perform a brute force axis rotation, or utilize the assumption that the intensity is jointly Gaussian and dependent with correlation coefficient ρ. New profiles could also be explored for future sizing value with streaked particles. Two profiles of particular interest are the log-normal normal independent (LNNI) and the Rayleight normal independent (RNI) probability density functions. These functions are summarized below. These profiles, along with rotation techniques, could provide a powerful tool for the estimation of diameter and particle shape using PIV.

3.4.1 Log Normal / Normal Independent (LNNI) PDF.

For the LNNI probability density function, two random variables x and y were considered to be independent random variables. The x r.v. was considered to be log-normally distributed with standard deviation σ_x and mean value μ_x. The y r.v. was considered to be normally distributed with standard deviation σ_y and mean value μ_y. For a log-normally distributed variable x, the pdf is defined as follows:

$$f_X(x) = \frac{1}{\sigma_x \sqrt{2\pi}} e^{\left(\frac{\ln(x) - \mu_x}{2\sigma_x}\right)^2} \quad \text{(Eq. 3.20)}$$

For a normally distributed variable y, the pdf is defined as follows:

$$f_Y(y) = \frac{1}{\sigma_y \sqrt{2\pi}} e^{\left(\frac{y - \mu_y}{2\sigma_y}\right)^2} \quad \text{(Eq. 3.21)}$$

For independent r.v.'s, the joint pdf can be expressed as (Stark and Woods, 1986):

$$f_{XY}(x, y) = f_X(x) * g_Y(y) \quad \text{(Eq. 3.22)}$$

Therefore, the joint pdf for an LNNI system can be written as:

$$f_{XY}(x, y) = \frac{1}{2\pi\sigma_x\sigma_y} e^{\left(-\left\{\left(\frac{\ln(x) - \mu_x}{2\sigma_x}\right)^2 + \left(\frac{y - \mu_y}{2\sigma_y}\right)^2\right\}\right)} \quad \text{(Eq. 3.23)}$$

where σ_x is the standard deviation of r.v. x, σ_y is the standard deviation for r.v. y direction, μ_x is the mean of r.v. x , and μ_y is the mean of r.v. y.

Figures 3.14 and 3.15 below show the a 2-D probability density function with x as a log-normal random variable with σ_x = 0.80 and μ_x = 1.00, and y as a Gaussian random variable with σ_y = 0.30 and μ_y = 0.00. The variables in these plots are assumed to be independent random variables x and y. This pdf may prove to be extremely useful in simulating streaked particles. The parameters σ_x and μ_x determine the skewness and length of the pdf's "tail." The parameters σ_y and μ_y can be manipulated to simulate particles of larger diameter. This probability density function allows the simulation of particles that exhibit skewness and streaking characteristics.

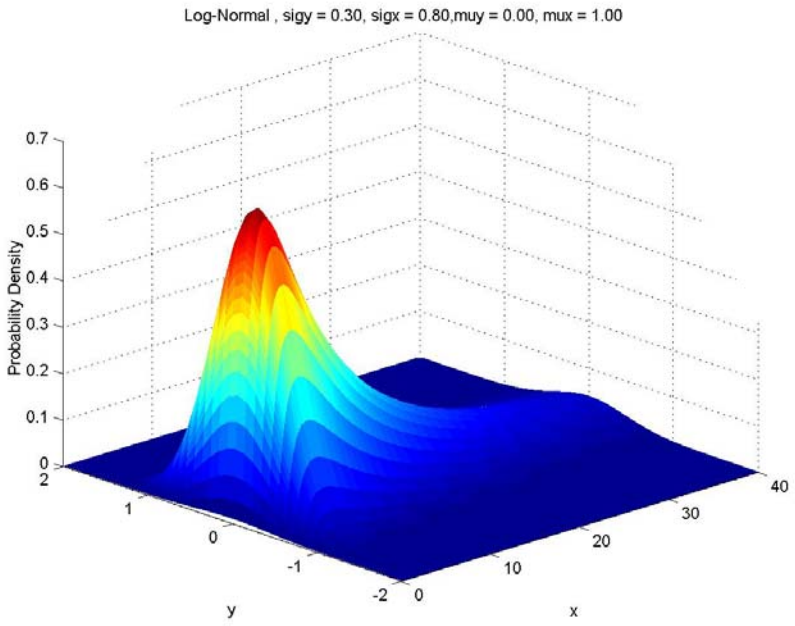

Figure 3.14: Log-Normal Surface Plot for $\sigma_x = 0.80$, $\sigma_y = 0.30$, $\mu_x = 1.00$, $\mu_y = 0.00$

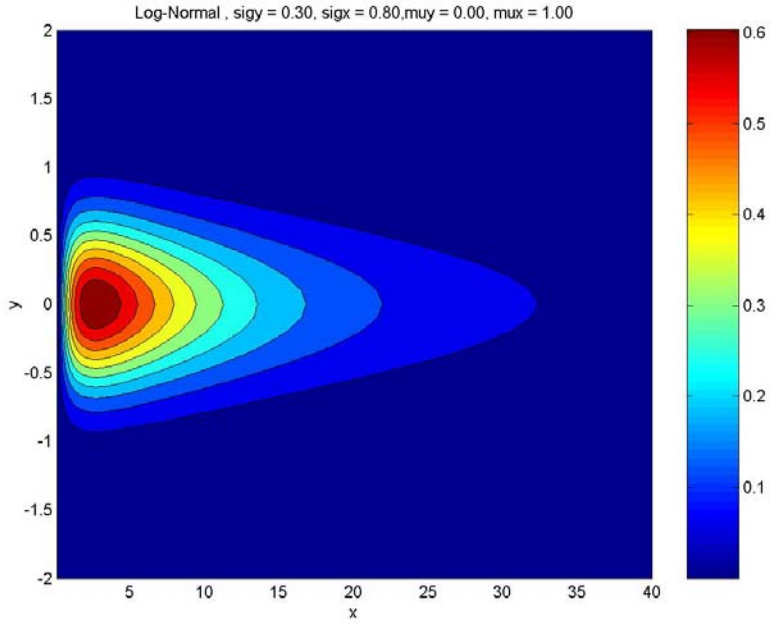

Figure 3.15: Log-Normal Contour Plot for $\sigma_x = 0.80$, $\sigma_y = 0.30$, $\mu_x = 1.00$, $\mu_y = 0.00$

3.4.2 Rayleigh Normal Independent (RNI) PDF.

For the RNI probability density function, two random variables x and y were considered to be independent random variables. The x r.v. was considered to be Rayleigh distributed with skewness

factor s. The y r.v. was considered to be normally distributed with standard deviation σ_y and mean value μ_y. For a Rayleigh distributed variable x, the pdf is defined as follows:

$$f_X(x) = \frac{x}{s^2} e^{-\left(\frac{x^2}{2s^2}\right)} \quad \text{(Eq. 3.24)}$$

For a normally distributed variable y, the pdf is defined as follows:

$$f_Y(y) = \frac{1}{\sigma_y \sqrt{2\pi}} e^{\left(\frac{y-\mu_y}{2\sigma_y}\right)^2} \quad \text{(Eq. 3.25)}$$

For independent r.v.'s, the joint pdf can be expressed as (Stark and Woods, 1986):

$$f_{XY}(x, y) = f_X(x) * g_Y(y) \quad \text{(Eq. 3.26)}$$

Therefore, the joint pdf for an RNI system can be written as:

$$f_{XY}(x, y) = \frac{1}{s^2 \sigma_y \sqrt{2\pi}} e^{\left(-\left\{\left(\frac{x^2}{2s^2}\right)+\left(\frac{y-\mu_y}{2\sigma_y}\right)^2\right\}\right)} \quad \text{(Eq. 3.27)}$$

Figures 3.16 and 3.17 below show the a 2-D probability density function with x as a log-normal random variable with s = 6.00, and y as a Gaussian random variable with σ_y = 0.20 and μ_y = 0.00. The variables in these plots are assumed to be independent random variables x and y. This distribution may be useful in quantifying particles that are slightly streaked or skewed. The parameter s determines the skewness of this distribution The parameters σ_y and μ_y can be manipulated to simulate particles of larger diameter. This probability density function allows the simulation of particles that exhibit noncircular or skewed profiles.

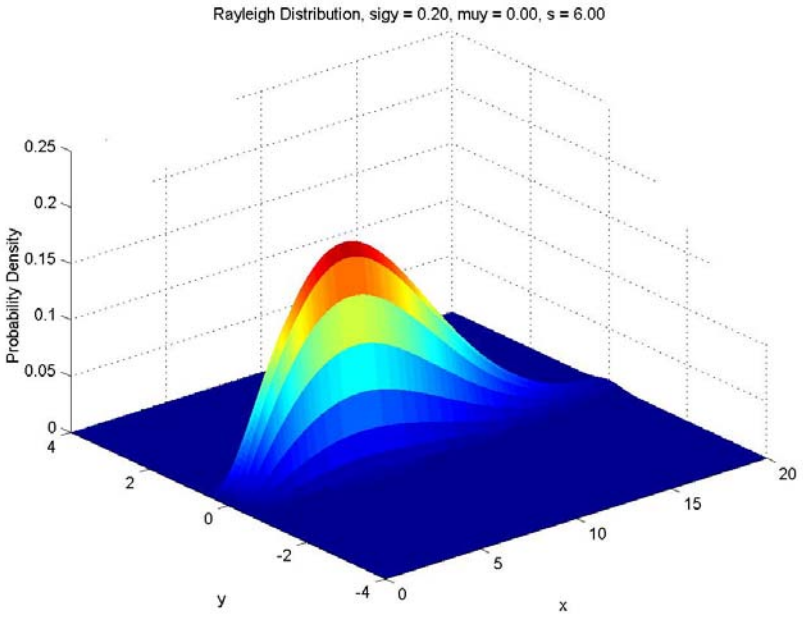

Figure 3.16: Log-Normal Surface Plot for $\sigma_y = 0.20$, $\mu_y = 0.00$, s = 6.00

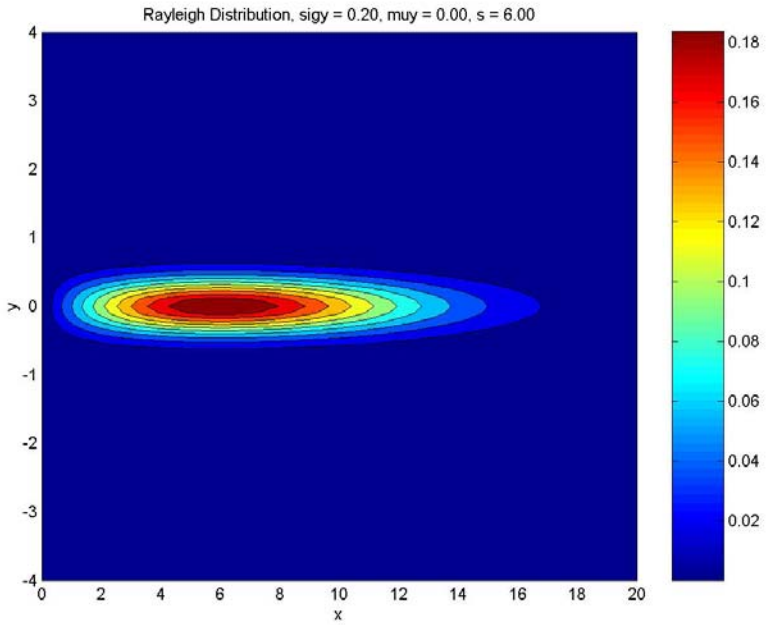

Figure 3.17: Log-Normal Contour Plot for $\sigma_y = 0.20$, $\mu_y = 0.00$, s = 6.00

These probability density functions approximate the shape of a streaked particle, and therefore may be of use in data recovery and high speed flow experiments. Future work should also include

the application of the elliptical sizing technique to the other methods, including the four point Gaussian, continuous four point Gaussian, and least squares sizing methods.

3.5 Summary of Original Contribution

In this Chapter, the major original contribution is the development of a Gaussian particle sizing method that is not limited to spherical particles. The method was confirmed with initial experimental Monte Carlo simulations. The potential of this method is apparent from the theoretical and experimental analysis presented in this chapter. The work on the development of the elliptical sizing method opens a door for the application of the sizing methods to elliptical and deformed seed particles in DPIV data sets, which represents a first next step in the development of advanced particle sizing methods. The work presented in this chapter is intended as an initial step for the continuation of the development of elliptical sizing algorithms.

Chapter 4

4 WALL SHEAR EXPERIMENTS

4.1 Introduction

A major aim of this work is to quantify the accuracy of wall velocity estimation using DPIV. Velocity measurement error for DPIV has been quantified in the past (Huang et al., 1997). Even in the presence of strong velocity gradients the accuracy of the velocity measurements is better than 0.1 pixels (px) for state-of-the-art systems. However, in the case of wall-bounded flows, cross-correlation induced spatial averaging effects can significantly affect the measurement due to very strong localized shear rates. The particle pattern displacements are determined with sub-pixel resolution from the cross-correlation peak for each interrogation window, using a Gaussian fit that is applied to the correlation coefficient matrix. Detailed analyses of these methods can be found in several of the referenced papers in this work (Marxen et al., 2000, Meunier and Leweke, 2003, Raffel et al., 1998, Wereley and Meinhart, 2001, Nogueira et al., 1999). For near wall measurements the cross-correlation signal to noise ratio is often compromised by reduced seeding density compared to the outer flow.

Evaluation of near-wall velocities from experimentally determined DPIV flow fields is most affected by the effect of spatial averaging due to window interrogation size. This is particularly true as the shear rate increases, which effectively skews the correlation matrix, the consequence of which is the inability of the conventionally utilized Gaussian three-point estimator to accurately determine the true displacement at the center of the window (Marxen et al., 2000). The signal is dominated by the flow away from the boundary due to higher velocities and better seeding, density causing a biasing of the displacement estimation. Only the effect of velocity gradient on the measurement accuracy will be considered here, as the near wall seeding is a system-dependent parameter.

4.2 Wall Shear Methods and Materials

Monte Carlo Simulations were performed in order to test the accuracy of several DPIV algorithms when measuring wall shear. One hundred artificial Couette flow images were created using in-house artificial image generation software for each shear rate studied in this work. In order to compare the error associated with DPIV measurements of velocity under velocity gradients, low shear rate images were generated in order to create centerline displacements of 0.1 to 0.5 pixels in 0.1 pixel increments. The shear rates used to produce these centerline displacements were 0.025, 0.050, 0.075, 0.100, and 0.125 pixels per pixel. Shear rates of 0.0625, 0.125, and 0..25 pixels per pixel were examined in order to determine the effects of increased shear rate on DPIV performance. The artificial images were then analyzed using several different DPIV methods. The methods tested in this work were no discrete window offset DPIV (single-pass DPIV), multi-grid DPIV (traditional DPIV algorithm), and a novel ultra-DPIV method developed in our laboratory. After the artificial data was analyzed using each DPIV method, the mean, RMS, and total errors were calculated for each case. The flow-field used in these experiments is shown below in Figure 4.1.

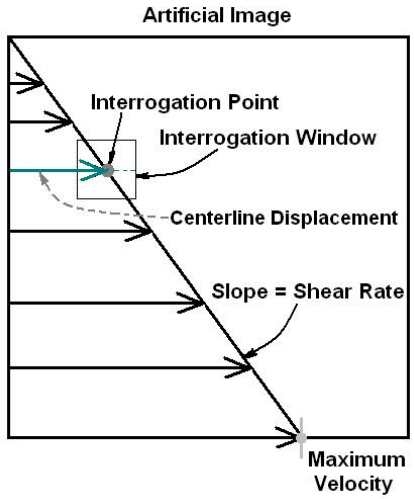

Figure 4.1: Artificial Image Diagram for Wall Shear Experiments

In order to obtain the desired shear rates, maximum velocities of 16, 32, 64, 128, and 256 were used in the artificial image generation software.

For the low shear portion of this work, maximum velocities of 6.4, 12.8, 19.2, 25.6, and 32 were used to yield shear rates of 0.025, 0.050, 0.075, 0.100, and 0.125. These shear rates were targeted in order to produce centerline displacements ranging from 0.1 to 0.5 pixels for error analysis and comparison to traditional PIV error uniform displacement results.

The tracking portion of this work utilized the Hybrid PTV algorithm available in Flow-IQ v2.2 to calculate the error associated with particle tracking in a shear flow. A search radius of 3 pixels was used in conjunction with No Discrete Window Offset PIV and 3 point Guassian sizing to track the particles in the artificial Couette images. The velocities from PTV were then compared to the known velocity at the particle's y postion obtained from the sizing algorithm and errors were plotted as a function of displacement for the low shear rates discussed above.

4.3 Wall Shear Results

The first goal of the wall shear portion of this work was to characterize the expected error associated with wall velocity measurements using DPIV. The wall shear characterization performed in this work was divided into two sections, a high shear section and a low shear section. The high shear section studied Couette flows with velocity gradients up to 1 pixel per pixel. The low shear section targeted shear rates that would produce centerline displacements of 0 to 0.5 pixels in 0.1 pixel increments.

4.3.1 Low Shear Rate Study

The shear rates examined in the high shear portion of this work were 0, 0.025, 0.05, 0.075, and 0.100, and 0.125 pixels per pixel shear rate. These shear rates produced the desired centerline displacement of 0 to 0.5 pixels at the first measurement point. The images generated for this work had zero background noise in order to isolate the effects of shear rate on the velocity error. Procedures identical to the high shear rates were used for the analysis of the low shear images. Errors were plotted to compare the performance of the various methods at different window sizes. Figure 4.2 below shows the total error for all methods studied in this work with a starting interrogation window of 64 pixels.

Figure 4.2 shows that the NDWO method has the highest error at a starting interrogation window of 64. The conventional multigrid method exhibits a spike in bias and rms error at centerline

displacements of 0.4 and 0.5 pixels. The DADPIV method, however, performs consistently over the range of displacements shown in Figure 4.2. The DADPIV and multigrid methods exhibit similar behavior at displacements ranging from 0 to 0.3 pixels.

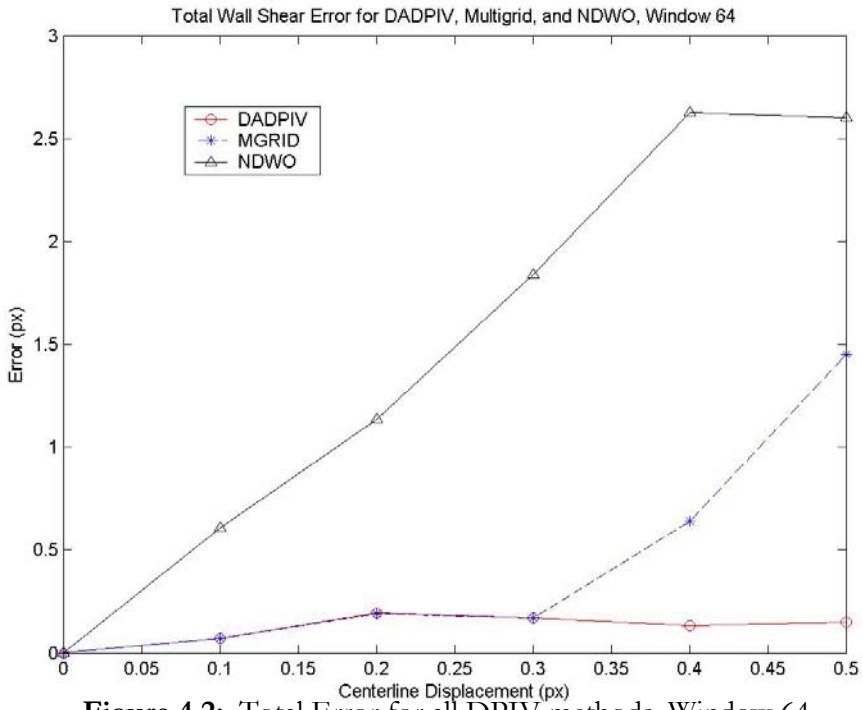

Figure 4.2: Total Error for all DPIV methods, Window 64

Figure 4.3 below shows the total errors for a starting interrogation window of 32 pixels.

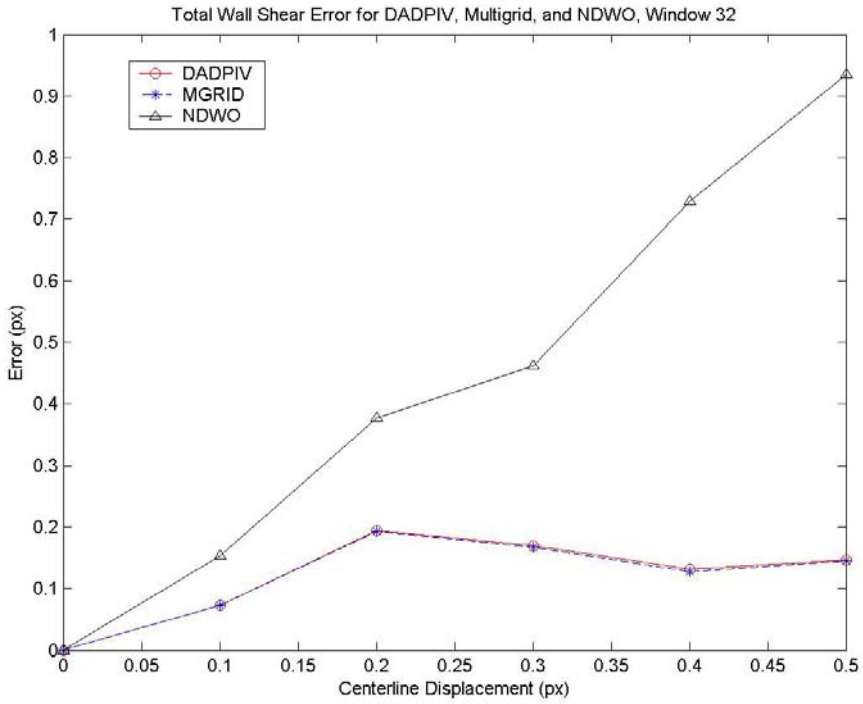

Figure 4.3: Total Error for all DPIV methods, Window 32

According to Figure 4.3, the multigrid and DADPIV algorithms have nearly identical performance over the range 0 to 0.5 pixels for an initial interrogation window size of 32 pixels. As in Figure 4.2, the RMS errors are an order of magnitude less than the associated mean errors. The NDWO method also exhibits a much higher error than the multigrid or DADPIV algorithms. Figure 4.4 below shows the total errors for an initial interrogation window of 16 pixels.

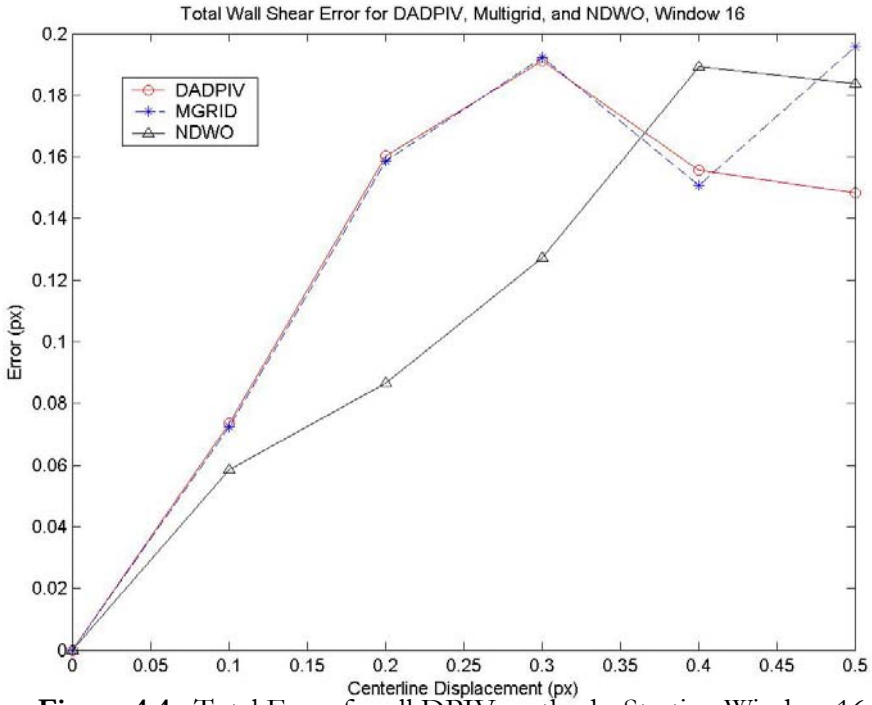

Figure 4.4: Total Error for all DPIV methods, Starting Window 16.

For an initial interrogation window size of 16, the multigrid and DADPIV methods have a higher error than the NDWO method, except at the displacements of 0.4 and 0.5, where all three methods have similar performance.

The above results suggest that for measurement of wall velocity in shear flows that exhibit relatively low velocity gradients, the initial interrogation window size plays a major role in the error associated with the measurement. The NDWO offset case represents the first pass in the multigrid and DADPIV methods. The errors shown in Figures 4.2 through 4.4 were calculated without taking the absolute value. Therefore, as initial interrogation window size increases, the first pass of all of the DPIV algorithms studied in this work overestimates. At an interrogation window size of 64, this overestimation reaches the level of 2 pixels. Since the multigrid and DADPIV methods exhibit a lower true error than the NDWO method, the refining passes in both the multigrid and the DADPIV methods must correct for the overestimation in some manner. The multiple pass methods can only correct by 0.5 pixels in each successive pass. If the overestimation is greater than 0.5 pixels, the multiple pass algorithms may not be able to correct for such an overestimation.

4.3.1.1 Comparison to Uniform Displacement Measurements

The wall shear results were compared to uniform displacement results in order to determine the difference between the measurement error in wall shear and the error associated with uniform displacement, which has been well documented. Figure 4.5 below shows the uniform displacement error in comparison to the wall shear velocity error for a starting interrogation window size of 32 pixels.

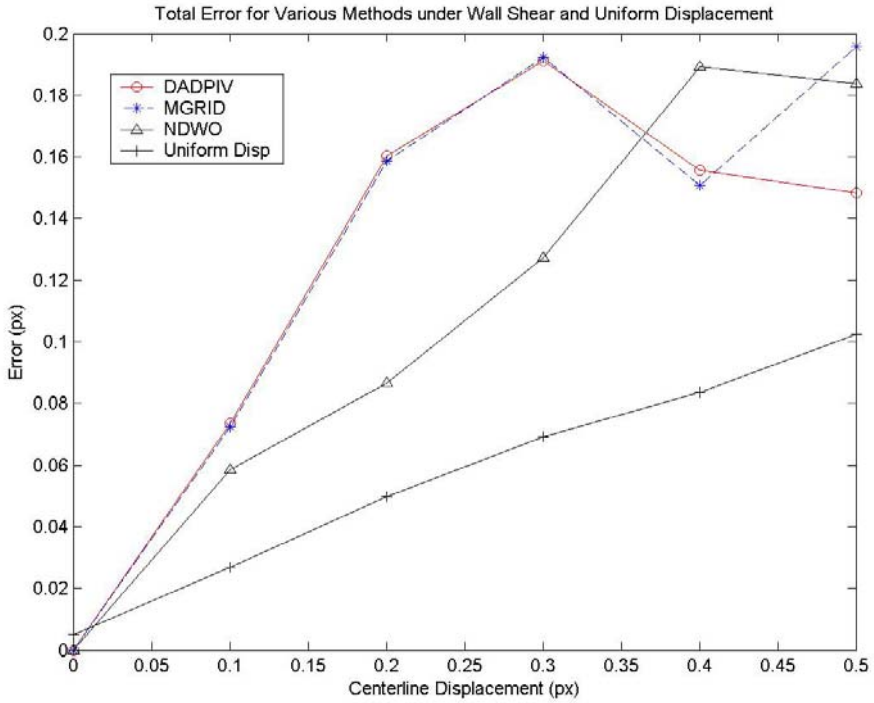

Figure 4.5: Wall Shear Error Compared to Uniform Displacement Error.

Figure 4.5 shows that the error for the shear flows studied in this work are much higher than the error associated with uniform displacement. The errors for uniform displacement agree with the error reported by Huang et al. (1997). Therefore, the introduction of velocity gradients into a flow significantly increases the error associated with DPIV velocity measurements.

4.3.1.2 Tracking Results

The artificial images used in the above analyses were also processed using the Hybrid Particle Tracking Velocimetry routine available in Flow-IQ v2.2. Unlike the PIV results, the tracking results produce a continuous velocity field. The errors at each y location were computed from the output of the Hybrid PTV algorithm. The shear rates analyzed were 0.025, 0.050, 0.075, 0.100, and 0.125 pixels per pixel. The total number of particles successfully tracked for each shear rate is listed below in Table 4.1. These results were obtained using a starting interrogation window of 16, which yielded approximately 5 to 6 particles per interrogation window.

Shear Rate (px/px)	Number of Particles Tracked (per 100 frames)
0.025	7068
0.050	4017
0.075	2748
0.100	1952
0.125	1667

Table 4. 1: Tracked Particle Populations for Each Shear Rate

The 16 starting interrogation window can only reliably resolve up to approximately 4 pixels displacement. For the higher shear rates, an increasing number of particles are in regions where accurate PIV measurement is impossible with a starting window of 16 pixels. Therefore, the number of tracked particles decreases with increasing shear rate.

Since the particle tracking process produces a continuous velocity field, the error can be plotted as a function of the centerline velocity. In order to compute this error, the velocity calculated by the algorithm was compared to the known velocity at the particles distance from the top of the image. The absolute value of the difference between the calculated and expected velocity values was used as the local error in this study.

In order to compare the Hybrid PTV results to the traditional PIV methods, the errors were calculated for the 0 to 1 pixel displacement range. The total error was defined by setting bins around pixel markers for the PTV method, and averaging the error for the measurements within the bin. The results are shown below in Figure 4.6.

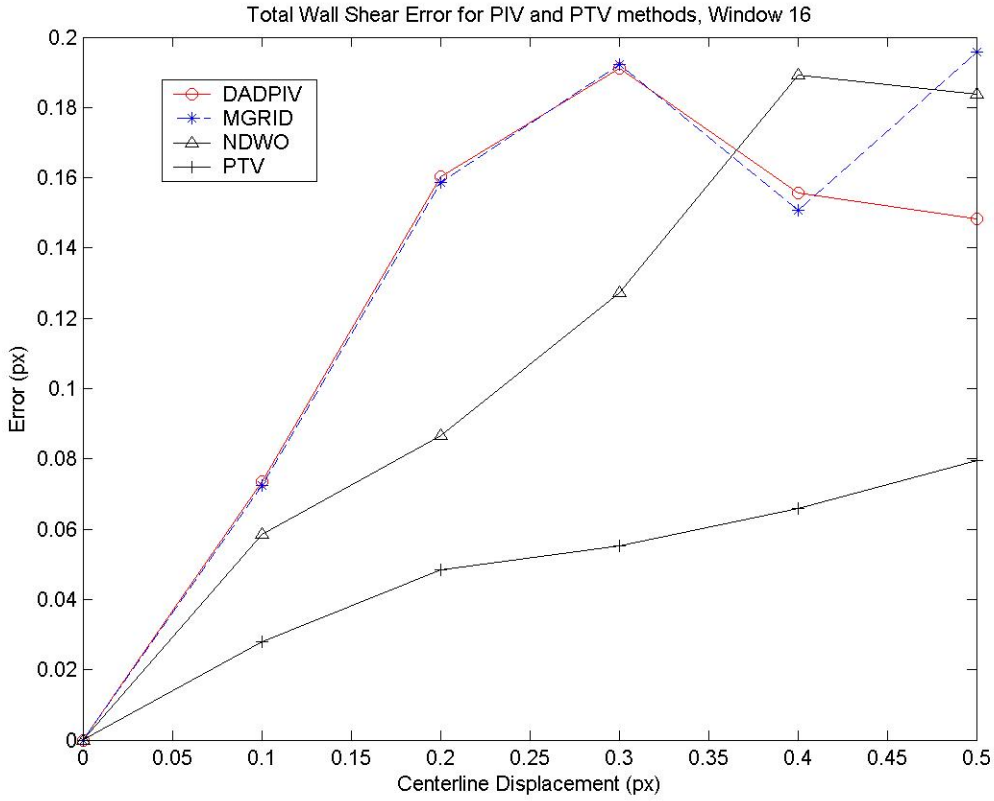

Figure 4.6: Total Error for all PIV methods and PTV

Figure 4.11 above shows that the PTV method performs much better than the PIV methods in the estimation of velocity in shear flows. The error for the PTV method is approximately half that of the PIV methods at corresponding displacements. A larger number of images must be analyzed in order to improve this assessment, however, since the particle populations at higher shear rates are relatively low and unreliable.

4.3.2 High Shear Rate Study

The shear rates examined in the high shear portion of this work were 0.0625, 0.125, 0.25, 0.50, and 1.00 pixels per pixel shear rate. The images generated for this work had zero background noise in order to isolate the effects of shear rate on the velocity error. The no discrete window offset case stands as the control case for these experiments.

For the no discrete window offset (NDWO) case, the interrogation windows were 64, 32, and 16. In this case, there were no consecutive passes performed in order to refine the velocity measurement. The results for the NDWO case are shown below in Figure 4.7.

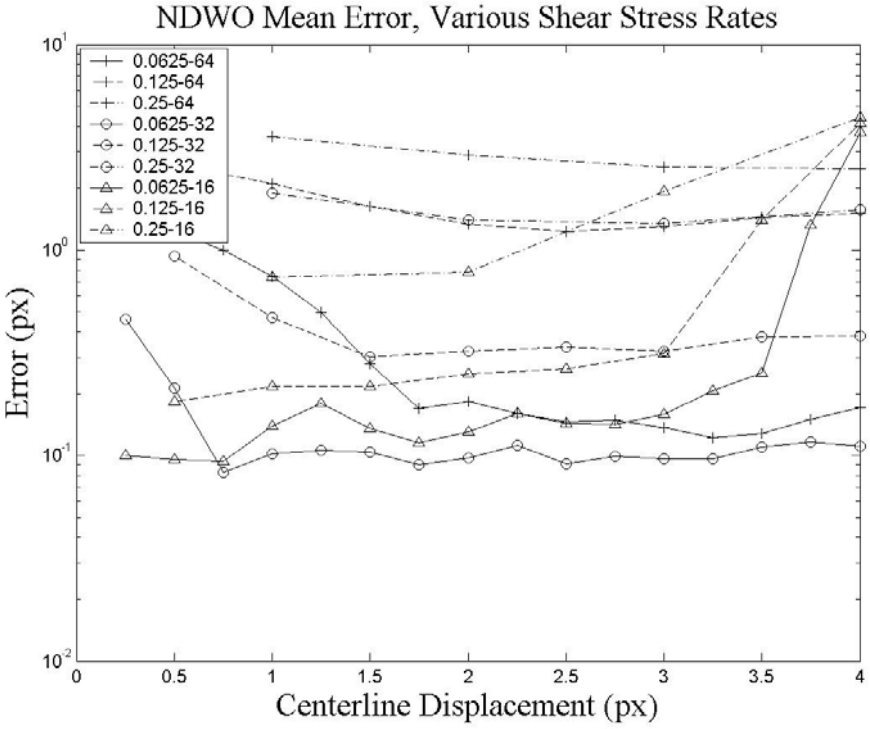

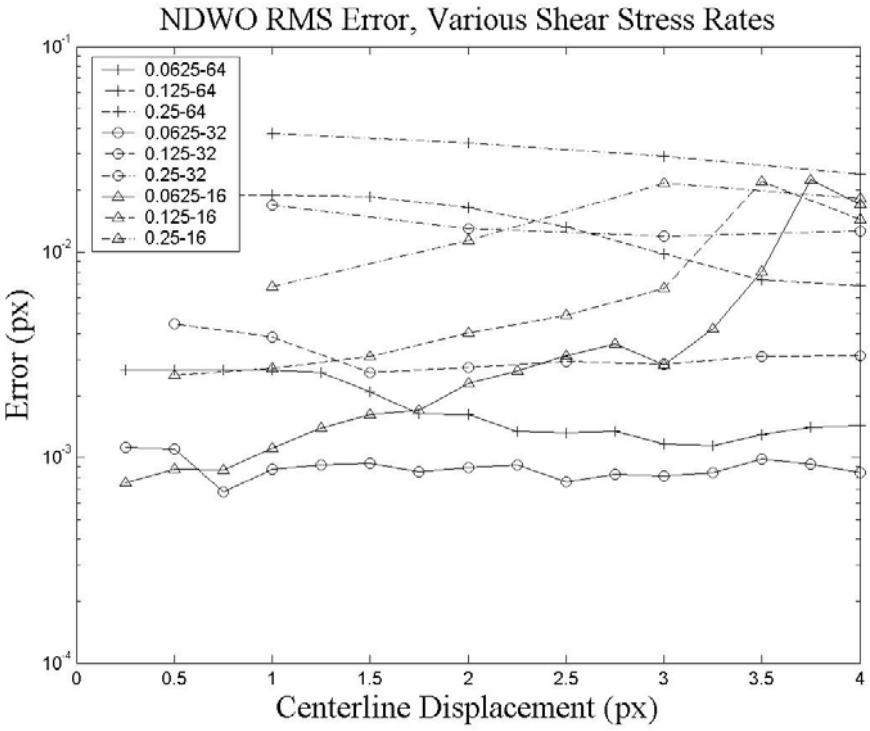

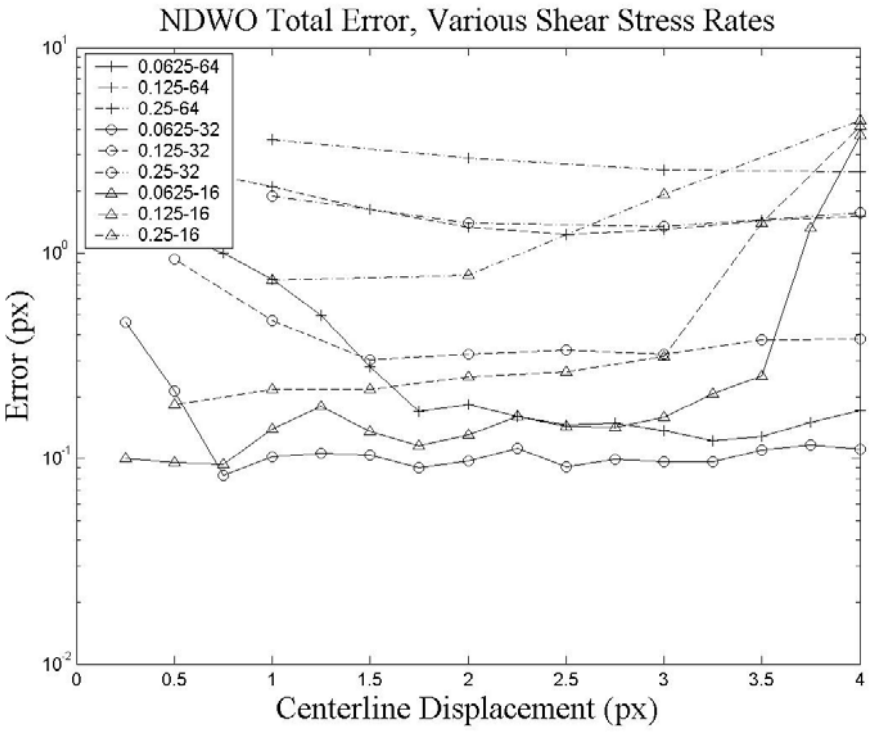

Figure 4.7: Mean, RMS, and Total Error for No Discrete Window Offset.

The trends seen in Figure 4.7 are the same as the trends seen in Figure 4.6. The RMS error is at least an order of magnitude less than the mean error at corresponding shear rates and interrogation window sizes. The shear rate is again the dominant factor in the velocity estimation error. The interrogation window size has an increasing effect on the velocity error as shear rate increases. In the NDWO case, as in the DADPIV case, the error associated with the measurement increases dramatically for every shear rate when the 16 window nears the maximum resolvable displacement of 4 pixels displacement.

Figure 4.8 below shows the mean, RMS, and total error for the conventional multigrid algorithm. The errors presented in Figure 4.6 are for the shear rates of 0.0625, 0.125, and 0.25 with interrogation window sizes of 64, 32, and 16. The error for shear rates of 0.50 and 1.00 were so high that they are not presented in this work. For the 64 window, consecutive window sizes of 64, 32, 16, and 8 were used in the multigrid algorithm. For the 32 window, consecutive window sizes of 32, 16, and 8 were used. Finally, for the 16 window, consecutive window sizes of 16 and 8 were

used. This pattern of window sizes was also used with the dynamically-adaptive DPIV algorithm presented later in this section.

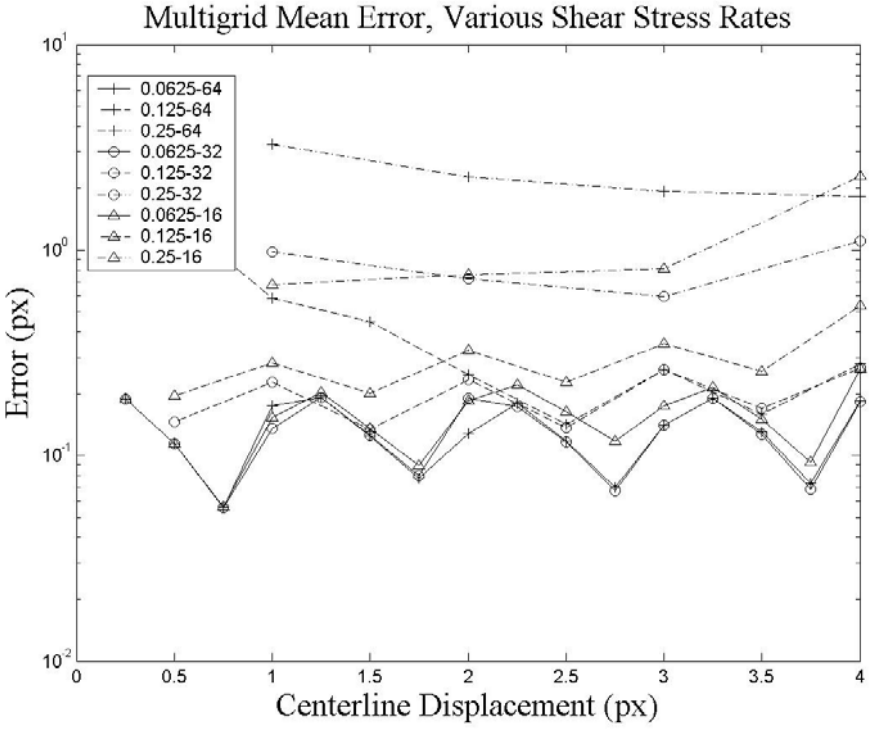

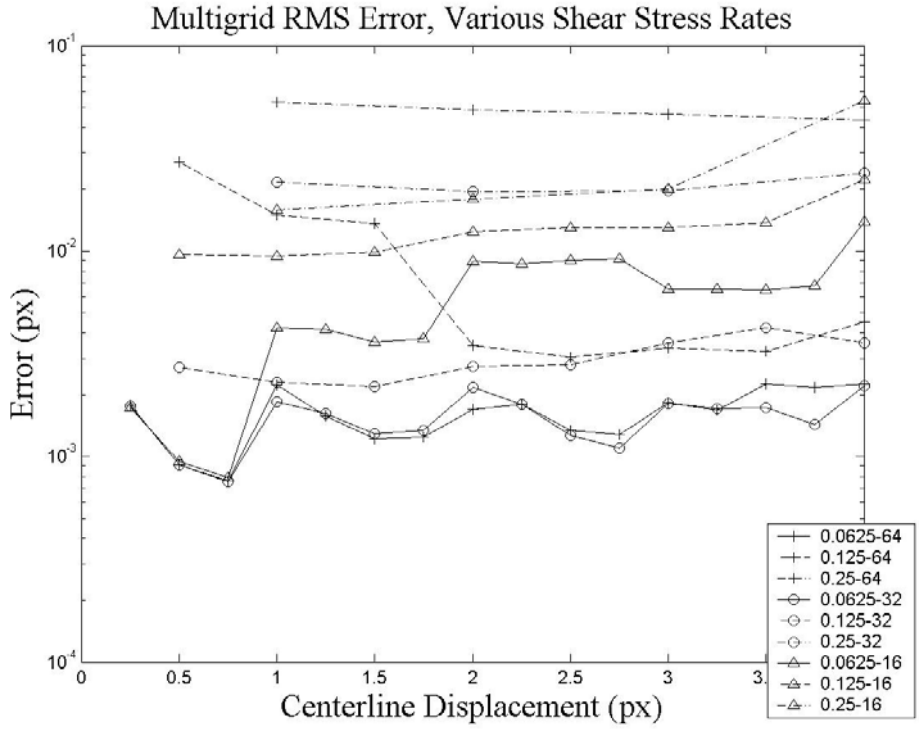

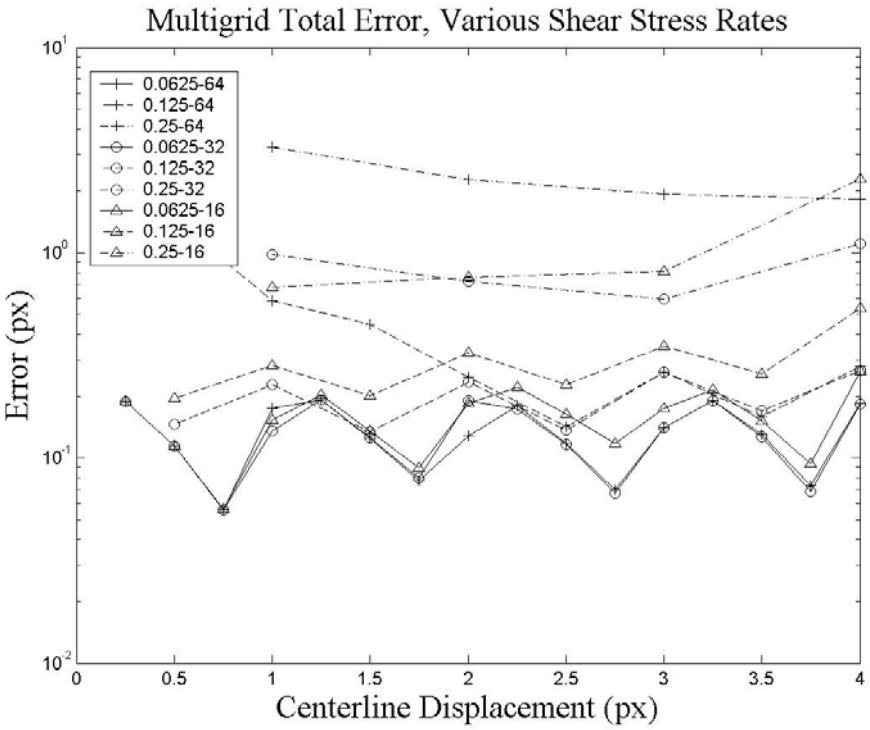

Figure 4.8: Mean, RMS, and Total Error for Multigrid DPIV Algorithm.

There are several important observations to make from Figure 4.6. Firstly, the RMS error is approximately one to two orders of magnitude less than the mean error at corresponding shear rates and interrogation window sizes. Therefore, the total error is almost identical to the bias error. The shear rate (represented as different line types) is clearly the dominant factor in the velocity estimation error. The interrogation window size has a marked effect on the velocity error at the higher shear rates. However, at low shear rates, the interrogation window size does not significantly affect the error associated with the measurement. It should also be noted that as the 16 window nears the maximum resolvable displacement (1/4 window rule) of 4 pixels displacement, the error associated with the measurement increases at shear rates of 0.125 and 0.25.

Figure 4.9 below shows the mean, RMS, and total error for the dynamically adaptive DPIV, or DADPIV, algorithm. Figure 4.7 exhibits many of the same phenomena seen in Figure 4.8. The RMS error is at least an order of magnitude less than the mean error at corresponding shear rates and interrogation window sizes. The shear rate is again the dominant factor in the velocity estimation error. The interrogation window size has an increasing effect on the velocity error as

shear rate increases. In the DADPIV case, the error associated with the measurement increases dramatically for every shear rate when the 16 window nears the maximum resolvable displacement of 4 pixels displacement.

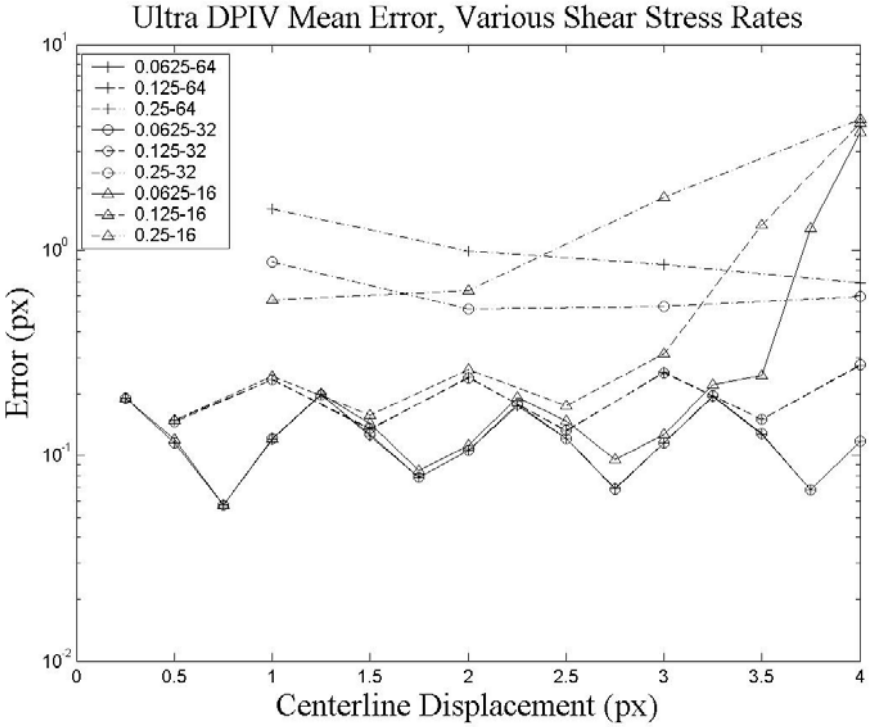

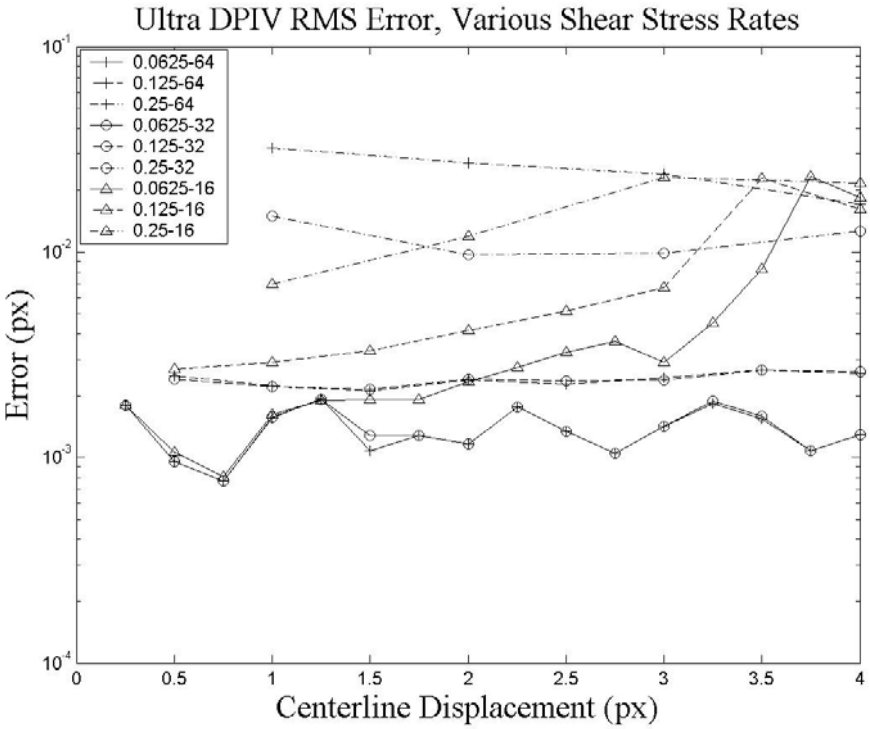

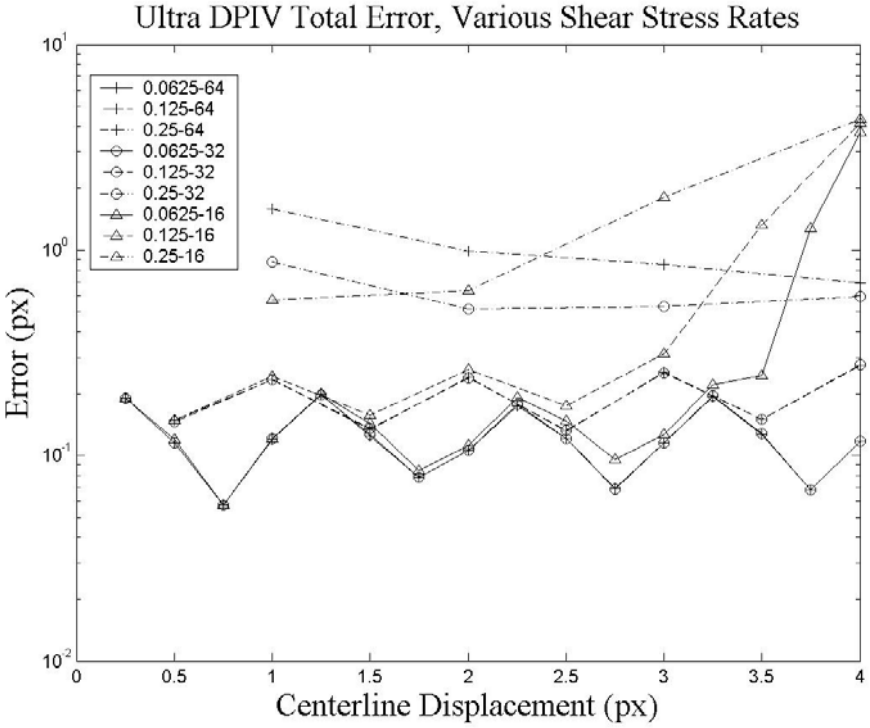

Figure 4.9: Mean, RMS, and Total Error for DADPIV Algorithm.

In addition to comparing the effects of shear rate and interrogation window size on the wall shear velocity measurement using DPIV, the effects of the various algorithms must also be compared. Since the RMS error was found to be an order of magnitude less than the bias error for all of the methods studied, only total error is presented in the remainder of this work. Figure 4.10 below compares the error of the various methods for various shear rates and an initial interrogation window size of 64 pixels.

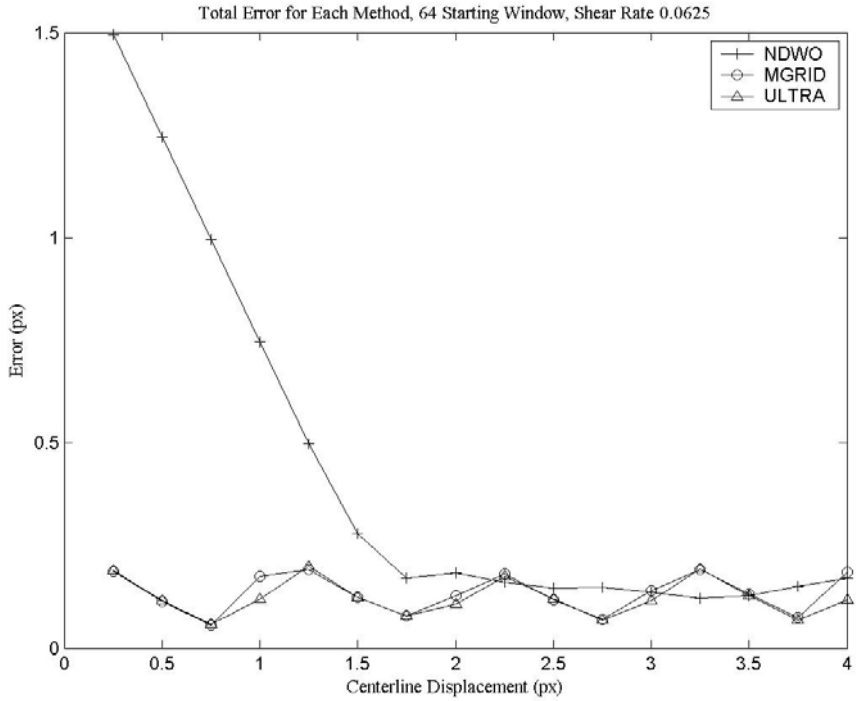
Total Error for Each Method, 64 Starting Window, Shear Rate 0.0625
NDWO
MGRID
ULTRA
Error (px)
Centerline Displacement (px)
0
0.5
1
1.5
0
0.5
1
1.5
2
2.5
3
3.5
4

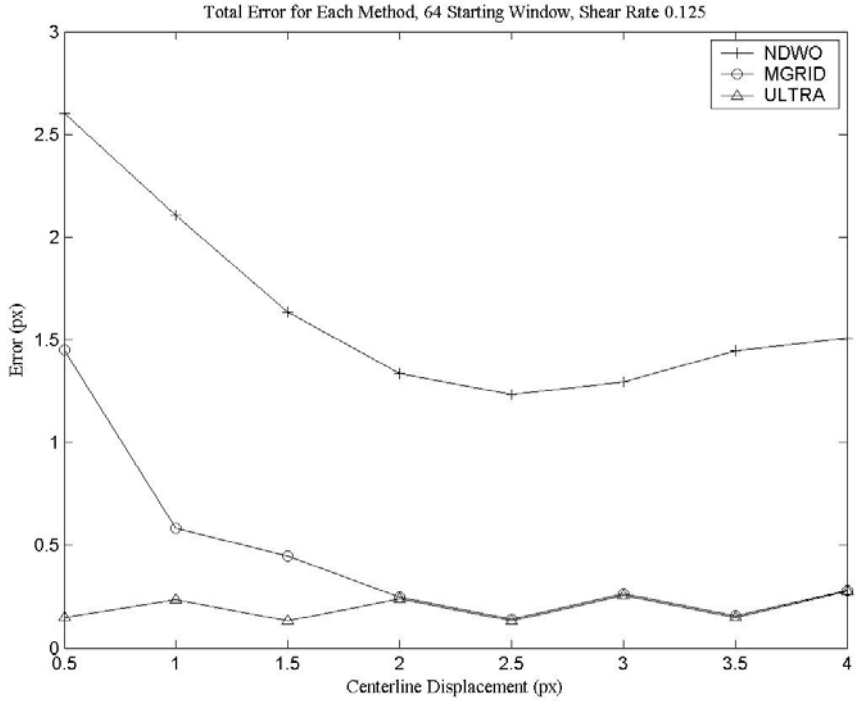
Total Error for Each Method, 64 Starting Window, Shear Rate 0.125
NDWO
MGRID
ULTRA
Error (px)
Centerline Displacement (px)
0
0.5
1
1.5
2
2.5
3
0.5
1
1.5
2
2.5
3
3.5
4

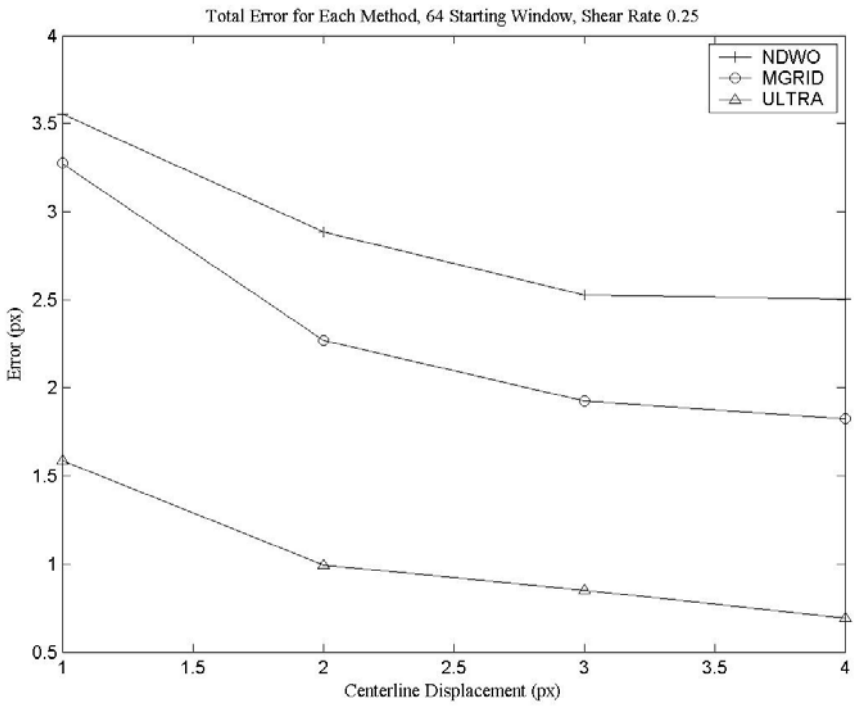

Figure 4.10: Error for Multigrid, DADPIV, and NDWO for Various Shear Rate, 64 Window.

Figure 4.10 shows that for the shear rates of 0.0625, 0.125, and 0.25 pixels/pixel, the NDWO case has the highest error. The traditional multigrid approach has comparable error to the DADPIV approach for a shear rate of 0.0625 pixels per pixel, but higher errors than the DADPIV algorithms for shear rates of 0.125 and 0.25 pixels per pixel. For the 0.25 shear rate, the DADPIV algorithm performs significantly better than the traditional multigrid algorithm and the NDWO method, averaging approximately 2 pixels less total error than the other methods. There appears to be a significant peak locking phenomenon occurring in the multigrid and DADPIV algorithms for a shear rate of 0.0625 and 0.125. Figure 4.11 below shows similar results as Figure 4.10, except for a starting interrogation window of 32 pixels.

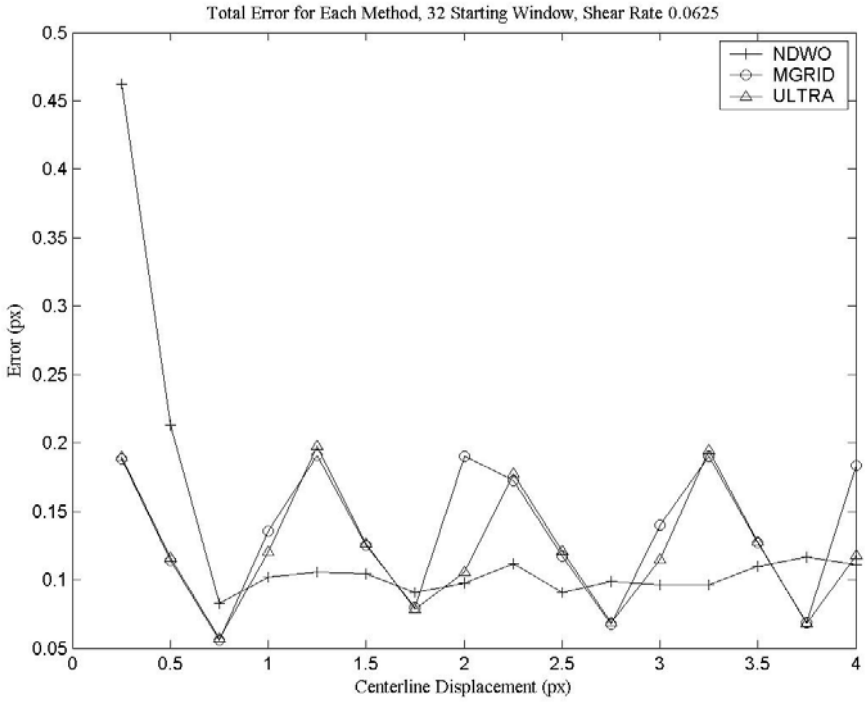
Total Error for Each Method, 32 Starting Window, Shear Rate 0.0625
NDWO
MGRID
ULTRA
Error (px)
Centerline Displacement (px)
0.5
0.45
0.4
0.35
0.3
0.25
0.2
0.15
0.1
0.05
0
0.5
1
1.5
2
2.5
3
3.5
4

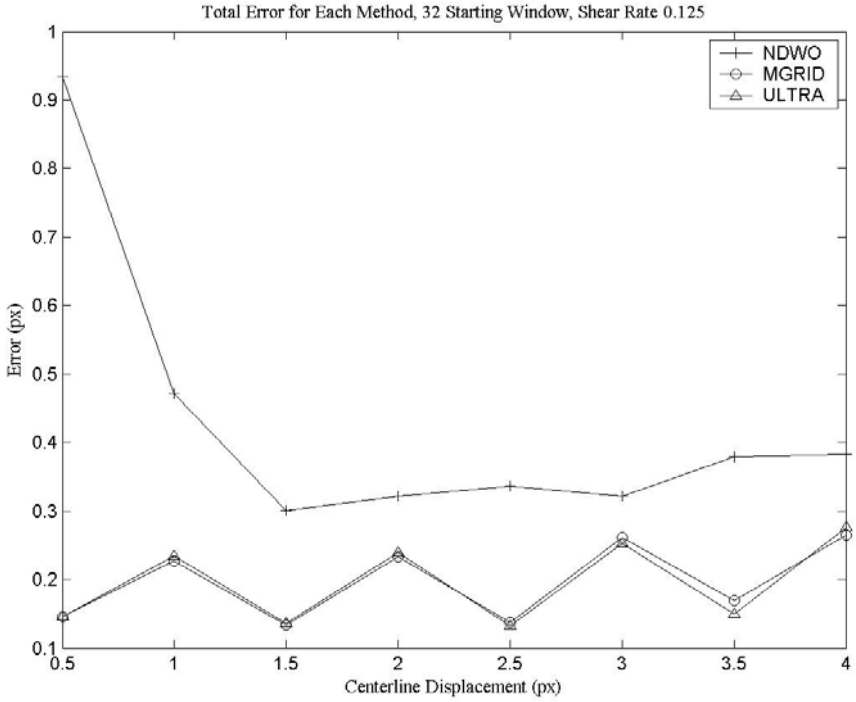
Total Error for Each Method, 32 Starting Window, Shear Rate 0.125
NDWO
MGRID
ULTRA
Error (px)
Centerline Displacement (px)
1
0.9
0.8
0.7
0.6
0.5
0.4
0.3
0.2
0.1
0.5
1
1.5
2
2.5
3
3.5
4

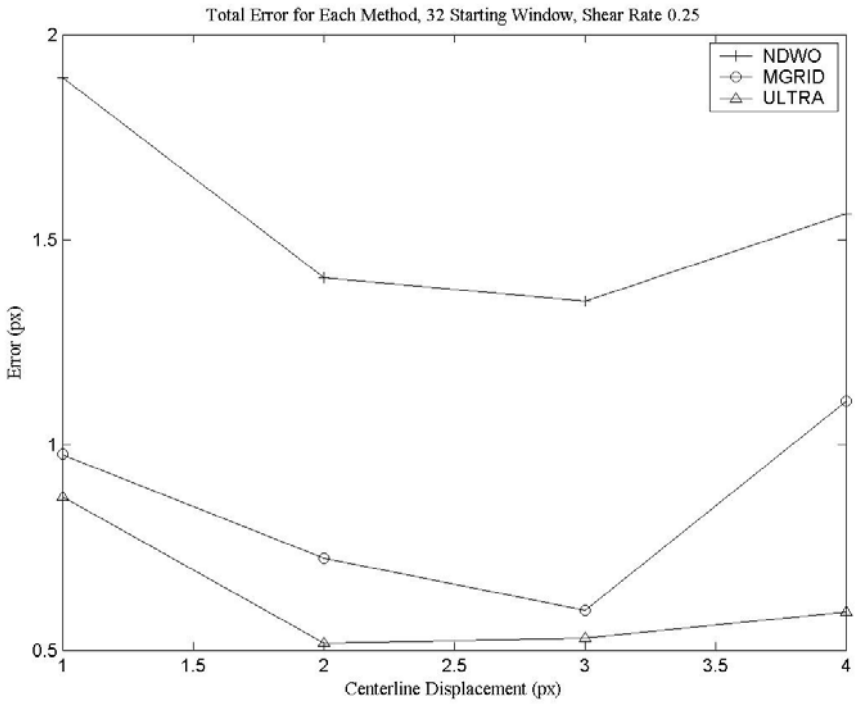

Figure 4.11: Error for Multigrid, DADPIV, and NDWO for Various Shear Rate, 32 Window.

Figure 4.11 hows that for the shear rates of 0.0625, 0.125, and 0.25 pixels per pixel, the NDWO case has the highest error close to the wall, but the peak locking phenomenon causes the multigrid and DADPIV algorithms to have a much higher oscillatory error at greater centerline velocities. The traditional multigrid approach has comparable error to the DADPIV approach for shear rates of 0.0625 and 0.125 pixels per pixel, but higher errors than the DADPIV algorithms for a shear rate of 0.25 pixels per pixel. For the 0.25 shear rate, the DADPIV algorithm performs better than the traditional multigrid algorithm and the NDWO method, averaging approximately 0.12 pixels less total error than the multigrid method and approximately 1 pixel less total error than the NDWO case. The peak locking phenomenon appears again at shear rates of 0.0625 and 0.125. There may be peak locking at the 0.25 shear rate, but the measurement increments may be too coarse to detect the phenomenon.

4.4 Conclusions and Future Work

The wall shear results presented in this work show that velocity gradients produce significant error in PIV measurements. The error associated with PIV measurements increases dramatically with shear rate. Increased interrogation window size also increases the error associated with the measurement because of the inclusion of higher-velocity particles in the interrogation area. The dominant factor in the error is the shear rate, however. This work also showed that the DADPIV method developed in the ESM Fluid Mechanics Laboratory performed better than other PIV algorithms currently in use. The bias error associated with shear flows was shown to be the largest contribution to the error. Methods for the reduction of velocity measurement error in shear flows were introduced, including the power law correction, which reduced the measurement error substantially. Therefore, this work succeeded in characterizing the performance of several PIV algorithms in the measurement of wall shear velocities with a wide range of velocity gradients.

In the wall shear area, more intense methods for correcting the error due to velocity gradients in the flow should be developed. A power law compensation should be explored, and novel correlation peak detection algorithms should be tested in an attempt to improve these errors. Another idea is the development of a correction scheme that will estimate the velocity at the centroid of the linear velocity profile. For a linear profile, the centroid is located at 2/3 of the window size from the top of the window, if the velocity profile is in accordance with Figure 4.1. This and other correction methods will be explored in future efforts.

4.5 Summary of Original Contribution

The major contribution of this chapter was the characterization of the performance of previously-developed PIV methods (multigrid, DADPIV, NDWO PIV) in the measurement of velocity in the presence of a velocity gradient. No new PIV methods or compensation methods were developed in the course of this work. The development of correction schemes for the measurement of wall shear error is left to future researchers in this area. To the knowledge of the author, no other researcher has performed this type of analysis on the error of DPIV measurements in the presence of velocity gradients. Therefore, this chapter comprises the most original and significant contribution contained in this work. This chapter also provides a basic

foundation for more work in the area of wall shear velocity measurement. The programs and algorithms developed in the course of this work will serve to quicken further research in this area.

Chapter 5

5 DPIV DOCUMENTATION AND TEST BED

5.1 DPIV Version 1.0 Documentation

A comprehensive user's manual for DPIV version 2.2 was developed in this work. The full user's manual is included below.

Flow-IQ Version 2.2
Documentation and Help

9/7/2004

Jason B. Carneal
Aeroprobe Corporation

Table of Contents

Introduction

The purpose of this manual is to familiarize the user with the functions of FLOW-IQ version 2.2. FLOW-IQ v2.2 is Digital Particle Image Velocimetry program with built-in image preprocessing, particle sizing, and post-processing tasks. FLOW-IQ v2.2 provides the user with several options not found in other packaged software currently on the market. The program provides excellent functionality in a user-friendly and easy-to-use windows-based environment. FLOW-IQ v2.2 also provides the user with many processing and task options that are novel in nature. This manual presents the functions available in FLOW-IQ v2.2, reviews the use of each function, and provides basic theoretical foundations for the algorithms used in FLOW-IQ v2.2. For more information on the algorithms used in FLOW-IQ v2.2, please review the References section of this manual.

This manual also includes Documentation relating to the test bed supplied with FLOW-IQ v2.2.

Chapter 1: Program Installation

In order to install FLOW-IQ 2.2 on your system, double-click on the Setup.exe in the root directory of the provided CD. The following dialog box will appear:

Use ALT+TAB to switch to other running programs in Windows, and shut them down. Then click on NEXT. The license agreement will appear. After reading through the license agreement, click on NEXT. The following dialog box will appear:

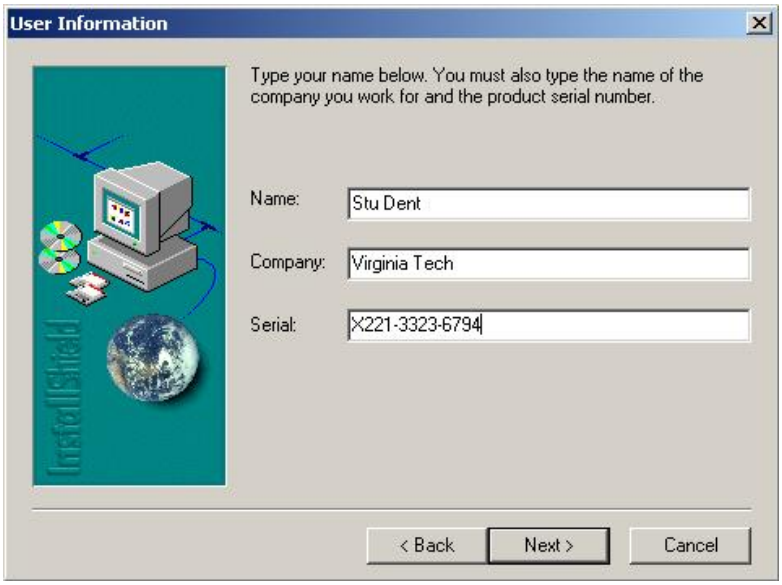

Enter your name, company, and serial number provided with your copy of FLOW-IQ 2.2 in the fields provided. Then click NEXT. Now, the destination folder dialog box will appear:

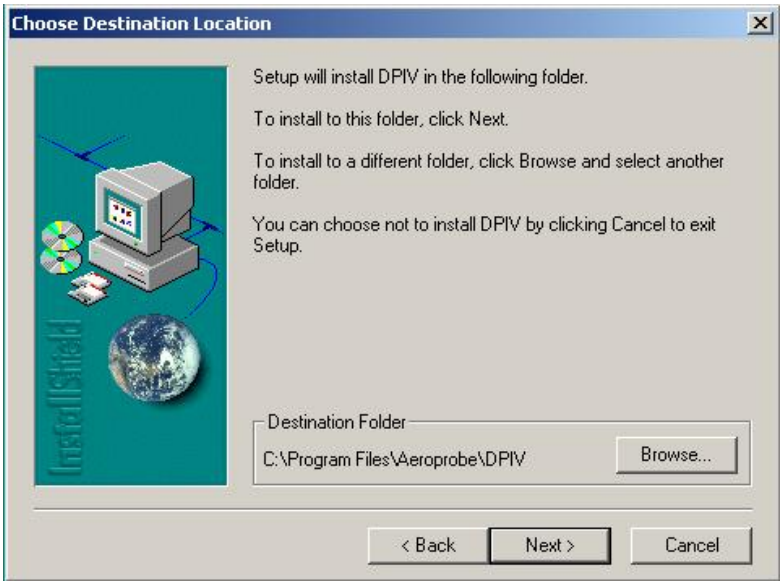

The default directory for installation is C:\Program Files\Aeroprobe\FLOW-IQ. If you wish to install the program to a different folder, click on Browse and find the desired destination folder. Once you have selected the destination folder, click NEXT. Now, the FLOW-IQ 2.2 program is ready to install. If you wish to install the software at this time, Click on NEXT in the following dialog box:

The files for FLOW-IQ will be copied to your computer. When installation is complete, the following dialog box appears:

You may select to view the Read Me file and/or launch FLOW-IQ 2.2 when you are finished installing. Choose the options, and click FINISH to complete the installation of FLOW-IQ 2.2 on your computer.

The installation program automatically creates a shortcut in your Start menu under Start → Programs → FLOW-IQ. Click on FLOW-IQ to start FLOW-IQ 2.2 on your computer.

Chapter 2: Basic Operations

Creating a New Project:

In order to create a new project, either click on File→New, Press Ctrl+N, or click the New icon in the top left corner of the FLOW-IQ GUI. A new project will initialize, as illustrated in Figure 2.1 below.

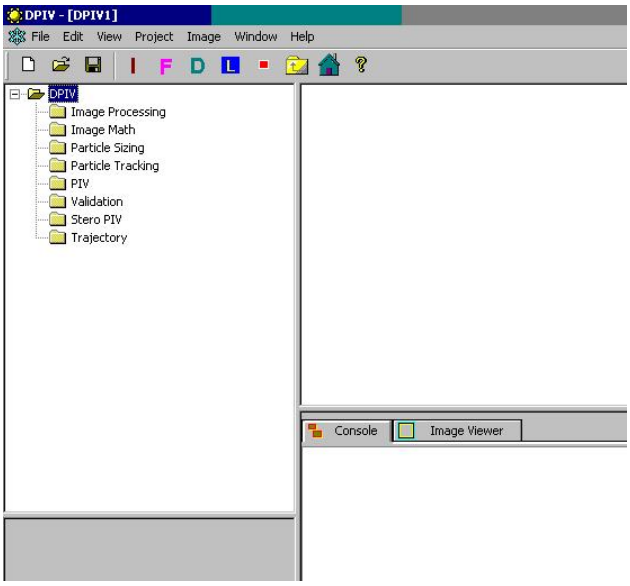

Figure 2.1: New Project Screen

This screen is the main GUI for the operation of FLOW-IQ 2.2. The upper-left box shows the project tasks. The lower-left shows the properties of selected tasks. The upper-right window displays images, directories, and file sequences included in the project. The lower-right window displays console commands, images, and output from the FLOW-IQ software.

Saving a Project

In order to save a project, click on File→Save, press Ctrl+S, or click on File→Save As. Browse for the directory in which you would like to save your project settings, provide a filename for your project, and click SAVE. All project settings, tasks, images, directories, and file sequences in the project will be saved. The directory in which the project is saved is the default directory for the output of files.

Loading a Project

To load a saved project, click on File→Open. Browse to the directory containing the saved project, click on the saved project, and click OPEN. The project will be loaded into the FLOW-IQ GUI.

Adding an Input Package to a Project

In FLOW-IQ v2.2, you must add an input package in order to process files. Images, Directories, and File Sequences can be added to the Input Package once it is created. This setup allows the user to process separate sets of files without interfering with saved work. To add an input package, either click on "I" in the toolbar or click on Project→Add→Input Package as shown below in Figure 2.2.

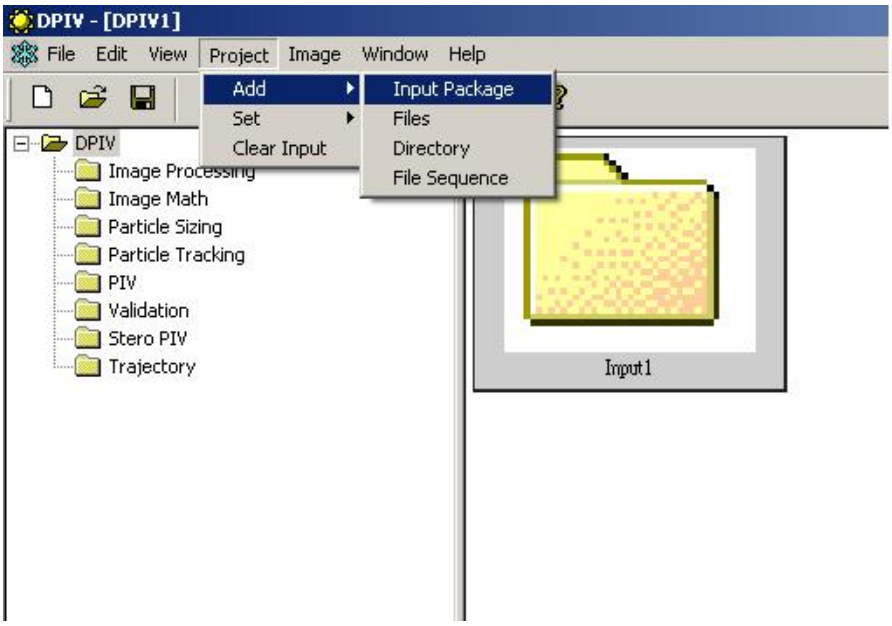

Figure 2. 2: Adding an Input Package

After clicking on "Input Package," the Input Package Dialog box, shown in Figure 2.3, will appear. In this box you can specify the desired name of the input package.

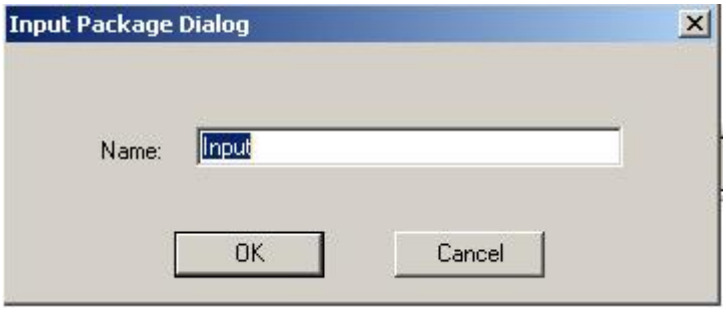

Figure 2. 3: Input Package Dialog Box

An icon will appear in the upper right box in the FLOW-IQ v2.2 window with the name inputted, as shown above in Figure 2.2. This icon is the created input package. All output will be stored in the base directory (where the project is saved) in a folder with the same title as the input package.

Deleting an Input Package From a Project

To delete an input package from the workspace, simply highlight the desired input package and press "Delete" on the keyboard. You may also right-click on the desired input package and click on "Delete" to delete the input package.

Modifying Input Package Properties

In order to modify the name of an input package, right-click on the input package and click on "Properties." The Input Package Dialog Box will appear again, and you will be able to input a new name for the input package.

Adding Images, File Sequences, and Directories to an Input Package

To add files, directories, or file sequences to an input package, simply double-click on the icon for the input package you wish to modify. Then, follow the instructions below for adding images, file sequences, or directories.

The FLOW-IQ program reads 8-bit .tif images with intensities ranging from 0 to 255. In order to add images to the project, either click on "I" in the toolbar or click on Project→Add→Files. Browse for and select the desired images to be added to the project, and click OK. The images will be displayed in the upper-right box in the FLOW-IQ software, as shown below in Figure 2.4.

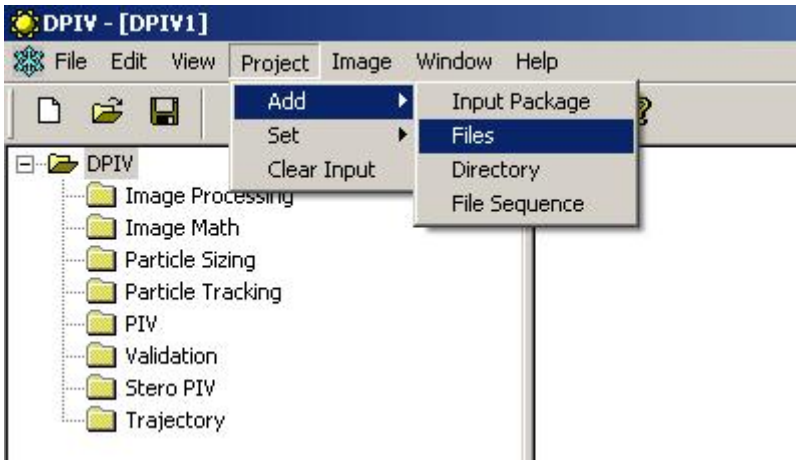

Figure 2. 4: Adding Images, Directories, and File Sequences to an Input Package

If you wish to perform tasks on a large number of images or data files, it is best to add directories or file sequences to the project instead of images.

In order to add a directory to the project, either click on "D" in the toolbar or click on Project→Add →Directory. The Directory Dialog box will appear as shown in Figure 2.5 below. Browse for the desired directory to be added to the project, and click OK.

Specify the extension of the files to be used in the directory, either .tif or .plt. The directory will be displayed in the upper-right box in the FLOW-IQ software.

Figure 2. 5: Directory Dialog Box

For file sequences, the procedure is the same as images and directories, except that the file sequence requires input from the user to run the desired file sequence. To add a file sequence, either click on "F" in the toolbar or click on Project→Add Add→File Sequence. Browse for the desired directory containing the images you wish to analyze, and click OK. The File Sequence Dialog Box, shown below in Figure 2.6, will appear.

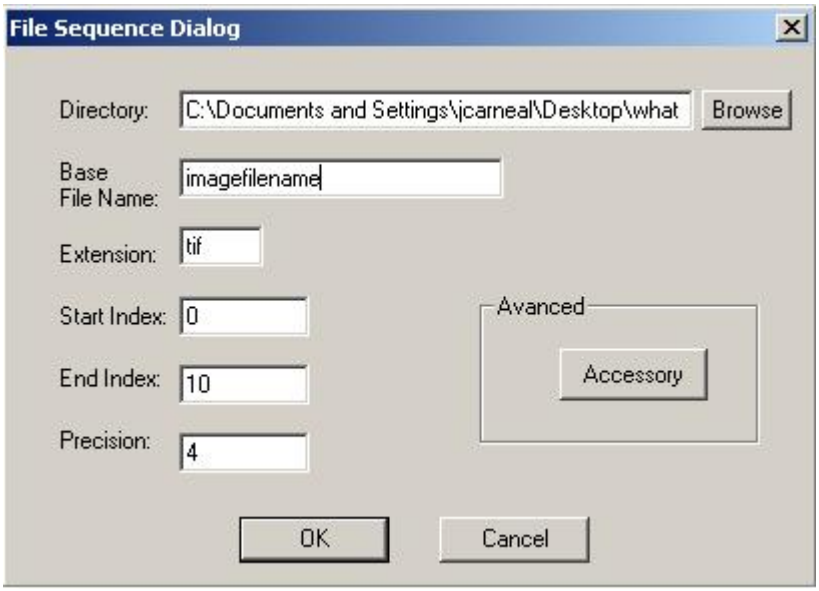

Figure 2.6: File Sequence Dialog Box

The program will automatically select the base filename, file extension, and precision. The user must select the start and end indices. The files must be numbered with the same basename. For example, the files for the options shown in Figure 2.6 would be named imagefilename0000.tif, imagefilename0001.tif, etc. Precision is the number of digits the integer in the filename is forced to have. If the integer is not forced to have a certain

number of digits, use 1 for precision. This will cause the program to look for filenames listed with only the integer value (no padding zeros).

Removing Images, File Sequences, and Directories from an Input Package

To remove files, directories, or file sequences from an input package, highlight the items to be deleted and press "Delete" on the keyboard, or right-click on the desired item and click on "Delete."

Setting Project Parameters

To set the experimental parameters, click on Project → Set→Experiment. The Project Settings Dialog Box, shown below in Figure 2.7, will appear. In this dialog box, you can specify the experimental parameters for the data you will process.

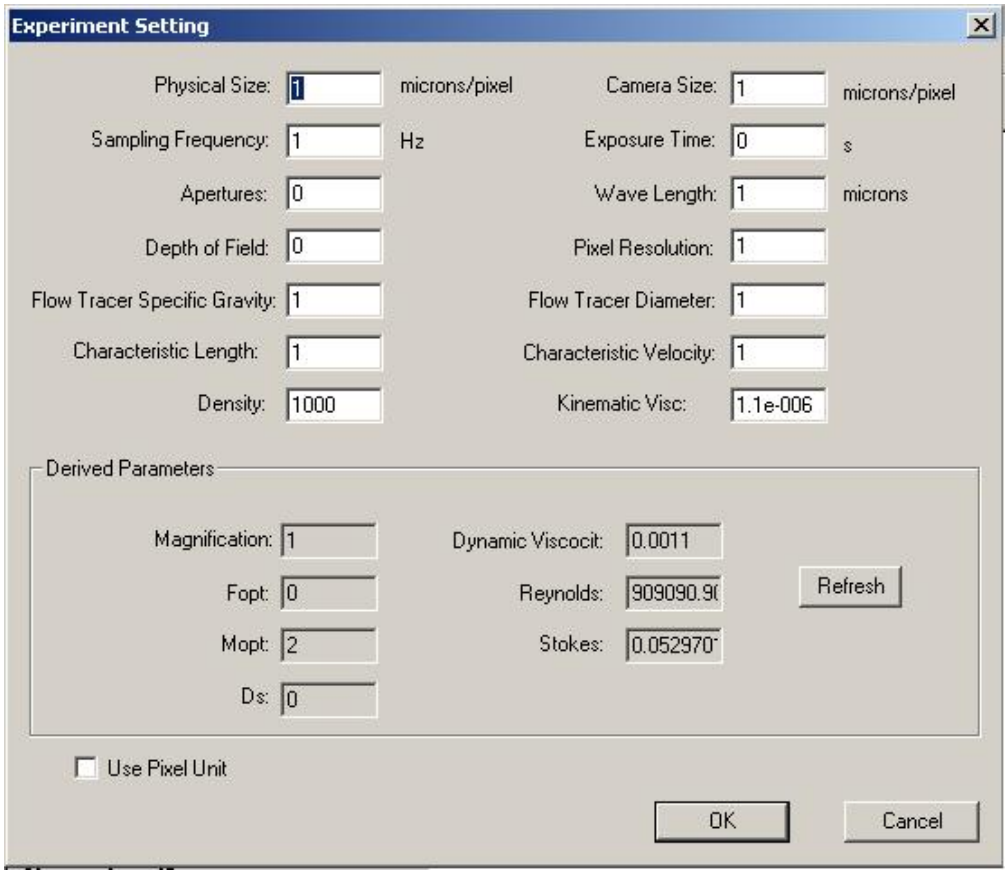

Figure 2. 7: Project Settings Dialog Box

The parameters specified in the Project Settings Dialog Box are used to convert the results from the tasks to the physical domain. The options include system aperature, magnification, camera pixel size, laser source wavelength, sampling time, and exposure time. Sampling time is the inverse of the frame rate of the data collection camera, and camera pixel size is the physical size of a single pixel in the data to be analyzed.

Other experimental parameters that can be specified are the Pixel Resolution, Depth of Field, Flow Tracer Specific Gravity, Flow Tracer Diameter, Characteristic Velocity and Length, Density of the fluid, and the kinematic viscosity of the fluid.

FLOW-IQ v2.2 is able to derive the magnification, dynamic viscosity, optimal focal length F_{opt}, Reynolds Number, Stokes Number, and diffraction-limited diameter D_s. If you wish to keep all measurements in the pixel domain, click on "Use Pixel Unit" in order to halt conversion to the physical domain.

Adding Tasks to the Project

To add tasks to the active project, click on the folder that represents the general task you wish to perform in the upper-left window (Image Processing, Particle Sizing, etc.). The desired folder should now be highlighted. Now, right-click on the folder and click on "Add Tasks." The Add message varies with each method, and the various methods will be discussed in the corresponding chapter for each type of operation. A dialog box will appear.

To add a task to the project, click on the desired task to highlight it, and then click 

The available tasks are listed on the left, and the tasks to be added are shown on the right. When you have selected the desired tasks, click OK. The added tasks will be shown in a tree under the selected folder. These tasks will be performed from top to bottom in the tree. If you wish to change the order of operations, click and drag the tasks to new positions until you are satisfied with the order of operations. The procedures for adding each type of task (Image Processing, Particle Image Velocimetry, etc.) will be discussed in the following chapters. An example dialog box for this process is shown below in Figure 2.8.

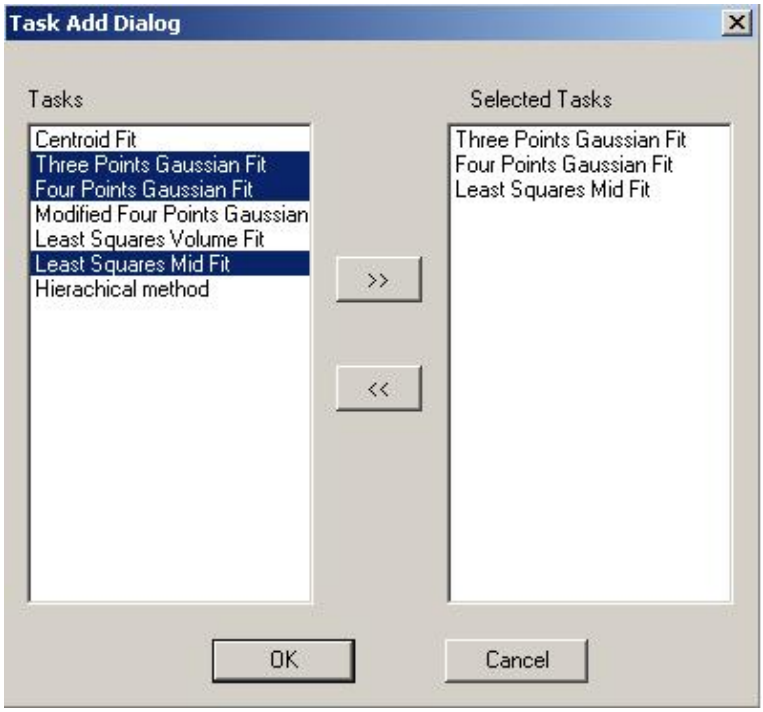

Figure 2. 8: Example Add Task Dialog Box

Editing Task Properties

When a task is highlighted, the properties of the task will be displayed in the lower-left window as shown. In order to edit these properties, click on the desired task to highlight the task. Then right-click on the highlighted task, and click "Properties." The corresponding dialog box will appear depending on the selected task. Enter the desired properties, and click OK. The individual properties are discussed below in detail for each PIV technique. Properties specific to each type of task (Image Processing, Particle Tracking, etc.) will be discussed in the following chapters.

Removing Tasks from a Project

There are two ways to remove tasks in FLOW-IQ 2.2, as a group or individually. To remove several tasks from the active project, click on the folder containing the tree you wish to modify in the upper-left window. The folder should now be highlighted. Now, right-click on the folder and click on "Remove Tasks." The Remove message will vary with the type of task. For example, the Image Preprocessing Remove Tasks Dialog Box is shown below in Figure 2.9.

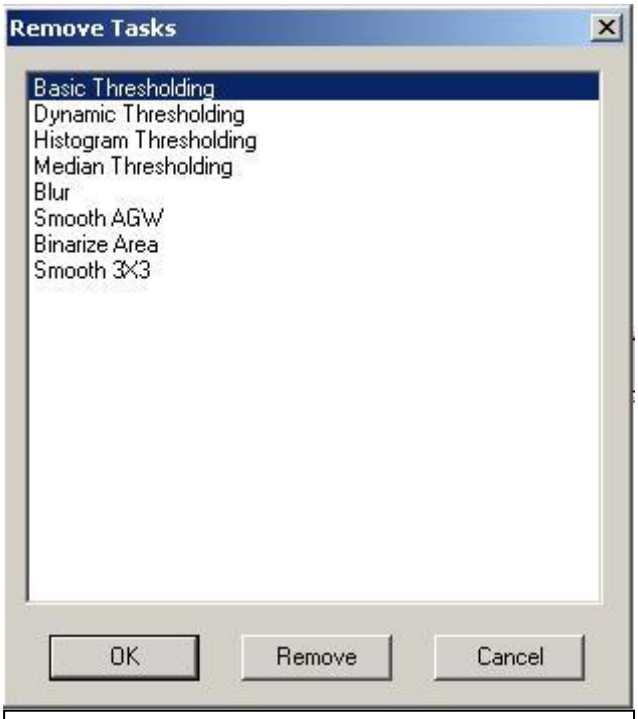

Figure 2. 9: Typical Remove Tasks Dialog Box

To remove a task, highlight the task by clicking on the task and click on REMOVE. This will remove the task from the list. When undesired tasks have been eliminated, click on

OK and the tree in the task folder will be updated accordingly. A detailed procedure for deleting tasks is presented in each chapter for the specific type of task.

To remove individual , click on the task to be removed. The task should now be highlighted. Now, right-click on the task to be removed and click on "Remove." The task will be deleted from the project.

Running Tasks

There are two ways to run tasks in FLOW-IQ 2.2, as a group or individually. To run all of the listed tasks in a tree, click on the folder containing the tree in the upper-left window. The folder should now be highlighted. Now, right-click on the folder and highlight "Run Tasks on." A submenu will appear that lists all of the available input packages. Click on the input package you wish to run the task on. This process is illustrated below in Figure 2.10. The Run message will vary with the type of task performed, and specific properties of each type of task are presented in the following chapters.

In order to run individual tasks, click on the desired task. The task should now be highlighted. Now, right-click on the task to be removed and click on "Run Task(s) on Data." A menu will appear with a list of the available input packages for analysis. Click on the input package to be processed to run the tasks on the desired data. The task will be run on all of the selected images or files in the project. Any task-specific procedures are covered in the following chapters.

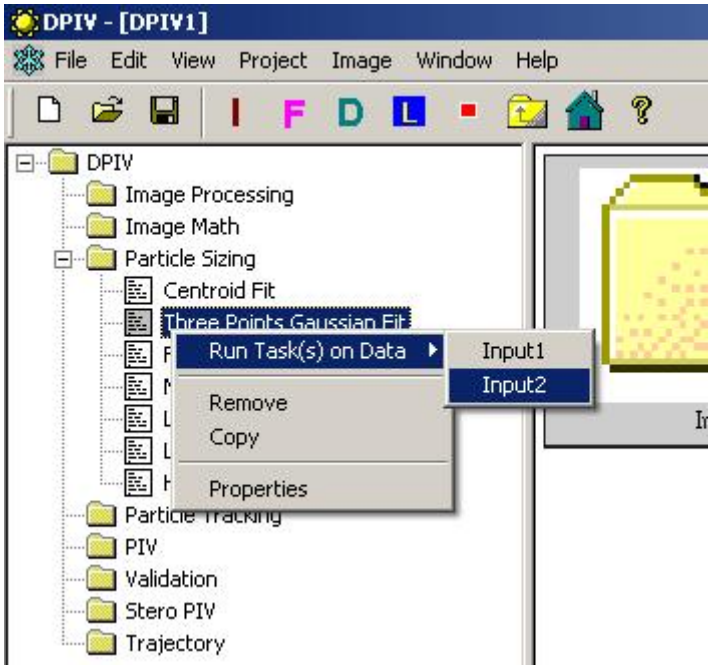

Figure 2. 10: Running a Task

When all running tasks have finished, a **##Finished Processing** message will appear in the lower-right window under "Console."

Navigating Windows and Checking Location in FLOW-IQ v2.2

In order to navigate between input packages in Flow-IQ v2.2, use the  buttons to navigate up one directory and return to the home directory, and to navigate into a directory double-click, as is standard in windows.

The following chapters discuss the setup and performance of each class of task provided in FLOW-IQ 2.2.

In order to check the current location of the files in the active file window (upper right window), right click in the upper-right window and select "Where Am I?" A dialog box will appear with the current location listed in the window.

Viewing Image Histograms in Flow-IQ v2.2

In order to view an image histogram, images must first be added as files to an input package. See *Adding Images to an Input Package* for more information. To view an image histogram, right-click on the image and select "Histogram." The image histogram will appear as shown in Figure 2.11 below. You may zoom in on an area by creating a box around the desired area with the mouse. The selected area will be enlarged to fit the full view.

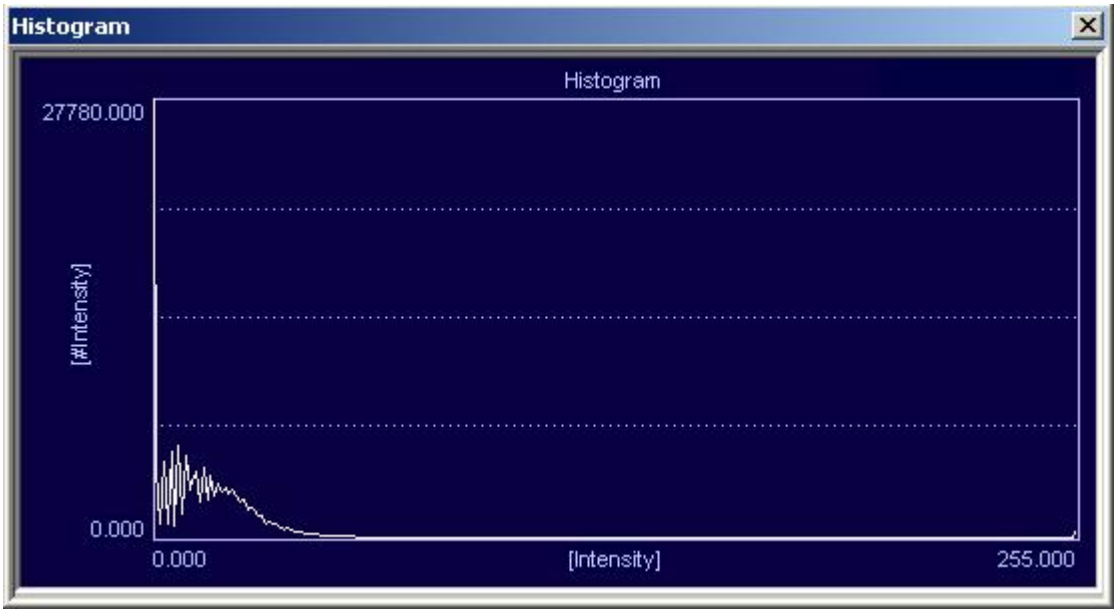

Figure 2. 11: Image Histogram

Chapter 3: Preprocessing Tasks

Several preprocessing tasks are included in Flow-IQ v2.2 to aid the user in producing quality results. The available preprocessing tasks and corresponding user-definable options are briefly summarized in this section. This section also deals with the addition, removal, and performance of preprocessing tasks. Preprocessing tasks may be run alone or in conjunction with other tasks. The input files for Preprocessing are 8 bit ".tif" images.

Adding Preprocessing Tasks

To add preprocessing tasks to the active project, click on "Image Processing" in the upper-left window. "Image Processing" should now be highlighted. Now, right-click on "Image Processing" and click on "Add ImagePro Tasks." The Image Preprocessing Add Task Dialog Box will appear. This process is shown in Figure 3.1 below.

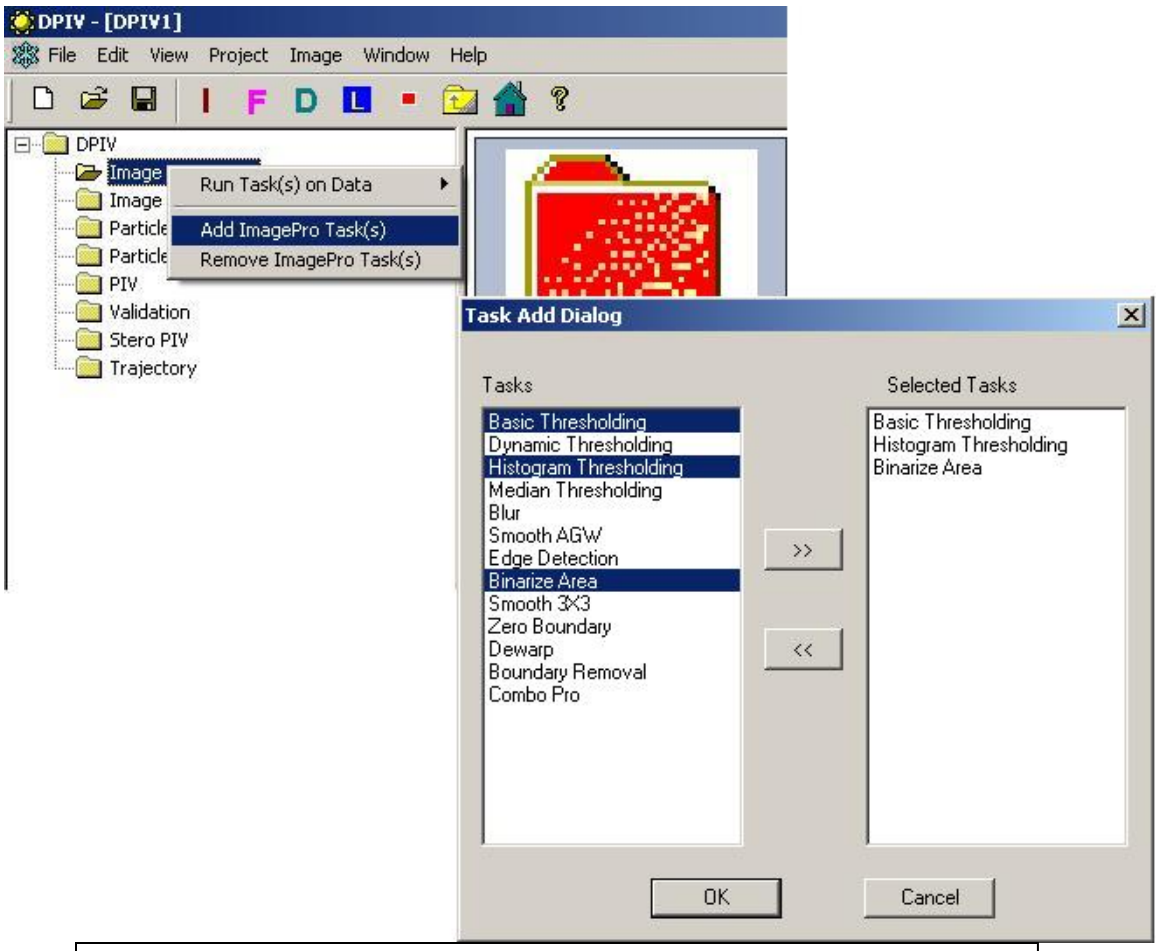

Figure 3. 1: Adding Image Preprocessing Tasks

To add a task to the project, click on the desired task to highlight it, and then click 

The available tasks are listed on the left, and the tasks to be added are shown on the right. When you have selected the desired tasks, click OK. The added tasks will be shown in a tree under "Image Processing," as shown below in Figure 3.2. These tasks will be performed from top to bottom in the tree. If you wish to change the order of operations, click and drag the tasks to new positions until you are satisfied with the order of operations.

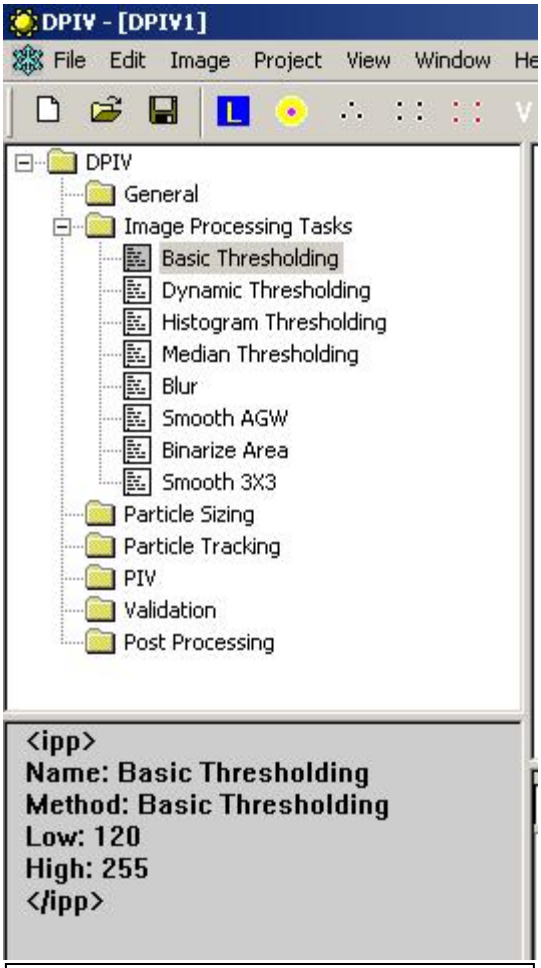

Figure 3. 2: Added Preprocessing Tasks

Editing Task Properties

When a task is highlighted, as "Basic Thresholding" is in Figure 3.2 above, the properties of the task will be displayed in the lower-left window as shown. In order to edit these properties, click on the desired task to highlight the task. Then right-click on the highlighted task, and click "Properties." The corresponding dialog box will appear depending on the selected task. Enter the desired properties, and click OK. You may also define the output directory for each task in the dialog box for the image processing tasks.

Removing Preprocessing Tasks

There are two ways to remove preprocessing tasks in FLOW-IQ V2.2, as a group or individually. To remove several preprocessing tasks from the active project, click on "Image Processing" in the upper-left window. "Image Processing" should now be highlighted. Now, right-click on "Image Processing" and click on "Remove ImagePro Tasks." The Image Preprocessing Remove Tasks Dialog Box will appear, as shown below in Figure 3.3.

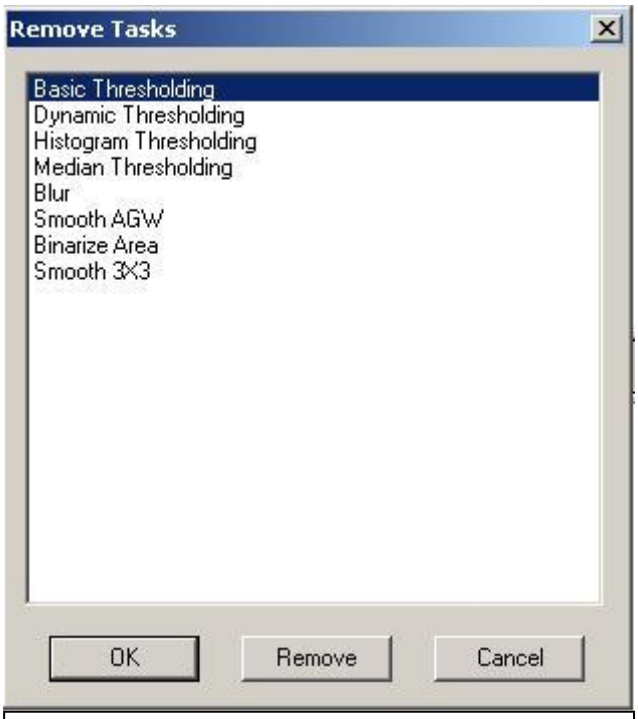

Figure 3. 3: Removing Preprocessing Tasks

To remove a task, highlight the task by clicking on the task and click on REMOVE. This will remove the task from the list. When undesired tasks have been eliminated, click on OK and the preprocessing tree will be updated accordingly.

To remove individual preprocessing tasks, click on the task to be removed. The task should now be highlighted. Now, right-click on the task to be removed and click on "Remove." The task will be deleted from the Image Preprocessing Task Tree.

Running Preprocessing Tasks

There are two ways to run preprocessing tasks in FLOW-IQ V2.2, as a group or individually. To run all of the listed preprocessing tasks in the tree, click on "Image Processing" in the upper-left window. "Image Processing" should now be highlighted. Now, right-click on "Image Processing" and click on "Run Task(s) on Data." A menu

will appear with a list of the available input packages for analysis. Click on the input package to be processed to run the tasks on the desired data. A list of the available input packages will appear. Click on the desired input package to be processed with the preprocessing tasks. The processed images will be saved in the ouput directory specified in the task. The input images will not be overwritten.

In order to run individual preprocessing tasks, click on the desired task. The task should now be highlighted. Now, right-click on the task to be removed and click on "Run Task(s) on." A list of the available input packages will appear. Click on the desired input package to be processed with the preprocessing task. The task will be run on all of the selected images in the project. The processed images will be saved in the ouput directory specified in the task. The input images will not be overwritten.

When the preprocessing tasks have finished processing, a **##Finished Processing** message will appear in the lower-right window under "Console." A description of each available preprocessing task follows.

Basic Thresholding

Basic thresholding eliminates integer intensity values in the selected images that are less than the user-specified threshold level, as shown in Figure 3.4 below. Fore example, in the case shown in Figure 3.4, the selected images, images in selected directories, or images in selected file sequences included in the project will be screened and any value less than 120 will be set to 0. If you wish to overwrite the original images, then click the check-box next to "Overwrite Original Image File." To specify an output directory, click on "Browse" and select the desired output directory.

Figure 3. 4: Basic Thresholding Options

Dynamic Thresholding

The dynamic thresholding task performs a dynamic threshold on the images included in the project. The user-definable attributes of this task are shown below in Figure 3.5. The "Coefficient" determines the strength of the dynamic thresholding. If you wish to overwrite the original images, then click the check-box next to "Overwrite Original Image File." To specify an output directory, click on "Browse" and select the desired output directory.

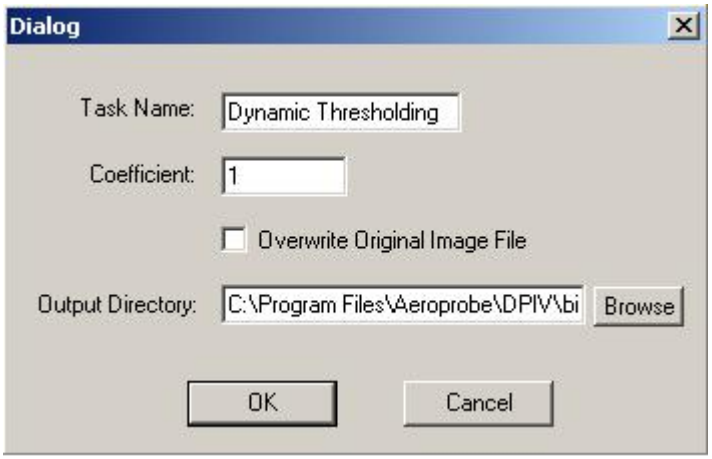

Figure 3. 5: Dynamic Thresholding Properties

Histogram Thresholding

Histogram thresholding creates a histogram of the intensities contained in an image, and sets a threshold based on this histogram. Any pixel intensity values less than this value are set to zero. This process is applied to all selected images in the project. Currently, there are no user-definable options for the task of histogram thresholding. The Dialog Box for Histogram Thresholding is shown below in Figure 3.6. If you wish to overwrite the original images, then click the check-box next to "Overwrite Original Image File." To specify an output directory, click on "Browse" and select the desired output directory.

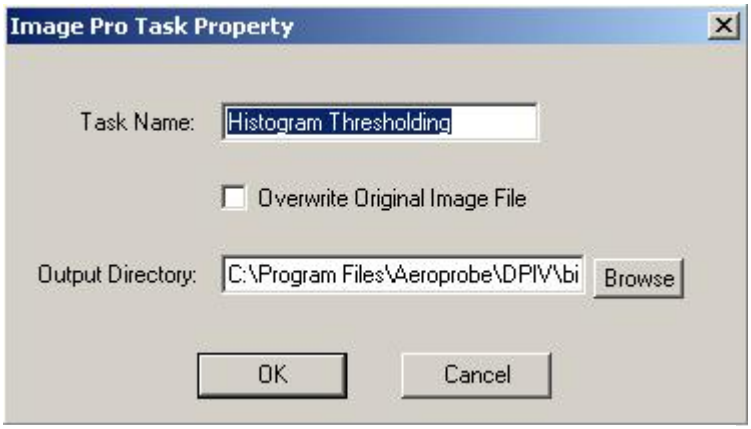

Figure 3. 6: Histogram Thresholding Options

Median Thresholding

In median thresholding, the median intensity for each image is found and any pixel with intensity less than the median intensity is set to zero. This process is applied to all selected images in the project. Currently, there are no user-definable options for the task of median thresholding. The Dialog Box for Median Thresholding is shown below in Figure 3.7. If you wish to overwrite the original images, then click the check-box next to "Overwrite Original Image File." To specify an output directory, click on "Browse" and select the desired output directory.

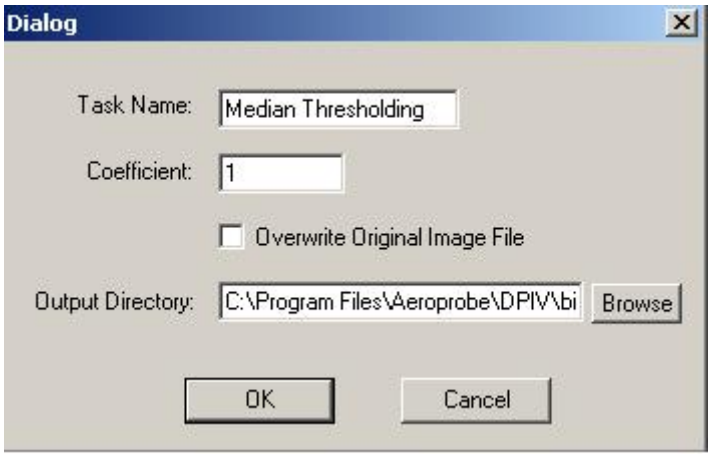

Figure 3. 7: Median Thresholding Options

Blur

The blur preprocessing task applies a blur filter to each selected image in the project. The user may select the strength of the blur filter, as shown below in Figure 3.8. If you wish to overwrite the original images, then click the check-box next to "Overwrite Original Image File." To specify an output directory, click on "Browse" and select the desired output directory.

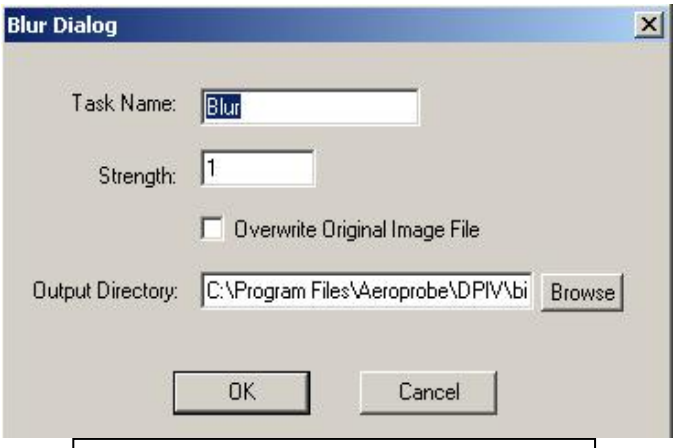

Figure 3.8: Blur Dialog Box

Smooth AGW

This task applies a smoothing Adaptive Gaussian Window filter to the selected project images. The user may select the strength of the Smooth AGW filter, as shown below in Figure 3.9. If you wish to overwrite the original images, then click the check-box next to "Overwrite Original Image File." To specify an output directory, click on "Browse" and select the desired output directory.

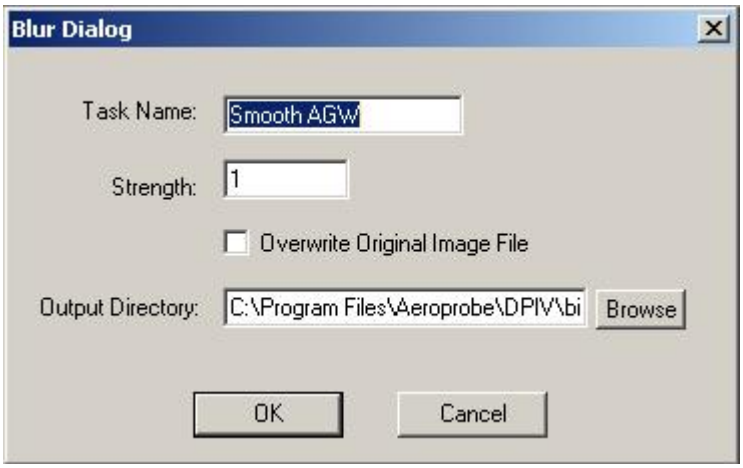

Figure 3. 9: Smooth AGW Strength

Edge Detection

The edge detection task uses an edge detection algorithm to detect and remove boundaries in the selected images. Currently, there are no user-definable attributes for the edge detection task. The Dialog Box for Edge Detection is shown below in Figure 3.10. If you wish to overwrite the original images, then click the check-box next to "Overwrite Original Image File." To specify an output directory, click on "Browse" and select the desired output directory.

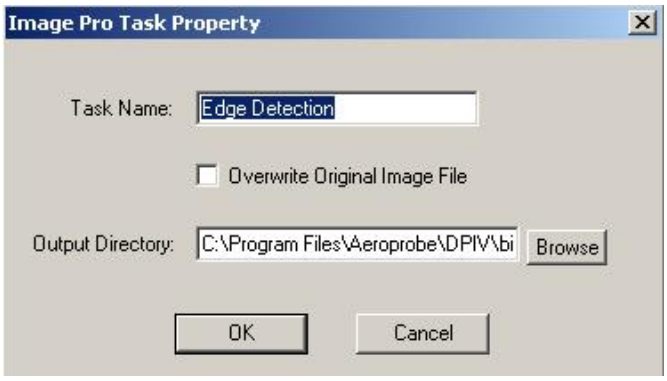

Figure 3. 10: Edge Detection Options

Binarize Area

The binarize area task identifies regions of interest in the image. Any intensity greater than the median threshold is set to 255, and any intensity less than the threshold is set to 0. This process binarizes the image into "on" and "off" regions. The strength of the Binarize Area algorithm may be defined by entering a number in the "Coefficient" box. The Dialog Box for Edge Detection is shown below in Figure 3.11. If you wish to overwrite the original images, then click the check-box next to "Overwrite Original Image File." To specify an output directory, click on "Browse" and select the desired output directory.

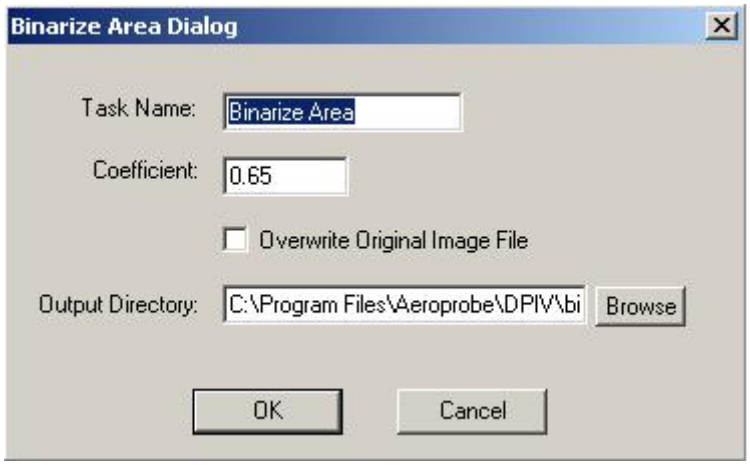

Figure 3.11: Binarize Area Options

Smooth 3X3

The smooth 3X3 task uses 3X3 blocks of the selected image to apply a smoothing filter to the image. Currently, there are no user-definable attributes for the smooth 3X3 filter. The Dialog Box for Edge Detection is shown below in Figure 3.12. If you wish to overwrite the original images, then click the check-box next to "Overwrite Original Image File." To specify an output directory, click on "Browse" and select the desired output directory.

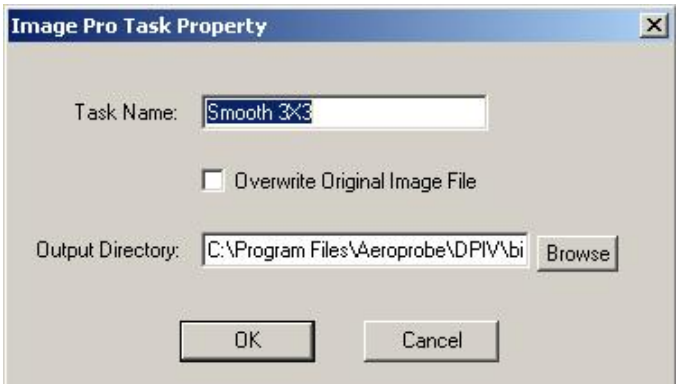

Figure 3. 12: Smooth 3X3 Options

Zero Boundary

The zero boundary task zeros the boundary of the image, as specified by the user. The variables m and n stand for the boundary width (in pixels) for the boundary to be zeroed in the x and y directions, respectively. The Dialog Box for Zero Boundary is shown below in Figure 3.13. If you wish to overwrite the original images, then click the check-box next to "Overwrite Original Image File." To specify an output directory, click on "Browse" and select the desired output directory.

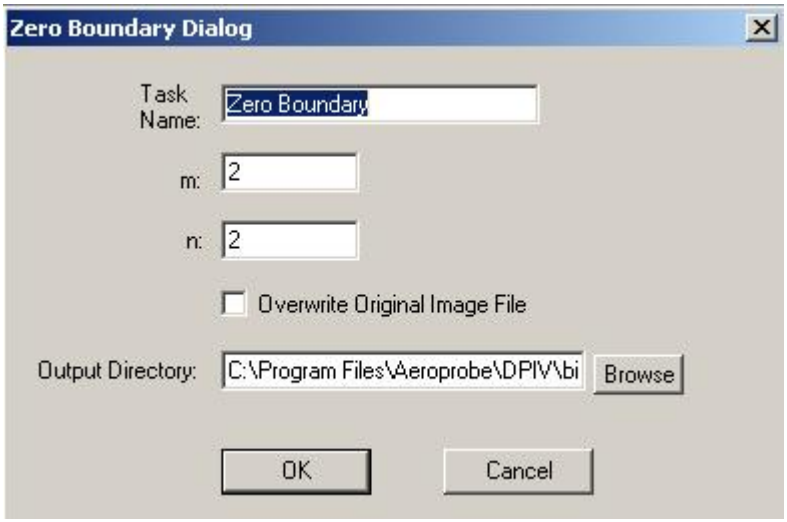

Figure 3. 13: Zero Boundary Options

Dewarp

The Dewarp task zeros is for use with Stereo-PIV images. The Dialog Box for Zero Boundary is shown below in Figure 3.14. The template file is the file that contains the template. It is an unwarped (orthogonal) image that shows the calibration target, which is usually rows and columns of circles or crosses. To specify the template file, click on "Browse" next to "Template File" and find the template image. The calibration file is a picture of the calibration target at the angle at which data was collected, which is warped. To specify the calibration file, click on "Browse" next to "Calibration File" and find the calibration image. Spacing is the approximate spacing of the markers on the calibration image, in pixels. Once these parameters are set, click on "Generate" to generate the necessary coefficients for dewarping. The "Calibration Matrix" will be updated according to the calculated values. You may either define a calibration matrix yourself, generate a new matrix as above, or import a calibration matrix. To export a calibration matrix, click on the "Export" button and save the file to the desired directory. You may now import this file for other projects, if necessary. If you wish to overwrite the original

images, then click the check-box next to “Overwrite Original Image File.” To specify an output directory, click on “Browse” and select the desired output directory.

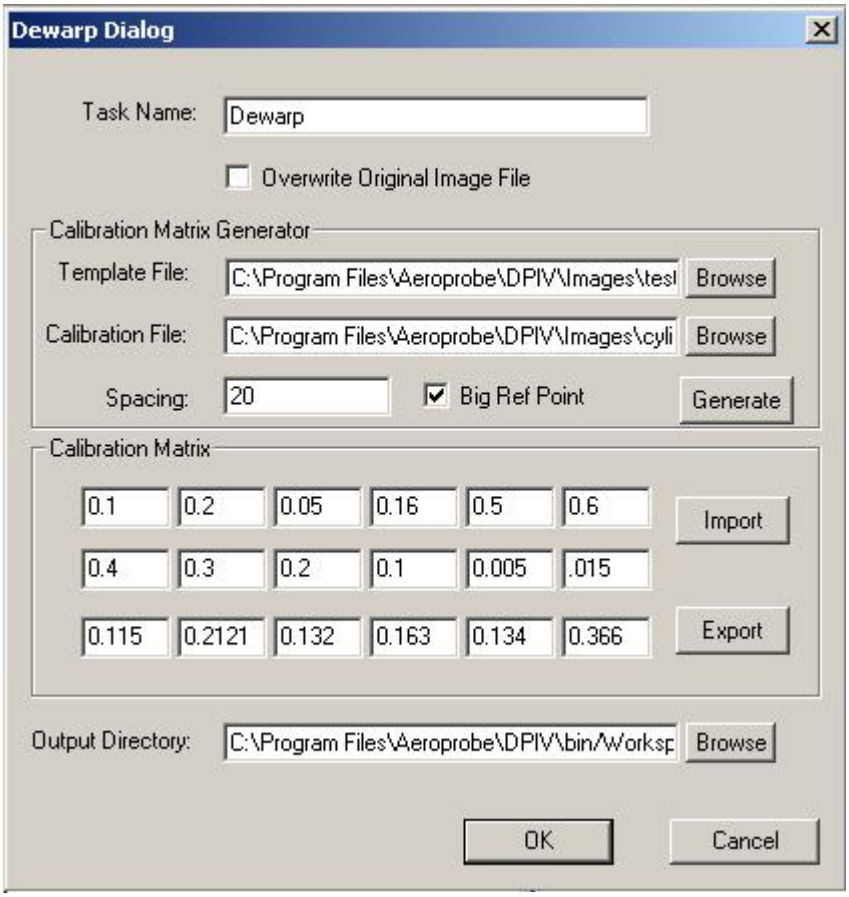

Figure 3. 14: Dewarp Function Options

Boundary Removal

The boundary removal task removes the boundaries in the image, as specified by the user. The strength of the algorithm can be increased by increasing the value of “Coefficient.” The Dialog Box for Boundary Removal is shown below in Figure 3.15. If you wish to overwrite the original images, then click the check-box next to “Overwrite Original Image File.” To specify an output directory, click on “Browse” and select the desired output directory.

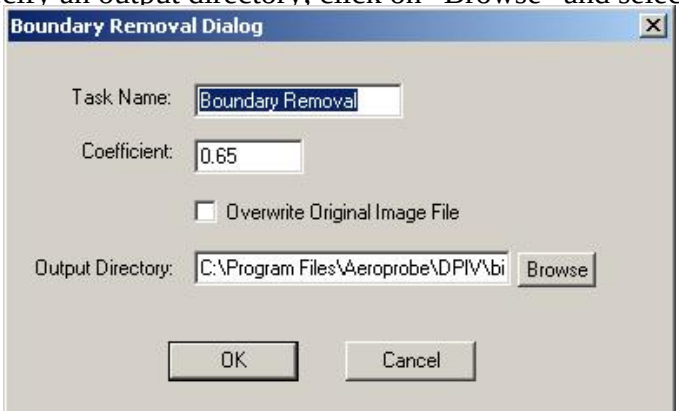

Figure 3. 15: Boundary Removal Dialog

Combo Processing

The Combo Pro task allows the user to do a variety of image preprocessing tasks in a single task. The Dialog Box for Combo Processing is shown below in Figure 3.16. To add a list of processing tasks, click on "Add" and add the tasks in the same manner described in Figure 3.1. To remove tasks from the list, simply click on "Delete" and remove the tasks as shown in Figure 3.3. To edit the properties of a specific task, highlight the task under "Image Preprocessing Task" and click on "Properties." The properties of each task will appear as shown above for each individual task. You may also select a blanket output directory for the combo processing by clicking on "Browse" and selecting the desired output directory.

Figure 3. 16: Combo Processing Options

Chapter 4: Image Math Tasks

In addition to the Image Preprocessing tasks available in Flow-IQ v2.2, several image mathematics tasks are included to aid the user in producing superior results. The available image mathematical tasks and corresponding user-definable options are briefly summarized in this section. This section also deals with the addition, removal, and performance of the image math tasks. Image math tasks may be run alone or in conjunction with other tasks. The input files for these tasks are 8 bit ".tif" images.

Adding Image Math Tasks

To add preprocessing tasks to the active project, click on "Image Math" in the upper-left window. "Image Math" should now be highlighted. Now, right-click on "Image Math" and click on "Add Image Math Tasks." The Image Preprocessing Add Task Dialog Box will appear. This process is shown in Figure 4.1 below.

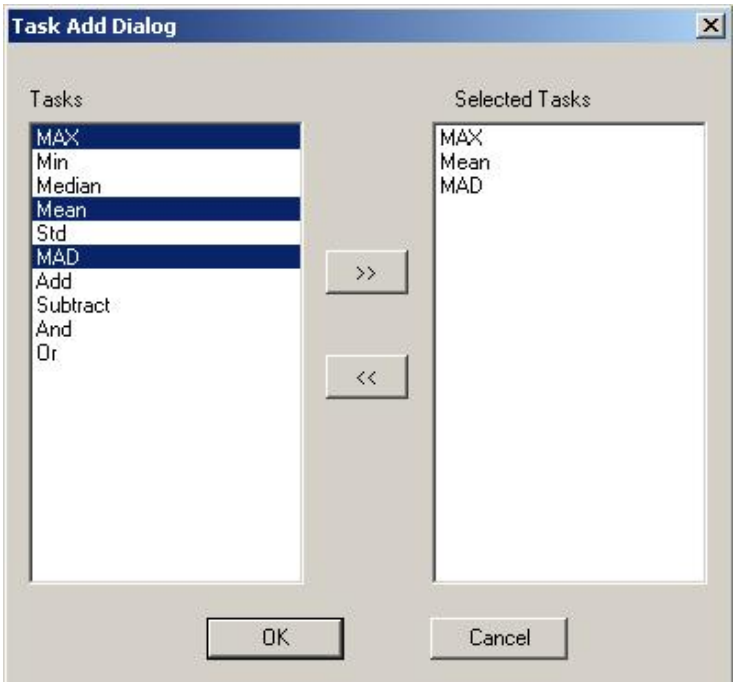

Figure 4. 1: Task Add Dialog Box

To add a task to the project, click on the desired task to highlight it, and then click 

The available tasks are listed on the left, and the tasks to be added are shown on the right. When you have selected the desired tasks, click OK. The added tasks will be shown in a tree under "Image Math," as shown below in Figure 4.2. These tasks will be performed from top to bottom in the tree. If you wish to change the order of operations, click and drag the tasks to new positions until you are satisfied with the order of operations.

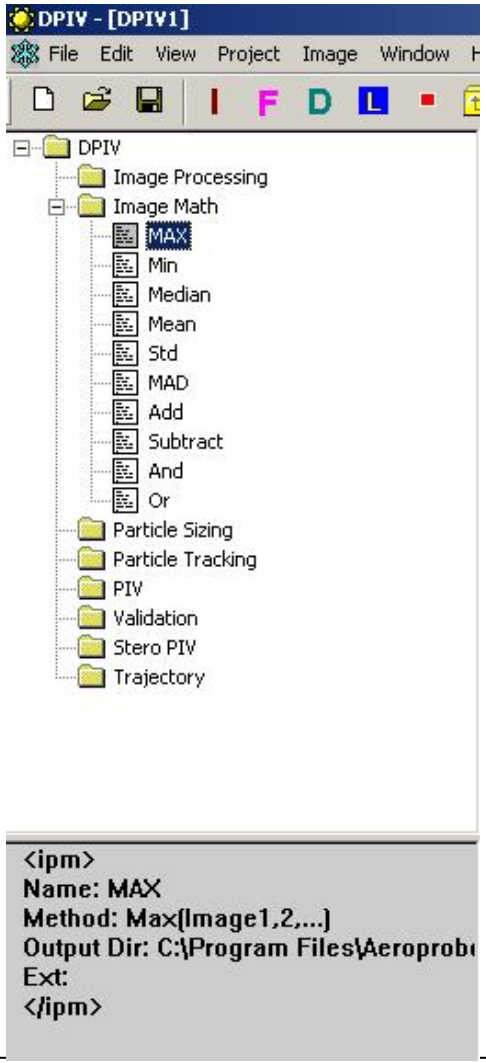

Figure 4. 2: Added Preprocessing Tasks

Editing Task Properties

When a task is highlighted, as "Max" is in Figure 4.2 above, the properties of the task will be displayed in the lower-left window as shown. In order to edit these properties, click on the desired task to highlight the task. Then right-click on the highlighted task, and click "Properties." The corresponding dialog box will appear depending on the selected task. Enter the desired properties, and click OK. You may also define the output directory for each task in the dialog box for the Image Math tasks.

Removing Image Math Tasks

There are two ways to remove image mathematics tasks in FLOW-IQ V2.2, as a group or individually. To remove several image mathematics tasks from the active project, click on "Image Math" in the upper-left window. "Image Math" should now be highlighted.

Now, right-click on “Image Math” and click on “Remove Image Math Tasks.” The Image Math Remove Tasks Dialog Box will appear, as shown below in Figure 4.3.

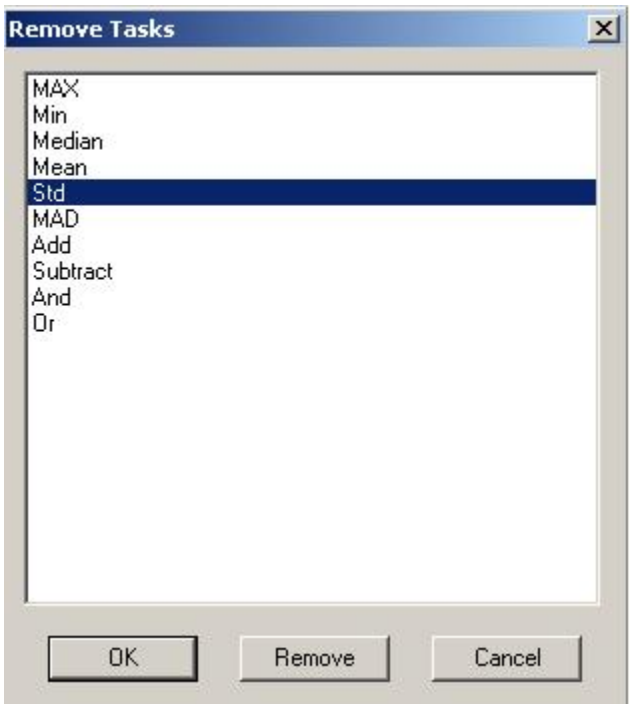

Figure 4. 3: Removing Preprocessing Tasks

To remove a task, highlight the task by clicking on the task and click on REMOVE. This will remove the task from the list. When undesired tasks have been eliminated, click on OK and the image math tree will be updated accordingly.

To remove individual image math tasks, click on the task to be removed. The task should now be highlighted. Now, right-click on the task to be removed and click on “Remove.” The task will be deleted from the Image Math Task Tree.

Running Math Tasks

There are two ways to run image mathematics tasks in FLOW-IQ V2.2, as a group or individually. To run all of the listed image mathematics tasks in the tree, click on “Image Math” in the upper-left window. “Image Math” should now be highlighted. Now, right-click on “Image Math” and click on “Run Task(s) on Data.” A menu will appear with a list of the available input packages for analysis. Click on the input package to be processed to run the tasks on the desired data. A list of the available input packages will appear. Click on the desired input package to be processed with the image mathematics tasks. The processed images will be saved in the ouput directory specified in the task. The input images will not be overwritten.

In order to run individual image mathematics tasks, click on the desired task. The task should now be highlighted. Now, right-click on the task to be removed and click on "Run Task(s) on." A list of the available input packages will appear. Click on the desired input package to be processed with the image mathematics task. The task will be run on all of the selected images in the project. The processed images will be saved in the ouput directory specified in the task. The input images will not be overwritten.

When the image mathematics tasks have finished processing, a **##Finished Processing** message will appear in the lower-right window under "Console." A description of each available image mathematics task follows.

Max Task

The Max task creates an array and stores the maximum value across the input set of images at each location. The algorithms searches from (x,y) = (0,0) to (x,y) = (255,255) and finds the maximum for each point in the input image set. Currently, there are no options available for the Max task algorithm. The Dialog box for the Max task is shown below in Figure 4.4. The output directory may be specified by clicking "Browse" and selecting the desired output directory.

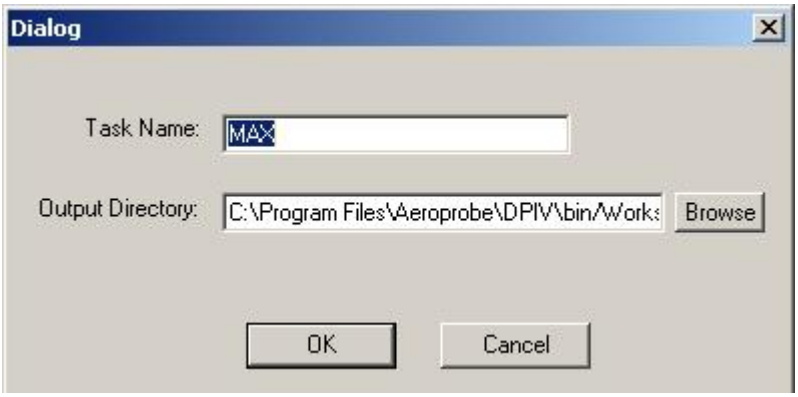

Figure 4. 4: Max Task Options

Min Task

The Min task creates a 256X256 array and stores the minimum value across the input set of images at each location. The algorithms searches from (x,y) = (0,0) to (x,y) = (255,255) and finds the minimum for each point in the input image set. Currently, there are no options available for the Min task algorithm. The Dialog box for the Min task is shown below in Figure 4.5. The output directory may be specified by clicking "Browse" and selecting the desired output directory.

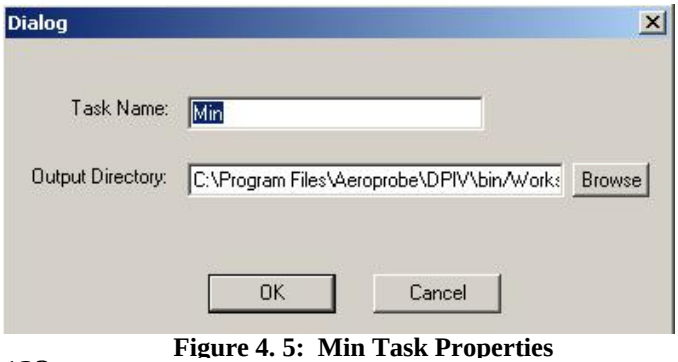

Figure 4. 5: Min Task Properties

Median Task

The Median task creates a 256X256 array and stores the median value across the input set of images at each location. The algorithms searches from (x,y) = (0,0) to (x,y) = (255,255) and finds the median for each point in the input image set. Currently, there are no options available for the Median task algorithm. The output directory may be specified by clicking "Browse" and selecting the desired output directory.

Mean Task

The Mean task creates a 256X256 array and stores the mean intensity value across the input set of images at each location. The algorithms searches from (x,y) = (0,0) to (x,y) = (255,255) and finds the Mean for each point in the input image set. Currently, there are no options available for the Mean task algorithm. The output directory may be specified by clicking "Browse" and selecting the desired output directory.

STD Task

The STD task creates a 256X256 array and stores the standard deviation of the intensity value across the input set of images at each location. The algorithms searches from (x,y) = (0,0) to (x,y) = (255,255) and finds the standard deviation for each point in the input image set. Currently, there are no options available for the standard deviation task algorithm. The output directory may be specified by clicking "Browse" and selecting the desired output directory.

MAD Task

The MAD task creates a 256X256 array and stores the mad values in an 8-bit '.tif' format. Currently, there are no options available for the standard deviation task algorithm. The output directory may be specified by clicking "Browse" and selecting the desired output directory.

Add

The Add task adds an object image to the images in the input package. The Dialog Box for the Add task is shown below in Figure 4.6. The user may select the object file by clicking "Browse" and selecting the desired image to be added to the images in the input package. The output directory may be specified by clicking "Browse" and selecting the desired output directory.

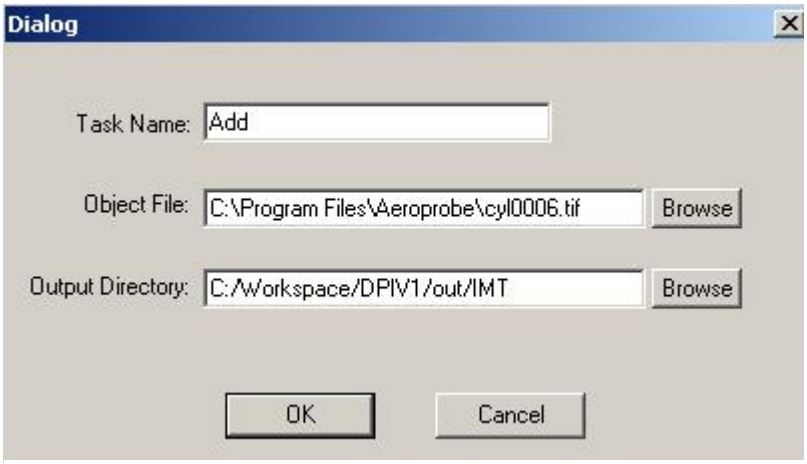

Figure 4. 6: Add Task Dialog Box

Subtract Task

The Subtract task subtracts an object image from the images in the input package. The Dialog Box for the Subtract task is shown below in Figure 4.7. The user may select the object file by clicking "Browse" and selecting the desired image to be subtracted from the images in the input package. The output directory may be specified by clicking "Browse" and selecting the desired output directory.

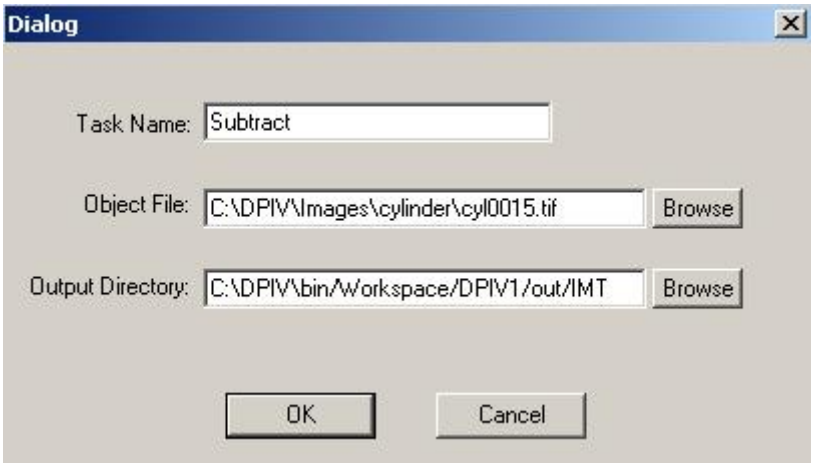

Figure 4. 7: Subtract Task Dialog Box

And Task

The And task performs an AND operation between an object image and the images in the input package. The Dialog Box for the And task is shown below in Figure 4.8. The user may select the object file by clicking "Browse" and selecting the desired image to be subtracted from the images in the input package. The output directory may be specified by clicking "Browse" and selecting the desired output directory.

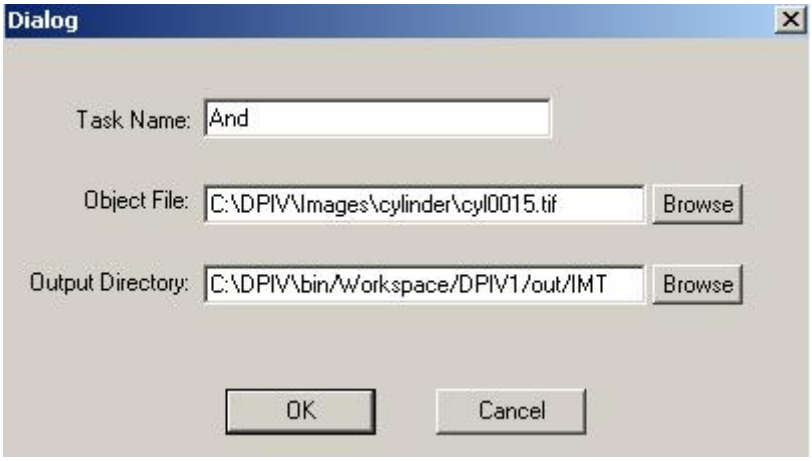

Figure 4. 8: And Task Dialog Box

Or Task

The Or task performs an OR operation between an object image and the images in the input package. The Dialog Box for the Or task is shown below in Figure 4.9. The user may select the object file by clicking "Browse" and selecting the desired image to be subtracted from the images in the input package. The output directory may be specified by clicking "Browse" and selecting the desired output directory.

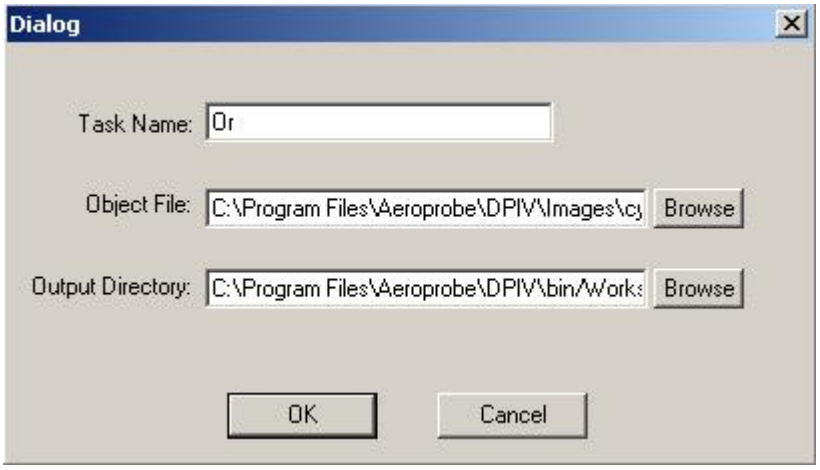

Figure 4. 9: Or Task Dialog Box

Chapter 5: Particle Sizing Tasks

Several particle sizing techniques are included in Flow-IQ v2.2 to aid the user in producing quality results. This section deals with the addition, removal, and performance of preprocessing tasks. The available particle sizing tasks are briefly summarized in this section. Preprocessing tasks can be run alone or in conjunction with other tasks. The input files for Particle Sizing tasks are 8 bit ".tif" images.

Adding Particle Sizing Tasks

To add particle sizing tasks to the active project, click on "Particle Sizing" in the upper-left window. "Particle Sizing" should now be highlighted. Now, right-click on "Particle Sizing" and click on "Add Sizing Tasks." The Particle Sizing Dialog Box will appear, as shown in Figure 5.1 below.

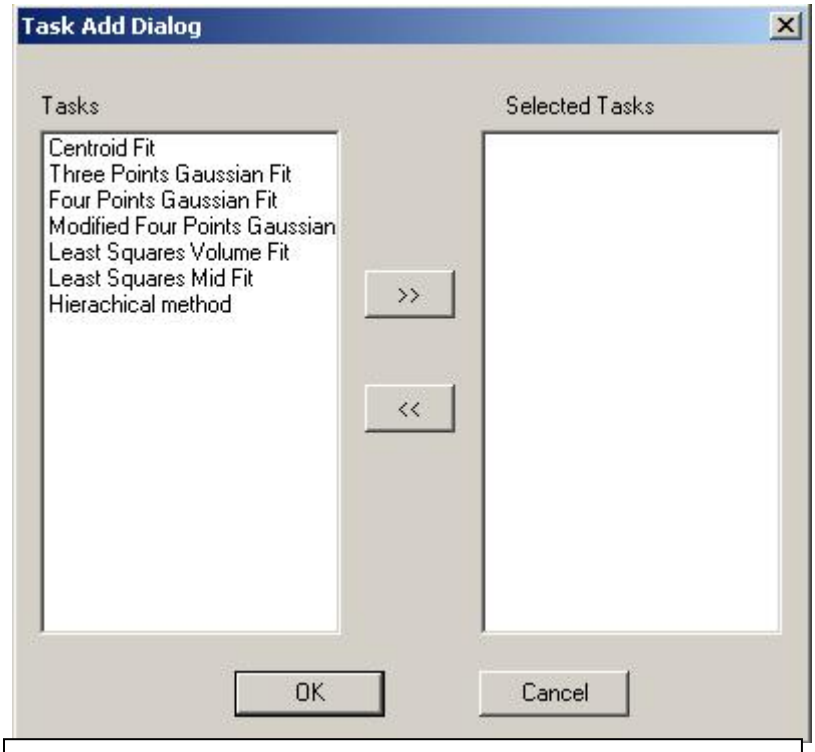

Figure 5. 1: Add Particle Sizing Task Dialog Box

To add a task to the project, click on the desired task to highlight it, and then click 

The available tasks are listed on the left, and the tasks to be added are shown on the right. When you have selected the desired tasks, click OK. The added tasks will be shown in a tree under "Particle Sizing," as shown below in Figure 5.2. These tasks will be performed from top to bottom in the tree. If you wish to change the order of operations, click and drag the tasks to new positions until you are satisfied with the order of operations.

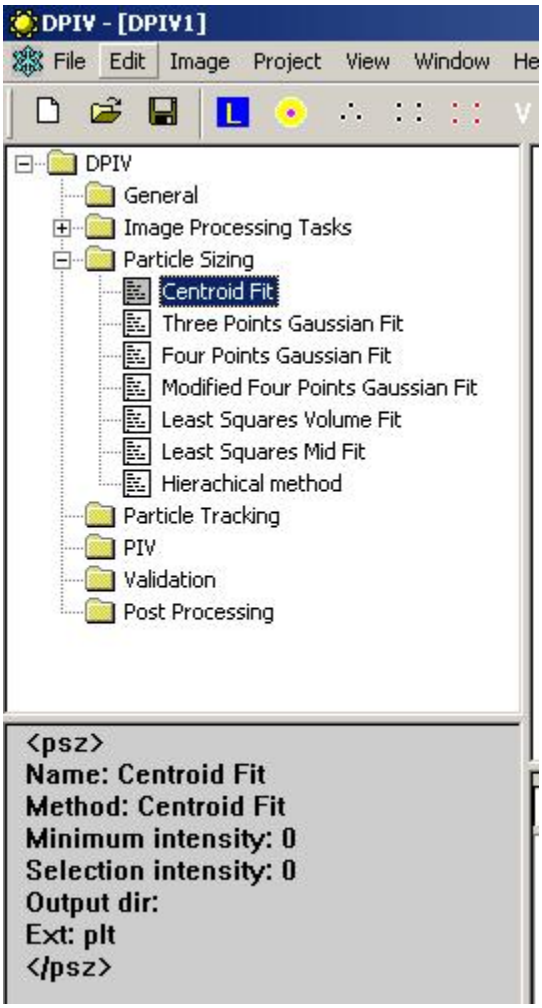

Figure 5. 2: Added Particle Sizing Tasks

Editing Task Properties

When a task is highlighted, as "Centroid Fit" is in Figure 5.2 above, the properties of the task will be displayed in the lower-left window as shown. In order to edit these properties, click on the desired task to highlight the task. Then right-click on the highlighted task, and click "Properties." The Edit Sizing Task Properties Dialog Box will appear, as shown below in Figure 5.3.

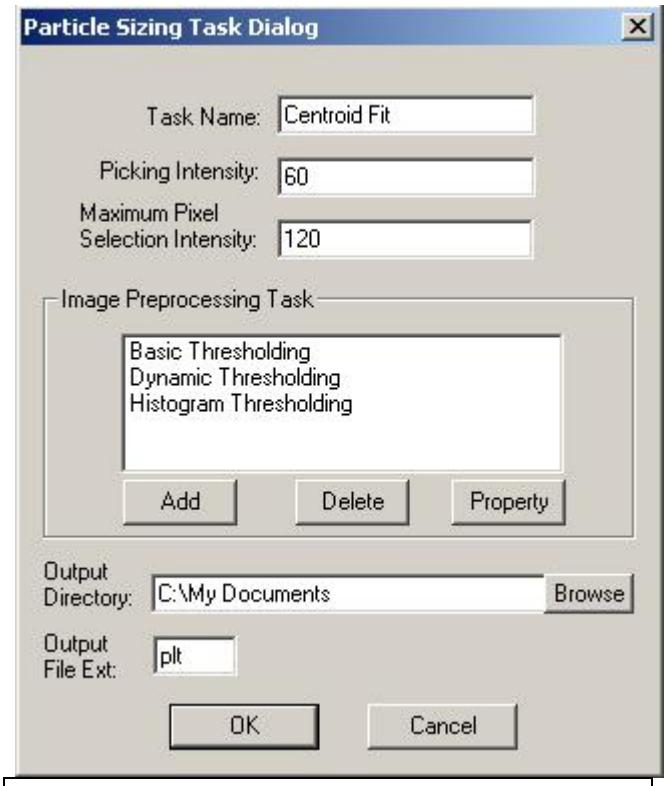

Figure 5. 3: Editing Particle Sizing Task

"Maximum Pixel Selection Intensity" is the minimum intensity a local maximum pixel intensity in the image must have to be considered a particle by the algorithm. Around this local maximum, every pixel greater than "Picking Intensity" will be considered part of this particle. All pixels with intensity less than "Picking Intensity" surrounding the peak pixel will be ignored.

Image preprocessing tasks may be added, and will be performed before the particle sizing algorithm is run. Clicking the ADD button brings up the Add Preprocessing Task Dialog Box (See Figure 3.1). Select the desired tasks, and click OK. To change the properties of the preprocessing tasks, click on the desired task and then click on "PROPERTIES". The properties can then be modified as discussed in Chapter 2.

To set the output directory, click on BROWSE and select the desired destination directory. The default output type is Tecplot ".plt" format.

The rest of the particle sizing tasks are edited in a manner similar to that discussed above.

Removing Particle Sizing Tasks

There are two ways to remove particle sizing tasks in FLOW-IQ V2.2, as a group or individually. To remove several sizing tasks from the active project, click on "Particle Sizing" in the upper-left window. "Particle Sizing" should now be highlighted. Now,

right-click on “Particle Sizing” and click on “Remove Sizing Tasks.” The Particle Sizing Remove Tasks Dialog Box will appear, as shown below in Figure 5.4.

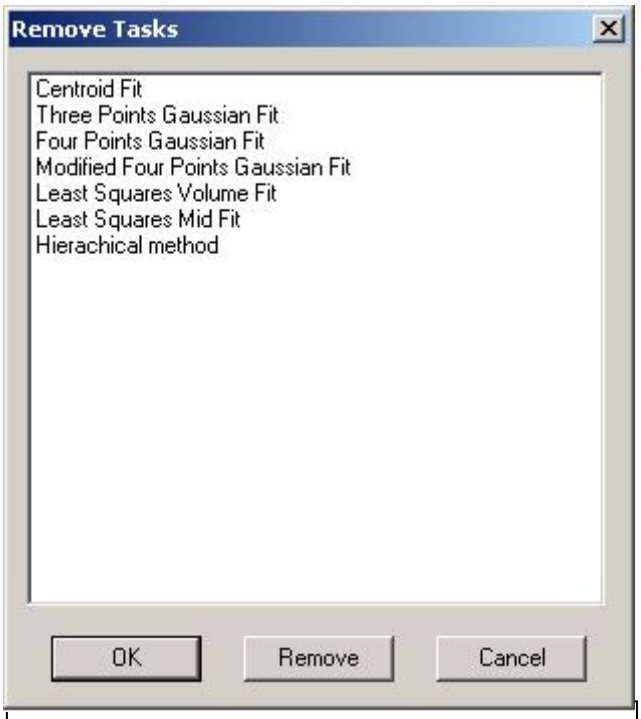

Figure 5. 4: Removing Particle Sizing Tasks

To remove a task, highlight the task by clicking on the task and click on REMOVE. This will remove the task from the list. When undesired tasks have been eliminated, click on OK and the preprocessing tree will be updated accordingly.

To remove individual particle sizing tasks, click on the task to be removed. The task should now be highlighted. Now, right-click on the task to be removed and click on “Remove.” The task will be deleted from the Particle Sizing Tree.

Running Particle Sizing Tasks

There are two ways to run particle sizing tasks in FLOW-IQ V2.2, as a group or individually. To run all of the listed particle sizing tasks in the tree, click on “Particle Sizing” in the upper-left window. “Particle Sizing” should now be highlighted. Now, right-click on “Particle Sizing” and click on “Run Task(s) on Data.” A menu will appear with a list of the available input packages for analysis. Click on the input package to be processed to run the tasks on the desired data. A menu will appear with a list of the available input packages for analysis. Click on the input package to be processed to run the tasks on the desired data. This will run the specified particle sizing tasks on the selected images in the project.

In order to run individual particle sizing tasks, click on the desired task. The task should now be highlighted. Now, right-click on the task to be removed and click on "Run Task(s) on Data." A menu will appear with a list of the available input packages for analysis. Click on the input package to be processed to run the tasks on the desired data. The individual task will be run on all of the selected images in the project.

When the particle sizing tasks have finished processing, a **##Finished Processing** message will appear in the lower-right window under "Console." A theoretical description of each available particle sizing task follows.

Nomenclature for Fitting Schemes

The nomenclature for the description of each fitting scheme is listed below.

a_i = discrete intensity value
d = particle diameter
d_r= pixel resolution of recording medium
d_t = geometric image diameter
d_s =diffraction limited spot diameter
$D_r(i,j)$ = true particle position
$D_m(i,j)$ = measured particle position
E_{true} = RMS error with respect to true value
E_{mb} = mean bias error
E_{rms} = RMS error with respect to mean
f# = f-number of the lens
I_o = maximum intensity
M = magnification of image
(x_c,y_c) = particle center
(x_i,y_i) = pixel location
λ = illumination wavelength
σ = standard deviation of gaussian curve
σ_n = standard deviation of added noise level

Centroid Fit

The Centroid Fit uses pixel counting and center-of-mass estimation algorithms to determine the centroid and diameter of a particle. A center-of-mass (intensity weighted centroid) estimator provides the simplest approach for estimating the center and area of a particle. Although not limited by the size of a particle the accuracy of this method is significantly compromised by saturation and noise. Moreover, it is subject to severe peak locking effects for particles with small diameters.

Pixel Counting gives an estimate of the apparent diameter of a particle with a easy to implement algorithm. The image is first preprocessed with a basic threshold filter. Each pixel is then sorted by its distance from an estimated center (using centroid method). The intensity of each pixel from the sorted list is summed until it is equal to four standard deviations (defined as the particle diameter as explained below). Pixel counting is computationally fast, however the method is very sensitive to the preprocessing task as will be shown.

Three Point Gaussian Fit

The three-point Gaussian estimator is a simple one-dimensional approximation of the geometric particle image.

$$\mathbf{a_i = I_0 e^{-\frac{(x_i - x_c)^2}{2\sigma^2}}} \quad \textbf{(1)}$$

The three independent variables: Io, σ , and x_c represent the maximum intensity, the Gaussian distribution standard deviation and the center position, respectively. If the three points chosen to solve these equations are the maximum intensity pixel, and the two neighboring pixels along the x-axis, then the standard three-point Gaussian estimator can be derived (Willert and Gharib 1991).

$$\mathbf{x_c = x_o + \frac{\ln a_{o-1} - \ln a_{o+1}}{2(\ln a_{o-1} + \ln a_{o+1} - 2\ln a_o)}} \quad \textbf{(2)}$$

The equation for finding y_c is equivalent, therefore five points are actually needed. The diameter measurement is directly related to the variance,

$$\sigma^2 = \frac{\ln \mathbf{a_{o+1}} - \ln \mathbf{a_o}}{(\mathbf{x_o - x_c})^2 - (\mathbf{x_{o+1} - x_c})^2} \quad \textbf{(3)}$$

The three point estimator is computationally fast and easy to implement. Its limitations are that it is a one-dimensional approximation thus when employed in 2-D it is practically a five point scheme that restricts the selection of points to the highest intensity pixel and its four neighbors along the rows and columns of the image. In addition, the diagonal pixels do not contribute to the measurement. Because of its nature, the three-point Gaussian fit does not allow discarding any pixels on the basis of their intensity, thus saturated pixels do contribute to the measurement. Finally, one more limitation stems from the fact that the center pixel which is the one with the highest intensity, is an upper bound for the maximum intensity value of the particle thus always constraining its calculation. Although this is not significant for the position estimation, it is of great importance for the diameter measurement, since it adjusts the height and spread of the Gaussian distribution and can be more detrimental when pixels are saturated. The three point fit is also very susceptible to high errors for particles larger than three pixels in diameter.

Four Point Gaussian Fit

A four point estimator is now presented. The motivation behind this method was to overcome the limitations of the three-point Gaussian fit and allow determining the center and diameter of a particle when it contains saturated pixels. For this scheme, if

saturated pixels exist, it is enforced that they do not contribute to the measurements. They are discarded and the measurements are then performed from the adjacent un-saturated pixels. This is significant in the case of the maximum intensity pixel that is the one most likely to be saturated. By removing the saturated high intensity pixels from the calculation we allow the accurate estimation of the particle maximum intensity value and the Gaussian spread, thus reducing the overall error of the method. Finally, the method is truly two-dimensional and accounts for the diagonal pixels.

Consider the two-dimensional intensity distribution:

$$\mathbf{a_i = I_0 e^{\frac{(x_i - x_c)^2 + (y_i - y_c)^2}{2\sigma^2}}} \quad \textbf{(4)}$$

We can solve for the four independent variables using the unsaturated intensities and coordinates at four points. The solutions for the center and variance are shown in Equations 6-8, and depend upon twelve constants defined as:

$$\alpha_1 = x_4^2(y_2 - y_3) + (x_2^2 + (y_2 - y_3)(y_2 - y_4))(y_3 - y_4) + x_3^2(y_4 - y_2)$$
$$\alpha_2 = x_4^2(y_3 - y_1) + x_3^2(y_1 - y_4) - (x_1^2 + (y_1 - y_3)(y_1 - y_4))(y_3 - y_4)$$
$$\alpha_3 = x_4^2(y_2 - y_1) + x_2^2(y_1 - y_4) - (x_1^2 + (y_1 - y_2)(y_1 - y_4))(y_2 - y_4)$$
$$\alpha_4 = x_3^2(y_2 - y_1) + x_2^2(y_1 - y_3) - (x_1^2 + (y_1 - y_2)(y_1 - y_3))(y_2 - y_3)$$

$$\gamma_1 = -x_3^2 x_4 + x_2^2(x_4 - x_3) + x_4(y_2 - y_3)(y_2 + y_3) + x_2(x_3 - x_4^2 + y_3^2 - y_4^2) + x_3(x_4^2 - y_2^2 + y_4^2)$$
$$\gamma_2 = x_1^2(x_3 - x_4) + x_3^2 x_4 + x_4(y_3^2 - y_1^2) - x_3(x_4^2 - y_1^2 + y_4^2) + x_1(-x_3^2 + x_4^2 - y_3^2 + y_4^2)$$
$$\gamma_3 = x_1^2(x_2 - x_4) + x_2^2 x_4 + x_4(y_2^2 - y_1^2) - x_2(x_4^2 - y_1^2 + y_4^2) + x_1(-x_2^2 + x_4^2 - y_2^2 + y_4^2)$$
$$\gamma_4 = x_1^2(x_2 - x_3) + x_2^2 x_3 + x_3(y_2^2 - y_1^2) - x_2(x_3^2 - y_1^2 + y_3^2) + x_1(-x_2^2 + x_3^2 - y_2^2 + y_3^2)$$

$$\beta_1 = x_4(y_2 - y_3) + x_2(y_3 - y_4) + x_3(y_4 - y_2)$$
$$\beta_2 = x_4(y_3 - y_1) + x_3(y_1 - y_4) + x_1(y_4 - y_3)$$
$$\beta_3 = x_4(y_1 - y_2) + x_1(y_2 - y_4) + x_2(y_4 - y_1)$$
$$\beta_4 = x_3(y_2 - y_1) + x_2(y_1 - y_3) + x_1(y_3 - y_2)$$

$$x_c = \frac{\ln(a_1)\alpha_1 + \ln(a_2)\alpha_2 + \ln(a_3)\alpha_3 + \ln(a_4)\alpha_4}{2(\ln(a_1)\beta_1 + \ln(a_2)\beta_2 + \ln(a_3)\beta_3 + \ln(a_4)\beta_4)} \quad \textbf{(5)}$$

$$y_c = \frac{\ln(a_1)\gamma_1 + \ln(a_2)\gamma_2 + \ln(a_3)\gamma_3 + \ln(a_4)\gamma_4}{2(\ln(a_1)\beta_1 + \ln(a_2)\beta_2 + \ln(a_3)\beta_3 + \ln(a_4)\beta_4)} \quad \textbf{(6)}$$

$$\sigma^2 = \frac{(x_4 - x_c)^2 + (y_4 - y_c)^2 - (x_3 - x_c)^2 - (y_3 - y_c)^2}{2(\ln(a_3) - \ln(a_4))} \quad \textbf{(7)}$$

It is interesting to note that if any three points used in the four-point fit are the same as the ones used in the three point fit for the x-axis, then the solution to x_c, Equation 6, reduces to the three point estimator (Equation 3), and similarly for the y-axis. It is also important to emphasize that the points selected for the four-point Gaussian estimation are not arbitrary and do not always yield a unique solution. The topology of the chosen points is paramount for the accuracy of the methodology and is determined by two additional

conditions. The first condition depends upon the pixel coordinates (x_i,y_i) only and is independent of the intensities. Assuming that the previously stated requirement of unsaturated pixels is satisfied, by observation of equations 5 and 6, it is obvious that if the denominators of x_c and y_c go to zero, a solution cannot be determined. It is possible to have the entire sum in the denominator go to zero, but each term in the sum is independent and that solution is trivial. Therefore each term must individually go to zero. Solving for $\beta_i=0$ yields:

$$\mathbf{x}_1 = \frac{\mathbf{x}_3\mathbf{y}_1 - \mathbf{x}_4\mathbf{y}_1 + \mathbf{x}_4\mathbf{y}_3 - \mathbf{x}_3\mathbf{y}_4}{\mathbf{y}_3 - \mathbf{y}_4} \qquad \mathbf{x}_2 = \frac{\mathbf{x}_3\mathbf{y}_2 - \mathbf{x}_4\mathbf{y}_2 + \mathbf{x}_4\mathbf{y}_3 - \mathbf{x}_3\mathbf{y}_4}{\mathbf{y}_3 - \mathbf{y}_4} \qquad \textbf{(8)}$$

Equation 8 represents the condition for all four points lying on the same line, which does not result to a solution in the four point fit and therefore must be avoided.

The second combination of points that does not yield a unique solution occurs if the four selected points all lie in a circle of any arbitrary center or radius. Assume any four points randomly located on a gaussian shaped particle as shown in Figure 2 (left). If the fourth point belongs on the circle determined by the first three, then it can be shown that the solution to the particle center, Equation 6 and 7 reduce to the solution of the center of the circle intersecting the four points, and is independent of any intensity values. In addition, the variance in Equation 8 goes to zero. The mathematical proof of the above condition is apparent by inspection. However, defining a circle using the first three points, and then inspect if the fourth point satisfies the equation of the circle can be used as a criterion for the point selection. Figure 2 shows examples of a acceptable (left) and unacceptable (center, right) groups of points.

The four-point Gaussian fit has the advantage over the three-point fit in that it is more flexible in selecting virtually any four of the pixels that satisfy the above conditions. Our practice showed that it is desirable to select pixels with high intensity and as close as possible to the maximum intensity pixel in order to reduce noise effects and minimize the error.

Least Squares Fit

Local least-squares (LLS) have been used in the past as alternatives to the three point Gaussian fit. The position and the diameter can be estimated with sub-resolution accuracy using a number of pixels greater than or equal to four. The local least squares fit is employed in this study by minimizing χ^2 described by Equation 10.

$$\chi^2 = \sum \left(a_i - I_o e^{-\frac{(x_i - x_c)^2 + (y_i - y_c)^2}{2\sigma^2}}\right)^2 \qquad (9)$$

The minimization was performed using a Gauss-Newton algorithm. The least squares fit allow for selecting certain points while leaving others out with no topological constrains. Two methods of point selection were investigated in the Monte Carlo simulations presented later. First, the conventional 3x3 pixel area around the one with highest intensity similarly to the standard three point Gaussian fit. This scheme was also

investigated by (Marxen and Sullivan 2000). Second, all the available points with intensity over a certain threshold value are accounted for. This is the equivalent of a high pass threshold filter and it is employed only for the larger particles in order to reduce excessive computational time.

Modified (Continuous) Four Point Gaussian Fit

Based on the above, an improved implementation of the four-point fit is now proposed. This is an integrated four point fit that eliminates the systematic error introduced by the pixel descretization. The integrated four point fit simply corrects for the pixel discretization by equating the integrated Gaussian profile over each pixel to the discrete gray value.

$$\mathbf{a_i} = \iint \mathbf{I_0 e}^{-\frac{(\mathbf{x_i}-\mathbf{x_c})^2+(\mathbf{y_i}-\mathbf{y_c})^2}{2\sigma^2}} \mathbf{dydx} \qquad \textbf{(10)}$$

Equation 9 cannot be solved in a closed-form, the expanded equations are shown in Equation 10 where Erf is the error function. Here x_i and y_i represent the position of the lower corner of each pixel, not the midpoint as in the Gaussian fits described above.

$$\mathbf{a_i} = \frac{\pi \mathbf{I_o}\sigma^2}{2}\left(\mathbf{Erf}\left[\frac{(\mathbf{x_i}-\mathbf{x_c})}{\sqrt{2}\sigma}\right]-\mathbf{Erf}\left[\frac{(\mathbf{x_i}+1-\mathbf{x_c})}{\sqrt{2}\sigma}\right]\right)\left(\mathbf{Erf}\left[\frac{(\mathbf{y_i}-\mathbf{y_c})}{\sqrt{2}\sigma}\right]-\mathbf{Erf}\left[\frac{(\mathbf{y_i}+1-\mathbf{y_c})}{\sqrt{2}\sigma}\right]\right) \qquad \textbf{(11)}$$

The nonlinear equations were solved using a form of the Powell dogleg optimization routine as described by Powell (1970). The same rules for point selection used in the Four Point fit were employed to the Integrated Four Point fit.

Least Squares Volume Fit

The third novel sub-resolution scheme developed during this study is the integrated local least square fit. Similarly to the integrated four point fit, introduced above, this scheme improves the error by taking into account the discretization error of the individual pixels.

$$\chi^2 = \sum\left(\mathbf{a_i} - \iint \mathbf{I_0 e}^{-\frac{(\mathbf{x_i}-\mathbf{x_c})^2+(\mathbf{y_i}-\mathbf{y_c})^2}{2\sigma^2}} \mathbf{dydx}\right)^2 \qquad \textbf{(12)}$$

As with the standard least squares, χ^2 was minimized using a Gauss-Newton algorithm. The same analysis as the standard least square for the point selection was performed on the integrated least square.

Hierarchical Fit

The hierarchical fit allows the user to select a series of sizing methods to perform. The options for the hierarchical fit are shown below in Figure 5.5. The setup for this method is the same as all of the other methods, except that the user may select a third method to perform after the Centroid and Three Point Gaussian Fit.

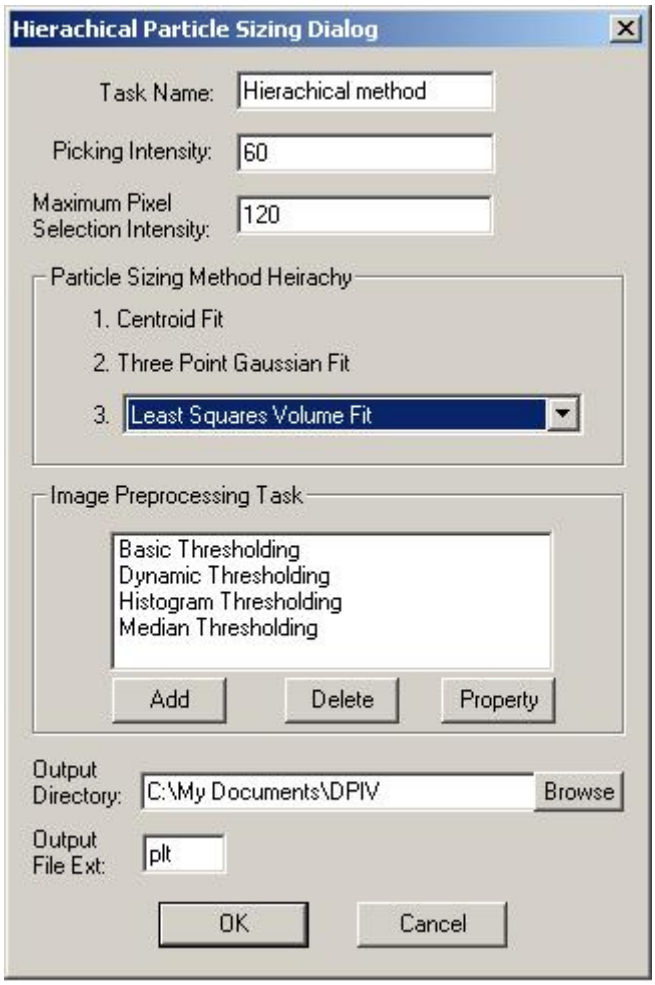

Figure 5. 5: Hierarchical Sizing Properties

The user may select the third method with the pull-down menu under "Particle Sizing Method Hierarchy." The methods will be performed in order 1 to 3, and the output will contain the *last* method that succeeds. For instance, if the Least Squares Volume Fit produces no result in this hierarchy, the results from the Three Point Gaussian Fit will be outputted to the destination file.

Chapter 6: Particle Image Velocimetry (PIV) Tasks

Several Particle Image Velocimetry techniques are included in Flow-IQ v2.2. This section deals with the addition, removal, and performance of PIV tasks. The available PIV techniques are briefly summarized in this section. PIV tasks can be run alone or in conjunction with particle tracking. The input files for PIV tasks are 8 bit ".tif" images.

Adding PIV Tasks

To add PIV tasks to the active project, click on "PIV" in the upper-left window. "PIV" should now be highlighted. Now, right-click on "PIV" and click on "Add PIV Tasks." The PIV Dialog Box will appear, as shown in Figure 6.1 below.

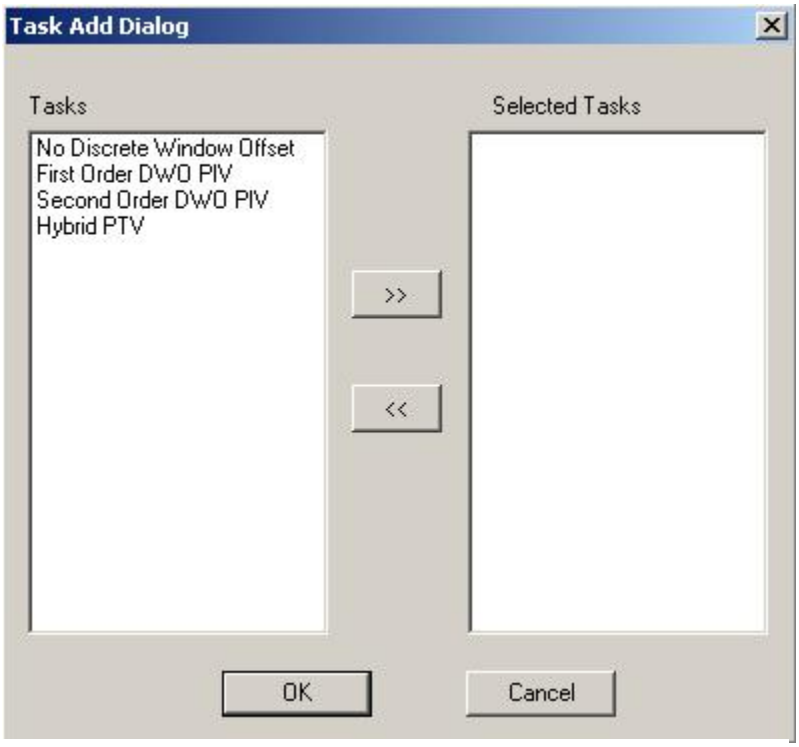

Figure 6. 1: Add PIV Task Dialog Box

To add a task to the project, click on the desired task to highlight it, and then click 

The available tasks are listed on the left, and the tasks to be added are shown on the right. When you have selected the desired tasks, click OK. The added tasks will be shown in a tree under "PIV," as shown below in Figure 6.2. These tasks will be performed from top to bottom in the tree. If you wish to change the order of operations, click and drag the tasks to new positions until you are satisfied with the order of operations.

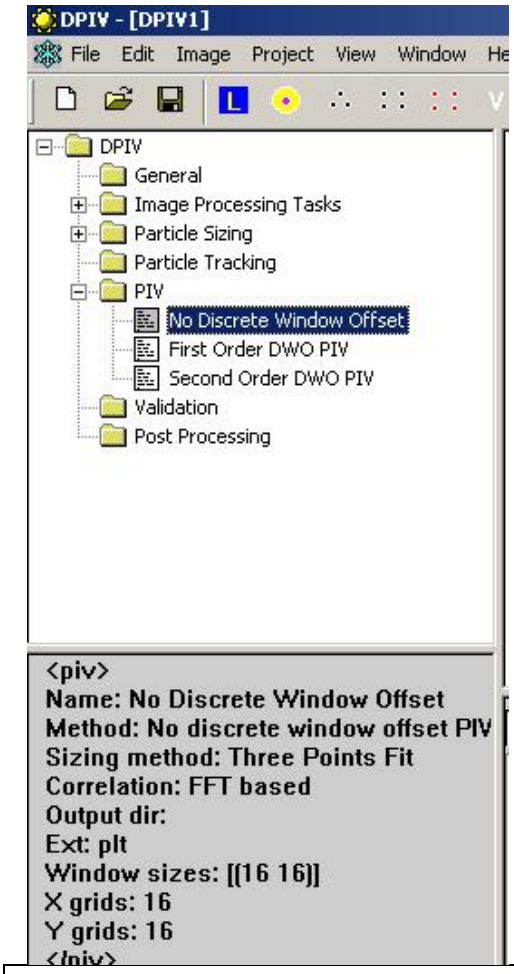

Figure 6. 2: Added PIV Tasks

Editing Task Properties

When a task is highlighted, as "No Discrete Window Offset" is in Figure 6.2 above, the properties of the task will be displayed in the lower-left window as shown. In order to edit these properties, click on the desired task to highlight the task. Then right-click on the highlighted task, and click "Properties." The corresponding dialog box will appear depending on the selected task. Enter the desired properties, and click OK. The individual properties are discussed below in detail for each PIV technique.

Removing PIV Tasks

There are two ways to remove PIV tasks in FLOW-IQ V2.2, as a group or individually. To remove several sizing tasks from the active project, click on "PIV" in the upper-left window. "PIV" should now be highlighted. Now, right-click on "PIV" and click on "Remove PIV Tasks." The PIV Remove Tasks Dialog Box will appear, as shown below in Figure 6.3.

Figure 6. 3: Removing PIV Tasks

To remove a task, highlight the task by clicking on the task and click on REMOVE. This will remove the task from the list. When undesired tasks have been eliminated, click on OK and the preprocessing tree will be updated accordingly.

To remove individual PIV tasks, click on the task to be removed. The task should now be highlighted. Now, right-click on the task to be removed and click on "Remove." The task will be deleted from the PIV Tree.

Running PIV Tasks

There are two ways to run PIV tasks in FLOW-IQ V2.2, as a group or individually. To run all of the listed PIV tasks in the tree, click on "PIV" in the upper-left window. "PIV" should now be highlighted. Now, right-click on "PIV" and click on "Run Task(s) on Data." A menu will appear with a list of the available input packages for analysis. Click on the input package to be processed to run the tasks on the desired data. This will run the specified PIV tasks on the selected images in the project.

In order to run individual PIV tasks, click on the desired task. The task should now be highlighted. Now, right-click on the task to be removed and click on "Run Task(s) on Data." A menu will appear with a list of the available input packages for analysis. Click on the input package to be processed to run the tasks on the desired data. The individual task will be run on all of the selected images in the project. A message similar to the following will appear in the lower-right window under "Console:"

Name: No Discrete Window Offset

Method: No discrete window offset PIV
Sizing method: Three Points Fit
Correlation: FFT based
Output dir: C:\Documents and Settings \My Documents
Ext: plt
Window sizes: [(16 16)]
X grids: 16
Y grids: 16
</piv>
Processing Frames 0~1 . . .
[16.320000000 seconds]
Processing Frames 0~1 . . .
[16.320000000 seconds]
##Finished Processing

When the PIV tasks have finished processing and all the frames have been completed, a **##Finished Processing** message will appear in the lower-right window under "Console." A description of each available PIV task follows.

No Discrete Window Offset (DWO) PIV

In No Discrete Window Offset (DWO) PIV, only a single interrogation pass is made. Regions within the two consecutive images undergoing PIV analysis will have the same coordinates in No Discrete Window Offset PIV. The user selects the interrogation window size as shown in Figure 6.4 below. The available window sizes are 8,16,32, and 64 pixels.

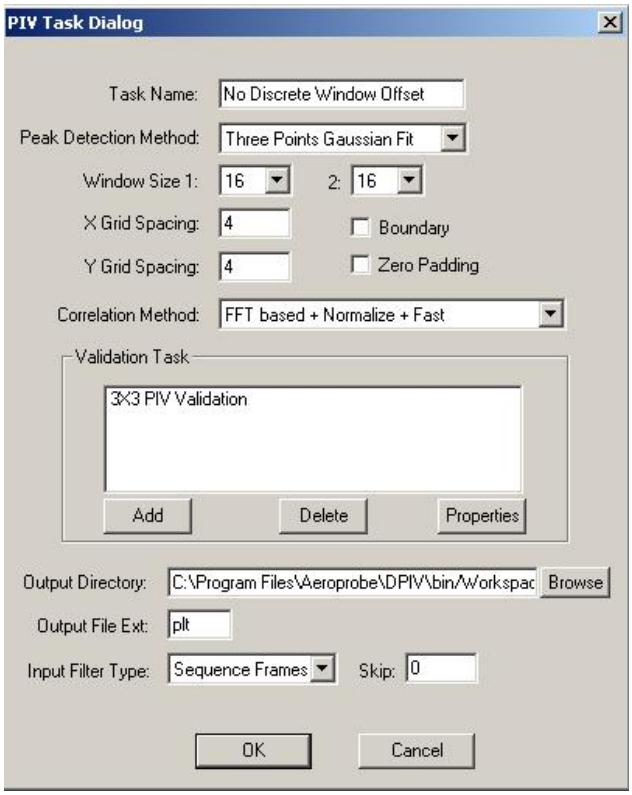

Figure 6. 4: No Discrete Window Offset Task Dialog Box

Peak Detection Method controls the method used to estimate displacement on the correlation. Window Size 1 determines the window size to use initially. Window Size 2 specifies a second try, which allows the user to specify a smaller window for attempting the NDWO PIV algorithm. X Grid Spacing and Y Grid Spacing specify the x and y grid spacing in the final output, and can take any value specified by the user. Boundary specifies whether boundary detection should be used to detect and remove the boundaries in the image. Zero padding, if clicked, forces the algorithm to pad the interrogation window sizes with zeros near the boundary in order to allow measurements very close to the wall. The user may add a validation task to the PIV algorithm in order to perform validation during PIV analysis by clicking on "Add" under "Validation Task." The properties of the validation task can be modified by highlighting the task and clicking "Properties." The user may specify the output directory by clicking BROWSE, selecting the desired output directory, and clicking OK. The user may also specify the output file extension, which defaults to Tecplot ".plt" format. Input Filter Type Specifies the sequence for the input files in the input package to be read, whether single-frame, double-frame, or sequence frames. Skip determines the desired skip between the input files, which defaults to 0 (no skip).

Correlation allows the user to select between FFT based and direct correlation and a variety of other options, which are listed below.

FFT Based – Fast Fourier Transform (FFT) correlation.
FFT Based + Normalize – Normalized Fast Fourier Transform (FFT) correlation.
FFT Based + Fast – Efficient Fourier Transform (FFT) correlation.
FFT Based + Normalize + Fast – Normalized and Efficient FFT correlation.
Direct – Direct correlation.
Direct + Normalize – Normalized Direct correlation.
Direct+ Fast – Efficient Direct correlation.
Direct + Normalize + Fast – Normalized and Efficient Direct correlation.

These options are available in all of the PIV algorithms used in Flow-IQ v2.2.

First-Order DWO PIV

In First Order DWO PIV, the initial pass is performed on identical areas in two corresponding image. For successive passes, the interrogation area in the second image is shifted by the rounded result from the initial pass. All successive passes are made on the resulting areas, and the final pass is added to the rounded integer initial estimate. If a pass fails, the previous pass is used to update the estimated displacement. For more information, see Chapter 9 on Output Types. The First Order DWO Process is shown below in Figure 6.5.

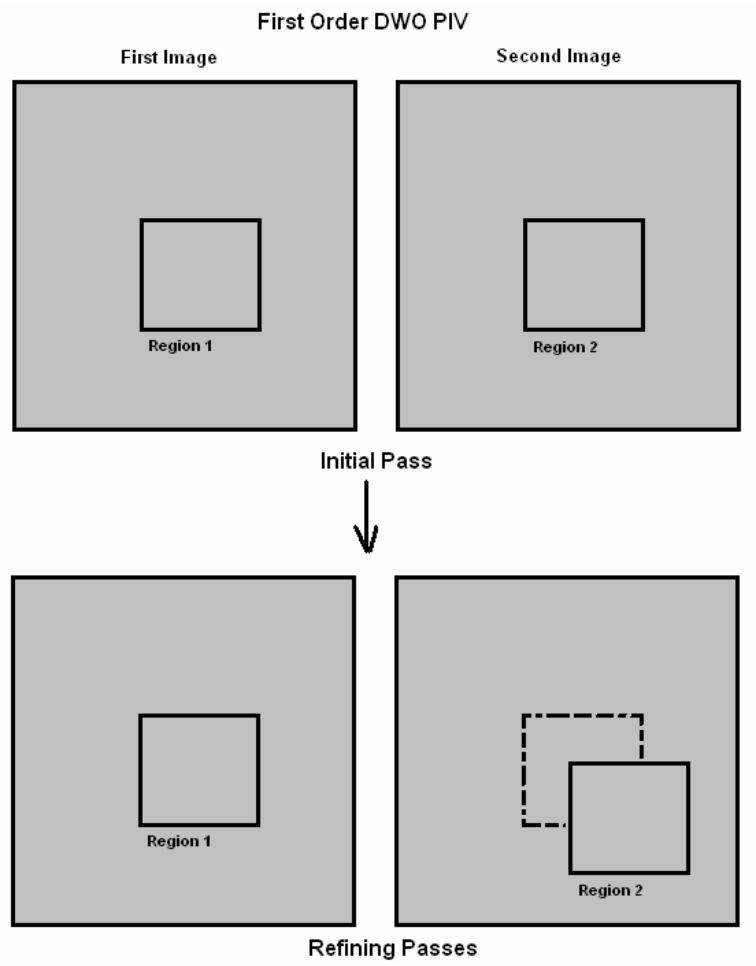

Figure 6. 5: First Order Discrete Window Offset

The options for First Order DWO PIV are much the same as in No DWO PIV, except that the user can specify a sequence of interrogation window sizes to be performed. There is no limit on the number of passes that can be performed. The windows must be a power

of 2 in order to use the FFT based correlation. If a non-power of 2 window is entered, the user will be prompted and direct correlation will be used for correlating regions of interest. The task option dialog box for First Order DWO PIV is shown below in Figure 6.6. Another feature added to the First Order DWO PIV is the Aggressive Multiple Pass, which is the dynamically-adaptive algorithm developed by Claude Abiven and Dr. Pavlos Vlachos in the ESM Fluid Mechanics Laboratory.

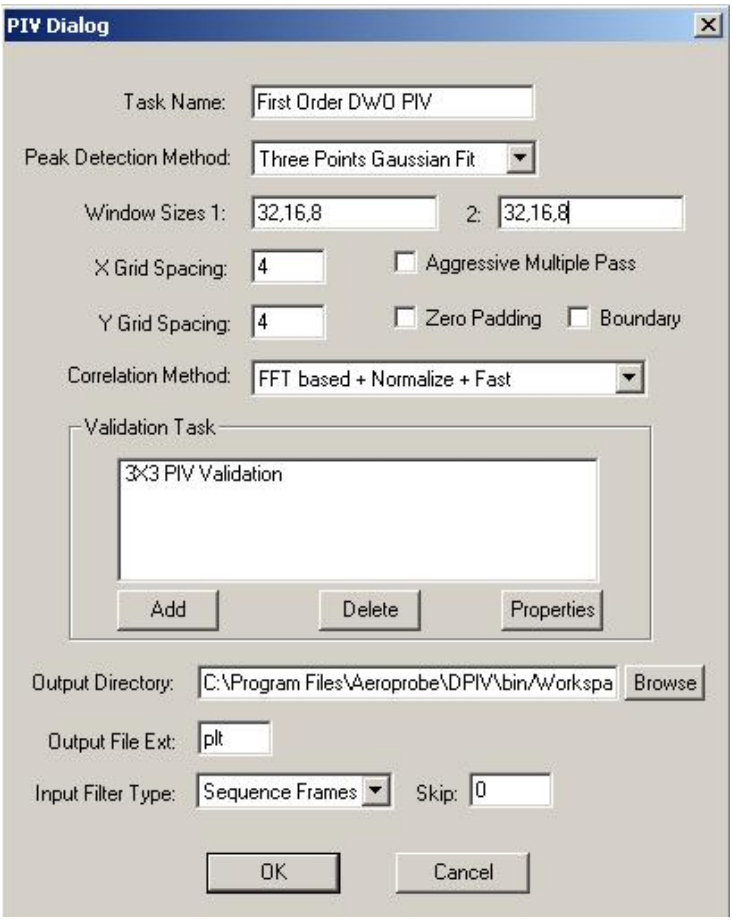

Figure 6. 6: First Order DWO PIV Options

To enter a series of interrogation window sizes, enter the desired sequence as shown in Figure 6.6, with commas separating the window sizes. In this example, FLOW-IQ V2.2 will perform PIV with 3 interrogation passes of 32, 16, and 8 pixels in that order.

Second-Order DWO PIV

In Second Order DWO PIV, the initial pass is performed on identical areas in two corresponding image. For successive passes, the interrogation area in the second image is shifted by half of the rounded result from the initial pass, and the interrogation window in the first image is shifted by negative one-half of the rounded result from the initial pass. If the rounded result is an odd number, then the second window is shifted by the ceiling of the rounded result from the initial pass, and the first window is shifted by the floor of the rounded result from the initial pass. All successive passes are made on the resulting interrogation areas, and the final pass is added to the rounded integer initial estimate. If a pass fails, the previous pass is used to update the estimated displacement. For more information, see Chapter 9 on Output Types. The Second Order DWO Process is shown below in Figure 6.7.

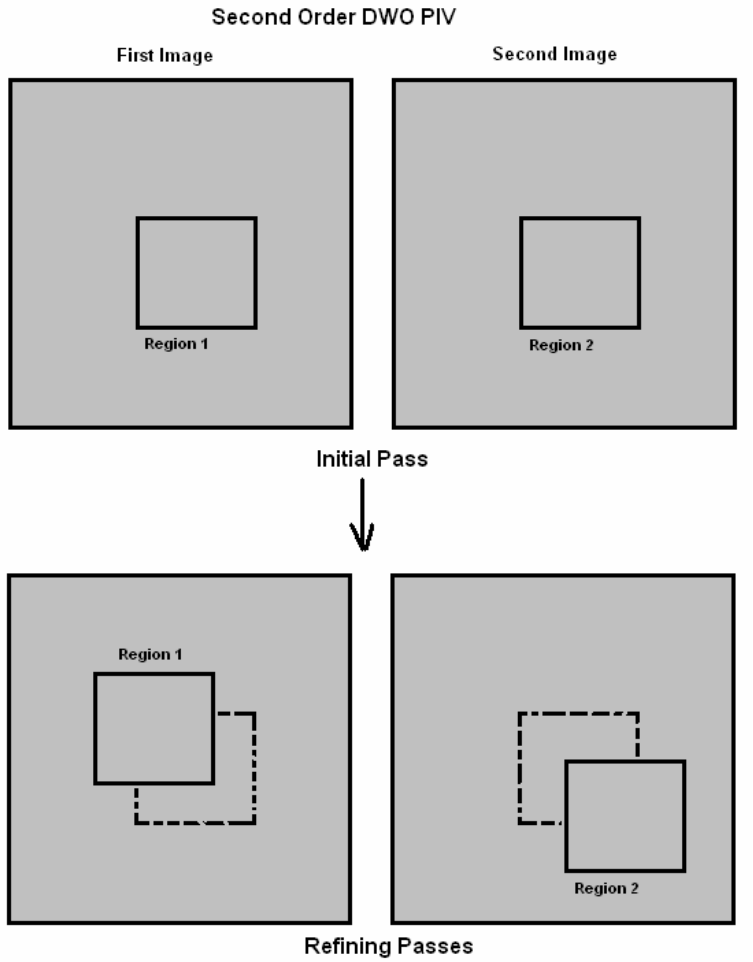

Figure 6. 7: Second Order Discrete Window Offset

The options for Second Order DWO PIV are the same as the options for First Order DWO PIV. See Figure 6.6 for a description of the available options in Second Order DWO PIV.

Hybrid PTV

In hybrid Particle Tracking Velocimetry (PTV), the results from PIV output are used to track particles using the local velocity field. The options for Hybrid PTV are shown below in Figure 6.8. The algorithm uses the output from particle sizing and PIV to produce the hybrid PTV results. The user must select a Particle Sizing method under "Particle Sizing" by clicking on "Add" and adding the desired sizing tasks. The properties of the sizing tasks can be modified by highlighting the desired task and clicking on "Properties" under "Particle Sizing." The user must also select a PIV method under "PIV" by clicking on "Add" and adding the desired sizing tasks. The properties of the sizing tasks can be modified by highlighting the desired task and clicking on "Properties" under "PIV." Distance specifies the search radius the algorithm uses to determine tracked particles, and is in pixel units. In the example shown in Figure 6.8, three point Gaussian sizing and First Order Discrete Window Offset PIV will be used with a search radius of 3 pixels to produce hybrid PTV results. The user may also specify an output directory for the PTV results by clicking on "Browse" and selecting the desired output directory. The default output type is Tecplot ".plt" format.

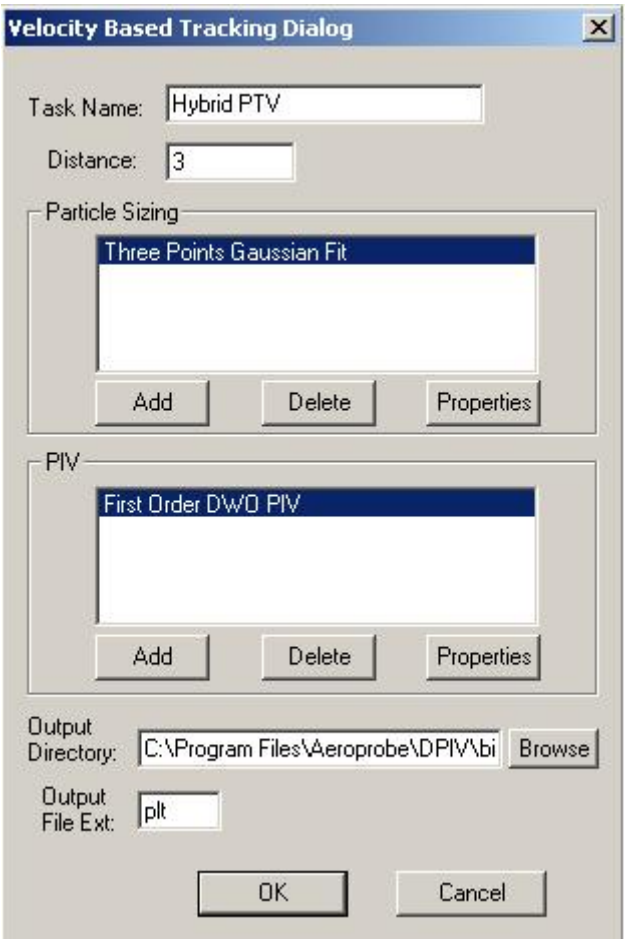

Figure 6. 8: Hybrid PTV Properties Dialog

Chapter 7: Validation

FLOW-IQ V2.2 includes validation algorithms for support with PIV applications. This section deals with the addition, removal, and performance of validation tasks. FLOW-IQ V2.2 includes several validation options to the user. Validation must be run on the ".plt" output from PIV tasks.

Adding Validation Tasks

To add particle tracking tasks to the active project, click on "Validation" in the upper-left window. "Validation" should now be highlighted. Now, right-click on "Validation" and click on "Add Tracking Tasks." The Validation Dialog Box will appear, as shown in Figure 7.1 below.

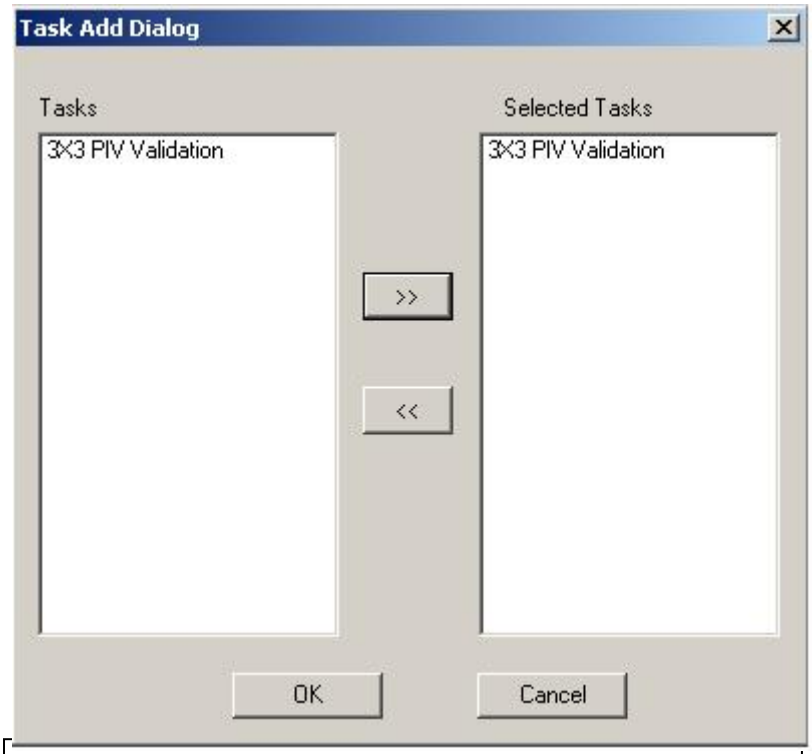

Figure 7. 1: Add Validation Task Dialog Box

To add a task to the project, click on the desired task to highlight it, and then click 

The available tasks are listed on the left, and the tasks to be added are shown on the right. When you have selected the desired tasks, click OK. The added tasks will be shown in a tree under "Validation."

Editing Task Properties

When a task is highlighted, the properties of the task will be displayed in the lower-left window as shown. In order to edit these properties, click on the desired task to highlight the task. Then right-click on the highlighted task, and click "Properties." The corresponding dialog box will appear depending on the selected task. Enter the desired properties, and click OK. The individual properties are discussed below in detail for each Validation technique.

Removing Validation Tasks

There are two ways to remove Validation tasks in FLOW-IQ V2.2, as a group or individually. To remove several sizing tasks from the active project, click on "Validation" in the upper-left window. "Validation" should now be highlighted. Now, right-click on "Validation" and click on "Remove Tracking Tasks." The Validation Remove Tasks Dialog Box will appear, as shown below in Figure 7.2.

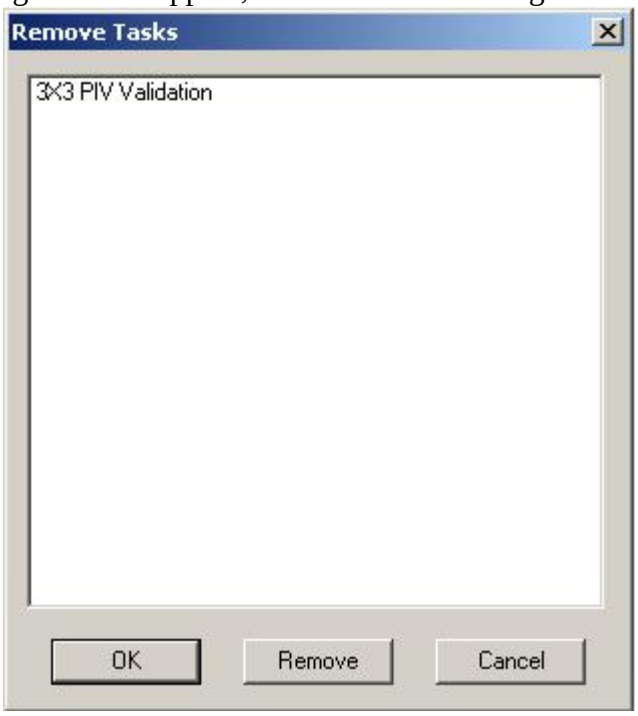

Figure 7. 2: Removing Validation Tasks

To remove a task, highlight the task by clicking on the task and click on REMOVE. This will remove the task from the list. When undesired tasks have been eliminated, click on OK and the preprocessing tree will be updated accordingly.

To remove individual Validation tasks, click on the task to be removed. The task should now be highlighted. Now, right-click on the task to be removed and click on "Remove." The task will be deleted from the Validation Task tree.

Running Validation Tasks

There are two ways to run Validation tasks in FLOW-IQ V2.2, as a group or individually. To run all of the listed Validation tasks in the tree, click on "Validation" in the upper-left window. "Validation" should now be highlighted. Now, right-click on "Validation" and click on "Run Task(s) on Data." A menu will appear with a list of the available input packages for analysis. Click on the input package to be processed to run the tasks on the desired data. This will run the specified Validation tasks on the selected images in the project.

In order to run individual Validation tasks, click on the desired task. The task should now be highlighted. Now, right-click on the task to be removed and click on "Run Task(s) on Data." A menu will appear with a list of the available input packages for analysis. Click on the input package to be processed to run the tasks on the desired data. The individual task will be run on all of the selected images in the project. A message similar to the following will appear in the lower-right window under "Console:"

<vld>
Name: 3X3 PIV Validation
Method: 3X3 PIV Validation
Output dir: C:\Documents and Settings\jcarneal\Desktop
Ext: plt
Standard deviation threshold: 0.100
</vld>
##Finished Processing

When the Validation tasks have finished processing and all the frames have been completed, a **##Finished Processing** message will appear in the lower-right window under "Console." A description of each available Validation task follows.

3X3 PIV Validation

The 3X3 PIV Validation task takes a 3 X 3 window centered around each velocity vector, and calculates the standard deviation and mean of the vectors surrounding the center vector to be validated. The algorithm then compares the center vector to the mean of the surrounding vectors, and if the difference between the center vector and the mean of the surrounding vectors is greater than the user-defined standard deviation threshold, the center vector is replaced by the mean of the surrounding vectors and is flagged as "invalid" in the output file. This process is illustrated below in Figure 7.3.

In Figure 7.3, the red vector is the vector to be validated. The black vectors are the surrounding vectors for which the mean and standard deviation are calculated. In this case, the center vector would most likely be flagged as invalid.

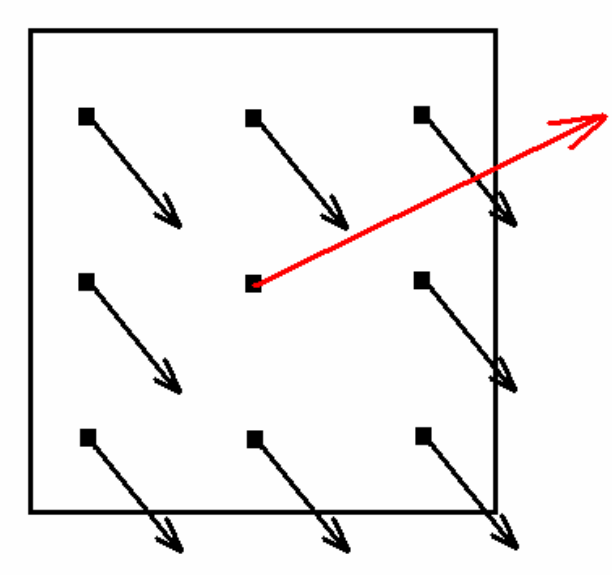

Figure 7. 3: 3X3 PIV Validation Scheme

The options for 3X3 PIV Validation are shown below in Figure 7.4. Standard Deviation Threshold High is the upper threshold the algorithm uses to flag vectors as valid or invalid. Low is the lower threshold value used to flag vectors as valid or invalid. Nx and Ny are the number of measurements in the x and y direction to use in the calculation of the standard deviation in a validation area. Filter can be set to "Mean" or "Median," depending on which parameter the user wishes to use in the validation analysis. The user can also check the "Adaptive" box to use an adaptive algorithm, which sequentially decreases the threshold values for the validation by half for each validation pass. The number of passes is determined by the value in "Number of Loops." The user can specify the output directory by Clicking on BROWSE and selecting the desired output directory. When the desired options have been selected, press OK to update the task to the specified options. The default output file extension is Tecplot ".plt" format.

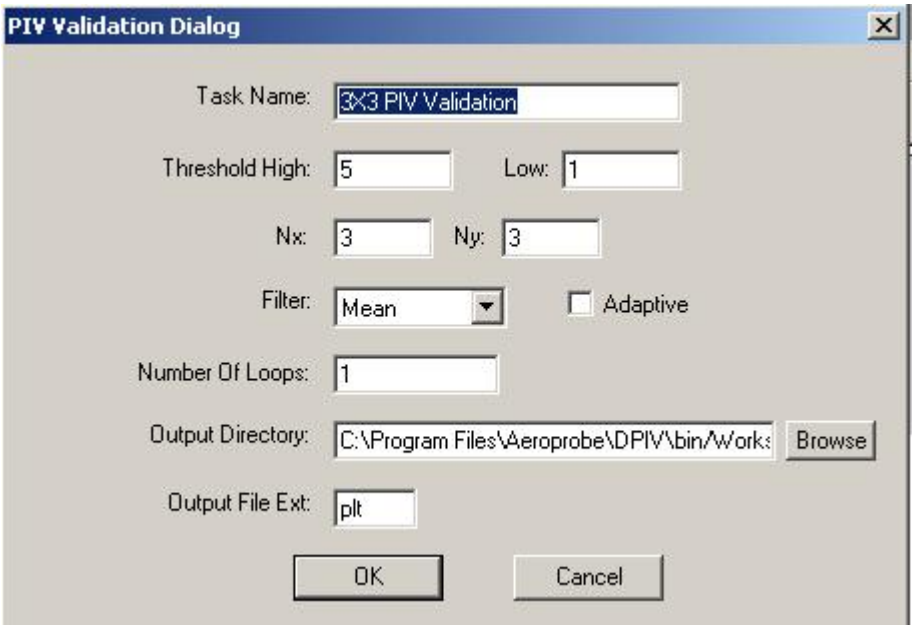

Figure 7. 4: 3X3 PIV Validation Options

Chapter 8: Stereo-PIV Tasks

FLOW-IQ V2.2 includes algorithms for the performance of Stereo-PIV. This section deals with the addition, removal, and performance of Stereo-PIV tasks.

Adding Stereo-PIV Tasks

To add STEREO-PIV tasks to the active project, click on "STEREO-PIV" in the upper-left window. "STEREO-PIV" should now be highlighted. Now, right-click on "STEREO-PIV" and click on "Add STEREO-PIV Tasks." The STEREO-PIV Dialog Box will appear, as shown in Figure 8.1 below.

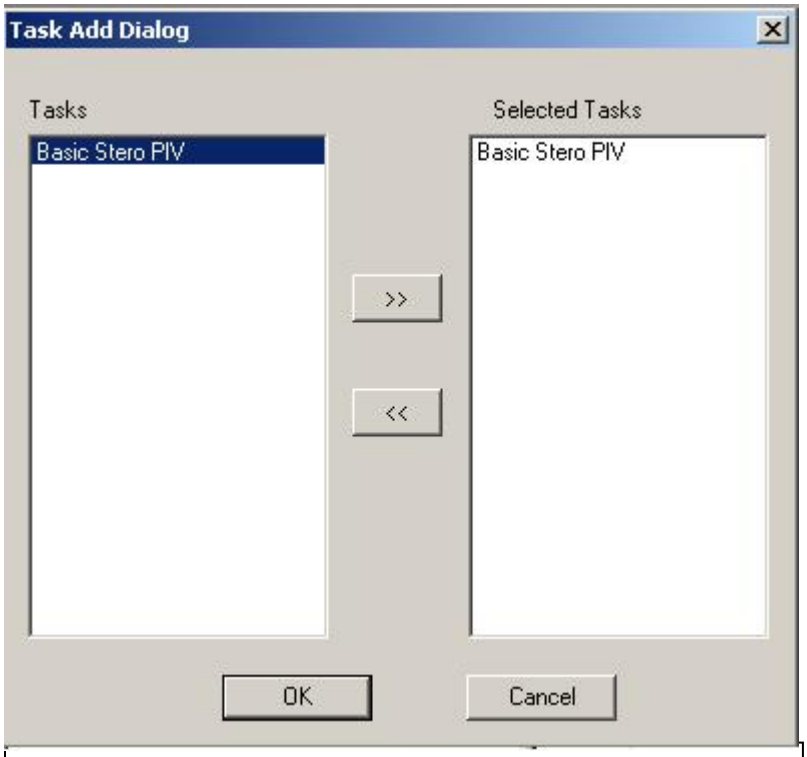

Figure 8. 1: Add Stereo-PIV Task Dialog Box

To add a task to the project, click on the desired task to highlight it, and then click 

The available tasks are listed on the left, and the tasks to be added are shown on the right. When you have selected the desired tasks, click OK. The added tasks will be shown in a tree under "STEREO-PIV." These tasks will be performed from top to bottom in the tree. If you wish to change the order of operations, click and drag the tasks to new positions until you are satisfied with the order of operations.

Editing Task Properties

When a task is highlighted, the properties of the task will be displayed in the lower-left window. In order to edit these properties, click on the desired task to highlight the task. Then right-click on the highlighted task, and click "Properties." The corresponding dialog box will appear depending on the selected task. Enter the desired properties, and click OK. The individual properties are discussed below in detail for each STEREO-PIV technique.

Removing STEREO-PIV Tasks

There are two ways to remove STEREO-PIV tasks in FLOW-IQ V2.2, as a group or individually. To remove several sizing tasks from the active project, click on "STEREO-PIV" in the upper-left window. "STEREO-PIV" should now be highlighted. Now, right-click on "STEREO-PIV" and click on "Remove STEREO-PIV Tasks." The STEREO-PIV Remove Tasks Dialog Box will appear, as shown below in Figure 8.2.

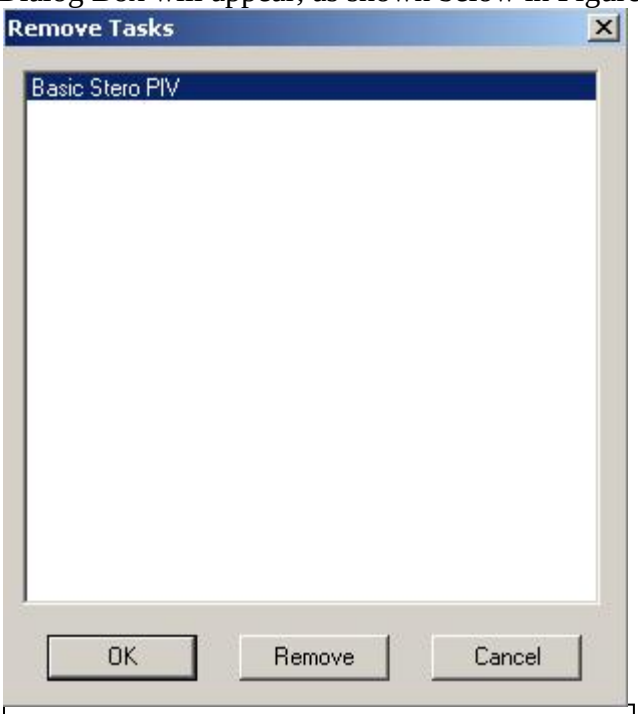

Figure 8. 2: Removing Stereo-PIV Tasks

To remove a task, highlight the task by clicking on the task and click on REMOVE. This will remove the task from the list. When undesired tasks have been eliminated, click on OK and the preprocessing tree will be updated accordingly.

To remove individual Stereo-PIV tasks, click on the task to be removed. The task should now be highlighted. Now, right-click on the task to be removed and click on "Remove." The task will be deleted from the Stereo-PIV Tree.

Running Stereo-PIV Tasks

There are two ways to run Stereo-PIV tasks in FLOW-IQ V2.2, as a group or individually. To run all of the listed PIV tasks in the tree, click on "Stereo PIV" in the upper-left window. "Stereo PIV" should now be highlighted. Now, right-click on "Stereo PIV" and click on "Run Task(s) on Data." A menu will appear with a list of the available input packages for analysis. Click on the input package to be processed to run the tasks on the desired data. This will run the specified Stereo-PIV tasks on the selected images in the project.

In order to run individual Stereo-PIV tasks, click on the desired task. The task should now be highlighted. Now, right-click on the task to be removed and click on "Run Task(s) on Data." A menu will appear with a list of the available input packages for analysis. Click on the input package to be processed to run the tasks on the desired data.

When the Stereo-PIV tasks have finished processing and all the frames have been completed, a **##Finished Processing** message will appear in the lower-right window under "Console." A description of each available Stereo-PIV task follows.

Basic Stereo PIV

In Basic Stereo PIV, the user must input the angles used in the Stereo-PIV experiment. The user must define Alpha left, Alpha Right, Beta Left, and Beta Right. The user may also select the output directory for the results by clicking on "Browse" and selecting the desired output directory. Figure 8.3 below shows the available options for the Basic Stereo PIV task in Flow-IQ v2.2.

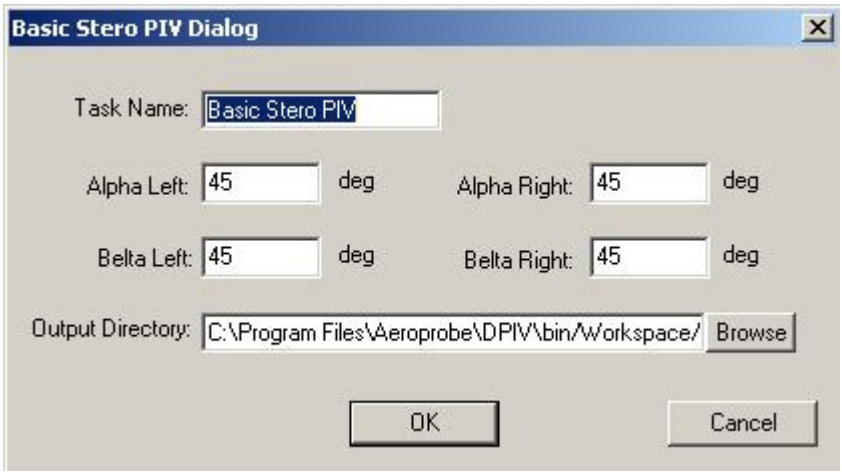

Figure 8. 3: No Discrete Window Offset Task Dialog Box

Chapter 9: Trajectory Tasks

In addition to Particle Image Velocimetry, FLOW-IQ V2.2 also includes particle tracking algorithms. This section deals with the addition, removal, and performance of particle tracking tasks. FLOW-IQ V2.2 includes basic tracking and Particle Tracking Velocimetry (PTV) tasks. As with the other available tasks, particle tracking can be run alone or in conjunction with particle tracking. The input files for particle tracking tasks are the output files from the Particle Sizing and PIV processes, which are Tecplot format ".plt" files (See Chapter 11 on Output Types).

Adding Particle Tracking Tasks

To add particle tracking tasks to the active project, click on "Particle Tracking" in the upper-left window. "Particle Tracking" should now be highlighted. Now, right-click on "Particle Tracking" and click on "Add Tracking Tasks." The Particle Tracking Dialog Box will appear, as shown in Figure 9.1 below.

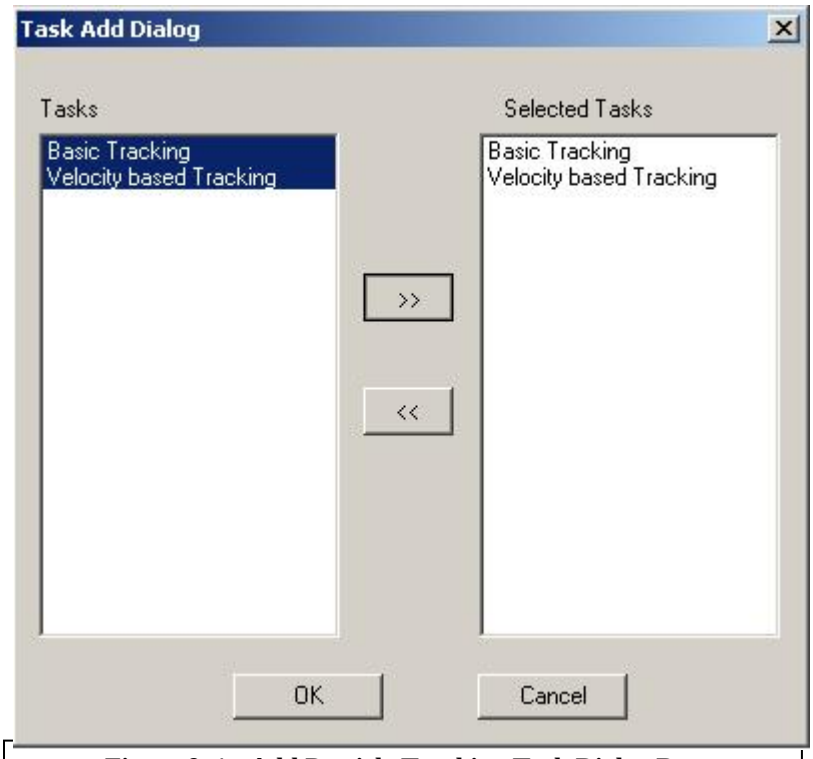

Figure 9. 1: Add Particle Tracking Task Dialog Box

To add a task to the project, click on the desired task to highlight it, and then click 

The available tasks are listed on the left, and the tasks to be added are shown on the right. When you have selected the desired tasks, click OK. The added tasks will be shown in a tree under "Particle Tracking."

Editing Task Properties

When a task is highlighted, the properties of the task will be displayed in the lower-left window as shown. In order to edit these properties, click on the desired task to highlight the task. Then right-click on the highlighted task, and click "Properties." The corresponding dialog box will appear depending on the selected task. Enter the desired properties, and click OK. The individual properties are discussed below in detail for each Particle Tracking technique.

Removing Particle Tracking Tasks

There are two ways to remove Particle Tracking tasks in FLOW-IQ V2.2, as a group or individually. To remove several sizing tasks from the active project, click on "Particle Tracking" in the upper-left window. "Particle Tracking" should now be highlighted. Now, right-click on "Particle Tracking" and click on "Remove Tracking Tasks." The Particle Tracking Remove Tasks Dialog Box will appear, as shown below in Figure 9.2.

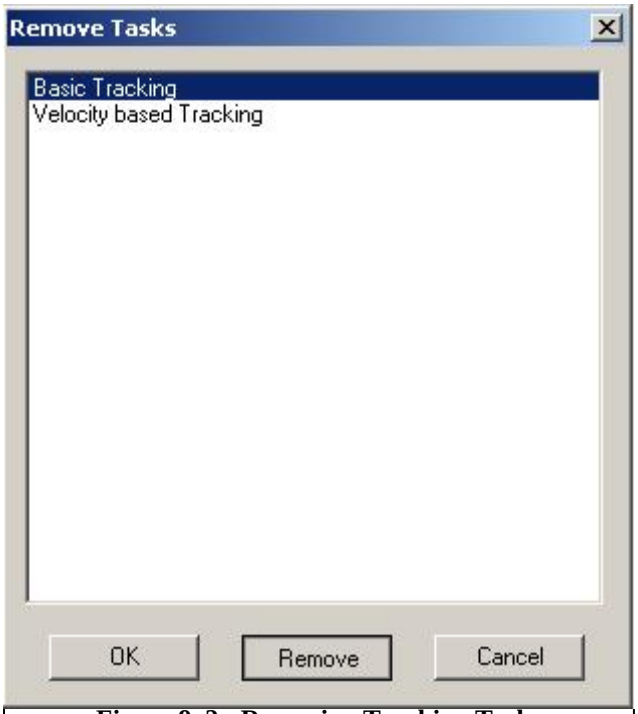

Figure 9. 2: Removing Tracking Tasks

To remove a task, highlight the task by clicking on the task and click on REMOVE. This will remove the task from the list. When undesired tasks have been eliminated, click on OK and the preprocessing tree will be updated accordingly.

To remove individual Particle Tracking tasks, click on the task to be removed. The task should now be highlighted. Now, right-click on the task to be removed and click on "Remove." The task will be deleted from the Particle Tracking Task tree.

Running Particle Tracking Tasks

There are two ways to run Particle Tracking tasks in FLOW-IQ V2.2, as a group or individually. To run all of the listed Particle Tracking tasks in the tree, click on "Particle Tracking" in the upper-left window. "Particle Tracking" should now be highlighted. Now, right-click on "Particle Tracking" and click on "Run Task(s) on Data." A menu will appear with a list of the available input packages for analysis. Click on the input package to be processed to run the tasks on the desired data. This will run the specified Particle Tracking tasks on the selected images in the project.

In order to run individual Particle Tracking tasks, click on the desired task. The task should now be highlighted. Now, right-click on the task to be removed and click on "Run Task(s) on Data." A menu will appear with a list of the available input packages for analysis. Click on the input package to be processed to run the tasks on the desired data. The individual task will be run on all of the selected images in the project. A message similar to the following will appear in the lower-right window under "Console:"

<ptk>
Name: Velocity based Tracking
Method: Velocity Based Tracking
Distance limit: 0.000000
Step count: 2
Output dir: none
Ext:plt
</ptk>
##Finished Processing

When the Particle Tracking tasks have finished processing and all the frames have been completed, a **##Finished Processing** message will appear in the lower-right window under "Console." A description of each available Particle Tracking task follows.

Basic Trajectory

The basic trajectory algorithm simply searches for particles in consecutive images within a user-defined search radius. Particles must be identified in each frame using the Particle Sizing tasks in Chapter 4 before running basic trajectory. The basic trajectory algorithm reads the Particle Sizing ".plt" files consecutively, and searches for particles within a certain radius. If a particle is found within the search radius, the algorithm assigns this particle as tracked and continues the trajectory until no particle is found in the search radius. Each tracked particle is assigned a number, and is stored in the corresponding output ".plt" file for particle trajectory in the destination directory. The options screen for Basic Trajectory is shown below in Figure 9.3.

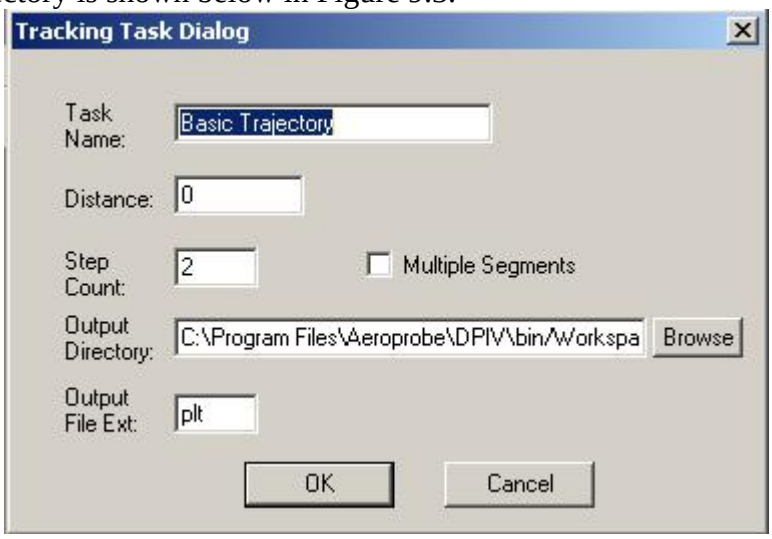

Figure 9. 3: Basic Tracking Options

Distance is the search radius, in pixels, that the algorithm will use to search for particles in successive frames. Step count is the incremental step between frames, in case the user wishes to skip a certain number of frames for processing. Output directory can be specified by clicking BROWSE and selecting the desired output directory. The output type for particle trajectory is Tecplot format ".plt."

Chapter 10: Output Types

This chapter discusses the output types for each class of tasks in detail.

Particle Sizing Output

A portion of an output ".plt" file using the Three Point Gaussian Fit is shown below. The first three lines are the header required by the Tecplot ".plt" format. The data is arranged in columns, with the first column listing the x coordinate of the particle. The second column contains the y coordinate of the particle. The third column is the estimated diameter of the particle, and the fourth column is a flag identifying the sizing method.

```
TITLE="Particle Sizing Data File"
VARIABLES="X" "Y" "Diameter" "MID"
Zone I=6
135.493496 253.628721 2.848859 1
239.724143 253.009294 2.850054 1
125.454566 252.157295 2.839976 1
223.564297 252.016439 2.846193 1
48.457762 249.068571 2.844447 1
89.926630 249.042028 2.889702 1
```

A list of the flags for the different sizing methods is shown below in Table 10.1.

Sizing Method	Output Flag
Centroid	0
Three Point Gaussian	1
Four Point Gaussian	2
Modified Four Point Gaussian	3
Least Squares Volume	4
Least Squares Mid	5

Table 10. 1: Output Flags for Sizing Methods

If a hierarchical fit is used, then the flag inserted in the output file will be the last sizing method that returned a result on the sizing.

PIV Output

A portion of an output ".plt" file using the Three Point Gaussian Fit is shown below. The first three lines are the header required by the Tecplot ".plt" format. The data is arranged in columns, with the first column listing the x coordinate of the velocity measurement. The second column contains the y coordinate of the velocity measurement. The third column is the estimated x component of the velocity "U", and the fourth column is the estimated y component of the velocity "V." The fifth column, "W," is the z component of the velocity. The sixth and seventh columns list the number of measurements in the x and y directions, respectively. The eighth column, "Correlation," shows the value of the

normalized correlation peak. The ninth column, “Valid,” lists a valid vector as “1,” and invalid vector as “-1,” and an unvalidated vector as “0.”

```
TITLE="FLOW-IQ Data File"
VARIABLES="X" "Y" "U" "V" "W" "Wx" "Wy" "Correlation" "Valid"
"Boundary"
Zone I=16 J=16
15.000000 241.000000 0.544723 3.497631 0.000000 16 16 0.481796 0 0
31.000000 241.000000 2.900743 1.608065 0.000000 16 16 0.496196 0 0
47.000000 241.000000 0.868580 -0.099177 0.000000 16 16 0.386605 0 0
63.000000 241.000000 -2.261536 -0.880877 0.000000 16 16 0.325937 0 0
79.000000 241.000000 1.252156 6.046097 0.000000 16 16 0.359740 0 0
95.000000 241.000000 -2.127558 0.524451 0.000000 16 16 0.391176 0 0
111.000000 241.000000 1.755754 -0.549097 0.000000 16 16 0.389217 0 0
127.000000 241.000000 2.095121 1.906425 0.000000 16 16 0.418114 0 0
143.000000 241.000000 0.000000 0.000000 0.000000 0 0 0.000000 -1 0
```

Hybrid PTV Output

Particle Trajectory Output

A portion of an output “.plt” file using Velocity-Based Tracking is shown below. The first three lines are the header required by the Tecplot “.plt” format. The data is arranged in columns, with the first column listing the x coordinate of the tracked particle. The second column contains the y coordinate of the tracked particle. The third column is the diameter of the tracked particle. The fourth column is the “FID” or Frame ID of the tracked particle. The fifth column is the Particle ID or “PID” of the tracked particle. Each time a new particle is found for tracking, it is assigned a sequentially increasing PID starting with 0. Then, the particle is tracked through the successive frames and FID is updated if the particle is tracked. For example, the first particle, PID 0, in this data set was tracked from frame 0 to frame 1 from (x,y) = (135.493496, 253.628721) in frame 0 to (x,y) = (140.790380, 248.332298) in frame 1, but not beyond.

```
TITLE="Particle Tracking Data File"
VARIABLES="X" "Y" "Diameter" "FID" "PID"
Zone I=168
135.493496 253.628721 2.848859 0 0
140.790380 248.332298 2.866822 1 0
239.724143 253.009294 2.850054 0 1
245.026787 247.708276 2.859587 1 1
125.454566 252.157295 2.839976 0 2
130.746163 246.854155 2.844657 1 2
```

Chapter 11: Advanced Topics

Flow-IQ v2.2 has been updated to allow more efficient use of the provided algorithms by using the "Copy" Feature. This feature allows the user to copy properties between classes of tasks. For instance, the user may select a image preprocessing task that is already set up and copy its properties to a particle sizing task. This feature allows the user to quickly set up new tasks with saved properties from other projects.

Copy Feature

In order to use the Copy Feature, click on a task that has already been set up by the user. The task may then be copied into the same tree, or the copied task can be dragged to another tree that uses the features of the copied task. A list of the compatible tasks is shown below in Table 11.1.

Task Type	Compatible With (Can be copied and dragged to)
Image Processing	Particle Sizing
Image Math	None
Particle Sizing	Hybrid PTV
PIV	Hybrid PTV
Validation	PIV tasks
Stereo-PIV	None
Trajectory	None

Table 11. 1: Copy Feature Compatibility

Copy Feature Example

In this example, the workspace has been set up by adding an Input Package named "Input," a Basic Thresholding Image Processing Task, and a Centroid Fit Sizing Task. The Basic Thresholding was updated using the procedures outline in Chapter 3. In order to copy the feature to the Centroid Sizing Tasks, the user simply clicks on the Basic Thresholding tasks and drags it to the Centroid task, as shown below in Figure 11.1. If the task is successfully copied, the following message appears in the console window.

##Image Pro Task "Basic Thresholding" Added to Sizing Task "Centroid Fit"

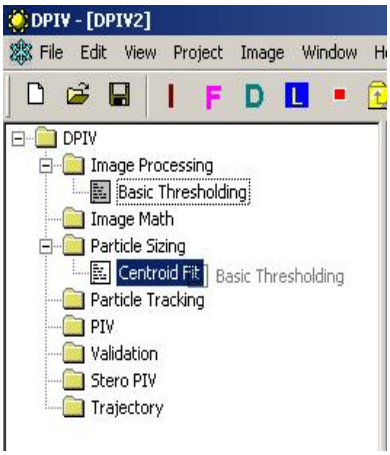

Figure 11.1: Copy Example 1

Chapter 12: FLOW-IQ APIs Documentation

The purpose of the document is to describe in details how to use the FLOW-IQ APIs.

At the time the document is written, FLOW-IQ is composed of image preprocessing, particle sizing, particle tracking, and PIV modules. Each module is a Win32 DLL that can be used by any Win32 application. We don't include any MFC stuff in these DLLs in order to make it work with any Win32 application. All of them share the same utility module that is also a DLL. Particle sizing, particle tracking and PIV modules work depending on the existence of image preprocessing module. PIV module also depends on particle sizing module. Particle tracking module depends on both particle sizing and PIV modules.

The document is organized as follows: section 1 describes utility module; image preprocessing module is given in section 2; section 3 illustrate particle sizing module; PIV is demonstrated in section 4; next section is particle tracking module.

1. Utility Module

The purpose of the module provides functionality common to other modules. It is reusable across projects.

- **Class Matrix<T>**

As a first-class template class, it provides basic matrix operations such as '+', '-', '*', etc. Although it is a user-defined type, it can be used in the similar way to the basic types (i.e. int). It can be used with any first-class class as its template type that has constructor T(int value).

Operations:

(1) Matrix construction

- Create a m*n double matrix: Matrix<double> mat(m,n);
- Create a m*n double matrix based on a one dimension array X: Matrix<double> mat(m,n,X);
- Create a m*n double matrix based on a two dimension array Y: Matrix<double> mat(m,n,Y);

Note: X and Y must have longer life than mat.

(2) Subscript operator: m(0,0) represents the first row, first column element. If m is a double matrix and z is a double, then you can do

- m(0,0) = 10.3;
- z=m(0,0);

(3) '+' unary operator: positive matrix, i.e. +m

(4) '-' unary operator: negative matrix, i.e. –m

(5) '=' assignment operator: m1 = m2

(6) Arithmetic operators “+=”, “-=”, “*=”, “/=”, “^=” : m1+=m2, m1-=m2, m1*=3, m1/=3, m1^=5 (power)
(7) Logic operators “==”, “!=”: m1 == m2, m1 != m2
(8) Friend arithmetic operators “+”, “-“, “*”, “^”, “~”(transpose): m1=m2+m3, m1=m2-m3, m1=m2*3, m1=m2^5, m1=~m2
(9) I/O stream operators “<<”, “>>”: cout<<m, cin>>m, fout<<m, fin>>m
(10) Set all elements to a certain value: m.Value(0)
(11) Change the size of the matrix: m.SetSize(3,3)
(12) Change the values of a row: m.SetRow()
(13) Change the values of a column: m.SetColumn()
(14) Get a copy of a row: m.GetRow()
(15) Get a copy of a column: m.GetColumn()
(16) Get sub matrix: m.GetSubMatrix(0,0,2,2)
(17) Get sub matrix: m.GetSubMatrixEx(-1,-1,3,3)

Note: GetSubMatrixEx allows index out of left-to-right or top-to-bottom range of matrix m. And set those unavailable elements from m as T(0). You cannot do this using GetsubMatrix().

(18) Flip the matrix from left to right: m.FlipLR()
(19) Flip the matrix from top to down: m.FlipUD()
(20) Check if the matrix is square: m.IsSquare()
(21) Get the dimension of the matrix: m.GetRowNo(), m.GetColNo()
(22) A matrix can be accessed in the way like an way by using operator [ ]: suppose m is a 2x3 matrix, then m[2] means m(0,3), m[4] means m(1,0), m[6] means m(1,2).
(23) Get the address of a row: m.GetRowAddr(2). This operation is provided for efficiency. Use it only to get values of the row elements.
(24) Element by element matrix multiplication: Matrix<double> x(2,2), y(2,2);

- x.DotMultiply(y); result is saved to matrix x.
- Matrix<double> z = x^y; result is saved to matrix z.

(25) Treat a matrix as one dimension array: Matrix<double> x(2,2); Then x[0] is the same as x(0,0); x[1] is the same as x(0,1),…

- **Class RealMatrix<T>**

The class is a wrapper of class Matrix<T>. It only accepts Matrix<T> where T is real type. So it will not work properly if user passes it a std::complex matrix.

Operations:

(1) Creation: RealMatrix<double> rm(m), where m is Matrix<double>
(2) Matrix norm: rm.Norm()
(3) Matrix mean: rm.Mean()
(4) Matrix standard deviation: rm.StdDev()
(5) Find the max value: rm.Max()
(6) Find the min value: rm.min()
(7) Find the max value and return its indices: rm.Max(rowIndex, colIndex)
(8) Find the min value and return its indices: rm.Min(rowIndex, colIndex)
(9) Convert to a rounded matrix: Matrix<int> rounded = rm.Round()

(10) Convert to a double type matrix: Matrix<double> d=rm.ToDouble()
(11) Count the number of elements whose values greater than or equal to some value: rm.CountGEs(20.0)
(12) Count the number of elements whose values less than or equal to some value: rm.CountLEs(2.0)
(13) Set the elements, whose values greater than or equal to some value x, to x: rm.ThreshHigh(20.0)
(14) Set the elements, whose values less than or equal to some value x, to x: rm.ThreshLow(5)
(15) Set the elements, whose values less than or equal to some value x, to 0: rm.ThreshLow(5, true)
(16) Sort elements from left to right, top to bottom: m.Sort();

- **Class RealSquareMatrix<T>**

The class is derived from class RealMatrix<T>. It only accepts Matrix<T> where T is real type
and the matrix is square. All of its operations are supposed to work with a real square matrix.

Operations:

(1) Creation: RealSquareMatrix<double> rm(m), where m is Matrix<double>
(2) Determinant: m.Det()
(3) Inversion: m.Inv()
(4) Cofactor: m.Cofact()
(5) Adjoin: m.Adj()
(6) Condition number: m.Cond()
(7) Set to identity matrix: m.Unit()
(8) Find eigen values/vectors: m.eig()
(9) Solve linear equation by LU factorization: for AX=B, call A.solve(B) to get X
(10) Check if the matrix is singular: m.IsSingular()
(11) Check if the matrix is diagonal: m.IsDiagonal()
(12) Check if the matrix is scalar: m.IsScalar ()
(13) Check if the matrix is unit: m.IsUnit()
(14) Check if the matrix is symmetric: m.IsSymmetric()
(15) Check if the matrix is skew symmetric: m.IsSkewSymmetric()
(16) Check if the matrix is upper triangular: m.IsUpperTriangular()
(17) Check if the matrix is lower triangular: m.isLowerTriangular()

- **Class DSP**

The responsibility of this class is to provide digital signal processing routines.

Operations:

(1) 1D FFT
```
Matrix<std::complex<double> > min, mout;
mout = DSP::fft(min);
```
(2) 1D inverse FFT

```
Matrix<std::complex<double> > min, mout;
mout = DSP::ifft(min);
```
(3) 2D FFT
```
Matrix<std::complex<double> > min, mout;
mout = DSP::fft2d(min);
```
(4) 2D inverse FFT
```
Matrix<std::complex<double> > min, mout;
mout = DSP::ifft2d(min);
```
(5) direct 2D convolution
```
Matrix<double> A, B, C;
C=DSP::conv2d(A,B, DSP::CONV_SHAPE_FULL);
```
(6) fft-based 2D convolution
```
C=conv2(A,B);
```
(7) direct 2D cross correlation
```
Matrix<double> A, B, C;
C=DSP::xcorr2d(A,B);
```
(8) direct 2D auto correlation
```
Matrix<double> A, C;
C=DSP::xcorr2d(A);
```
(9) normalized direct 2D cross correlation
```
C=DSP::xcorr2_norm(A,B);
```
(10) fft-based 2D cross correlation
```
C=DSP::xcorr2(A,B);
```
(11) fft-based 2D auto cross correlation
```
C=DSP::xcorr2(A);
```
(12) normalized fft-based cross correlation
```
C=DSP::xcorr2_norm(A,B);
```

- **Class EigenValueVector**

This class is used to realize the algorithm for finding eigen values/vectors.
Example:
```
RealSquareMatrix<double> t(m);
EigenValueVector evv=t.eig();
std::vector<double> r=evv.GetRealEigenValues();
std::vector<double> imag=evv.GetImagEigenValues();
```

- **Class SVD**

This class is used to do singular value decomposition. We just use part of its implementation to calculate the norm of a matrix. User should not use it directly.

- **Class BaseException**

This is the base class for all exception classes in this project

- **Class MatrixException**

This is the generic exception class for matrix.

- **Class SingularMatrixException**

It is derived from class MatrixException. It is thrown when there is a singular matrix exception.

- **Class IOException**

It is thrown when there is error in reading/wriging file

- **Class UnsupportedDataFormat**

It is thrown when file contains bad data

- **Class UnsupportedImageFormat**

It is thrown when a file has unsupported image format.

- **Class ExperimentConfig**

This class models experiment configuration. It provides info about number of apertures, magnification, camera pixel size, etc. It is used to convert pixel unit to physical unit
Operations:

(1) Get particle diameter in physical unit:
ecf. GetTrueParticleDiameter(x), where x is particle diameter in pixel unit, ecf is an ExperimentConfig object.
(2) Get veleocity in physical unit:
ecf.GetTrueVelocity(x), where x is velocity in pixel unit per sampling time
(3) Convert to physical unit: ecf.Pixel2PhysicalUnit(x);
(4) Get the number of apertures: ecf.GetNumberOfApertures();
(5) Set the number of apertures: ecf.SetNumberOfApertures(x);
(6) Get magnification factor: ecf.GetMagnificationFactor();
(7) Set magnification factor: efc.SetMagnificationFactor(x);
(8) Get camera pixel size: ecf.GetCameraPixelSize();
(9) Set camera pixel size: ecf.SetCameraPixelSize(x);
(10) Get sampling time: ecf.GetSamplingTime();
(11) Set sampling time: ecf.SetSamplingTime(x);
(12) Get exposure time: ecf.GetExposureTime();
(13) Set exposure time: ecf.SetExposureTime(x);
(14) Get wave length: ecf.GetWaveLength();
(15) Set wave length: ecf.SetWaveLength(x);

- **Class Mathematics**

This class provides some mathematical utility used by this application.
Operations:

(1) test if a double is zero: Mathematics::IsZero(x); where x is double
(2) round a double: Mathematics::Round(x);
(3) get the max value from two doubles: Mathematics::Max(a,b);
(4) get the min value from two doubles: Mathematics::Min(a,b);
(5) integrate a one dimension function: Mathematics::Integral(low,high,func);
where low is lower limit, high is upper limit, func is the function.
(6) Solve nonlinear equation:
Mathemtaics::fsolve(n,x,calfun,dstep,dmax,acc,maxfun);
Where,
n is the number of variables in the equations
x is the initial value of the variables (note, it's an array starts from 1 not 0)
calfun is the function used to evaluate the equations
dstep is step length

dmax is the change in the vector x at each iteration does not exceed dmax
dmax must be greater than dstep
acc is the required accuracy
maxfun is the maximum number of iterations

(7) Levenburg Marquardt Least Squares: Mathematics::LMLeastSquare(x, na, a, ny, y, s, f,lambda, termepsilon, maxiter);
where,
x is the matrix contains input variables (x1,x2,...) data. Each column of the matrix represents an input variable
na is the dimension of 'a'
a is the estimated paramters(ex: Io, belta, xc, yc)
ny is the dimension of 'y' and 's'
y is the output variable data, y=f(x1,x2,...,a1,a2,...)
s is normally set to 1.0
f is the function y=f(x1,x2,...,a1,a2,...)
lambda is blend between steepest descent (lambda high) and
jump to bottom of quadratic (lambda zero).
termepsilon is termination accuracy
maxiter is max iterations

public member:
static const double pi; //3.1415926

- **Class PltFile**

This class is the base class for any other format of plt file. Don't use this class directly. Design and use a class that derives from it.
Operations:

(1) Get the number of lines in the plt file: pltfile.GetNumOfLines(); where pltfile is a PltFile object.
(2) Get file name: pltfile.GetFileName();

- **Class FileSequence**

This class models a sequence of files. For example: spray0000.tif, spray0001.tif, spray0002.tif,… If a FileSequence object has accessory directory and extension (.plt), then that means it not only represent a sequence of tif files but also plt files. In fact, there are two sequences with same base name, sequence no but different extension or location.

Operations:

(1) Get full file name of the ith file: fs.GetFullFileNameOfIndex(i, filename); where fs is a FileSequence object, filename is the returned file name.
(2) Convert to a string: fs.ToString(aString); where aString is the returned string.
(3) GetAccessoryDir()
(4) GetAccessoryExt()
(5) SetAccessories()

Public members:
char Dir[MAX_FN_SIZE]; //location of files

char BaseFileName[MAX_FN_SIZE]; //base name of files
unsigned int StartIndex; //index of the first file
unsigned int EndIndex; //index of the last file
unsigned int Precision;//i.e. for “spray0000.tif”, Precision=4.
char Ext[8]; //file extension
static const char id; //the beginning character of the info for a FileSequence object. fs.ToString()

2. Image Preprocessing Module

- **Class Image**

It is responsible for reading, writing image from a file, and storing pixels. This class is a wrapper about class CxImage. Except raw image file, read, write and draw operations are delegated to the CxImage object.

Operations:

(1) Read image
Image img(“test.bmp”);
(2) Write image
Img.Save(“test1.bmp”);
(3) Fork() is used to clone the image, then you can do image processing operation on the cloned image. In this way, original image is not affected.
Note: don’t forget to do this operation before do any image processing.
(4) Join(false) is used to update the original image using the cloned image then delete it. Join(true) is used to merge the cloned image and original image and forget the change.
(5) Access the pixel matrix: img.Pixel();
(6) Get the image full path: img.GetID();
(7) Get image type: img.GetType();
(8) Get dimension: img.GetHeight(); img.GetWidth();
(9) Test if a file is supported image file: img.IsSupportedImage();
(10) Draw the image: img.Draw(…);

- **Class ImageProTask**

The class is the virtual base class for other image processing task classes. It defines the image processing task interface that must be conformed by other image processing classes.

Operations:

(1) Process image
bool Run(Image* imag);
(2) DoTasks()
Does a set of processing tasks on an image.
(3) Accept a visitor: task.Accept(aVisitor);
(4) Reset the task state: task.Reset();
(5) Get info about the task type: task.GetDesc()
(6) Get info aobut the task: task.GetHelpInfo()

(7) Get type id: task.GetID();

Public member:

char m_Name[MAX_FN_SIZE];//task name

- **Class ThresholdImageTask**

Basic thresholding

Public members:

UBYTE m_Low,m_High;//low and high threshold values

- **Class DynamicThresholdImageTask**

Dynamic thresholding

- **Class HistogramThresholdImageTask**

Histogram thresholding

- **Class BlurImageTask**

Blur mage

Pubic member:

unsigned int strength;

- **Class SmoothAGWTask**

Smooth image

Pubic member:

unsigned int strength;

- **Class EdgeDetectionTask**

Edge detection

- **Class BinarizeAreaTask**

Binarize area

3. Particle Sizing Module

- **Class Particle**

The responsibility of this class is to implement particle detection and various particle-sizing methods.

Operations:

(1) Creation

There are two methods to create a Particle object:

a) Particle::MapParticles()

It extracts Particle objects from an image. Keep in mind that this function returns a vector of pointers. So delete them after use.

b) Particle(label, left, top, right, bottom, pixels)
If you have a matrix of pixels in hand, use this method to create a Particle object. 'label' is the particle id; 'left', 'top', 'right' and 'bottom' are the location of the particle in its container image.

(2) Least squares fit method to detect particle size and position
p. LeastSquaresFit(), where p is a Particle object. By passing maptype=VOLUME or MID, one of the two least squares method is used.

(3) Four points gaussian fit method
p. FourPointsGaussFit()

(4) Modified four points gaussian fit method
p.ModifiedFourPointsGaussFit()

(5) Three points gaussian fit method
p.ThreePointsGaussFit()

(6) Centroid method
p. CentroidDiamFun()

Note: to use (2) to (5), you must supply reasonable initial values for function arguments Io, beta, diam, xc and yc. If you don't want to bother giving good initial values, then use (7)

(7) Sizing() method that takes a method id as first argument. For example, if you want to use Three points gaussian fit method, do this: p.Sizing(ParticleBase:: THREE_POINTS_FIT, minint, Io,beta,xc,yc);

(8) Add noise: Particle::AddNoise()

(9) Conversion between beta and diameter: Particle::btod(), Particle::dtob()

(10) Filter particles: FilterParticles(particles,selint); where, 'particles' is a vector of particles, 'selint' means a particle has at least one pixel with value greater or equal to selint. If a particle cannot meet this requirement, it is filtered out.

(11) Destroy the particle list generated from MapParticles:
Particle::Destroy(particles)

Public members:

Matrix<UBYTE> pixels; //the pixel matrix

- **Class ParticleT<T>**

A template class cannot be exported. And we don't need it is exported. We only need ParticleT<double> is exported, which is used in PIV to find particle displacement.

- **Class PzMethod**

This class models a particle sizing task. Given an image, it can return you a ParticleSizingResults object (see class ParticleSizingResults). It implements a standard particle sizing workflow including image preprocessing, particle extraction, filtering and sizing. If you do have special workflow, you can design a new class derive the class.

Operations:

(1) Run in one step: pzm.Run(image, results); where, pzm is a PzMethod object, image is an Image object, results is the returned ParticleSizingResults object.

(2) Run in multiple steps:

Particles = Pzm.Start(image);
Pzm.RunAParticle(ParticleI, image, psr); //where ParticleI is the ith element of Particles, psr is the returned ParticleSizingResult object. Repeat this class until all particles are processsed.
Pzm.End(Particles); //this call must be made to free resources.

Note if you want to do sth for example, display info on console to let user know what's going on, then "Run in multiple steps".

(3) Accept a visitor: pzm.Accept(aVisitor); here we user Visitor design pattern to give user the flexibility to modify pzm attributes through dialog, serialize them into file, or implement any other extensible functionality. For example, PzUIVisitor and PzSrlzvisitor are implemented in DPIV.exe, so that we don't have any GUI and MFC stuff in the dll.
(4) Get description about the type of current task: pzm.GetDesc();
(5) Get detailed description about the task: pzm.GetHelpInfo(Info, Size); where Info is an array at least 1024 bytes, Size is the array size.
(6) Get the task type id: pzm.GetID();
(7) Reset the state of the task: pzm.Reset(); It is recommended to call this function before calling Run().

Public members:

```
char m_Name[MAX_FN_SIZE];//task name
UBYTE minint;//minimum intensity
UBYTE selint;//selection intensity
std::vector<ImageProTask*> m_ImgProTasks;
char m_OFDir[MAX_FN_SIZE];//output file directory
char m_OFExt[8]; //output file extension
ExperimentConfig m_ExpCfg;//experiment configuration
```

- **Class HrkPzMethod**

This class models hierarchical sizing method. There are three levels of methods. The first two are fixed. They are centroid fit and three point. User can choose the third method. By default it is least square volume method. If the first method succeeds, use the result as initial Io, beta, diameter, xc,yc and apply the second method. If it fails, return the result from the first method. Otherwise, apply the third method using the result. If the third method succeeds, return the result. Otherwise, return the result from the second method.

Operations:

(1) Get the last method id: hrkpzm.GetLastMethodID();
(2) Set the last method id: hrkpzm.SetLastMethodID();

- **Class NonlinearEquation**

It gives the nonlinear equation specification.
Operation:

(1) Evaluate nonlinear equations
f->eval(), where is f is a pointer to a NonlinearEquation or its derived type object

- **Class LMfunc**

It gives the least square function specification.
Operation:

(1) Evaluate least square functions
f->eval(),where is f is a pointer to a LMfunc or its derived type object

- **Class FourPointGaussFitEquation**

It specifies the nonlinear equations for four points gauss fit method. It is derived from class NonlinearEquation.

- **Class LMParticleSizing**

It specifies nonlinear least squares functions. It is derived from class LMfunc.

- **Class LabelConnectedComponent**

It is used to label connected components in a binary image.

Operations:

(8) Label the input image.
lcc.doLabel(img), where lcc is a **LabelConnectedComponent** object
(9) Get the number of labels
lcc.getNumberOfLabels()

4. PIV Module

- **Class CPIV**

This class is the base for other PIV classes. As an abstract class, it cannot be instantiated. It defines the PIV interface.

Operations:

(1) Get velocity vector: piv.Run(image1, image2, results); where image1 and image2 are consecutive images, results are the returned velocity vector.
(2) Accept a visitor: task.Accept(aVisitor);
(3) Reset the task state: task.Reset();
(4) Get info about the task type: task.GetDesc()
(5) Get info aobut the task: task.GetHelpInfo()
(6) Get type id: task.GetID();

Public members:

```
enum{NODMO_MULTIPASS, FIRST_ORDER_MULTIPASS,
     SECOND_ORDER_MULTIPASS, N_METHODS};
enum CorrType{FFT_BASED, DIRECT, N_CORRS};
m_Wss;// window size
m_Mx;// x grid
m_My;// ygrid
char m_Name[MAX_FN_SIZE];//task name
char m_OFDir[MAX_FN_SIZE];//output file directory
```

char m_OFExt[8]; //output file extension
int m_PzMethod;//particle sizing method
ExperimentConfig m_ExpCfg;//experiment configuration
int m_CorrType;//cross correlation type

- **Class NoDWOPIV**

This class models no discrete window offset PIV method.

- **Class FirstOrderPIV**

This class models the first order PIV method.

- **Class SecondOrderPIV**

This class models the second order PIV method.

- **Class WinSize**

This class models a window dimension.

Public members:

int x, y;

- **Class PIVPltFile**

This class models a PIV plt file for writing purpose only.
Operations:

(1) Creation: PIVPltFile pltfile(filename, nI, nJ); where nI is the number of rows, nJ is the number of columns of a velocity vector matrix.
(2) Output a velocity to file: pltfile.WriteVelocity(pivresults); where pivresults is a velcocity vector.

- **Class PIVFileReader**

This class is used to read velocity vectors from a plt file.
Operations:

(1) Creation: PIVFileReader reader(filename); if the file 'filename' doesn't exist, IOException is thrown.
(2) Read velocity vectors: reader.ReadAll(pivrs); where pivrs is a PIVResults object. If the file is not in correct format, this function returns false. As a user, check the return value to make sure reading is completed successfully.

- **Class PIVResult**

This class models a velocity vector.
Public members:

enum {INVALID=-1, PARTIAL_VALID=0, VALID=1};
INVALID – the vector is invalid
PARTIAL_VALID – the vector is not validated yet
VALID – the vector is validated and valid
double X;// X coordinate of position
double Y;// Y corrdinate of position
double U;// U component of velocity vector
double V;// V component of velocity vector
double W;// W component of velocity vector
int Wsx;//window size in x
int Wsy;//window size in y

double Ncc; //normalized cross correlation
int Valid;//validity flag
int Boundary;//boundary flag

- **Class PIVResults**

This class models a velocity vector matrix.
Public members:
std::vector<PIVResult> velocities;//velocity matrix in vector format
unsigned long nI;//number of row of velocity matrix
unsigned long nJ;//number of row of velocity matrix
int width; //image width
int height;//image height

- **Class PIVTaskVisitor**

The base class for PIV task visitors.

- **Class PivValidation**

This class defines the interface for validation task.

Operations:
(1) Validate a velocity vector matrix: pivv.Run(pivrs); where pivv is a PivValidation object, pivrs is a PIVResults object.
(2) Accept a visitor: task.Accept(aVisitor);
(3) Reset the task state: task.Reset();
(4) Get info about the task type: task.GetDesc()
(5) Get info aobut the task: task.GetHelpInfo()
(6) Get type id: task.GetID();

Public data members:
char m_Name[MAX_FN_SIZE];//task name
char m_OFDir[MAX_FN_SIZE];//output file directory
char m_OFExt[8]; //output file extension

- **Class C3x3PivValidation**

This class models 3X3 vector matrix validation. Get a 3X3 matrix with the validating vector as center from the input velocity vector matrix. Then calculate its mean and standard deviation without including the validating vector.

Public member:
double m_SdHigh;//standard deviation threshold

5. Particle Tracking Module

- **Class CParticleTracking**

This class defines the particle-tracking interface. This is an abstract class. So it cannot be instantiated.

Operations:

(1) Run next step: task.GoNextStep(fs); where task is an CParticleTracking object, fs is a FileSequence object. Each derived particle-tracking class has a step size. Some class allows its modification, but others does not.
(2) Query if the current file sequence is finished:: task.IsFinished(fs);
(3) Get start frame for current step: task.GetCurrentStartFrame(fs);
(4) Get end frame for current step: task.GetCurrentEndFrame(fs);
(5) Prepare for the next step: task.PrepareForNextStep();
Note: once finish or give up a file sequence, call task.Reset();

Public members:

```
double m_Distance;//distance limit
char m_Name[MAX_FN_SIZE];//task name
char m_OFDir[MAX_FN_SIZE];//output file dir
char m_OFExt[8];//output file extension
ExperimentConfig m_ExpCfg; //experiment configuration
```

- **Class BasicParticleTracking**

This class implements the basic particle-tracking method. It doesn't use any PIV information. Its input is particle sizing results in a plt file. It can be run in two modes: one-step-one-processing-unit and All-steps-one-processing-unit. In the first mode, particle list is reset at each step.

Operations:

(1) Set step size: task.SetStepNo(x); where x is new step size.

Public member:

```
bool m_MultiSeg;//if true, reset particle list at each step
```

- **Class VbParticleTracking**

This class implements the velocity-based particle-tracking method. It uses both PIV and sizing information.

Pubic members:

```
public:
  std::vector<PzMethod*> m_PzTasks;    //particle-sizing tasks
  std::vector<CPIV*> m_PIVTasks;    //PIV tasks
```

- **Class TrackingPltFile**

This class is used to output tracking result to a plt file.

- **Class TrackingTaskVisitor**

This class models a tracking task visitor.

References for DPIV Documentation

Adrian, R., Yao, C. Pulse laser technique application to liquid and gaseous flows and the scattering power of seed materials, *Applied Optics*, 24 (1985).

Adrian R.J.; Yao C.S., "Development of Pulsed Laser Velocimetry for Measurement of Fluid Flow," *Proceedings, Eight Biennial Symposium on Turbulence*, G. Patterson and J. L. Zakin, Eds. (University of Missouri, Rolla, 1983).

Bachalo WD, Experimental methods in multiphase flows. *Int J Multiphase Flow*, 20, pp. 261-295. (1994).

Black, D.L.; Mcquay, M.Q.; Bonin, M.P. Laser-based techniques for particle-sizing measurement: a review of sizing methods and their industrial applications. *Prog Energy Combust Sci*. 22. pp. 267-306 (1996).

Boedec, T; Simoens, S. Instantaneous and simultaneous planar velocity field measurements of tow phases for turbulent mixing of high pressure sprays. *Experiments in Fluids*, 31, pp. 506-518 (2001).

Cowen, E., Monismith, S., A hybrid digital particle tracking velocimetry technique. *Experiments in Fluids*, 22, pp. 199-211 (1997).

Fan, L.S.; Zhu, C., Principles of Gas-Solid Flows, Cambridge University Press, (1997).

Fincham AM; Spedding G. Low cost, high resolution DPIV for measure3ment of turbulent flow. *Experiments in Fluids*, 23 (1997).

Guezennec, Y.G.; Kiritsis, N. Statistical Investigation of Errors in Particle Image Velocimetry, *Experiments in Fluids*, 10 pp.138-146 (1990).

Hardalupas, Y.; Pantelides, K.; Whitelaw, J.H., Particle Tracking Velocimetry in Swirl-stabilized Burners, *Experiments in Fluids*, 29, pp. S220-S226 (2000).

Hassan, A.; Blanchat, T., *Experiments in Fluids*, 11, pp. 293 (1991).

Hassan, Y.; Blanchat, T.; Seeley, C.; Canaan, R., Simultaneous Velocity Measurements of Both Components of a Two-phase Flow Using Particle Image Velocimetry, *Int. J. Multiphase Flow*, 18, pp. 371-395, (1992).

Herpfer, D.C.; Jeng, S.M., Planar Measurements of Droplet Velocities and Sizes within a Simplex Atomizer, *AIAA J.*, 35, pp. 127-132 (1997).

Huang H; Dabiri D; Gharib M. On errors of digital particle image velocimetry. *Measurement Science and Technology* 8, pp. 1427-1440 (1997).

Jones, A.R., Light scattering for particle characterization. *Prog. Energy. Sombust. Sci*. 25, pp. 1-53 (1999).

Kadambi, J.R.; Martin, W.T.; Amirthaganesh, S.; Wernet, M.P. Particle Sizing Using Particle Image Velocimetry for Two Phase Flows, *Powder Technology*, 100, pp. 251-259 (1998).

Kato, H.; Nishino, A.; Shinshi, A.; Torii, K., Flow Visualization and Image Processing of Multiphase systems, FED-Vol. 209, ASME New York, pp. 115-122 (1995).

Keane, R.D.; Adrian, R.J. Optimization of Particle Image Velocimeters. Part 1: Double Pulsed Systems, . *Measurement Science and Technology* 1, pp. 1202-1215 (1990).

Keane, R.D.; Adrian, R.J. Optimization of Particle Image Velocimeters. Part 2: Multiple Pulsed Systems, *Measurement Science and Technology* 2, pp. 963-974 (1991).

Khalitov, D.A.; Longmire, E.K. Simultaneous two-phase PIV measurements for high speed flows. Third International Workshop on Particle Image Velocimetry. Santa Barbara. Sept. 16-18 (1999).

Lindken, R.; Gui, L.; Merzkirch, W., Velocity Measurements in Multiphase Flow by Means of Particle Image Velocimetry, *Chem. Eng. Technol*., 22, pp. 202-206 (1999).

Marxen, M., Sullivan, P., Loewen, M.,Jahne, B. Comparison of Gaussian particle center estimators and the achievagble measurement density for particle tracking velocimetry. *Experiments in Fluids*, 29 (2000).

Nishino, K; Kato, H; Torii, K. Stereo imaging for simultaneous measurement of size and velocity of particles in dispersed two-phase flow. *Meas. Sci. Tech*. 11 pp. 633-645 (2000)

Powell, M. J. D., "A Fortran Subroutine for Solving Systems of Nonlinear Algebraic Equations," *Numerical Methods for Nonlinear Algebraic Equations*, P. Rabinowitz, ed., Ch.7, (1970).

Sakakibara, J; Wicker, R.B.; Eaton, J.K., Measurements of the particle-fluid Velocity Correlation and the Extra Dissipation in a Round Jet, *Int. J. Multiphase Flow*. 22, pp. 863-881, (1996)

Udrea, D., Bryanston-Cross, P., Lee, W., Funes-Gallanzi, M. Two sub-pixel processing algorithms for high accuracy particle centre estimation in low seeding density particle image velocimetry. *Optics & Laser Technology*, Vol 28, no 5 (1996).

Wang X.S., Wu X.P., Liao G.X., Wei Y.X., Qin J.. Characterization of a water mist based on digital particle images. *Experiments in Fluids*, 33 (2002).

Willert, C.E.; Gharib, M. *Experiments in Fluids*. 10 pp. 181 (1991).

5.2 Test Bed for DPIV Software, Methods

Artificial and real PIV data were gathered and tested using the DPIV version 2.2 software. Eleven sets of 50 256X256 pixel uniform displacement images were generated using the existing software for image generation. The uniform displacement images ranged in displacement from -0.5 pixels to 0.5 pixels in 0.1 pixel increments. These images were analyzed using the DPIV version 2.2 software and the original *ultimate* software. Errors were calculated and plotted in order to compare the performance of the two systems. The output files from both tests were saved, and a comparison program was developed in C++ to characterize output by comparison with the original systems.

Several test cases were included in the test bed. PIV data from the IMP experiment, cylindrical vortex shedding (mining experiment), and spray data are included in the test bed, along with artificial Couette flow images and Osceen vortex images. The artificial image software generated by Claude Abiven (2002) was used for all artificial images in this work. All of the images in the test bed were analyzed with Flow-IQ v2.2 and *ultimate*. In the case of artificial input images, the errors were calculated and plotted. In the case of real PIV data, the results are compared directly to each other, using the *ultimate* output as the base for comparison.

The test bed was developed in C++ for data analysis and MATLAB for data visualization in order to provide ease of use for future participants in the analysis of DPIV software performance.

5.2.1 Test Bed for Flow-IQ v2.2 Results.

A test bed was developed in addition to the user's manual provided in this work. The basic error analysis portion of the test bed is included here. Uniform displacement images were generated in order to provide a test bed for the basic accuracy testing of Flow-IQ v2.2. Programs were developed for the analysis of the output ".plt" files from both Flow-IQ v2.2 and *Ultimate*. A comparison program was also developed to compare the output from the two programs. A set of basic images was constructed in order to provide a wide range of situational testing.

5.2.1.1 Uniform Displacement Results.

A set of uniform displacement images, with displacements ranging from -0.5 to 0.5 pixels, were created and analyzed using various options in Flow-IQ v2.2. Figure 5.1 below shows the mean, RMS, and total error for the *ultimate* code as compared to the Flow-IQ v2.2 No Discrete Window Offset, First Order Discrete Window Offset, and Second Order Discrete Window Offset algorithms with interrogation window sizes of 16 pixels square. Only a single pass was used, in order to check the accuracy of the first pass in all of the algorithms presented in the uniform case.

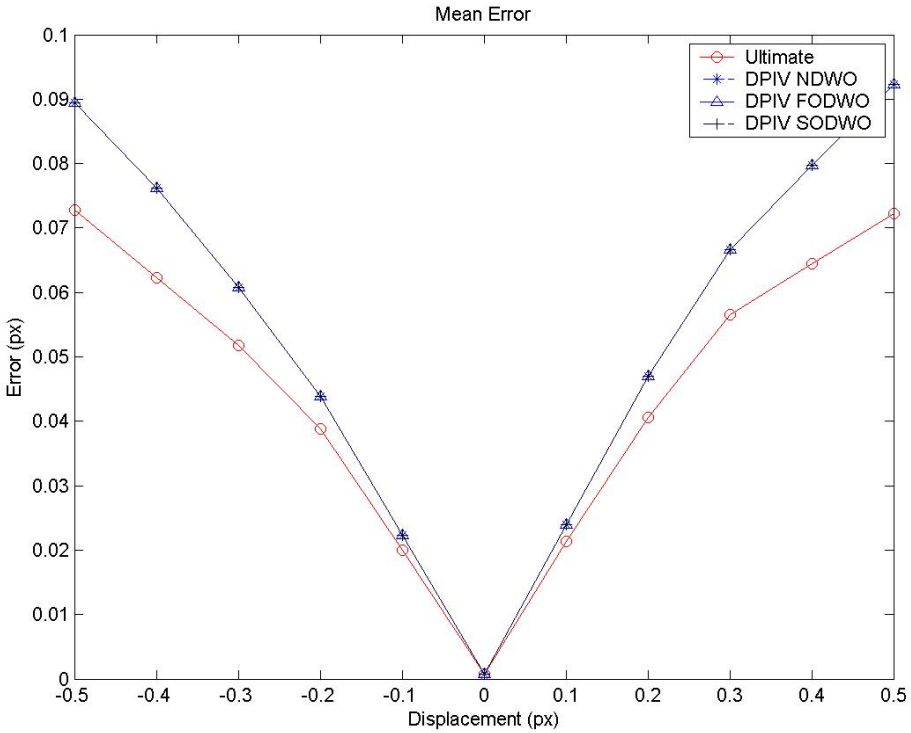

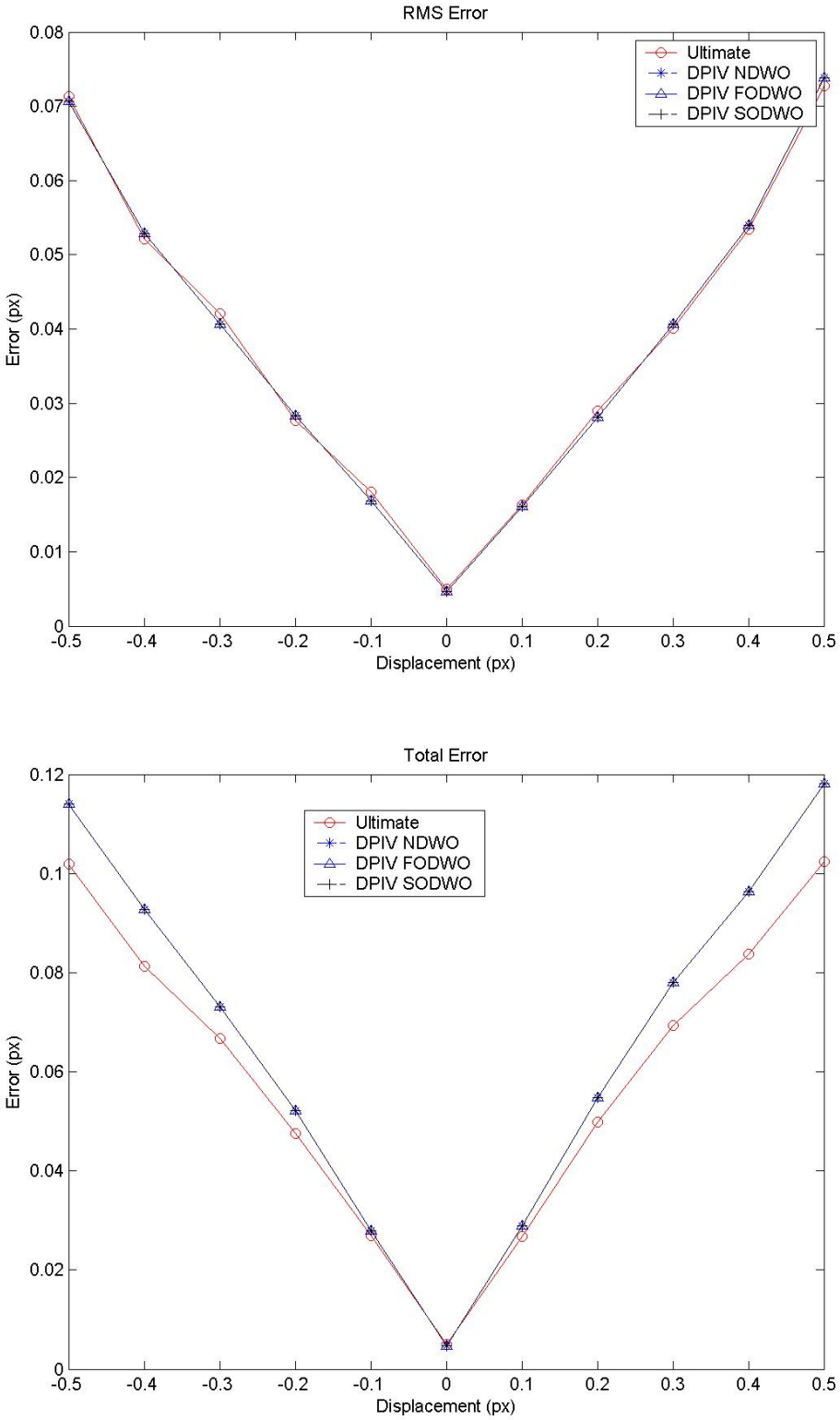

Figure 5.1: Mean, RMS, and Total Errors for Ultimate and Flow-IQ v2.2 NDWO and FODWO

Figure 5.1 shows that the mean error for Flow-IQ v2.2 is approximately 28% higher than the error for the *ultimate* code at a displacement of 0.5 pixels, and the total error for the Flow-IQ v2.2 program is approximately 20% higher than the *ultimate* code. The RMS errors are approximately

equal for all of the cases in Figure 5.1. All of the Flow-IQ v2.2 methods performed the same with no window offset, which means that the first pass in each method is consistent.

5.2.1.2 Vortex Results.

The results for a 3.0 maximum displacement vortex in the x and y direction for the First Order Discrete Window Offset, Second Order Discrete Window Offset, and No Discrete Window Offset are shown below in Figures 5.2 to 5.4. The algorithms used to obtain these results utilized a 16 pixel square first pass and an 8 pixel second pass, when applicable. The PIV algorithms analyzed in this section are the available algorithms in Flow-IQ v2.2. Figures 5.2 to 5.4 are included here as a proof-of-concept for the new test bed. No complete error analysis was performed on this data. The complete error analysis is left to future researchers.

The purpose of the test bed is to develop an interface for error analysis. Testbed2.m, a Matlab program, contains functionality for uniform and vortex error analysis for the Flow-IQ software. Future researchers should update the code to include ultimate processing capability, and to handle a wider variety of test cases.

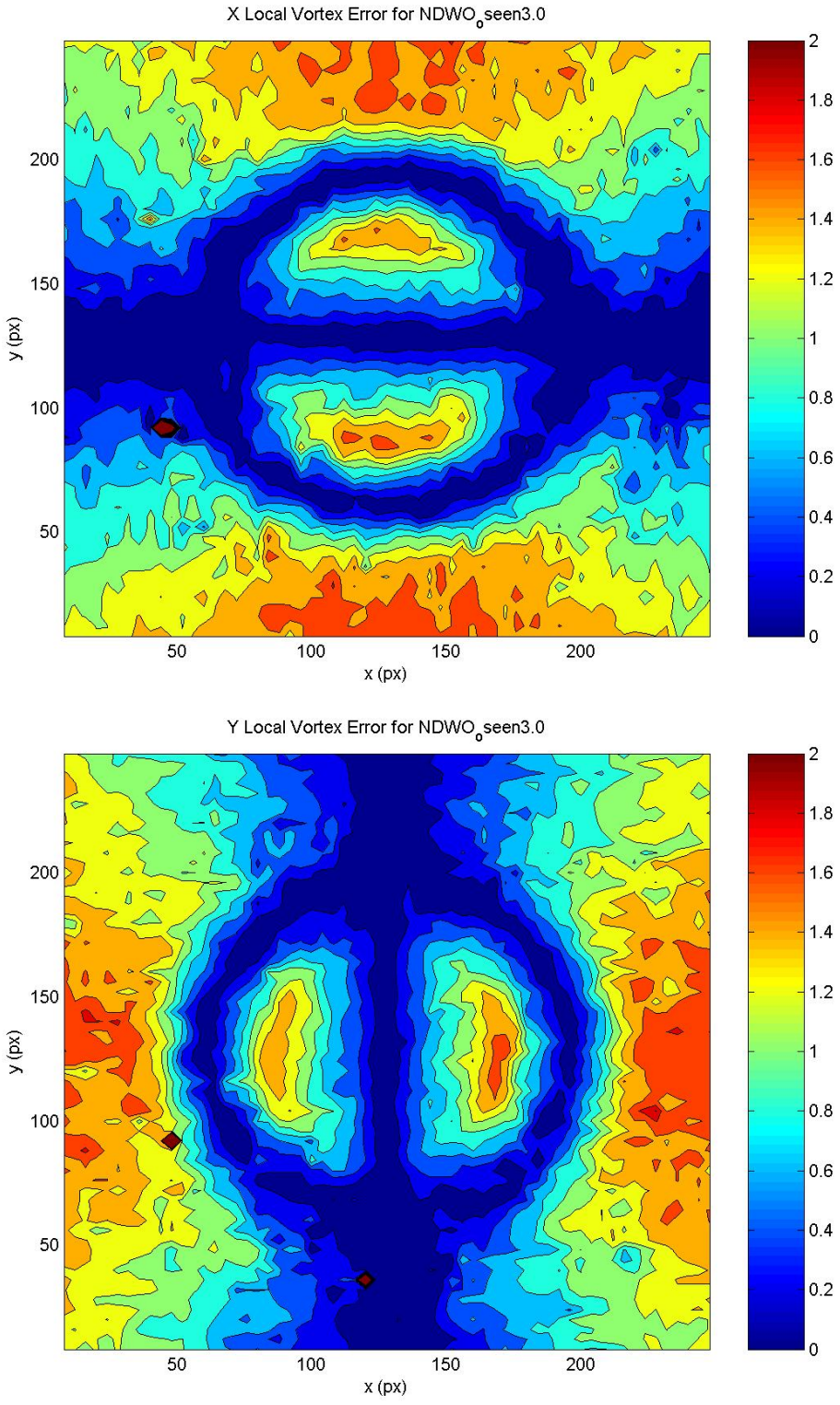

Figure 5.2: X and Y Local Error for No Discrete Window Offset

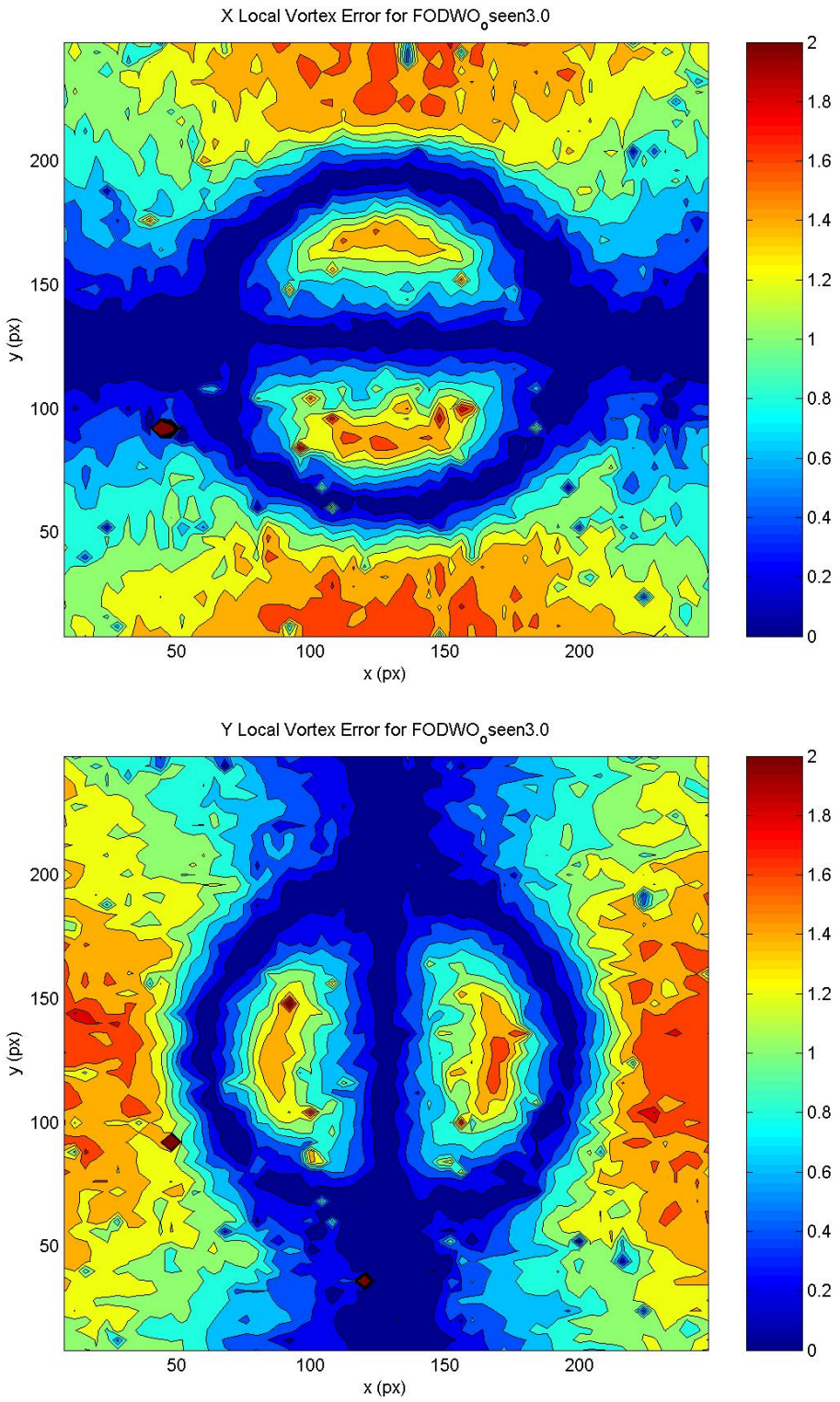

Figure 5.3: X and Y Local Error for First Order Discrete Window Offset

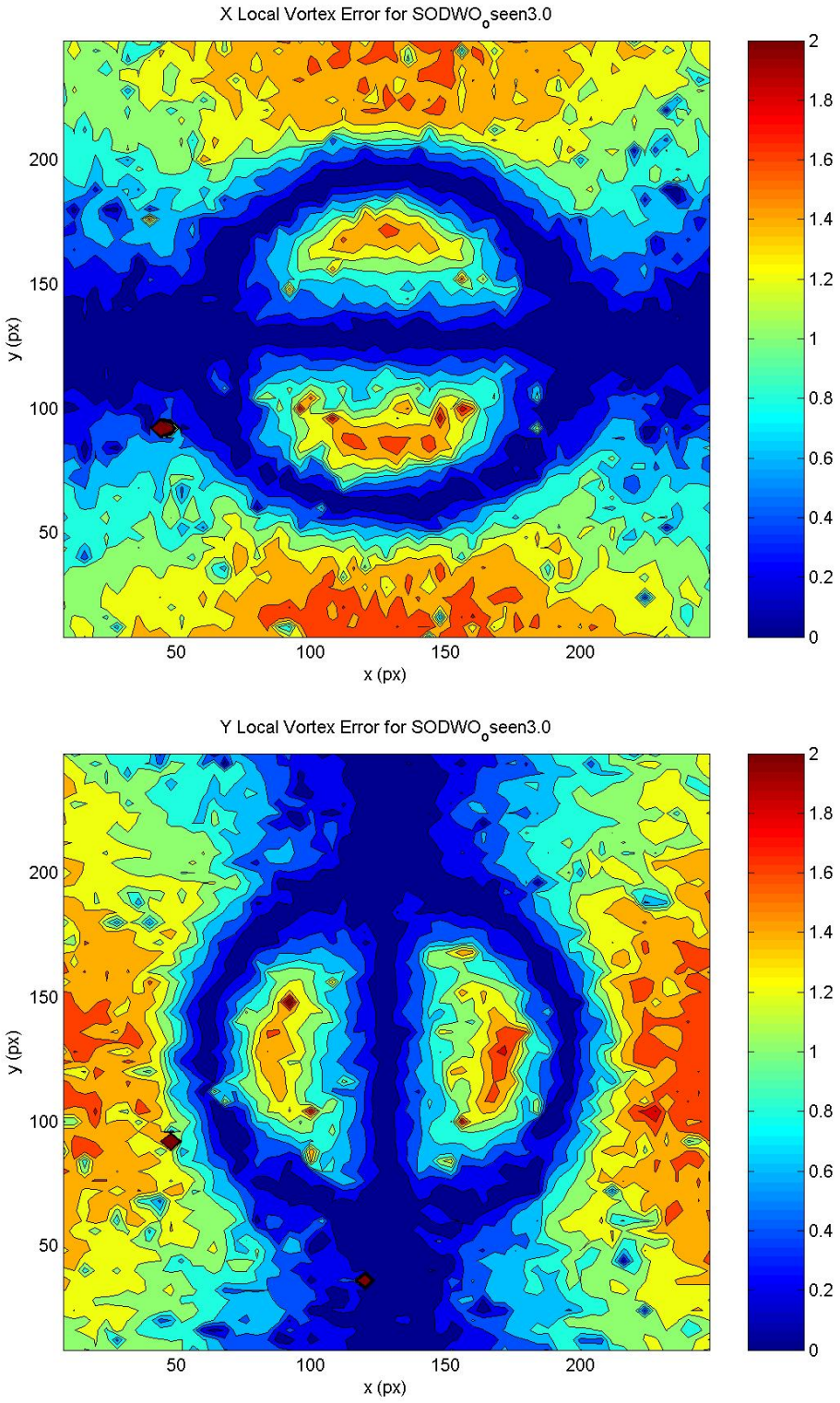

Figure 5.4: X and Y Local Error for First Order Discrete Window Offset

5.3 Summary of Original Contribution

The original contribution in this work is a complete and comprehensive user's manual for Flow-IQ software. All of the documented methods were developed by previous researchers. The document is a portion of the work completed in the course of this work. The other contribution in this chapter is a test bed that allows the comparison of .plt PIV output files and a base program for the execution of error analysis. This program will need to be modified by future researchers in order to handle multiple frames and multiple data sets.

REFERENCES

Abiven C., Vlachos P. P. (2002): Super spatio-temporal resolution, digital PIV system for multi-phase flows with phase differentiation and simultaneous shape and size quantification, Int. Mech. Eng. Congress, Nov. 17-22, 2002, New Orleans, LA

Abiven, C. Vlachos P. P. and. Papadopoulos G (2002): DPIV Strategies for resolving high shear and vortical flows, Int. Mech. Eng. Congress, Nov. 17-22, 2002, New Orleans, LA

Adrian, R., Yao, C. (1985), Pulse laser technique application to liquid and gaseous flows and the scattering power of seed materials, *Applied Optics*, **24**.

Adrian RJ (1991): Particle-Imaging techniques for experimental fluid mechanics. ARFM, 23, 261-304.

Adrian RJ, Meinhart CD, Barnhart DH and Papen GC (1995): An HPIV System for turbulence research. EP Rood (ed.), ASME FED, 148,17-21.

Adrian, R. J. (1996): Strategies for Imaging Flow Fields with PIV. AIAA 96-1988

Black, D.L.; Mcquay, M.Q.; Bonin, M.P. (1996), Laser-based techniques for particle-sizing measurement: a review of sizing methods and their industrial applications. *Prog Energy Combust Sci.* **22**. pp. 267-306.

Brady, M., and Vlachos, P. (2003). "Novel Particle Sizing and Centroid Estimation Techniques." Proceedings of IMECE 2003.

Brady, M., Abiven, C., Vlachos, P., and Papadopoulos, G. (2002). "Time–Resolved Spray–Droplet Velocity and Size Measurements via Single Camera Laser Sheet Imaging and Planar DPIV." Proceedings of IMECE 2002.

Boedec, T; Simoens, S. (2001), "Instantaneous and simultaneous planar velocity field measurements of tow phases for turbulent mixing of high pressure sprays." *Experiments in Fluids*, 31, pp. 506-518.

Cowen, E., Monismith, S. (1997), A hybrid digital particle tracking velocimetry technique. *Experiments in Fluids*, **22**, pp. 199-211.

Damaschke N, Nobach H, Tropea C (2002): Optical limits of particle concentration for multi-dimensional particle sizing techniques in fluid mechanics. *Experiments in fluids*, **32**, 143-152

Derou, D., and Herault, L., "A new paradigm for Particle Tracking Velocimetry, based on graph-theory and pulsed neural networks."

Dracos Th. and A. Gruen (1998): Videogrammetric methods in velocimetry. Appl. Mech. Rev. vol. 51, no. 6 1998.

Etebari, A, Carneal, J. B., Vlachos, P, 2004, "On the Accuracy of Wall Shear Stress Using DPIV," Proceedings of the ASME HTFE Summer Conference 2003.

Gharib, M. and Willert, C. "Particle Tracing: Revisisted." Review Paper.

Grant I (1997): Particle Image Velocimetry: A Review. Proceedings Institute of Mechanical Engineers

Grant I (1994): Selected papers on Particle Image Velocimetry. SPIE Milestone Series MS99, SPIE Optical Engineering Press, Bellingham, Washington

Guezennec, Y.G., and Kiritsis, N. (1990). "Statistical investigation of errors in particle image velocimetry." *Exp Fluids,* **10**, pp. 138-146.

Harris, J. W. and Stocker, H. "Ellipse." §3.8.7 in *Handbook of Mathematics and Computational Science.* New York: Springer-Verlag, p. 93, 1998.

Hasselinc L. (1988): Digital Image Processing in Flow Visualization. ARFM 20:421 85

Huang, H., Dabiri, D., Gharib, M., 1997, "On errors of digital particle image velocimetry," Meas. Sci. Technol. **8**, pp. 1427-1440.

Huang H. T. and Gharib M. (1997): Processing Error in Digital Particle Image Velocimetry. FEDSM97-3068.

Keane, R.D, Adrian, R.J., and Zhang, Y. (1995). "Super-resolution particle imaging velocimetry." *Meas. Sci. Tech.*, **6**, pp. 754-68.

Keane R. D. and Adrian R. J. (1990): Optimization of particle image velocimeters . Part I: Double pulsed systems. Meas. Sci. Tech. 1 1202-1205.

Khalitov, D.A.; Longmire, E.K. (1999).Simultaneous two-phase PIV measurements for high speed flows. Third International Workshop on Particle Image Velocimetry. Santa Barbara. Sept. 16-18.

Marxen, M., Sullivan, P., Loewen, M.,Jahne, B. (2000), Comparison of Gaussian particle center estimators and the achievagble measurement density for particle tracking velocimetry. *Experiments in Fluids*, **29**.

Meynard R. (1983): Measure de champs de vitesse d' ecoulements fluids par analyse de suites d'images obteneues par diffusion d'un fueillet lumineux. Ph.D Dissertation, Faculte des Science Appliquees, Universite Libre de Bruxelles.

McKenna, S.P., and McGillis, W.R., (2002). "Performance of digital image velocimetry processing techniques." *Exp. Fluids*, **32**, pp. 106-115.

Mayer, S. (2002). "A generalized processing technique in digital particle image velocimetry with direct estimation of velocity gradients." *Exp. Fluids*, **33**, pp. 443-457.

Meunier, P., Leweke, T., 2003, "Analysis and treatment of errors due to high velocity gradients in particle image velocimetry," Exp. in Fluids, **35**, pp 408-421

Nogueira, J., Lecuona, A., Rodriguez, P. A., 1999, "Local field correction PIV: on the increase of accuracy of digital PIV systems," Exp. in Fluids, **27**, pp. 107-116

Pereira, F., Gharib, M., Dabiri, D., and Modarress, D. (2000): Defocusing digital particle image velocimetry: a 3-component 3-dimensional DPIV measurement technique. Application to bubbly flows. Experiments in Fluids **29**(**7**), S078-S084.

Prasad A.K. and Adrian R J (1993): Stereoscopic particle image velocimetry applied to liquid flows. Experiments in Fluids 15, 49-60.

Raffel M. Willert C. E. Kompnhans, J., 1998, "Particle image velocimetry: a practical guide," Springer, Berlin Heidelberg, New York

Song, X., Yamamoto, F., (1999). "A new tracking algorithm of PIV and removal of spurious vectors using Delaunay tessellation." *Exp. Fluids*, **26**, pp. 371-80.

Stark, H. and Woods, J.W. (1994) *Probability, Random Processes, and Estimation Theory for Engineers.* 2nd ed., Prentice Hall, Upper Saddle River, NJ.

Scarano, F. and Rieuthmuller, M. L. (1999): Iterative multigrid approach in PIV image processing with discrete window offset. Experiments in Fluids, **26**, 513-523.

Udrea, D., Bryanston-Cross, P., Lee, W., Funes-Gallanzi, M. (1996), Two sub-pixel processing algorithms for high accuracy particle centre estimation in low seeding density particle image velocimetry. *Optics & Laser Technology*, Vol **28**, no 5.

Wereley ST, Meinhart CD (2001): Second-order accurate particle image velocimetry. *Experiments in Fluids*, **31**, 258-268

Westerweel, J (1997), "Fundamentals of particle image velocimetry," Meas. Sci. & Technol. **8**, pp. 1379-1392

Westerweel J. (1993a): Digital Particle Image Velocimetry, Theory and Application. Delft University Press
Westerweel J. (1993b):Optical Diagnostics in fluid and thermal flow. SPIE 2005 624-35

Willert C.E., Gharib, M., 1991, "Digital particle image velocimetry," *Exp. in Fluids* **10**, pp 181-193

VITA

Jason Bradley Carneal was born in Richmond, Virginia on July 20, 1979. He enjoyed a happy upbringing due to the generosity and kindness of his parents, James H. and Joan G. Carneal, and his grandparents, who lived next door. He lived in Ashland, VA, until his valedictory graduation from Patrick Henry High School and his matriculation at Virginia Tech in August of 1997. His early college years were marked by confusion, exhibited by his three major changes in a single year, from Physics, to Biology, to Aerospace Engineering, and finally to Engineering Science and Mechanics. This final decision of major reflected his natural inability to make rational decisions. During his senior year, he met and started dating the love of his life, Catherine Orifici, whom he married on July 31, 2004. He graduated Summa Cum Laude with a Bachelor of Science in Engineering Science and Mechanics and a Minor in Mathematics in May of 2001. In a fit of utter madness, he matriculated at the University of Michigan, Ann-Arbor in the Biomedical Engineering for a masters degree in August, 2002. One year, 50 pounds, and one Grave's Disease later, he returned to Virginia Tech for a masters degree in Engineering Mechanics, the culmination of which is this document. During his masters education, Jason developed an interest in shooting, and now owns five firearms. Perhaps his crowning achievement during graduate school was taking and passing a motorcycle class and the subsequent purchase of a 1998 Kawasaki Vulcan. All of this aside, he still doesn't know what he wants to do with his life, and he isn't quite sure that he should know at all. His life could easily meander into medicine, defense research, law, or real estate. Out of all the ambiguity the only certainty is that he hates engineering, or at least the engineering to which he has been exposed to date. With any luck, his career decisions in the future will reflect his desires, and not the desires of those around him.